Multicomponent assemblies for organic electronics

Wassima Rekab

UNIVERSITÉ DE STRASBOURG

ÉCOLE DOCTORALE DES SCIENCES CHIMIQUES

UMRS 7006 – Institut de science et d'ingénierie supramoléculaires

THÈSE

présentée par :

Wassima REKAB

soutenue le : **09 Janvier 2017**

pour obtenir le grade de : **Docteur de l'université de Strasbourg**

Discipline/ Spécialité : Chimie-Physique

Assemblage multi-composant pour l'électronique organique

THÈSE dirigée par :

M. SAMORÌ Paolo	Professeur, université de Strasbourg, France
M. ORGIU Emanuele	Professeur, université de Strasbourg, France

RAPPORTEURS :

Mme. LUDWIGS Sabine	Professeur, université de Stuttgart, Allemagne
Mme. VIGNAU Laurence	Professeur, université de Bordeaux, France

Résumé de la thèse

Mon travail de thèse porte sur l'assemblage supramoléculaire des multi-composants utilisés dans le domaine de l'électronique à base organique. En particulier, l'étude et l'optimisation des transistors organiques à effet de champ (OFETs), des phototransistors, et des inverseurs organiques, dans le but d'améliorer leurs performances électriques en rajoutant de nouvelles propriétés supplémentaires aux films semi-conducteurs (de type-n et ambipolaire).

Au cours de la dernière décennie, la fabrication et l'optimisation des transistors à effet de champ utilisant des semi-conducteurs organiques comme éléments actifs a fait l'objet de nombreux travaux avancés à l'interface de la chimie-physique et l'électronique, ces dispositifs représentent des éléments clés pour l'électronique de demain en raison de leurs multiples avantages par rapport aux transistors classiques à base de silicium, notamment, la flexibilité, la légèreté, la transparence et la facilité de fabrication à faible coût[1-5]. Les éléments électroniques à base organique peuvent aussi jouer un rôle important dans différents domaines tels que le domaine de l'identification par radiofréquence (RFID),[6-7] dans les circuits intégrés (CI),[8-9] les écrans, les codes-barres électroniques,[10-12] les senseurs,[13] les diodes électroluminescentes,[14-15] les photovoltaïques[16] et dans la technologie des inverseurs CMOS (complémentaire métal-oxyde-semi-conducteur)[17-18]. Par ailleurs, l'un des grands défis est le développement des composants multifonctionnels qui présentent de nouvelles propriétés intéressantes, ce qui nous permet de fabriquer des nouveaux dispositifs électroniques avec des fonctionnalités supplémentaires.

Les nouveaux progrès dans le domaine des matériaux organiques semi-conducteurs, ont mené à une nouvelle génération de composés organiques, qui sont solubles dans différents solvants organiques et capables d'être procédés en solution avec des méthodes à faible coût. Les semi-conducteurs organiques ont attiré l'attention de nombreuses entreprises travaillant sur diverses applications électriques, telles que, les écrans (LCD), les batteries des portables, et les écrans électroluminescents. Les semi-conducteurs organiques peuvent être déposer en couches minces sur des supports flexibles par des méthodes très simple à basse température, comme spin-coating (éduction centrifuge), drop-casting, et inject-printing (impression jet d'encre). Pour cela, ils peuvent donc remplacer les dispositifs classiques à base de semi-conducteurs inorganiques. Certains dispositifs basés sur des semi-conducteurs d'oxyde métallique peuvent être fabriquer qu'à des températures très

élevées, ce qui augmente le coût de production. Ceci est donc l'une des limitations pour certaines applications dans le domaine d'électronique. Des développements significatifs ont été réalisés, en ajustant les propriétés chimiques, optiques et électriques des molécules organiques, pour mettre en avance la technologie d'électronique et d'optoélectronique organique par rapport à l'électronique basés sur le silicium. Les performances des dispositifs organiques sont relativement liées à plusieurs paramètres, comme la cristallinité des couches semi-conductrices et l'efficacité de l'injections des charges. Pour ce fait, il est fortement indispensable d'optimiser les interfaces métal-semi-conducteur et semi-conducteur-diélectrique ainsi que les conditions de traitement, comme le choix des solvants, les techniques de dépôt et le recuit thermique.

La première partie de nos études porte sur la corrélation entre l'architecture moléculaire et les propriétés électriques des transistors à effet de champs basé sur un dérivé de Fullerène. La famille des fullerènes, comme [6,6]phenyl-C_{61}-butyric acide méthyle ester (PCBM) ont été souvent utilisés comme matériaux qui transportent les électrons dans les OFETs. Des efforts chimiques ont été déployés pour le développement de nouveaux dérivés de fullerène qui peuvent être traitées en solution, possédant en outre des mobilités d'électrons plus élevées. Parmi les différents dérivés, le 1′,1″,4′,4″-Tetrahydro-di[1,4]methanonaphthaleno [1,2:2′,3′,56,60:2″, 3″][5,6]fullerene-C60, aussi connu sur le nom Indene-C_{60} Bis-Adduct (ICBA),[19] a attiré particulièrement une grande attention, ceci nous a encouragé à mettre au point de nouveaux transistors organiques plus performants en utilisant cette molécule de fullerène mentionnée ci-dessus (ICBA) comme étant semi-conducteur de type-n. Ainsi, nous avons étudié les effets de la durée et la température d'annealing (recuit) des dispositifs OFETs sur leurs performances électriques et la morphologie des couches semi-conductrices. Les surfaces de SiO_2 ont été passivées par la formation des monocouches auto-assemblées de l'octadécyltrichlorosilane (OTS) et hexaméthyldisilazane (HMDS), afin d'étudier l'effet de l'optimisation de l'interface semi-conducteur-diélectrique sur les propriétés électriques des transistors à effet de champs qui ont été fabriqués en configuration 'bottom-contact bottom-gate'. Ces dispositifs ont été chauffés à différentes températures (90 °C, 140 °C, 200 °C). Les résultats obtenus montrent des valeurs de mobilités à effet de champ très élevées dans le cas des transistors traités par OTS suivi par annealing à 200 °C par rapport à ceux traités par HMDS, OTS rend la surface de SiO_2 énergétiquement favorable et plus hydrophobe comparé à l'HMDS. Cette différence de performances, peut être corrélée aux interactions molécule-molécule qui sont liées aux interactions molécule-substrat, ces dernières dépendent largement du type de traitement de la surface du substrat. Aussi, lors de cette étude nous avons démontré l'impact de la durée du traitement d'annealing sur l'amélioration du transport de charge. A notre connaissance, notre meilleure valeur de mobilité d'électrons de $0.1 cm^2V^{-1}s^{-1}$ est la plus élevée jamais reportée jusqu'à présent dans la littérature. L'étude caractéristique GIXRD (Grazing incidence

X-ray diffraction) n'a pas fourni d'éventuelles informations sur l'ordre structurel à l'échelle atomique. En outre, ce matériau ICBA connu par ces capacités de transport des charges de type-n (les électrons) a aussi montré un comportement ambipolaire en transportant à la fois des électrons et des trous (des charges positives). Cependant, les mobilités obtenues des électrons et des trous ne sont pas balancées. L'ambipolarité de ce matériau est en cours d'étude, et nécessite plus d'informations approfondies basées sur des calculs théoriques. La dépendance remarquable du transport de charge dans les couches semi-conductrices de ICBA, sur la température de recuit (annealing) et sa durée ainsi que sur l'énergie de surface de diélectrique SiO_2 est une preuve que les propriétés du transport de charge dans le matériau ICBA sont directement liés aux conditions de traitement et préparation des transistors à effet de champ.

La dépendance du transport de charge dans les couches semi-conductrices sur les conditions de traitement des dispositifs électriques a aussi été prouvée lors d'une étude d'un autre matériau semi-conducteur de type-n utilisé comme couche active dans la fabrication des phototransistors organiques.

La deuxième partie de nos travaux se focalise sur une comparaison optoélectronique et morphologique des différents assemblages moléculaires des couches actives des phototransistors organiques (OPTs). Ces derniers sont des transistors à effet de champ dans lequel une lumière incidente est utilisée en plus d'un champ à grille pour moduler la densité des porteurs de charge à l'intérieur du canal. Les phototransistors organiques présentent de nombreux avantages par rapport à leurs homologues inorganiques, tels que la possibilité de moduler leurs propriétés optoélectroniques *via* la conception moléculaire et l'auto-assemblage sur des supports non-planaires et flexibles,[20-22] en formant des structures microcristallines qui ont démontré des photosensibilités élevées[23]. Parmi les petites molécules organiques semi-conductrices utilisées comme composantes actives dans la fabrication des phototransistors, les dérivés de pérylène-di-imide (PDI) sont particulièrement appropriés en raison de leur absorption caractéristique dans la région visible combinée à leur haute capacité de transport des électrons[24-25]. L'une des limitations majeures des transistors organiques, en particulier ceux basés sur des systèmes de type-n (qui conduisent les électrons), est leur sensibilité à l'air. Pour surmonter cette limitation, nous avons étudié un dérivé de pérylène di-imide de type-n stable à l'air, nommé N, N'-1H, 1H-perfluorobutyl-dicyano pérylène di-imide (PDIF-CN2, commercialement disponible), cette molécule est connue pour sa capacité à former des fibres cristallines auto-assemblées par la méthode de la précipitation induite par solvant (SIP). Cette molécules a été intégré dans des dispositifs des phototransistors. Ainsi nous avons fabriqué des phototransistors à base de mono- et multi-fibres de PDIF-CN2 qui ont été optimisés par différents traitements de surfaces du diélectrique (fonctionnalisation par HMDS ou OTS). Les propriétés optoélectroniques de ces dispositifs ont été comparées à ceux des dispositifs à base des couches

minces déposés par spin-coating (éduction centrifuge). Nos dispositifs mono-fibres ont montré des valeurs de mobilité significativement plus élevées (supérieure à 2 $cm^2V^{-1}s^{-1}$) par rapport à ceux des multifibres et couches minces. Une telle efficacité de transport d'électrons est le résultat des interactions intermoléculaires assez fortes entre des molécules de PDIF-CN2 et d'une faible densité de défauts structurels. La cristallinité très élevée des fibres permet une collecte efficace des excitons photogénérés qui se traduit par la plus haute sensibilité à la lumière (R) et photosensibilité (P) rapportées pour les phototransistors à base de mono-fibre supérieure à 2×10^3 AW^{-1}, et 5×10^3 AW^{-1}, respectivement. Nos résultats ont démontré que la stabilité des performances électriques après exposition à l'air est très élevée pour les dispositifs dont les architectures cristallines sont utilisées en tant que couche semi-conductrice. Ces résultats confirment en effet le rôle important de l'ordre supramoléculaire cristallin dans les propriétés des matériaux intégrés dans la fabrication des phototransistors stable à l'air avec de meilleures photo-réponses R et photosensibilité P. Ces résultats démontrent clairement l'importance du degré d'ordre moléculaire pour présenter d'excellentes mobilités d'effet de champ ainsi que de bons dispositifs opérationnels. Les OPT organiques à base de mono-fibre fabriqués par un procédé de traitement très simple sont des candidats très prometteurs pour des dispositifs à commande optique dans l'optoélectronique, en raison de leur grande réactivité à la lumière et d'une bonne stabilité opérationnelle à l'air. Nos résultats confirment sans ambigüité que les propriétés d'auto-assemblage des molécules PDIF-CN2 et les performances électriques correspondantes sont largement améliorées lorsque les surfaces de SiO_2 sont passivées à l'aide de la formation des monocouches auto-assemblées d'OTS ou d'HMDS.

Dans le même contexte des matériaux organiques intégrés dans des dispositifs électriques. Nous avons concentré notre attention sur la réalisation des nouveaux composants électroniques multifonctionnels par des procédés de fabrications facilement réalisables, non complexes et qui ouvrent des nouvelles perspectives pour l'industrie de l'électronique organique. Ces nouveaux composants peuvent engendrer plusieurs fonctionnalités différentes dans un même dispositif électronique. De ce fait, nous avons combiné des semi-conducteurs organiques avec d'autres fragments moléculaires ayant différentes propriétés dans la fabrication des transistors, et inverseur organique. Notre objectif a été d'obtenir des dispositifs multifonctionnels en intégrant des molécules sensibles à la lumière telles que les diaryléthènes.

En ce qui concerne l'utilisation des polymères dans la fabrication des composants multi-fonctionnels, nous avons développé pour la première fois des dispositifs photo-modulés à base de trois composants, en utilisant un polymère ambipolaire en tant que semi-conducteur possédant des mobilités élevées (électrons-trous)[26]. Afin d'obtenir des mobilités ambipolaires élevées du polymère,

ce dernier devrait être chauffé à 320°C. Du fait de cette température élevée, les molécules photochromiques diaryléthènes (DAEs) sont intégrées dans la matrice polymèrique par diffusion thermiquement active à une température de 90°C, car ces molécules photochromiques se dégradent au-delà de cette température. Cette approche nous a permis de fabriquer des transistors ambipolaires à effet de champ avec un courrant de drain commandé par la lumière grâce aux intéractions entre le polymère est les diaryléthènes. Ces derniers subissent une isomérisation réversible entre deux isomères (forme ouverte et forme fermée) après une irradiation à différente longueurs d'ondes. Ceci mène à une fabrication facile des inverseurs organiques (CMOS) dont leur gain en tension (dc) devient photomodulable, grâce au contrôle de la population des isomères de diaryléthène par la longueur d'onde et le nombre des photons frappant la surface active des dispositifs. Dans ce travail, nous avons réussi à intégrer deux dérivés du diaryléthène avec différentes substitutions appelés DAE_tBu et DAE_F dans la matrice d'un polymère ambipolaire, le Diketopyrrole-thiéno [3,2-b] thiophène (DPPT-TT). En fonction de leur degré de conjugaison (élevé pour la forme fermée ou faible pour la forme ouverte), les molécules diaryléthènes utilisées possèdent différentes bandes de gap et différents niveaux énergétiques associés HOMO et LUMO. Lorsque le DAE_tBu est dans son état isomérique fermé, son niveau HOMO se situe dans la bande interdite du copolymère, il piége donc les trous en diminuant le courant qui passent dans le canal semi-conducteur. C'est également le cas pour le niveau LUMO du DAE_F, piégeant ainsi les électrons. Dans le cas contraire, lorsque DAE_tBu et DAE_F sont dans leurs formes ouvertes, leurs niveaux d'énergie HOMO et LUMO respectivement se situent à l'extérieur de la bande interdite du polymère, ceci ne conduit alors à aucune interaction électronique. Cette approche a déjà été utilisée au sein de notre laboratoire en utilisant des semi-conducteurs de type-p (P3HT, BTBT)[27-28] et des semi-conducteurs de type-n (ICBA, PCBM)[29] avec différents mélanges de DAEs. Mais lors de ce travail nous avons pu l'appliquer sur un semi-conducteur ambipolaire (à la fois semi-conducteur de type-n et -p). Nous avons effectué des cycles de commutation optique en alternant entre l'irradiation ultraviolet (365 nm) et visible (546 nm) sur les dispositifs de OFET basés sur trois composés le DPPT-TT, DAE_tBu et DAE_F. Nous avons observé que les courants de drain des électrons et des trous ont diminué après chaque étape lors de l'irradiation UV et ont ensuite augmenté lors de l'irradiation avec la lumière visible, jusqu'au atteindre les valeurs initiales. Ces résultats confirment la possibilité de réaliser des dispositifs optiquement controlés, sélectifs et complètement réversible pour le transport des trous et des électrons. En se basant sur ces résultats prometteurs, nous avont employé ces dispositifs dans la réalisation d'inverseurs organiques photomodulables. Un inverseur est l'unité de base dans les circuits électroniques, constitué de deux transistors de type-n et -p, conduisant à une inversion logique (0 - 1/1 - 0) d'une tension d'entrée.[30] Nos dispositifs fabriqués d'inverseurs organiques opèrent dans le premier quadrant à V_{DD} = -70 V, avec un gain en tension élevé ~ 180 avant l'irradiation (dans le noir). Le gain a augmenté progressivement lors de l'irradiation UV (365 nm) jusqu'à atteindre une valeur très élevée à environ

504 après 25 minutes d'irradiation. Ensuite, les dispositifs ont été irradiés par la lumière visible (546 nm), le gain a diminué à nouveau jusqu'à regagner la valeur initialale (180). Ce comportement confirme la possibilité de contrôler et améliorer le gain des inverseurs par irradiation UV/Visible. Grace à notre approche, les valeurs de gain obtenues pour les inverseurs ambipolaires sont relativement élevées (504), par rapport à celles rapportées dans la littérature (gain ~ 86).

En conclusion, nous avons démontré dans un premier temps l'influence de l'ordre supramoléculaire des matériaux semi-conducteurs sur les performances des transistors à effet de champ. Les structures cristallines des fibres de pérylène (PDIF-CN2) ont montré des mobilités (2 $cm^2s^{-1}V^{-1}$) supérieurs à celles des couches minces désordonnées. L'ordre structurel élevé des assemblages de fibres de PDIF-CN2, particulièrement lorsque on utilise une seule fibre cristalline tant que semi-conducteur organique, résulte à une sensibilité à la lumière (R) et photosensibilité (P) les plus élevées rapportées en littérature pour les phototransistors à base de PDI, dépassant 2×10^3 AW^{-1} et 5×10^3 respectivement. Les dispositifs à base de fibres auto-assemblées du PDIF-CN2 fabriqués par des procédés facile et compatible avec différentes applications de grande échelle sont très prometteurs pour le domaine de l'optoélectronique, en offrant ainsi, des bonnes performances électriques, une stabilité à l'air, et surtout une grande sensibilité à la lumière.

Ainsi, nous avons réalisé par le procédé d'annealing à des températures élevées des dispositifs plus performants à base d'un semi-conducteur de type-n (ICBA), sachant que ces derniers ont été traités par l'OTS afin d'améliorer l'hydrophobicité des surfaces SiO_2. Ces dispositifs ont montré un transport de charge à la fois de type-n et de type-p (transport ambipolaire), ce qui n'est pas habituel pour ce matériau. Néanmoins, les mobilités de trous extraites sont moins élevées (entre 10^{-4} et 10^{-3} $cm^2s^{-1}V^{-1}$) comparées à celles des électrons (0.1 $cm^2s^{-1}V^{-1}$ à une température de recuit de 200°C). Cela est encore en cours de traitement pour avoir plus d'informations qui pourraient nous expliquer ce phénomène inattendu. Bien que, les valeurs de mobilités d'électron sont les meilleures comparées à celles reportées dans la littérature jusqu'à présent.

Lors de ces travaux de thèse, nous nous sommes intéressés non seulement à des petites molécules semi-conductrices de type-n (PDIF-CN2 et ICBA), mais aussi à un polymère ambipolaire (DPPT-TT) ayant des performances électriques très élevées. Ce polymère a été utilisé lors de la fabrication de nouveaux dispositifs multifonctionnels par l'addition des molécules diaryléthénes (DAE_tBu et ou DAE_F), dont les propriétés électriques sont contrôlées par la lumière. Enfin, nous avons validé une nouvelle approche dans la fabrication des inverseurs organiques en ajoutant la lumière comme facteur de contrôle optique de gain en tension, ces dispositifs sont caractérisés par des

gain en tensions très élevées (jusqu'au 504). Ces travaux réalisés durant cette thèse offrent de nouvelles perspectives dans les domaines de l'optoélectronique et la conception des mémoires optiques.

Abstract

This thesis focuses on the investigation of charge carrier transport across organic single, bi- and three-component materials used as the active layer in organic transistors, phototransistors and complementary inverters.

The fabrication and optimization of organic field-effect transistors (OFETs) have been the subject of an intense research endeavor during the last decades because such devices represent key elements for low-cost flexible electronics including radiofrequency identification (RFID) tags,[1-7] integrated circuits (ICs) [8-9] for logic and memory chips, smart cards[10-12] and sensors.[13] Organic-based electronics can play an important role also in other applications including electronic bar codes or active matrix elements for displays, light-emitting diodes, [14-15], photovoltaics[16], and in complementary inverters (CMOS).[17-18] However, one of the grand challenges is still the development of multicomponent materials that can combine a set of new interesting properties while leading to new functionalities.

Recent performance improvements in molecular materials area, gives rise to new generation of organic compounds; that are highly soluble in organic solvents and capable to be processed with low-cost methods. Organic semiconductors have attracted the attention of numerous companies working on various electronic applications, like liquid crystal displays data storage, portable batteries, and light-emitting displays. Simple fabrication techniques such as spin-coating, drop-casting, inject-printing of organic semiconductors that can be processed at low temperature, make them good replacements for conventional devices based on inorganic semiconductors. Some of devices based on metallic oxide semiconductors can be fabricated only at elevated temperatures and needs high-tech manufacturing technology and high-cost production, which are considered as limitations for several applications. Significant progress was made by tuning the chemical, optical, and electrical properties of organic molecules, to put molecular electronics and optoelectronics in advance of the silicon available technology. Organic devices performances are strongly related to different parameters such as crystallinity and the efficiency of the charge injection. To overcome such limitations, it is highly required to optimize metal-semiconductor and semiconductor-dielectric interfaces as well as processing conditions, like solvents choice, deposition techniques, and thermal annealing.

First, we have focused our attention on the correlation between semiconductor film properties at different processing conditions and the corresponding field-effect devices performances, using a Fullerene derivative. Fullerene derivatives including [6,6]phenyl-C_{61}-butyric acid methyl ester (PCBM) have been often used as electron transporting materials in OFETs. Intensive chemical effort has been put towards the development of fullerene moieties that can be solution-processed, resulting in higher electron mobility with the desired molecular packing. Among all the different derivatives, certainly the 1′,1″,4′,4″-Tetrahydro-di[1,4]methanonaphthaleno[1,2:2′,3′,56,60:2″, 3″][5,6]fullerene-C_{60}, also known as Indene-C_{60} Bis-Adduct (ICBA),[19] has garnered a great attention. We investigate the effects of the annealing temperature and duration as well as SiO_2 surface functionalization (of the above-mentioned fullerene molecule (ICBA) and correlate the film morphology to the transport of electrons in thin-film transistors fabricated in bottom-contact bottom-gate configuration. To study the influence of semiconductor-dielectric interface on the device electrical performances, we functionalized SiO_2 with different self-assembled monolayers hexamethyldisilazane (HMDS) and octadecyltrichlorosilane (OTS). After dielectric surface treatments, OFET devices were annealed at different temperatures (90 °C, 140 °C, and 200 °C). The electron mobility revealed a monotonic increase upon annealing for HMDS-treated SiO_2. Whilst an abrupt enhancement was recorded at 200°C on OTS-functionalized substrates which lead to a more hydrophobic surface compared to HMDS. This difference can be correlated to a molecule-molecule interaction intimately entwined to molecule-substrate interaction owing to the type of surface treatment. ICBA molecules are freer to move and undergo self-assembly when supported on an OTS-treated SiO_2 owing to the lower surface energy they experience. The highest extracted electron mobility approaching 0.1 $cm^2V^{-1}s^{-1}$, to the best of our knowledge, is the highest ever reported value for ICBA within the scientific literature. The ability of promoting electron transport within the film at a given temperature has been found to depend on the particular kinetically-trapped phase in which the molecules are found in time. Grazing Incidence X-Ray Diffraction (GIXRD) study did not provide strong evidence of structural order at the atomic scale. Besides its use as electron transporting semiconductor, ICBA material have showed an ambipolar behavior by transporting both electrons and holes, although with unbalanced mobilities. This ambipolar behavior is still under investigation to have further information from theoretical studies. The remarkable dependence of the charge transport upon the annealing duration and temperature as well as from the surface energy is unambiguous evidence that ICBA transport properties strongly depend on the processing conditions.

The charge transport dependence on processing treatments was also proved using another n-type semiconductor small molecule used for the fabrication of organic phototransistors.

Organic phototransistors in which an incident light is used in addition to a gate field to tune the charge-carrier density inside the transistor channel, have gained considerable attentions due to their molecular assemblies supported on flexible substrates .[20-22] Low-dimensional organic architectures such as crystalline micro/nanowire, microribbon structures exhibited high light-sensitivity and good charge carrier mobilities.[23] Among organic small molecules that can be self-assembled forming crystalline structures. Perylene di-imide (PDI) derivatives are highly employed as semiconductor layer in field-effect transistors, owing to their ability to transport electron charge carriers.[24-25]. Organic self-assembled fibers produced *via* solvent induced precipitation of an air stable n-type perylene derivative i.e. N, N'-1H, 1H-perfluorobutyl-dicyano perylene di-imide called PDIF-CN2 (commercially available) were used as solution-processed active materials for the fabrication of light sensitive field effect transistors. Their absorption capacity of visible light made it possible to fabricate phototransistors based on single fiber or multifibers that serve as active layers. We have fabricated organic phototransistors based on either single or multi-fibers integrated in three-terminal devices. It is well known that thin film continuity and surface morphology are thought to enhance charge transport efficiency. In order to form highly ordered organic films, a surface modification was applied to SiO_2 dielectric, substrates were modified with UV-Ozone treatment and functionalized with HMDS and OTS self-assembled monolayers. The optoelectronic properties of these devices were compared to those of devices incorporating more disordered spin-coated PDIF-CN2 thin-films. The single-fiber devices revealed significantly higher field-effect mobilities, compared to multifiber and thin-films, exceeding 2 $cm^2V^{-1}s^{-1}$. Such high charge transport is attributed to the strong intermolecular coupling between closely packed PDIF-CN2 molecules and of a low density of structural defects. The improved crystallinity allows efficient collection of photogenerated Frenkel excitons which results in the highest reported responsivity (R) for single-fiber PDI-based phototransistors, and photosensitivity (P) exceeding 2×10^3 AW^{-1}, and 5×10^3, respectively. Our results show also that the air-stability performances are superior in devices where highly crystalline supramolecularly engineered architectures serve as the active layer. These findings clearly illustrate the importance of the high degree of molecular order for exhibiting excellent field-effect mobilities as well as good operational devices. Organic single fiber based-OPTs fabricated by a very simple processing method are highly promising candidates for light-controlled devices in optoelectronics because of their high light responsivity, and good operational stability in air atmosphere.

New multifunctional components can be fabricated combining organic small molecules and polymers semiconductors with other molecular moieties having different chemical, optical, and electrical properties such as photochromic switches with the aim of tuning the semiconductors functional performances to be able to perform devices with new functionalities. Based on that, we

have fabricated multifunctional transistors and complementary inverter devices combining organic semiconductors with molecules sensitive to light like diarylethenes.

We have developed for the first time three-component photoswitchable devices using an ambipolar polymer featuring good electron and hole mobilities[26] as the active layer. Due to the high temperatures at which the chosen polymer films had to be processed (320 ºC) in order to exhibit a good ambipolar behavior, the photochromic diarylethene molecules could be integrated in the material only by thermally activated diffusion into the polymer matrix through a gentle post-processing annealing (90 ºC). This made it possible to fabricate OFETs where the drain current can be phototuned thanks to the interactions between the polymer and the DAE species. The latter can undergo reversible isomerization between a closed and an open form upon irradiation at different wavelengths. This leads to the facile fabrication of inverters whose gain becomes photomodulable because it can be tuned by controlling the different population of closed vs. open isomers in the blend by playing with the number and wavelength of the photons shone over the active layer. In particular, diarylethene moieties possess different band gap and associated HOMO and LUMO levels, depending on their stronger (closed form) or weaker (open form) degree of conjugation, that can be controlled upon irradiation at different wavelengths. In this work, we report on the integration of two diarylethene synthesized derivatives, i.e. DAE_tBu and DAE_F, into an ambipolar polymer Diketopyrrole-Thieno[3,2-b]thiophene Copolymer (DPPT-TT) called DPPT-TT in order to exploit the optically responsive nature of the photochromic systems to photo-gate the charge transport of both electrons and holes through the three-component material. The DAEs in their open and closed states feature different HOMO and LUMO levels. In particular, when they are in their closed isomeric state, the HOMO sits in the bandgap of the copolymer, thus they act as intragap hole-accepting levels. Likewise, is the case for the LUMO, thus for electron-accepting levels. Conversely, the HOMO and LUMO energetic levels of the open form of DAE_tBu and DAE_F respectively sit outside the bandgap, thus no electronic interaction takes place . This approach has been previously employed in our lab using p-type semiconductors (P3HT, BTBT)[27-28] and n-type semiconductors (PCBM, ICBA)[29] with different DAE blends. We have performed photoswitching cycles alternating ultraviolet (365 nm) and green (546 nm) irradiation onto the OFET devices based on three-compounds DPPT-TT, DAE_tBu and DAE_F. We observed that both electrons and holes drain currents decreased upon UV irradiation after each step and increased upon visible light irradiation. After visible light irradiation, the drain current is completely recovered. These results confirm the light-switching process, which is completely reversible and selective for holes and electrons charge transport, as found in bi-component devices, by inserting just one DAE type (DAE_tBu of DAE_F) which plays the role of traps in the closed state for only electrons (using DAE_F) or only holes (using DAE_tBu). The basic aim of this work is to fabricate organic inverters based on this polymer (DPPT-TT) and DAE moieties with a photocontrolable gain voltage. An

inverter is a basic unit in electronic circuits, it leads to logical inversion (0 - 1 / 1 - 0) of an input that is voltage in our study.[30] We fabricated organic complementary inverters employing identical ambipolar OFETs based on DPPT-TT polymer with diarylethene molecules (DAE_tBu and DAE_F) inserted *via* permeation into DPPT-TT matrix in order to tune the voltage gain of complementary inverter by UV/Visible irradiation. The inverter devices fabricated by integrating DAEs in the semiconductor layer operate in the first quadrant at V_{DD} = -70, with a high gain ~ 180 in dark. The voltage gain increased progressively with UV illumination (365 nm) exhibited a high static gain value of 504 after 25 minutes of UV irradiation. Upon visible light (546 nm), the voltage gain decreased to recover the initial value after 25 minutes of visible irradiation. This behavior confirms the ability to tune the inverter's gain using light irradiation. The resulted gain values in dark and under light irradiation are relatively high for organic complementary inverters based on ambipolar transistors, compared to those reported in literature (gain ~ 86).

In summary, we have provided evidence for the influence of the order at the supramolecular level on the electrical performances of both field-effect transistors and phototransistors supported on SiO_2 substrates. In particular, the comparison of perylene single fibers (of PDIF-CN2) with high crystallinity produced by solution processable method (SIP) and multifiber assemblies with spin-coated thin films, revealed that the former outperform by exhibiting good reproducibility and field-effect mobilities up to 2 $cm^2s^{-1}V^{-1}$ when the SiO_2 is treated with OTS self-assembled monolayers. The higher structural order of fiber assemblies especially when using one single crystalline fiber results in the highest reported responsivity (R), and photosensitivity (P) for PDI-based phototransistors comparing with literature, exceeding 2×10^3 AW^{-1}, and 5×10^3, respectively. Our results clearly highlight that the self-assembling properties of PDIF-CN2 molecules and the related electrical performances are strongly improved when hydrophobic surfaces treated with OTS or HMDS self-assembled monolayers are used for the film growth. Pointing out that air stable and high ordered PDIF-CN2 fibers can be used for fundamental studies in light-controlled devices in optoelectronics.

OTS monolayers enhanced the silicon dioxide surface enhancements using OTS monolayers led to the highest electron mobility (around 0.1 $cm^2s^{-1}V^{-1}$) reported up to date, owing to the more favorable energetic surface than HMDS for annealed devices based on ICBA small molecule. All ICBA fabricated transistor devices showed an ambipolar behavior with low hole mobilities (in the range of 10^{-4} et 10^{-3} $cm^2s^{-1}V^{-1}$), this is under investigation for providing more informations to understant this behavior. We demonstrated that the thermal annealing has high impact on the film morphology and permit the formation of crystalline domains. Based on our results, the optimization of

OFET interfaces and processing conditions change the organic semiconductor film properties and thus the devices performances. This can be considered as an alternative route to perform high organic semiconducting materials with easy and low-cost methods, instead of looking forward to synthesize new novel materials.

In our work, we performed studies not only on high performing n-type small semiconductor molecules but also on ambipolar polymer (DPPT-TT) material with high electrical performances. Using DPPT-TT polymer as an ambipolar semiconductor, we fabricated organic photo-switching transistors and complementary inverters based on bi- and three-components integrating into DPPT-TT matrix two diarylethene molecules (DAE_tBu and or DAE_F) with completely reversible and selective photocontrollable drain currents. The reported voltage gain values were higher (in the range of 504 after UV irradiation) than those already recorded in literature (gain ~86). This work highlighted the possibility to provide new properties to the electronic devices by adding other molecules. This approach reliable for other ambipolar materials can be used in industrial manufacturing, reducing manufacturing costs. The realization of such high complementary organic inverters functioning with light as an optical remote motor controller, can be considered as new and novel approach opening new perspectives in optoelectronic research area.

References

1. Dimitrakopoulos, C. D.; Malenfant, P. R. L., Organic Thin Film Transistors for Large Area Electronics. *Adv. Mater.* **2002,** *14* (2), 99-117.
2. Tian, H. K.; Shi, J. W.; Yan, D. H.; Wang, L. X.; Geng, Y. H.; Wang, F. S., Naphthyl end-Capped Quarterthiophene: A Simple Organic Semiconductor with High Mobility and Air Stability. *Adv. Mater.* **2006,** *18* (16), 2149-2152.
3. Facchetti, A., Semiconductors for Organic Transistors. *Mater. Today* **2007,** *10* (3), 28-37.
4. Zaumseil, J.; Sirringhaus, H., Electron and Ambipolar Transport in Organic Field-Effect Transistors. *Chem. Rev.* **2007,** *107* (4), 1296-1323.
5. Murphy, A. R.; Frechet, J. M. J., Organic Semiconducting Oligomers for Use in Thin Film Transistors. *Chem. Rev.* **2007,** *107* (4), 1066-1096.
6. Mas-Torrent, M.; Rovira, C., Novel Small Molecules for Organic Field-Effect Transistors: Towards Processability and High Performance. *Chem. Soc. Rev.* **2008,** *37* (4), 827-838.
7. Würthner, F.; Stolte, M., Naphthalene and Perylene Diimides for Organic Transistors. *Chem. Commun.* **2011,** *47* (18), 5109-5115.
8. Klauk, H.; Halik, M.; Zschieschang, U.; Schmid, G.; Radlik, W.; Weber, W., High-Mobility Polymer Gate Dielectric Pentacene Thin Film Transistors. *J. Appl. Phys.* **2002,** *92* (9), 5259-5263.

9. Torsi, L.; Farinola, G. M.; Marinelli, F.; Tanese, M. C.; Omar, O. H.; Valli, L.; Babudri, F.; Palmisano, F.; Zambonin, P. G.; Naso, F., A Sensitivity-Enhanced Field-Effect Chiral Sensor. *Nat Mater* **2008,** *7* (5), 412-417.
10. Caboni, A.; Orgiu, E.; Barbaro, M.; Bonfiglio, A., Flexible Organic Thin-Film Transistors for pH Monitoring. *Ieee Sens J* **2009,** *9* (12), 1963-1970.
11. Arias, A. C.; MacKenzie, J. D.; McCulloch, I.; Rivnay, J.; Salleo, A., Materials and Applications for Large Area Electronics: Solution-Based Approaches. *Chem. Rev.* **2010,** *110* (1), 3-24.
12. Olivier, Y.; Niedzialek, D.; Lemaur, V.; Pisula, W.; Müllen, K.; Koldemir, U.; Reynolds, J. R.; Lazzaroni, R.; Cornil, J.; Beljonne, D., 25th Anniversary Article: High-Mobility Hole and Electron Transport Conjugated Polymers: How Structure Defines Function. *Adv. Mater.* **2014,** *26* (14), 2119-2136.
13. Caboni, A.; Orgiu, E.; Scavetta, E.; Barbaro, M.; Bonfiglio, A., Organic-Based Sensor for Chemical Detection in Aqueous Solution. *Appl Phys Lett* **2009,** *95* (12), 123304-123304-3.
14. Burroughes, J. H.; Bradley, D. D. C.; Brown, A. R.; Marks, R. N.; Mackay, K.; Friend, R. H.; Burn, P. L.; Holmes, A. B., Light-Emitting-Diodes Based on Conjugated Polymers. *Nature* **1990,** *347* (6293), 539-541.
15. Greenham, N. C.; Moratti, S. C.; Bradley, D. D. C.; Friend, R. H.; Holmes, A. B., Efficient Light-Emitting-Diodes Based on Polymers with High Electron-Affinities. *Nature* **1993,** *365* (6447), 628-630.
16. Brabec, C. J.; Cravino, A.; Meissner, D.; Sariciftci, N. S.; Fromherz, T.; Rispens, M. T.; Sanchez, L.; Hummelen, J. C., Origin of the Open Circuit Voltage of Plastic Solar Cells. *Adv. Funct. Mater.* **2001,** *11* (5), 374-380.
17. Baeg, K. J.; Kim, J.; Khim, D.; Caironi, M.; Kim, D. Y.; You, I. K.; Quinn, J. R.; Facchetti, A.; Noh, Y. Y., Charge Injection Engineering of Ambipolar Field-Effect Transistors for High-Performance Organic Complementary Circuits. *ACS Appl. Mater. Interfaces* **2011,** *3* (8), 3205-3214.
18. Singh, T. B.; Senkarabacak, P.; Sariciftci, N. S.; Tanda, A.; Lackner, C.; Hagelauer, R.; Horowitz, G., Organic inverter circuits employing ambipolar pentacene field-effect transistors. *Appl Phys Lett* **2006,** *89* (3).
19. He, Y. J.; Chen, H. Y.; Hou, J. H.; Li, Y. F., Indene-C-60 Bisadduct: A New Acceptor for High-Performance Polymer Solar Cells. *J Am Chem Soc* **2010,** *132* (4), 1377-1382.
20. Qi, Z.; Liao, X. X.; Zheng, J. C.; Di, C. A.; Gao, X. K.; Wang, J. Z., High-Performance n-Type Organic Thin-Film Phototransistors Based on a Core-Expanded Naphthalene Diimide. *Appl Phys Lett* **2013,** *103* (5), 053301-053301-4.
21. Kim, J.; Cho, S.; Kim, Y. H.; Park, S. K., Highly-Sensitive Solution-Processed 2,8-difluoro-5,11-bis(triethylsilylethynyl) Anthradithiophene (diF-TESADT) Phototransistors for Optical Sensing Applications. *Org. Electron.* **2014,** *15* (9), 2099-2106.
22. Kim, M.; Ha, H. J.; Yun, H. J.; You, I. K.; Baeg, K. J.; Kim, Y. H.; Ju, B. K., Flexible Organic Phototransistors Based on a Combination of Printing Methods. *Org. Electron.* **2014,** *15* (11), 2677-2684.
23. Guo, N.; Hu, W. D.; Liao, L.; Yip, S.; Ho, J. C.; Miao, J. S.; Zhang, Z.; Zou, J.; Jiang, T.; Wu, S. W.; Chen, X. S.; Lu, W., Anomalous and Highly Efficient InAs Nanowire Phototransistors Based on Majority Carrier Transport at Room Temperature. *Adv. Mater.* **2014,** *26* (48), 8203-8209.
24. Nollau, A.; Hoffmann, M.; Fritz, T.; Leo, K., Dissociation of Excitons in Organic Dye Layers of Perylene Derivatives. *Thin Solid Films* **2000,** *368* (1), 130-137.
25. Feng, Y.; Feng, W., Photo-Responsive Perylene Diimid–Azobenzene Dyad: Photochemistry and its Morphology Control by Self-Assembly. *Opt Mater* **2008,** *30* (6), 876-880.
26. Chen, Z. Y.; Lee, M. J.; Ashraf, R. S.; Gu, Y.; Albert-Seifried, S.; Nielsen, M. M.; Schroeder, B.; Anthopoulos, T. D.; Heeney, M.; McCulloch, I.; Sirringhaus, H., High-Performance Ambipolar Diketopyrrolopyrrole-Thieno 3,2-b thiophene Copolymer Field-Effect Transistors with Balanced Hole and Electron Mobilities. *Adv. Mater.* **2012,** *24* (5), 647-652.
27. Orgiu, E.; Crivillers, N.; Herder, M.; Grubert, L.; Patzel, M.; Frisch, J.; Pavlica, E.; Duong, D. T.; Bratina, G.; Salleo, A.; Koch, N.; Hecht, S.; Samori, P., Optically switchable transistor via energy-level phototuning in a bicomponent organic semiconductor. *Nat. Chem.* **2012,** *4* (8), 675-679.

28. El Gemayel, M.; Borjesson, K.; Herder, M.; Duong, D. T.; Hutchison, J. A.; Ruzie, C.; Schweicher, G.; Salleo, A.; Geerts, Y.; Hecht, S.; Orgiu, E.; Samori, P., Optically switchable transistors by simple incorporation of photochromic systems into small-molecule semiconducting matrices. *Nat. Commun.* **2015,** *6*.

29. Borjesson, K.; Herder, M.; Grubert, L.; Duong, D. T.; Salleo, A.; Hecht, S.; Orgiu, E.; Samori, P., Optically switchable transistors comprising a hybrid photochromic molecule/n-type organic active layer. *J Mater Chem C* **2015,** *3* (16), 4156-4161.

30. Khim, D. Y.; Han, H.; Baeg, K. J.; Kim, J. W.; Kwak, S. W.; Kim, D. Y.; Noh, Y. Y., Simple Bar-Coating Process for Large-Area, High-Performance Organic Field-Effect Transistors and Ambipolar Complementary Integrated Circuits. *Adv. Mater.* **2013,** *25* (31), 4302-4308.

Table of Contents

Chapter 7. High-performance phototransistors based on PDIF-CN2 solution-processed single fiber and multifiber assembly

Chapter 8. Organic-based inverters with photomodulable gain

Chapter 9. Conclusions and outlooks

Symbols and Abbreviations

AFM	Atomic force microscopy
Au	Gold
Ag	Silver
$CHCl_3$	Chloroform
C_i	Dielectric capacitance
Cr	Chrome
D	Drain electrode
DAE	Diarylethene
DAE_F	1,2-Bis(2-(3,5-bis(trifluoromethyl)phenyl)-5methylthiazol-4-yl)perfluorocyclopent-1-ene
DAE_tBu	(1,2-Bis(5-(3,5-di-tert-butylphenyl)-2-methylthiophen-3-yl)cyclopent-1-ene)
DPPT-TT	Poly(2,5-bis(2-octyldodecyl)-3-(5-(thieno[3,2-b]thiophen-2,5-yl)thiophen-2-yl)-6(thiophen-2,5-yl)pyrrolo[3,4-c]pyrrole-1,4(2H,5H)-dione
DOS	Density of states
Eq	Equation
ε	Permittivity
e^-	Electron
ε_0	Vacuum permittivity
E_C	Conduction band
E_V	Valance band
E_G	Band gap
E_F	Fermi level
ε_r	Relative permittivity
E_a	Activation energy
eV	Electronvolt
E_{vac}	Vacuum level
FET	Field-effect transistor
GIXD	Grazing incident X-ray diffraction
h^+	hole
HMDS	Hexamethyldisilazane
HOMO	Highest occupied molecular orbital
I_D	Drain-source current
IE	ionization energy
I_{GS}	Leakage current

ICBA	1’,1”,4’,4”tetrahydrodi[1,4]methanonaphthaleno[1,2:2’,3’,56,6:2”,3”][5,6]fullerene-C60
I_{light}	Drain current measured under light irradiation
I_{dark}	Drain current measured in dark
I_{ph}	Photocurrent
I_{off}	Lowest drain current value
I_{on}	Highest drain current value
k_B	boltzman constant
L	Channel length
LUMO	Lowest unoccupied molecular orbital
MTR	Multiple trap and release model
MS	Mott-Schottky
MO	Molecular orbital
NML	Noise margin low
NMH	Noise margin high
OTFT	Organic thin-film transistor
OTFT	Organic field-effect transistor
OPT	Organic phototransistors
OTS	Octadecyltrichlorosilane
P	Photoresponsivity
PDIF-CN2	N,N'-1H,1H-perfluorobutyldicyanoperylene-carboxydi-imide
PDI	Perylene di-imide
PMMA	Poly(methylmethacrylate)
Φ_B	work function
Φ_M	Injection barrier
R	Responsivity
R_{ch}	Channel resistance
R_c	Contact resistance
R_{bulk}	Resistance of the bulk
R_{TOT}	Total resistance
RF	Radio frequency
RPM	Rounds per minute
R_{rms}	Root-mean-squared roughness
SAM	Self-assembled monolayer
S-D	Source-drain electrodes
S	Subthreshold voltage
SE	Secondary eletrons
Si	Silicon
SiO_2	Silicon dioxide
T	Temperature
TLM	Transfer length method
UV	Ultraviolet

V_{DS}	Drain-source bias
V_{GS}	Gate-source bias
V_{Th}	Threshold voltage
$V_{Th,e}$	Threshold voltage for electrons
$V_{Th,h}$	Threshold voltage for holes
VRH	Variable range hopping
wt %	Total weight %
W	Channel width
XRD	X-ray diffraction
2D-GIXD	Two dimentional grazing incident X-Ray diffraction
α	Tilt angle
λ	Wavelength
μ	Field effect mobility
μ_{eff}	Effective mobility
μ_p	hole field-effect mobility
μ_n	Electron field-effect mobility

Chapter 1. Introduction

1.1. Background

The transistor is the key building block for several electronic devices used in our daily life. The first field-effect transistor constituted of copper-sulfide semiconductor and three-electrodes was made in 1921 by Julies E.[1] The first microprocessor chip (the 4004), has been manufactured in 1971 by Intel using 10 µm process technology, it had a clock speed of 108 kHz and contained 2300 transistors. From that time, Intel has manufactured chips on smaller wafers using hundreds of millions of transistors. They developed prototype transistors based on conventional silicon used in different Intel's logic product, which show promise for future high-speed and very low-power logic applications. In modern technology, transistors are integrated in cell phones, smart cards, and computers, etc…Therefore, silicon-based electronics have multiple limitations, that can be attributed to the high cost wafer processing and manufacturing equipment, which required clean room environment. In contrast, the cost reduction of organic electronic manufacturing and fabrication facilities open new perspectives to the field of electronics.

In 1959, the physicist Richard Feynman predicted the promising future of nanoscale organic electronics, his prediction had been confirmed over the last 30 years. During that period, the concept of organic electronics has been proved from the fundamental science and applications points of view. In 1977, Alan Heeger, MacDiarmid and Hideki Shirakawa working in the field of organic electronics, discovered oxidized iodine-doped polyacetylene. Later in 2000, they have been awarded the Nobel Prize in chemistry for their great contribution in conductive conjugated polymers.

Organic electronic is an attractive field for scientists in physical chemistry. Relevant research activities have been achieved since the discovery of electronic conduction property of π-conjugated polymers and small molecules. This new field is considered as an exciting and encouraging domain, which opens new perspectives to overcome inorganic based electronics technology limitations. The exploitation of organic compounds properties in electronic devices offers multiple advantages for a variety of flexible and low-cost applications. They can be self-assembled *via* intermolecular interactions on different and flexible supports forming high packing structures at the nanometric scale. The charge transport within an organic material can be tuned by varying the semiconductor structural

properties *via* organic synthesis. Another important advantage comparing with the inorganic based devices, is the capacity to build and design new devices with new functionalities combining organic semiconductors with other organic molecules having different chemical and physical properties. These advantages serve as high motivations for scientists to investigate in organic electronics and optoelectronics field.

Organic semiconducting devices, such as organic field-effect transistor, have gained considerable research interest in recent years. They are becoming attractive for various industrial applications, due to their great promise for low-cost, large area, and flexible electronics integrated in logic circuits (CI)[2-3] for memory chips, smart cards and sensors.[4-7] A number of organic materials have been successfully commercialized in different electronic applications, including liquid crystal displays (LCD), radiofrequency identification (RFID) tags,[8-9] light emitting diodes, [10-11] and photovoltaics [12]. More applications continue to evolve as the organic technology develops. Several electronic companies, such as Solvay, Sumitomo, BASF, DuPont, Merck, and Ciba, etc…are now engaged in research developments focused on organic electronic applications. Ambipolar organic semiconductors capable to transport negative and positive charge carriers (electrons and holes) are promising for the implementation of organic complementary inverters in logic circuits. [13-14]

1.2. Thesis objectives and motivations

The construction of electronic and optoelectronic devices based on organic materials became an alternative approach for conventional technologies funded on silicon integrated devices. The growth of organic electronics industry is greatly accelerated in the recent years owing to the rapid improvements in organic materials capacity to form excellent performing devices, and the availability of state-of-the-art materials that can compete with silicon based devices. For instance, our big challenge and real attempt as researcher scientists in this field is to optimize the different properties of organic semiconductor material from its conception to film deposition. The former can be realized by modifying several molecular parameters during synthesis, such as molecular weight, side-chain groups, and length, that affect the molecular solubility. Other key parameter to improve organic electronic devices efficiency is the interfaces engineering of both metal-semiconductor and semiconductor-dielectric. These parameters have a great influence in molecular self-organization at the devices surface and charge injection.

The challenge in the nowadays research activities in molecular electronics is to use organic materials as active component in electronic devices, thereby replacing silicon and other inorganic semiconductors. The several advantages discussed above are the real motivation for this replacement attempt. Above all, a bonus can be expected in terms of reduced cost, mechanical flexibility, and

large-area capability of organic thin film based electronics. Over the last 30 years, a great progress has been achieved. However, the optimization of the properties of (macro)molecular components through lab work is required towards a reliable technology. The present thesis is focused on the multiscale study and control over key physical and chemical properties of specific (macro)molecules and their use as active components to fabricate field-effect transistors.

The electronic technology has evolved after employing solution-processable materials, which reduces the deposition techniques cost, by using simple processes like spin coating, drop-casting, inject printing. New multifunctional components can be fabricated using solution processing methods, and combining organic small molecules and polymers semiconductors with other molecular moieties; having different chemical and electrical properties such as photochromic switches in the aim of making photo-tuned switching devices.

In this thesis, we have focused our attention on the investigation of (i) charge carrier transport across organic bi and three-component materials acting as the active layers for organic transistors integrated in complementary logic circuits, and (ii) the light-sensitivity properties of crystalline structures produced from an air n-type small molecule. Upon optimizing the order at the supramolecular level in single and multi-component materials, charge transport properties of different studied organic semiconductors (n-type and ambipolar) have been correlated with their optical, morphological and structural characterization.

However, organic electronics has some limitations that need to be improved, including the limited stability of the components in air and low performances. The cooperative efforts during last years, between academia research in laboratories, industry companies and government institutions are vital to the development of a novel organic material with good properties, as well as the manufacturing fabrication, to overcome organic electronics limitations. I believe that with potential efforts, organic electronics will provide the next generation of electronic devices and will take important directions in research in near future.

1.3. Structure of the thesis

The thesis work is divided into the following nine chapters:

Chapter 1 briefly introduces the molecular electronic field and history, and describe the thesis work motivations in both fundamental science and technological applications points of view.

Chapter 2 gives a basic-background on the physics and chemistry of organic materials. It offers an overview of some of the current models that have been reported to describe the charge transport mechanisms in organic materials. Expressing the major advances that have recently been achieved in the description of the parameters impacting charge transport in organic semiconductors to achieve significant improvements.

Chapter 3 presents a background overview of organic electronic technology including organic field-effect transistors (OFETs), organic phototransistors (OPTs) and organic complementary inverters. It provides their fundamental properties, basic operation and important devices-extracted parameters. It also discusses the factors and different features that directly affect the devices performances.

Chapter 4 presents an overview on molecular properties, chemical and physical characteristics of organic semiconductors and molecules encompassed and studied in this thesis.

Chapter 5 briefly describes the main experimental techniques and different instruments used to evaluate and perform organic-based devices characteristics. More details are provided in this chapter on the device fabrication, materials preparation and deposition methods.

Chapter 6 reports on the charge transport properties of ambipolar-based field-effect transistors. Demonstrating the effect of thermal annealing, silicon dioxide surface treatments with self-assembled monolayers on the OFETs electrical, optical and morphological characteristics. Chapter studies are focused on spin-coated thin films of a fullerene derivative, i.e. the indene-C60 bis-adduct (ICBA).

Chapter 7 focuses on the fabrication of organic phototransistors based on either single or multifibers integrated in three-terminal devices. These self-assembled fibers have been produced by solvent-induced precipitation of an air stable and solution-processable perylene di-imide derivative, i.e., PDIF-CN2. The optoelectronic properties of these devices were compared to devices incorporating more disordered spin-coated PDIF-CN2 thin-films.

Chapter 8 presents for the first-time high gain light-induced complementary inverters based on one single ambipolar layer. In this chapter, light-induced single, bi-and three-component based field-effect and complementary inverters were optimized due to the light-transformation of inserted diarylethene systems into an ambipolar polymer matrix accompanied by photo-isomerization. It also shows that multi-component based photo-switched transistors and complementary inverters can be optically controlled via irradiation with UV and Visible light irradiation.

Chapter 9 summarizes the main conclusion of the thesis work and gives an overview of future outlooks.

1.4. References

1. Lilienfeld, J. E., Method and Apparatus for Controlling Electric Currents. *U. S. Patent No. 1,745,175* **1930**.

2. Klauk, H.; Halik, M.; Zschieschang, U.; Schmid, G.; Radlik, W.; Weber, W., High-Mobility Polymer Gate Dielectric Pentacene Thin Film Transistors. *J. Appl. Phys.* **2002,** *92* (9), 5259-5263.

3. Torsi, L.; Farinola, G. M.; Marinelli, F.; Tanese, M. C.; Omar, O. H.; Valli, L.; Babudri, F.; Palmisano, F.; Zambonin, P. G.; Naso, F., A Sensitivity-Enhanced Field-Effect Chiral Sensor. *Nat. Mater.* **2008,** *7* (5), 412-417.

4. Caboni, A.; Orgiu, E.; Scavetta, E.; Barbaro, M.; Bonfiglio, A., Organic-Based Sensor for Chemical Detection in Aqueous Solution. *Appl. Phys. Lett.* **2009,** *95* (12), 123304-123304-3.

5. Caboni, A.; Orgiu, E.; Barbaro, M.; Bonfiglio, A., Flexible Organic Thin-Film Transistors for pH Monitoring. *Ieee Sens. J.* **2009,** *9* (12), 1963-1970.

6. Arias, A. C.; MacKenzie, J. D.; McCulloch, I.; Rivnay, J.; Salleo, A., Materials and Applications for Large Area Electronics: Solution-Based Approaches. *Chem. Rev.* **2010,** *110* (1), 3-24.

7. Olivier, Y.; Niedzialek, D.; Lemaur, V.; Pisula, W.; Müllen, K.; Koldemir, U.; Reynolds, J. R.; Lazzaroni, R.; Cornil, J.; Beljonne, D., 25th Anniversary Article: High-Mobility Hole and Electron Transport Conjugated Polymers: How Structure Defines Function. *Adv. Mater.* **2014,** *26* (14), 2119-2136.

8. Mas-Torrent, M.; Rovira, C., Novel Small Molecules for Organic Field-Effect Transistors: Towards Processability and High Performance. *Chem. Soc. Rev.* **2008,** *37* (4), 827-838.

9. Würthner, F.; Stolte, M., Naphthalene and Perylene Diimides for Organic Transistors. *Chem. Commun.* **2011,** *47* (18), 5109-5115.

10. Burroughes, J. H.; Bradley, D. D. C.; Brown, A. R.; Marks, R. N.; Mackay, K.; Friend, R. H.; Burn, P. L.; Holmes, A. B., Light-Emitting-Diodes Based on Conjugated Polymers. *Nature* **1990,** *347* (6293), 539-541.

11. Greenham, N. C.; Moratti, S. C.; Bradley, D. D. C.; Friend, R. H.; Holmes, A. B., Efficient Light-Emitting-Diodes Based on Polymers with High Electron-Affinities. *Nature* **1993,** *365* (6447), 628-630.

12. Brabec, C. J.; Cravino, A.; Meissner, D.; Sariciftci, N. S.; Fromherz, T.; Rispens, M. T.; Sanchez, L.; Hummelen, J. C., Origin of the Open Circuit Voltage of Plastic Solar Cells. *Adv. Funct. Mater.* **2001,** *11* (5), 374-380.

13. Baeg, K. J.; Kim, J.; Khim, D.; Caironi, M.; Kim, D. Y.; You, I. K.; Quinn, J. R.; Facchetti, A.; Noh, Y. Y., Charge Injection Engineering of Ambipolar Field-Effect Transistors for High-Performance Organic Complementary Circuits. *ACS Appl. Mater. Interfaces* **2011,** *3* (8), 3205-3214.

14. Singh, T. B.; Senkarabacak, P.; Sariciftci, N. S.; Tanda, A.; Lackner, C.; Hagelauer, R.; Horowitz, G., Organic inverter circuits employing ambipolar pentacene field-effect transistors. *Appl. Phys. Lett.* **2006,** *89* (3).

Chapter 2. Organic materials: Theoretical background

Introduction

The invention of the transistor in 1947 by John Bardeen, William Shockley and Walter Brattain represented a real technological revolution which was recognized with the Nobel Prize in Physics in 1956. The vast majority of transistors have been mostly based on inorganic semiconductors and, in particular, on silicon. However, due to technological limitations associated with the use of silicon, such as the high-power dissipation, high-cost manufacturing and processing fabrications, and non-mechanical flexibility. Substantial efforts are currently devoted to developing organic semiconductors that offer the benefits that they can be deposited on glass, paper or plastic substrates.[1-2]The organic semiconductors are characterized by ability to be deposited at low temperature with low-cost solution processable methods, which make them effective and attractive for different electronic commercial applications.[3] This chapter provides an introduction to the organic semiconductors describing briefly their theoretical background and giving some details on the chemical bonding, the crystalline nature, and physical properties of organic semiconducting materials offering an overview on the most important and interesting charge transport models.

Depending on their electrical conductivity, solid-state materials are composed into three main groups: insulators, semiconductors and conductors. Conductors, or metals, have high conductivities of $\sigma = (10^{7} – 10^{6})$ S m^{-1}, semiconductors show intermediate conductivities of $\sigma = (10^{-8} – 10^{6})$ S m^{-1}, and insulators have low conductivities of $\sigma = (10^{-8} – 10^{-16})$ S m^{-1}. The reason for such quite different conductivity behavior of metals, semiconductors and insulators is the distribution of energy bands. In a metal the conduction and valence bands overlap, thus electrons can easily pass into the conduction band. This means that the number density of free charge carriers is very high. In semiconductors and insulators, there is a gap between the valence band and conduction band. For semiconductors, the valence band is completely full and charge carriers are not mobile. To become free to move charge carriers must first be activated. The activation requires some energy, this energy can be provided, for example, by thermal excitation, then, electrons can jump the gap into the conduction band. However, the number of

free electrons in the conduction band is still much less than that of a conductor. In an insulator, the energy gap (E_G) is much larger, thus a large amount of energy would be needed for electrons to jump into the conduction band. For this reason, there are far fewer electrons in the conduction band of an insulator than that of a semiconductor (see **Figure 2.1**).

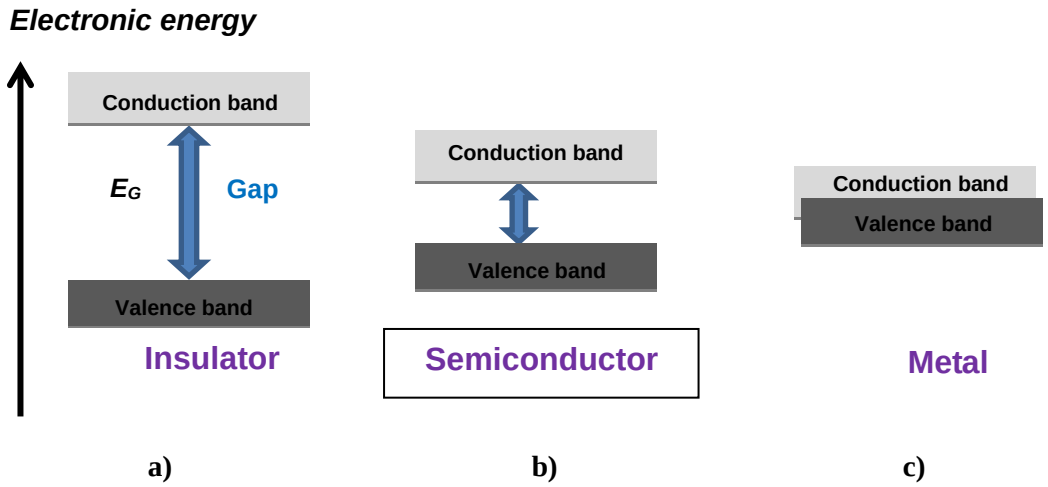

Figure 2.1. Energy diagram for **a)** an insulator metal, **b)** semiconductor and **c)** metal.

2.1. Organic semiconductors

2.1.1. Background

Organic molecules contain carbon atoms associated with hydrogen and other heteroatoms like oxygen, nitrogen, sulfur…etc. These molecules are constructed by a number of single, double, or triple bonds, arranged together forming the molecular structure. Organic semiconductors are organic molecules with a conjugated system, their backbone can be constituted with carbon atoms and heteroatoms like Sulfur. There are two main classes of organic semiconductors: low-molecular weight (small molecules) and polymers. Both have in common a conjugated π-electron system formed by the p_z orbitals of sp^2-hybridized C atoms in the molecules (see **Figure 2.2**).

Devices based on semiconducting organic (non-metallic) molecules are of interest for large area electronics, owing to their fundamental charge transport properties, that can be exploited in molecular solids.[4] Because of this reason, they have been the focus of intense investigation during the past 50 years.[5] The solid-state of these materials is based on molecules/polymer chains interacting through non-covalent (weak) bonds, principally of van der Waals and dipole-dipole type.[6]

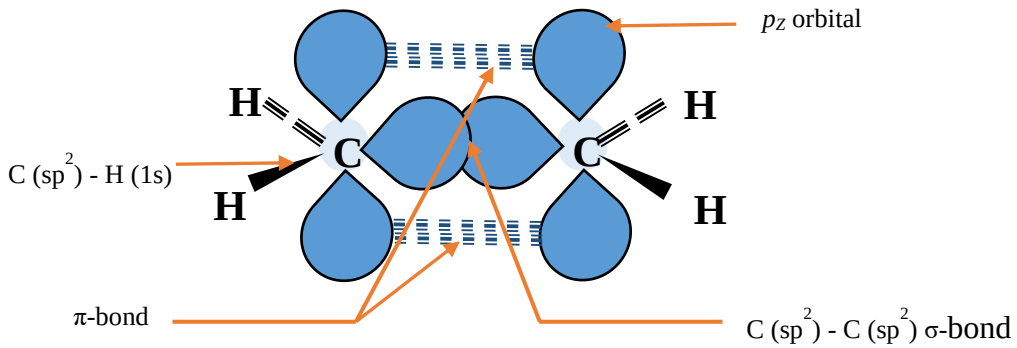

Figure 2.2. Carbon-Carbon single bond C(sp^2)-C(sp^2) (σ) and double bond in ethylene CH_2=CH_2. The ethylene double bond consists of a σ-bond and a π-bond. The π-bond is resulted from overlap of two p_z un-hybridized orbitals.

Carbon has an atomic number of six, its electron configuration is $1s^2$, $2s^2$, $2p^2$. The inner shell $1s^2$ is filled with two electrons, two other electrons are distributed in $2s^2$ orbital and the other rest two are in p orbital. The last four orbitals (in $2s^2$ and $2p^2$) can be involved in hybridization that explained by the construction of hybrid orbitals by linear combination of both wave functions of the 2s and 2p orbitals to form excited orbitals called sp. Orbitals combinations lead to different hybridization i.e., sp, sp^2 and sp^3, for example, when three groups bonded to a central carbon atom, the combination of the orbital s and two p orbitals (p_x and p_y) constructs three sp^2 hybrids, each hybrid orbital is 33.3% s and 66.7% p. Polyenes conjugated systems (C_nH_{n+2}) contain conjugated double bonds, alternating single and double bonds. They are interested compounds for molecular electronics. Two sp^2 hybrids on each carbon bond form with the neighboring carbon atoms single bonds C(sp^2)-C(sp^2), a third sp^2 hybrid on each carbon bond with hydrogen atom forming σ-bond, leaving a free p_z un-hybridized orbital on each carbon. The two p_z orbitals lie perpendicular to the carbon atoms plane, forming a *pi* or π-bond (see **Figure 2.3**). In comparison to the single bond (σ) constituting the backbone of the molecules, π bonding is relatively weaker.

Usually, electrons forming π-bonds are localized. However, in semiconductor small molecules and polymers, the presence of conjugation with alternation of single and double bonds in the backbone gives rise to an overlap of their atomics orbitals. The intermolecular interactions in conjugated structures between the atoms yield to a splitting of the carbon $2p_z$ orbitals and thus to a π electrons delocalization. π electrons can move from one bond to the neighboring one and over the whole molecule as illustrated in **Figure 2.3** showed various representation of the hexatriene as an example of polyenes systems and benzene molecule as an example of aromatic conjugated systems.[7]

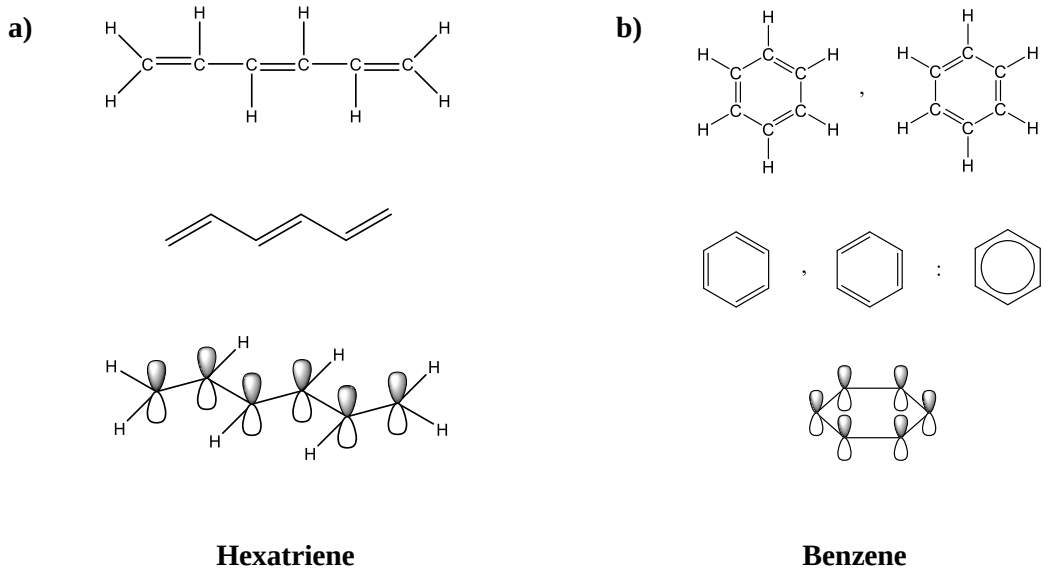

Figure 2.3. Different structures representations because of the π-electrons delocalization of the a) hexatriene and the b) benzene molecule used as examples for linear hydrocarbon molecules and aromatic conjugated systems respectively.

According to the molecular orbital (MO) theory and the linear combination of atomic orbitals (LCAO) concept, the system of alternating double and single bonds in the conjugated backbone and superposition of all the molecular orbitals gives rise to a separation of bonding and anti-bonding states. Resulting in the formation of valance and conduction bond respectively, and an energy gap that spatially separate them.,[8] as illustrated in **Figure 2.4**. HOMO and LUMO orbitals are analogous to the valance and conduction bands in inorganic semiconductors. The highest occupied molecular orbital (HOMO) is filled with electrons, and corresponds to the bonding state of the π-orbitals. However, the LUMO orbital is the lowest unoccupied molecular orbital (empty anti-bonding (π*)). The difference in energy between the HOMO and LUMO levels corresponds to the band-gap energy (E_G), which depends on molecular structure, and generally decreases with the number of repeat units in the molecular chain.

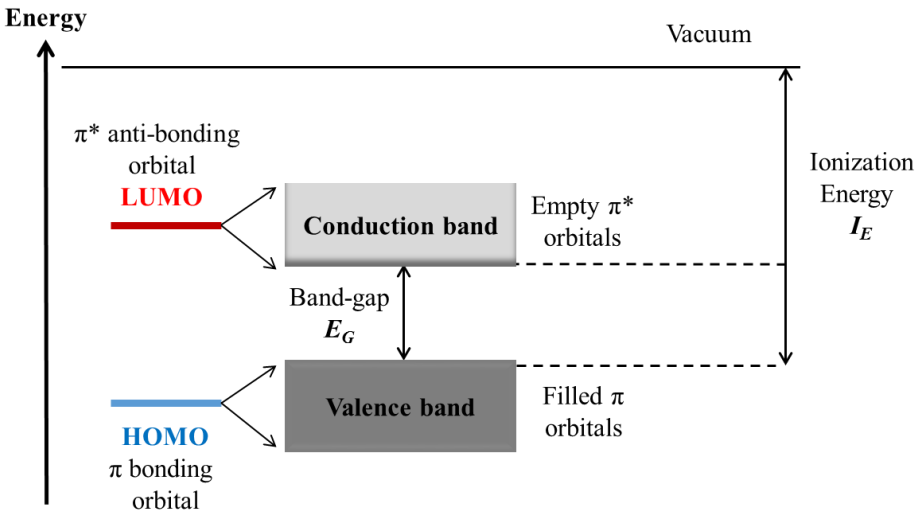

Figure 2.4. Representative energy band diagram of an organic semiconductor band structure of bonding and anti-bonding states separated by a band-gap energy (E_G) (reproduced from[8]).

The organic materials are classified based on the nature of charge carriers capable to be transferred within the π-conjugated system. Depending on the chemical composition of the backbone, the organic semiconducting materials with strongly withdrawing groups such as fluorinated groups can easily transport electrons (e^-) and called n-type semiconductors. While, those with more electronegative systems are holes (positive charges h^+) transporting organic semiconductors called p-type semiconductors.[9] In n-type semiconductors, the majority of carriers are electrons and holes are the minority carriers, which means that they primarily transport electrons rather than holes. Most of the known organic materials exhibit p-type characteristics and tend to conduct holes better than electrons, this means that holes are more easily injected than electrons.[10] Comparatively, there are considerably fewer reports on n-type organic semiconductors[11] with good characteristics.[12-13] n-type semiconductors are characterized by poorer air stability, limited solubility and lower field-effect mobility compared to p-type semiconductors.[14] The development in devices based on electron transporting semiconductors is still far from the performance already achieved with p-type organic materials due to the fact that charge transport in n-channel semiconductors is degraded by air, which acts as electron traps together with the dielectric surface trapping sites. For that reason, most of the studied organic materials have tendency to conduct holes better than electrons. In an n-type semiconductor, the Fermi level is larger than that of the intrinsic semiconductor and lies closer to the conduction band. However, for p-type semiconductors the Fermi level is below the intrinsic Fermi level and closer to the valence band than the conduction band[15-16] as represented in **Figure 2.5**.

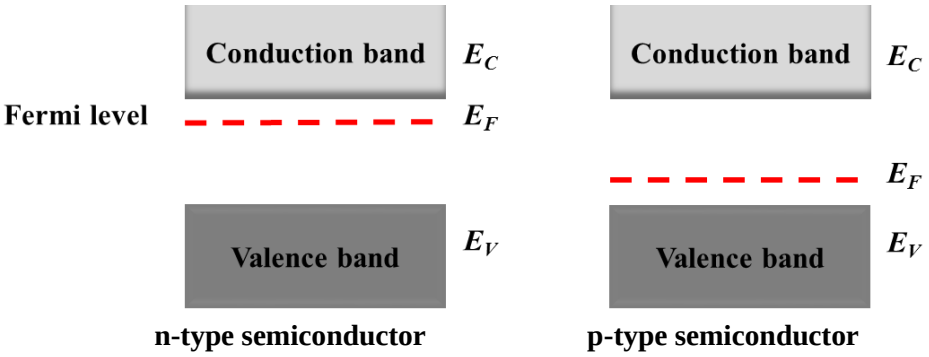

Figure 2.5. Representative energy diagram for n-type and p-type semiconductors.

2.1.1.1. Small molecules

As mentioned before, the studied organic semiconductors are divided on two families, polymers and small conjugated molecules including oligomers. Depending on the material, semiconductivity occurs in single molecules, short and long chains. Small molecule semiconductors are monodispersed. They include pentacene, anthracene and rubrene, as well as larger molecules such as fullerene derivatives. Typically, organic small molecules are low molecular mass. They exhibit high field-effect mobility (the mobility is the drift velocity which characterizes how quickly the charge carriers move along the semiconductor channel under the field-effect). The high mobility is attributed to the high molecular packing of small molecule and their ability to form well-ordered and crystalline thin films on device surfaces. The most studied p-type small molecule semiconductor is pentacene from acenes family, due to its chemical and thermal stability as well as good hole mobility compared to other organic semiconductor materials. Hole mobility of vacuum deposited pentacene based TFTs devices reported in literature are in the range 0.5-1.5 $cm^2V^{-1}s^{-1}$ and as high as 5 $cm^2V^{-1}s^{-1}$[12, 17] and on/off current ratio (which is the ratio between the highest and lowest measured drain current I_D) of such devices ranging from 10^5 to 10^8 due to their polycrystalline films. Most of n-type semiconductor materials are deposited by vacuum evaporation. However, there is a great attention in developing soluble n-type molecules with improved processability and good mobilities for low-cost electronics. Different other acene and thiophene derivative reported for thin films provide mobilities of more than 1 $cm^2V^{-1}s^{-1}$, 1.1 $cm^2V^{-1}s^{-1}$ for alkyl-substituted oligothiophene[18] and pentacene.[19] Other promising organic semiconductors based on p-extended heteroarenes and tetrathiafulvalene derivatives have resulted in high mobilities between 2.1 and 2.9 $cm^2V^{-1}s^{-1}$.[20] Fullerene,[21-24] naphthalene[25] and perylene diimide[26-27] derivatives are good acceptor molecules and have been extensively studied as n-type semiconductors, they are considered from the most performing n-type semiconductors exhibiting high electron mobility exceeding 0.01 $cm^2V^{-1}s^{-1}$. The highest mobility is around 6 $cm^2V^{-1}s^{-1}$ reported on epitaxy epitaxy-grown fullerene thin films naphthalenetetracarboxylic diimide with fluorinated alkyl chains (NDI-CF).[25] Which is the first air-stable n-channel OFET that was successfully integrated with

solution-deposited p-channel OFET providing an organic complementary inverter circuit from liquid phase deposition. During the last years, strong efforts have been devoted to synthesize high performing air -stable n-type semiconductor materials desirable for electronic devices. In particular, semiconductors with a good processibility and solvents solubility, which strongly depends on side chain groups. Different examples on p- and n-type small molecules organic semiconductors are presented in **Figure 2.6**.

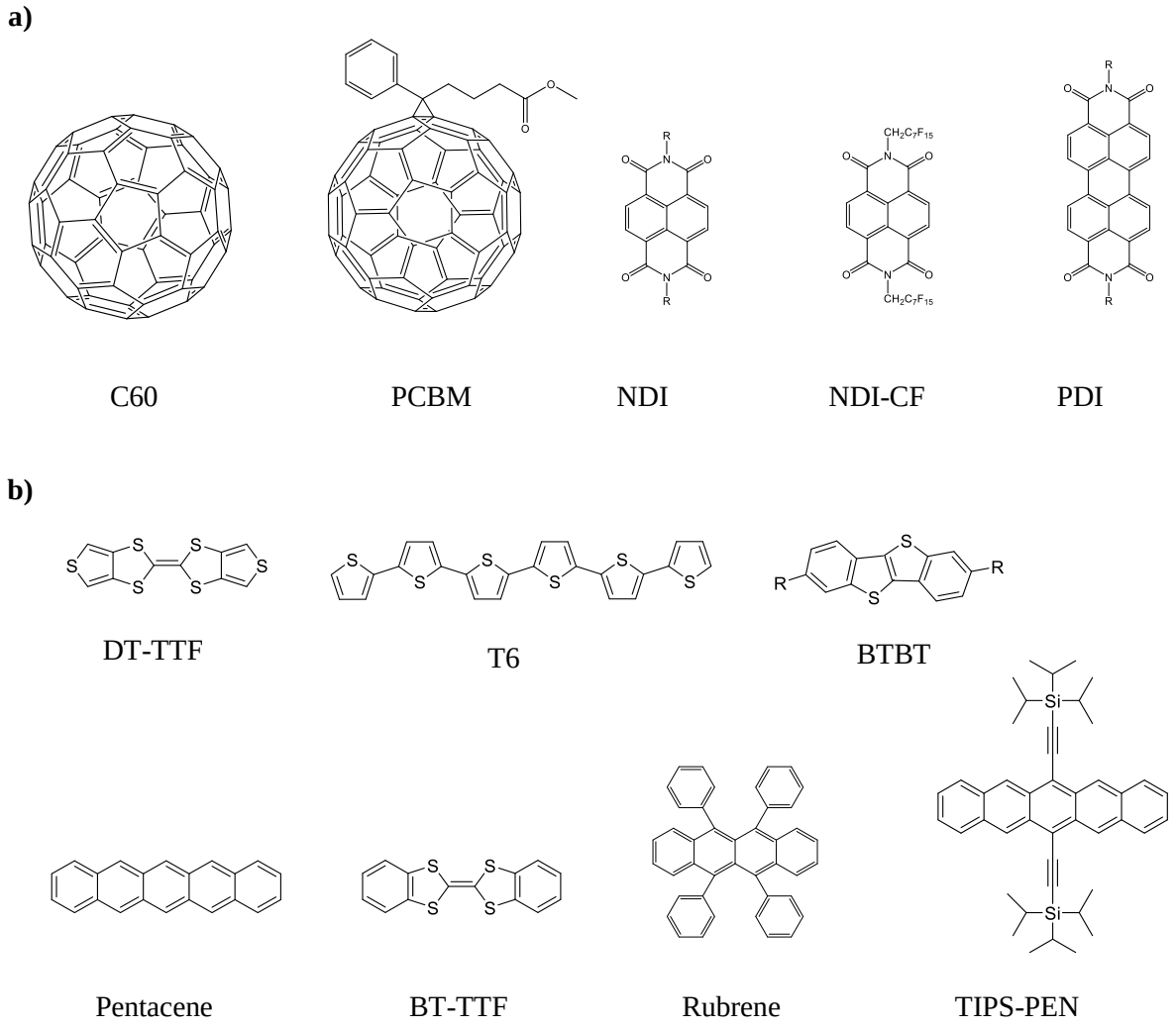

Figure 2.6. Chemical structures of some organic **a)** n-type and **b)** p-type semiconductors.

2.1.1.2. Polymers

Organic conjugated polymers are polydispersed molecules with long molecular chains and high molecular mass (> 50 carbon atoms) made of monomer repeating units and consist of a conductive backbone with alternated single, double, and triple bonds giving rise to an overlapping of their atomic orbitals. The delocalization of π-bond is responsible of charge transport within the polymer. The alkyl side chains determine the polymer solubility to ensure solution processing deposition methods. The polymer conjugation length and rotational freedom affect the semiconductor polymer conductivity and environmental sensitivity.[28] Typically, organic polymers are more soluble than organic small conjugated molecules. The polymer disordered matrix and its difficulty to form crystalline and well-ordered films (they form small crystalline domains) influence the charge transport performance. Their polydispersity affect the defects formation and limits the charge transport resulting in low field-effect mobilities compared to that of crystalline vacuum evaporated small molecules. Most polymeric materials comprise regions that are both crystalline and amorphous with defects. One of the most studied p-type conjugated polymers is poly(3-hexylthiophene) (P3HT), which exhibited OFET mobilities ranging from 0.1 and 1.2 $cm^2V^{-1}s^{-1}$.[29] Poly(2,5-bis(3-alkylthiophen-2yl)thieno[3,2-b]thiophene) (PBTTT) is another high performing p-type polymer exhibited a mobility of up to 0.7 $cm^2V^{-1}s^{-1}$.[30]

Although some polymer semiconductors have been used as electron transporting components in polymer electronic devices for a long time,[30-31] the first demonstration of n-channel polymer field-effect transistors was only reported in the early 2000s.[32-33] The polymer semiconductors are poly[(7-oxo-7,10H-benz[de]imidazo[4′,5′:5,6]benzimidazo[2,1-a]isoquinoline-3,4:10,11-tetrayl)-10-carbonyl] (BBL) and poly(6,9-dihydro-6,9-dioxobisbenzimidazo[2,1-b:1′,2′-j]benzo[lmn][3, 8]phenanthroline-3,12-diyl) (BBB).[32] BBL exhibited high electron mobility (∼0.1 $cm^2V^{-1}s^{-1}$) in air, comparable to the hole mobility of P3HT. Complementary inverter circuits based on BBL as n-channel transistor and P3HT as p-channel have been successfully demonstrated.[34] In the recent years, many researchers have tried to design and synthesize new n-type polymers that have suitable functionalities and a sufficient solubility in selective organic solvents. In 2007, another breakthrough in n-type polymer semiconductors was reported by exploiting the donor–acceptor approach based on fused thiophenes and a PDI or NDI units which is a suitable for electron transport as PDI[35] and NDI are excellent n-type small molecules. Copolymerization of PDI and NDI[36] with various thiophene units resulted in different polymer semiconductors.[37] Among these polymers, poly{[N,N′-bis(2octyldodecyl)-3,4,9,10-perylenedicarboximide(1,7&1,6)diyl]alt5,5′(2,2′bithiophene)} called P(PDI2OD-T2) is one of the most studied n-type polymers, with an electron mobility of 2×10^{-3} $cm^2V^{-1}s^{-1}$ in vacuum.[38] Different examples on p- and n-type polymer semiconductors are presented in **Figure 2.7**.

a)

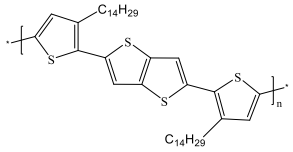

PBTTT

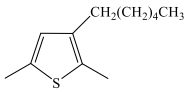

P3HT

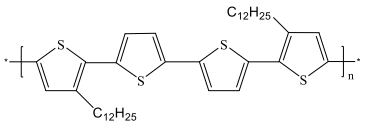

PQT

b)

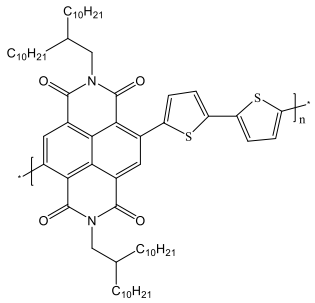

P(NDI2OD-T2)

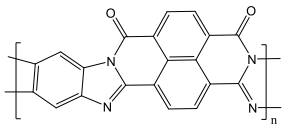

BBL

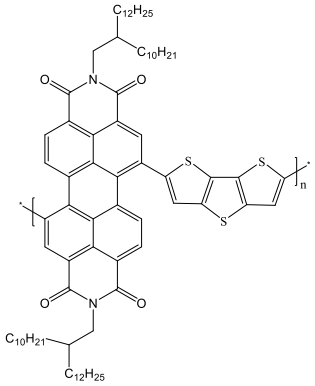

PPDI-DTT

Figure 2.7. Chemical structures of some organic **a)** p-type and **b)** n-type polymer semiconductors.

2.2. Charge transport models in organic semiconductors

The conduction mechanism in organic semiconductors is found to be rather different than those for their inorganic counterpart. This is especially due to the weak intermolecular forces such as Van der Waals interactions which hold together the molecules forming a "molecular solids". Conversely, in inorganic semiconductors like those containing Si or Ge, the atoms are bonded with strong covalent bonds making an ordered crystalline lattice permitting to the charge to take place via delocalized states.[39] In view of that, true band-like transport is rarely observed in organic semiconductors as it happens in silicon or graphene.[40] The charge transport and mobility in organic semiconductors are lower than that of inorganic crystals because of the large distance and poor contacts between different crystalline domains, and the presence of defects in amorphous disordered phases.[5, 28]. Therefore, molecular ordering and alignment of the conjugated segments in the thin film based on organic semiconductors plays an important role in attaining efficient charge transport.[41] The

polaronic and disorder charge-transport mechanisms have been already discussed and reviewed in more details in literature.[42-45] Here, we simply outline the main characteristics of the most popular models. In this section, we will present a brief overview of the different models for the transport of field-induced carriers on molecular surfaces.

2.2.1. Polaron model

Inorganic semiconductors can usually be well described via one-electron (band structure) approaches, while organic semiconductors require theories and approaches that are valid for arbitrary strengths of electronic coupling that takes both electron-electron and local electron-phonon interactions into account over temperature. The charge carrier created in a conjugated solid polarizes the intramolecular vibration modes of the molecule on which it is located as well as dipole active modes of the neighboring molecules, thus forming an extended ionic state. This refers to the electronic polarization effect due to the delocalization of the charge on a molecular site, the charge move associated with the induced polarization cloud. This entity is no a naked charge, but a 'dressed' charge and the resulted quasi-particle (the charge associated with its cloud) is called polaron.[46] The polaron stability is strongly related to two factors (i) the residence time (τ_{res}) corresponds to the average time a charge will reside on a molecule (ii) the electronic polarization time (τ_{el}) is the needed time for the polarization cloud to form around the charge. An order of magnitude can be estimated for both residence and electronic polarization time using Heisenberg's uncertainty principle by the following formula:

$$\tau \leq (\hbar/\Delta E)$$

Where ΔE is a characteristic energy. Concerning the residence time (τ_{res}), the pertinent energy is the width W of the allowed band, typically 0.1 eV in an organic semiconductor and 10 eV in an inorganic semiconductor, which gives a residence time of 10^{-14} s for the former and 10^{-16} s for the latter. For the electronic polarization time (τ_{el}), the corresponding energy is that of an electron transition i.e., the energy gap (around 1 eV) and the time τ_{el} is of the order of 10^{-15} s for both organic and inorganic semiconductors. In inorganic semiconductors, the electrons and holes move so fast and does not lead enough time to form electronic polaron. Whereas, in organic molecular solids, the electronic polaron has enough time to form, and the energy levels of the charged molecule are shifted with respect to that of a natural molecule. The most detailed transport theories are those based on elaborations of the one dimensional Holstein molecular model including band theory[47] and the polaron effective mass approach.[48] The charge mobility depends on the electron-phonon coupling. In the case of weak local electron-phonon couplings, the mobility is dominated by tunneling and displays a bandlike temperature dependence ($\mu \sim T\text{-}n$, where $n > 0$) in the whole range of temperature.[49] For

intermediate couplings, the mobility is bandlike at low temperatures; however, due to an increase in hopping contributions, it exhibits a weaker temperature dependence at high temperatures. For strong local couplings, three distinct temperature regimes:

(i) At low temperature, the mobility is bandlike dominant.

(ii) As temperature increases, the hopping starts to dominate.

(iii) When system achieves very high temperatures, the thermal energy becomes great enough to dissociate the polaron, and the residual electron is scattered by thermal phonons. As a consequence, the mobility decreases again with temperature.

2.2.2. Hopping model

Charge carries are known to move by tunneling from localized states (see figure 2.8), commonly called "hopping".[50]. This transport mechanism is phonon assisted and thermally activated.[50-51]

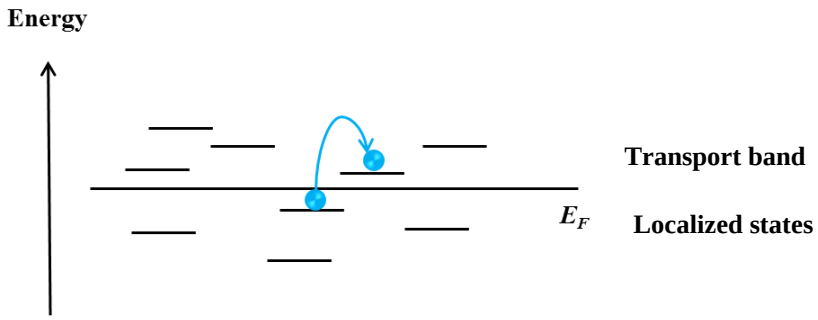

Figure 2.8. Schematic representation of charge carriers hopping transport from localized states in disordered semiconductor systems.

Hopping transport can be defined as the transfer of holes and electrons along (i) conjugated molecular chain (i.e., intramolecular transport) because of the π orbitals overlap, (ii) from one molecule to the neighboring one (between molecules) which called intermolecular transport and it is more difficult. (iii) The last type of charge transfer in organic materials is called inter-grain, is the hopping of carriers in between crystalline domains, the three-different hopping charge transfer types are illustrated in **Figure 2.9**.

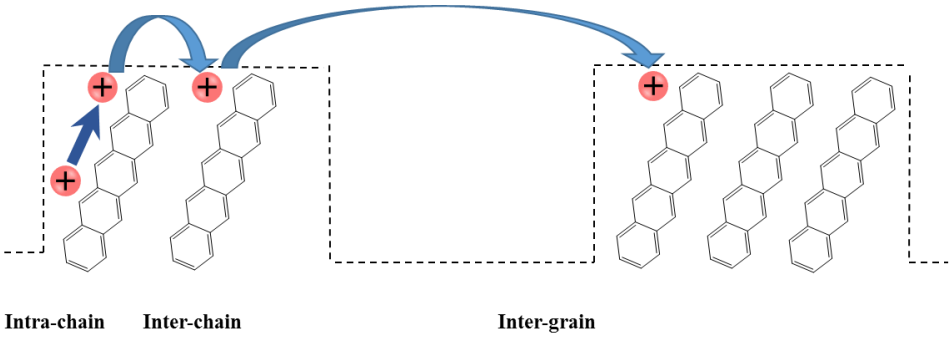

Figure 2.9. Schematic representation of different charge carriers hopping transport in pentacene molecular chain (intra-molecular transport), between one chain to the neighboring one (inter-molecular transport), and inter-grain transport. Here, the conjugated molecule is symbolized by pentacene.

Most organic semiconductor thin films consist of a mixture of amorphous disorder phase and polycrystalline domains. Charge transport via hopping of charge carriers between molecules in the disordered regions often limits charge carrier mobility. Thus, it is important to suppress the disordered phases and gain boundaries to achieve efficient charge transport. By providing an ordered and closer stuck molecule, thus high efficient carrier transport can be achieved.[41] In inorganic crystalline semiconductors, the charge mobility decreases with temperature. Whereas, it increased by increasing temperatures for organic molecules.[52] The temperature dependence of the mobility (μ) of such "hopping" transport generally follows the form proposed by Mott:[53]

$$\mu = \mu_0 \exp\left[-(T_0 - T)^{1/\alpha}\right]$$

Where μ_0 and T_0 are materials parameters (constants), T is temperature, and α is integer ranging from 1 to 4.[50] In addition to temperature, the density of states (DOS) in organic semiconductors is not uniform and defined by a Gaussian or an exponential function, in which the charge mobility becomes dependent at a high electric field (> 10^5 Vcm^{-1}).[17] this phenomenon occurs through Gill's[54] or a pool-Frenkel[55] mechanism, where the applied field changes the potential near the localized states, which increase the transfer rate of carriers between sites. The general field dependence of the mobility is described by:

$$\mu = \mu(0) \exp\left[\frac{q}{KT} \beta\sqrt{E}\right]$$

Where μ(0) is the mobility at zero field (E=0), E is the magnitude of the electric field and β is the Pool-Frenkel factor defined as :

$$\beta = (\varepsilon/\pi\, \varepsilon\, \varepsilon_0)^{1/2}$$

The observed semiconductor materials mobility dependence on the gate voltage came from the fact that as the gate voltage increases, injected carriers attend to fill the traps, so trapping becomes less efficient, which improves the charge transport. Therefore, by applying lower gate bias, charge carriers will occupy the lower states of the density of states (DOS), while, at high gate bias, injected carriers will also occupy high energy states as illustrated in **Figure 2.10.**

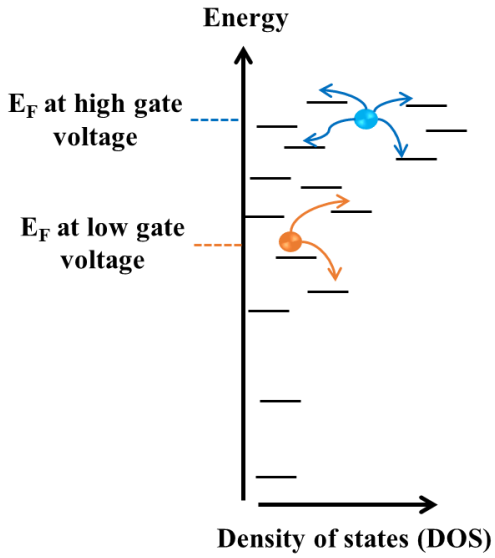

Figure 2.10. Schematic representation of charge transport at low and high gate voltage bias, the Fermi energy increases with increasing the applied gate voltage due to the accumulation of more charges.

2.2.3. Multiple trapping and release model

The charge carriers-transport in organic transistors is limited by localized states induced by defects and impurities. Hopping model is appropriate to describe charge transport within disordered organic materials, the multiple trapping and release (MTR) model[56] developed for the first time for describing the charge transport in amorphous silicon. MTR can be also applied to high ordered organic materials, like vapor deposited small molecules or the crystalline oligothiophenes in which, the field effect mobility is thermally activated. The basic statement of this model is the localized states distribution in the vicinity of the transport band-edges.[57] The charges may interact with the localized levels and gets captured instantaneously after arriving to a trap, then, the trapped carriers are released through thermal release process as illustrated in **Figure 2.11**.

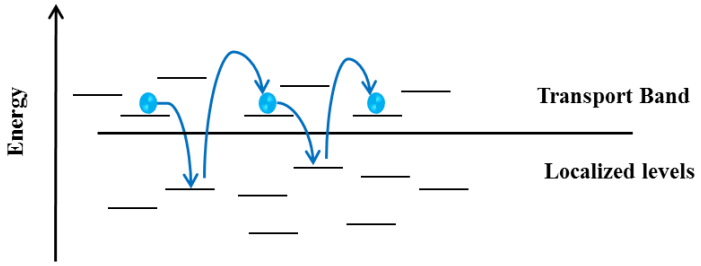

Figure 2.11. Schematic representation of charge transport by multiple trapping and release model, in which charge carriers are trapped and released through thermal release process.

In the case of homogeneous dispersed traps, the resulting effective mobility μ_{eff} is related to the mobility μ_0 in the transport band by the following equation:

$$\mu_{eff} = \mu_0 \alpha e^{-(Ec-Et)/KT}$$

Where E_t is the energy difference between the transport band edge and a single trap level, E_t is the energy of the transport band edge, μ_0 is the undisturbed mobility in the transport band, and α is the ratio between the density of available delocalized states and that of traps.[58]

2.2.4. Variable range hopping (VRH) and Mobility Egde model

Most of organic semiconductors contains crystalline and amorphous regions, so their electronic band are mostly like that of amorphous semiconductor. The mobility edges exist in the localized states in the band tails, that separate the region of localized state of that of extended states present in the band interior. The concept of mobility edges model was used for amorphous semiconducting materials, this concept is described by the energy difference separating both localized and delocalized states either in valence or conductance bands.[59-61]

There have been many theoretical treatments of the tunneling process. Hopping model is valid for carriers transfer between localized states. It is generally assumed that the states are distributed randomly in energy and space and that the fermi level lies within delocalized states. The variable range hopping model states that charges can hop with high energy activation over small distance or with a low energy through a long distance. The hoping distance vary with the temperature, and from that comes the name variable range hopping. This temperature dependence is relatively related to the localized states density. The VRH model developed by Vissenberg and Matters[51] gives the following equation for the temperature (T) and the occupation of localized states (δ) dependence of the conductivity:

$$\sigma(\delta,T)=\sigma_0\left(\frac{\pi N_t\delta(T_0/T)^3}{(2\alpha)^3 B_c\,\Gamma(1-T/T_0)\Gamma(1+T/T_0)}\right)^{T_0/T}$$

Where σ_0 is the preexponential factor of the conductivity, α is a parameter of effective overlap between localized sites, N_t is the number of states per unit volume, T_0 is a parameter that indicates the width of the exponential distribution, and B_c is a critical number of bonds defined by the density of bonds (N_b) divided by the the density of sites (N_s) in the percolating system.

Conclusion

This chapter presented a background overview of organic semiconductors. The fundamental properties of organic semiconducting molecules (small molecules and conjugated polymers). The basic and most important charge transport models were reviewed. First, we have described the different classes of materials depending on their energy levels and electrical behaviors, and regarding the nature of the charge carriers, paying a particular attention to the recent works on novel soluble small molecules and polymers employed for organic electronics. Then we have discussed the charge transport in organic semiconductors, accomplished by the overlapping of π-orbitals of the conjugated semiconductors, makes the conduction of charge carriers possible along the molecular system. Finally, we have discussed the major advances that have been achieved in the description of the charge transport across organic semiconductors.

2.3. References

1. Arias, A. C.; MacKenzie, J. D.; McCulloch, I.; Rivnay, J.; Salleo, A., Materials and Applications for Large Area Electronics: Solution-Based Approaches. *Chem. Rev.* **2010,** *110* (1), 3-24.
2. Bao, Z. N.; Dodabalapur, A.; Katz, H.; Raju, V. R.; Rogers, J., Organic Semiconductors for Plastic Electronics. *Abstr. Pap. Am. Chem. Soc.* **2001,** *221*, U627-U627.
3. Mas-Torrent, M.; Rovira, C., Novel Small Molecules for Organic Field-Effect Transistors: Towards Processability and High Performance. *Chem. Soc. Rev.* **2008,** *37* (4), 827-838.
4. Molinari, A. S.; Alves, H.; Chen, Z.; Facchetti, A.; Morpurgo, A. F., High Electron Mobility in Vacuum and Ambient for PDIF-CN2 Single-Crystal Transistors. *J. Am. Chem. Soc.* **2009,** *131* (7), 2462-2463.
5. Facchetti, A., Semiconductors for Organic Transistors. *Mater. Today* **2007,** *10* (3), 28-37.
6. Goodwin, A. L., Organic crystals: Packing down. *Nat Mater* **2010,** *9* (1), 7-8.
7. Farges, J. P., *Organic Conductors: Fundamentals and Applications* **1994,** *4*, CRS Press.

8. Brooks, J. S., Organic Crystals: Properties, Devices, Functionalization and Bridges to Bio-Molecules. *Chem. Soc. Rev.* **2010,** *39* (7), 2667-2694.

9. Sakamoto, Y.; Suzuki, T.; Kobayashi, M.; Gao, Y.; Fukai, Y.; Inoue, Y.; Sato, F.; Tokito, S., Perfluoropentacene: High-Performance p-n Junctions and Complementary. Circuits with Pentacene. *J. Am. Chem. Soc.* **2004,** *126* (26), 8138-8140.

10. Chua, L. L.; Zaumseil, J.; Chang, J. F.; Ou, E. C. W.; Ho, P. K. H.; Sirringhaus, H.; Friend, R. H., General Observation of n-Type Field-Effect Behaviour in Organic Semiconductors. *Nature* **2005,** *434* (7030), 194-199.

11. Jones, B. A.; Ahrens, M. J.; Yoon, M. H.; Facchetti, A.; Marks, T. J.; Wasielewski, M. R., High-Mobility Air-Stable n-Type Semiconductors with Processing Versatility: Dicyanoperylene-3,4 : 9,10-bis(dicarboximides). *Angew. Chem., Int. Ed.* **2004,** *43* (46), 6363-6366.

12. Bao, Z. A.; Lovinger, A. J.; Brown, J., New air-stable n-channel organic thin film transistors. *J. Am. Chem. Soc.* **1998,** *120* (1), 207-208.

13. Babel, A.; Jenekhe, S. A., n-Channel Field-Effect Transistors from Blends of Conjugated Polymers. *J. Phys. Chem. B* **2002,** *106* (24), 6129-6132.

14. Choi, J.; Song, H.; Kim, N.; Kim, F. S., Development of n-Type Polymer Semiconductors for Organic Field-Effect Transistors. *Semicond. Sci. Technol.* **2015,** *30* (6), 16.

15. Irie, T.; Endo, S.; Kimura, S., Electrical Properties of p- and n-Type CuInSe2 Single Crystals. *Jpn. J. Appl. Phys.* **1979,** *18* (7), 1303-1310.

16. Zaumseil, J.; Sirringhaus, H., Electron and Ambipolar Transport in Organic Field-Effect Transistors. *Chem. Rev.* **2007,** *107* (4), 1296-1323.

17. Jackson, T. N.; Lin, Y. Y.; Gundlach, D. J.; Klauk, H., Organic Thin-Film Transistors for Organic Light-Emitting Flat-Panel Display Backplanes. *IEEE J. Sel. Top. Quantum Electron.* **1998,** *4* (1), 100-104.

18. Halik, M.; Klauk, H.; Zschieschang, U.; Schmid, G.; Ponomarenko, S.; Kirchmeyer, S.; Weber, W., Relationship Between Molecular Structure and Electrical Performance of Oligothiophene Organic Thin Film Transistors. *Adv. Mater.* **2003,** *15* (11), 917-922.

19. Klauk, H.; Halik, M.; Zschieschang, U.; Schmid, G.; Radlik, W.; Weber, W., High- Mobility Polymer Gate Dielectric Pentacene Thin Film Transistors. *J. Appl. Phys.* **2002,** *92* (9), 5259-5263.

20. Yamamoto, T.; Takimiya, K., Facile Synthesis of Highly pi-Extended Heteroarenes, Dinaphtho[2,3-b:2‘,3‘-f]chalcogenopheno[3,2-b]chalcogenophenes, and Their Application to Field-Effect Transistors. *J. Am. Chem. Soc.* **2007,** *129* (8), 2224-2225.

21. Ball, J. M.; Bouwer, R. K. M.; Kooistra, F. B.; Frost, J. M.; Qi, Y. B.; Domingo, E. B.; Smith, J.; de Leeuw, D. M.; Hummelen, J. C.; Nelson, J.; Kahn, A.; Stingelin, N.; Bradley, D. D. C.; Anthopoulos, T. D., Soluble Fullerene Derivatives: The Effect of Electronic Structure on Transistor Performance and Air Stability. *J Appl Phys* **2011,** *110* (1), 014506.

22. He, Y. J.; Chen, H. Y.; Hou, J. H.; Li, Y. F., Indene-C-60 Bisadduct: A New Acceptor for High-Performance Polymer Solar Cells. *J Am Chem Soc* **2010,** *132* (4), 1377-1382.

23. Anthopoulos, T. D.; de Leeuw, D. M.; Cantatore, E.; van 't Hof, P.; Alma, J.; Hummelen, J. C., Solution Processible Organic Transistors and Circuits Based on a C-70 Methanofullerene. *J Appl Phys* **2005,** *98* (5), 054503.

24. Anthopoulos, T. D.; Tanase, C.; Setayesh, S.; Meijer, E. J.; Hummelen, J. C.; Blom, P. W. M.; de Leeuw, D. M., Ambipolar Organic Field-Effect Transistors Based on a Solution-Processed Methanofullerene. *Adv Mater* **2004,** *16* (23-24), 2174-2179.

25. Katz, H. E.; Lovinger, A. J.; Johnson, J.; Kloc, C.; Siegrist, T.; Li, W.; Lin, Y. Y.; Dodabalapur, A., A soluble and Air-Stable Organic Semiconductor with High Electron Mobility. *Nature* **2000,** *404* (6777), 478-481.

26. Weitz, R. T.; Amsharov, K.; Zschieschang, U.; Villas, E. B.; Goswami, D. K.; Burghard, M.; Dosch, H.; Jansen, M.; Kern, K.; Klauk, H., Organic n-Channel Transistors Based on Core-Cyanated Perylene Carboxylic Diimide Derivatives. *J. Am. Chem. Soc.* **2008,** *130* (14), 4637-4645.

27. Zschieschang, U.; Amsharov, K.; Jansen, M.; Kern, K.; Klauk, H.; Weitz, R. T., Separating the Impact of Oxygen and Water on the Long-Term Stability of n-Channel Perylene Diimide Thin-Film Transistors. *Org. Electron.* **2015,** *26*, 340-344.

28. Chason, M.; Brazis, P. W.; Zhang, H.; Kalyanasundaram, K.; Gamota, D. R., Printed Organic Semiconducting Devices. *Proc. IEEE* **2005,** *93* (7), 1348-1356.

29. Mena-Osterit, E.; Meyer, A.; W., L.-V. B. M.; Janssen, R. A. J.; Meijer, E. W.; Baduerle, P., Two-Dimensional Crystals of Poly(3-Alkyl- thiophene)s: Direct Visualization of Polymer Folds in Submolecular Resolution. *Angew. Chem. Int. Ed.* **2000,** *39*, 2679-2684.

30. McCulloch, I.; Heeney, M.; Bailey, C.; Genevicius, K.; Macdonald, I.; Shkunov, M.; Sparrowe, D.; Tierney, S.; Wagner, R.; Zhang, W. M.; Chabinyc, M. L.; Kline, R. J.; McGehee, M. D.; Toney, M. F., Liquid-Crystalline Semiconducting Polymers with High Charge-Carrier Mobility. *Nat Mater* **2006,** *5* (4), 328-333.

31. Halls, J. J. M.; Walsh, C. A.; Greenham, N. C.; Marseglia, E. A.; Friend, R. H.; Moratti, S. C.; Holmes, A. B., Efficient Photodiodes from Interpenetrating Polymer Networks. *Nature* **1995,** *376* (6540), 498-500.

32. Babel, A.; Jenekhe, S. A., High Electron Mobility in Ladder Polymer Field-Effect Transistors. *J. Am. Chem. Soc.* **2003,** *125* (45), 13656-13657.

33. Alam, M. M.; Jenekhe, S. A., Efficient Solar Cells from Layered Nanostructures of Donor and Acceptor Conjugated Polymers. *Chem. Mat.* **2004,** *16* (23), 4647-4656.

34. Briseno, A. L.; Kim, F. S.; Babel, A.; Xia, Y. N.; Jenekhe, S. A., n-Channel Polymer Thin Film Transistors with Long-Term Air-Stability and Durability and Their Use in Complementary Inverters. *J. Mater. Chem.* **2011,** *21* (41), 16461-16466.

35. Zhan, X. W.; Tan, Z. A.; Domercq, B.; An, Z. S.; Zhang, X.; Barlow, S.; Li, Y. F.; Zhu, D. B.; Kippelen, B.; Marder, S. R., A High-Mobility Electron-Transport Polymer with Broad Absorption and Its Use in Field-Effect Transistors and All-Polymer Solar Cells. *J. Am. Chem. Soc.* **2007,** *129* (23), 7246-7247.

36. Guo, X. G.; Watson, M. D., Conjugated Polymers from Naphthalene Bisimide. *Org. Lett.* **2008,** *10* (23), 5333-5336.

37. Guo, X. G.; Kim, F. S.; Seger, M. J.; Jenekhe, S. A.; Watson, M. D., Naphthalene Diimide-Based Polymer Semiconductors: Synthesis, Structure-Property Correlations, and n-Channel and Ambipolar Field-Effect Transistors. *Chem. Mat.* **2012,** *24* (8), 1434-1442.

38. Chen, Z. H.; Zheng, Y.; Yan, H.; Facchetti, A., Naphthalenedicarboximide- vs Perylenedicarboximide-Based Copolymers. Synthesis and Semiconducting Properties in Bottom-Gate N-Channel Organic Transistors. *J. Am. Chem. Soc.* **2009,** *131* (1), 8-9.

39. Coropceanu, V.; Cornil, J.; da Silva, D. A.; Olivier, Y.; Silbey, R.; Bredas, J. L., Charge Transport in Organic Semiconductors. *Chem. Rev.* **2007,** *107* (4), 926-952.

40. Bassler, H., Charge Transport in Disordered Organic Photoconductors a Monte Carlo Simulation Study. *Phys. Status Solidi B-Basic Res.* **1993,** *175* (1), 15-56.

41. Liu, L.; Yang, G. C.; Duan, Y. A.; Geng, Y.; Wu, Y.; Su, Z. M., The Relationship Between Intermolecular Interactions and Charge Transport Properties of Trifluoromethylated Polycyclic Aromatic Hydrocarbons. *Org. Electron.* **2014,** *15* (9), 1896-1905.

42. Böttger, H.; Bryksin, V. V., *Hopping Conduction in Solids* **1985**, VCH: Deerfield Beach, FL.

43. Emin, D., Phonon-Assisted Transition Rates I. Optical-Phonon-Assisted Hopping in Solids. *Adv. Phys.* **1975,** *24* (3), 305-348.

44. Klinger, M. I.; Sykes, J. B., *Problems of Linear Electron (Polaron) Transport Theory in Semiconductors* **1979**, 1st ed.; Pergamon Press: Oxford; New York,.

45. Movaghar, B., Theory of Conduction in Molecular-Solids .1. Theory. *J. Mol. Elecron.* **1987,** *3*, 183.

46. Holstein, T., Studies of polaron motion Part I. The Molecular-Crystal Model (Reprinted from *Annals of Physics*, vol 8, pg 325-342, 1959). *Ann. Phys.* **2000,** *281* (1-2), 706-724.

47. Glaeser, R. M.; Berry, R. S., *J. Chem. Phys.* **1966,** *44*, 3797.

48. Silinsh, E.; Càpek, V., Organic Molecular Crystals: Interaction, Localization, and Transport Phenomena. *American Institute of Physics : New York* **1994**.

49. Silbey, R.; Munn, R. W., General Theory of Electronic Transport in Molecular Crystals. I. Local Linear Electron–Phonon Coupling. *J. Chem. Phys.* **1980,** *72*, 2763.

50. Dimitrakopoulos, C. D.; Malenfant, P. R. L., Organic Thin Film Transistors for Large Area Electronics. *Adv. Mater.* **2002,** *14* (2), 99-117.

51. Vissenberg, M.; Matters, M., Theory of the Field-Effect Mobility in Amorphous Organic Transistors. *Phys. Rev. B* **1998,** *57* (20), 12964-12967.

52. Li, F. M.; Nathan, A.; Wu, Y.; Ong, B. S., Organic Thin Film Transistor Integration: A Hybrid Approach. **2011,** *Weinheim, Germany: Wiley-VCH*.

53. Mott, N. F., Conduction in non-Crystalline Materials : 3. Localized States in a Pseudogap and Near Extremities of Conduction and Valence Bands. *Philos. Mag.* **1969,** *19*, 835-852.

54. Gill, W. D., Drift Mobilities in Amorphous Charge-Transfer Complexes of Trinitrofluorenone and Poly-N-Vinylcarbazole. *J. Appl. Phys.* **1972,** *43*, 5033-5040.

55. Frenkel, J., On Pre-Breakdown Phenomena in Insulators and Electronic Semi-Conductors. *Phys. Rev.* **1938,** *54*, 647-648.

56. Le Comber, P. G.; Spear, W. E., Electronic Transport in Amorphous Silicon Films. *Phys. Rev. Lett.* **1970,** *25*, 509.

57. Horowitz, G.; Hajlaoui, M. E., Mobility in Polycrystalline Oligothiophene Field-Effect Transistors Dependent on Grain Size. *Adv. Mater.* **2000,** *12* (14), 1046-1050.

58. Bao, Z.; Locklin, J., Organic Field-Effect Transistors. CRC Press- Taylor & Francis. Group: **2007**.

59. Khan, M. A.; Jiu-Xun, S., Improvement of Mobility Edge Model by Using New Density of States with Exponential Tail for Organic Diode. *Chin. Phys. B* **2015,** *24* (4), 6.

60. Mott, N., The Mobility Edge Since 1967. *J. Phys. C: Solid State Phys.* **1987,** *20* (21), 3075-3102.

61. Okamoto, H.; Toyama, T.; Hattori, K., An Extended Model for the Mobility Edge Carrier Transport. *J. Non-Cryst. Solids* **2004,** *338*, 341-344.

Chapter 3. Organic electronic devices

Introduction

The first idea and design of field effect transistor dates back to 1920.[1] However, the concept of field-effect transistors was successfully demonstrated with the metal-oxide-semiconductor FET (MOSFET) invention in 1960 year.[2] The developments in organic based transistors area only started in the late 1980s.[3-4] Field-effect transistors are the basic unit of more complex electronic circuits. They have gained a great attention from their invention to date[5-7]. Today, they are part of our daily life, they are integrated in micro-chips and used by billion users in microprocessors and everyday electronics such as smartphones, displays, memory chips, smart cards and sensor arrays.[8-9] The micro-electronics industry based on the inorganic silicon has been expanding since 1960s and is continuing to advance every year.[10] However, field-effect transistors based on inorganic semiconductors present multiple limitations as they are non-flexible, non-transparent, and are produced at high cost owing to the high resolution lithography tools and equipment required. Organic semiconductor-based devices can be fabricated on flexible and transparent supports using solution processing methods.[11] They offer the advantage of being processable at low temperature, low cost and feature large area electronic products,[12] such as organic photovoltaics (OPVs),[13] and light-emitting diodes (OLEDs).[14-15]

In this chapter, we focus our attention on the working principles of devices such as organic field-effect transistors, organic phototransistors, and organic complementary inverters. The different OFET geometries, as well as their crucial interfaces are also tackled within this chapter.

3.1. Organic field-effect transistors (OFETs)

3.1.1. OFET device architecture and operation mode

The field-effect transistor (FET) is a three-terminal device that uses an electric gate field to control the charge density and therefore the conductance of a given semiconductor material. Within the family of field-effect transistors there are also those called thin film transistors (TFT) that use a

thin semiconductor film as the active layer. **Figure 3.1** shows a three-dimensional view of an organic thin-film transistor (OFET), in which the active part of the device is constituted of an organic semiconductor thin film. Generally, an organic field-effect transistor is composed of three main parts: a semiconductor thin layer, an insulator (dielectric) layer, and three metal electrodes (terminals) called source (the grounded electrode), drain and gate. The source (S) and drain (D) electrodes directly contact the organic semiconductor material. The distance between the source and the drain is called the channel length L. The electrode width is called W. The area W x L identifies the so-called channel, where charges are transported between source and drain electrodes. A third electrode, the gate (G), is electrically separated from the semiconductor thin film by a thin insulating layer, forming a metal-insulator-semiconductor (MIS) structure. The gate electrode controls the charge density in the channel area and it is therefore able to turn the device on and off depending on the applied voltage. The charge density defines the current intensity between from source to drain, I_D, in the semiconductor channel. The current flows through the insulator layer is called the leakage current I_{GS}, which should be negligible compared to the drain current.

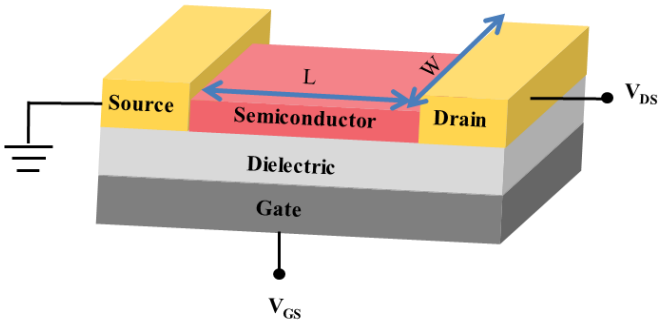

Figure 3.1. Schematic view of a three-terminal organic field-effect transistor (OFET).

In principle, four different transistor's geometries can be employed for organic FETs: bottom-contact bottom-gate, bottom-contact top-gate, top-contact bottom-gate and top-contact top-gate (see **Figure 3.2**).

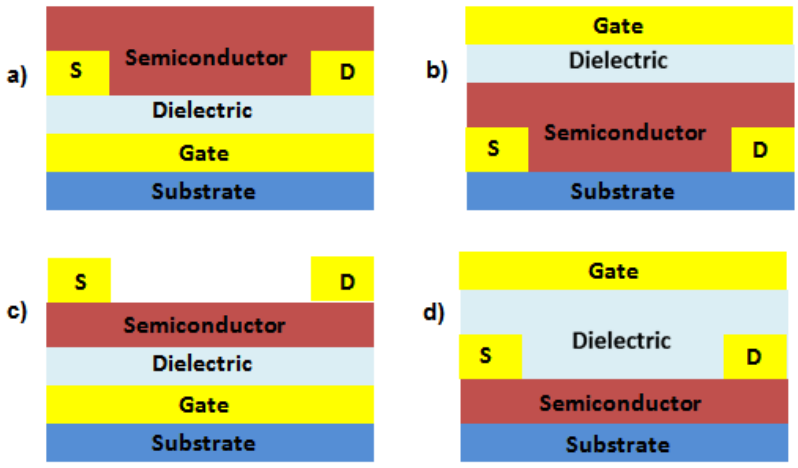

Figure 3.2. Schematic view of the four different OFET configurations: **a)** bottom-contact, bottom-gate; **b)** bottom-contact, top-gate; **c)** top-contact, bottom-gate; **d)** top-contact, top-gate.

In top-contact configuration, the source and drain electrodes are evaporated on the top of organic semiconductor whereas in bottom-contact configuration they lie on the dielectric before depositing the organic semiconductor. In top-gate configuration the gate electrode is realized on the top of dielectric while in bottom-gate configuration the gate lies under the dielectric.

Depending on the type of the major carrier, three types of OFET can be identified: (organic) p-channel FET, (organic) n-channel, and (organic) ambipolar. The p-channel transistor is based on a p-type semiconductor and operates at negative gate bias, n-channel transistor is based on n-type semiconductor and operates at positive gate potential, and ambipolar transistor is based on an ambipolar organic semiconductor capable to transport both electrons and holes, for that, it can operate on negative (to transport holes) and positive (to transport electrons) biases. In a field-effect transistor, two independent voltages perpendicular to each other are applied; the gate voltage (V_{GS}) and the drain voltage (V_{DS}), both referred to the potential between source and gate, and source and drain respectively. By applying a positive or negative voltage V_{GS} (positive for n-type and negative for p-type semiconductors) between source and gate, electrons or holes charge carriers respectively are accumulated at the semiconductor-dielectric interface forming a channel between source and drain electrodes. While, the applied drain voltage V_{DS} drives these induced charges from the source to the drain electrode. The source serves as the reference (grounded) electrode (see **Figure 3.3**).

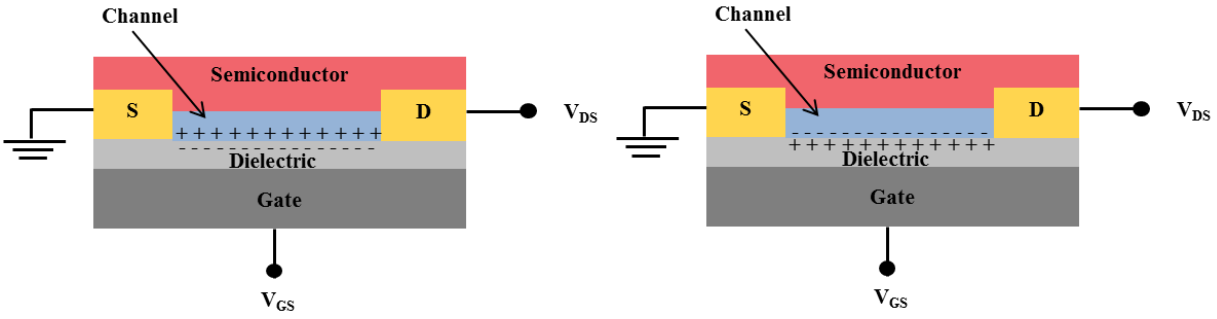

a) **b)**

Figure 3.3. Schematic representation of organic field-effect transistor based on **a)** a p-type semiconductor and **b)** an n-type semiconductor. The electrons (represented by a negative charges (-)) and holes (represented by positive charges (+)) are accumulated in the semiconductor-dielectric interface under gate bias effect.

Depending on the applied drain (V_{DS}) and gate (V_{DS}) biases, two transport regimes occur through the semiconductor channel: the linear and the saturation regimes (see **Figure 3.4**). A linear regime is observed at low drain voltage $V_{DS} \leq (V_{GS} - V_{th})$ in which the current between source and drain (I_D) follows Ohm's law. When the drain voltage increases, and approaches the gate voltage and reaching a certain point where $V_{DS} = (V_{GS} - V_{th})$ called 'pinch-off', on which the potential close the drain electrode drops to zero and charge carriers at this region form a depletion region. When the drain bias keep increasing ($V_D > V_{GS} - V_{th}$), the drain current does not increase but tends to saturate, and start to be independent to the gate bias, here the regime is changes from the linear to saturation. The drain current in both regimes is described according the following equations:

$$I_D = \frac{W}{L} C_i \mu_{LIN} (V_{GS} - V_{th}) V_{DS}$$

$$I_D = \frac{W}{2L} C_i \mu_{SAT} (V_{GS} - V_{th})^2$$

Where μ indicates the field-effect carrier mobility of the semiconductor, L is the channel length, i.e. the length of the transistor from the source to drain in the direction of the current flow, W is the channel width which represents the width of the injecting electrode, both L and W are defined in the **Figure 3.1**. V_{Th} is the threshold voltage which is a characteristic parameter of the material and the geometry, represents the gate voltage value at which the OFET device turns on, V_{DS} is the source-drain voltage, V_{GS} is the source-gate voltage, and C_i indicates the capacitance per unit area of the insulator layer which is given by the following formula:

$$C_i = \frac{\varepsilon_0 \varepsilon_r}{d_i}$$

With ε_0 the permittivity of vacuum, ε_r the relative permittivity of the dielectric and d_i the thickness of the dielectric layer.

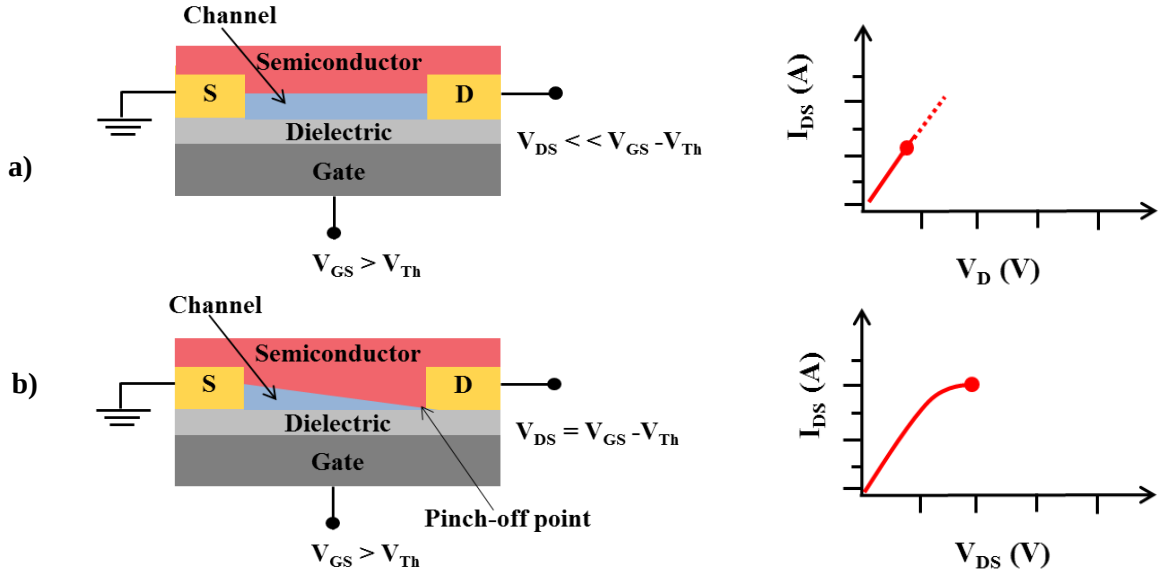

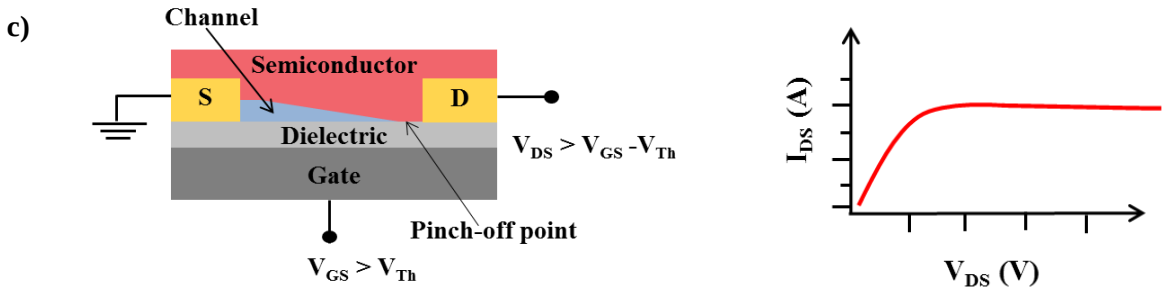

Figure 3.4. Schematic representation of an organic field-effect transistor in operation with the corresponding output characteristics in different operation regimes, depending on V_{GS}, V_{DS}, and V_{th} voltages: **a)** in the linear regime, **b)** at the pinch-off point, and **c)** in the saturation regime. The blue area is the semiconductor channel (reproduced from[16]).

Based on the previous equations, the field-effect carriers mobility in both linear and saturation regimes can be extracted and defined by the flowing equations:

$$\mu_{LIN} = \frac{L}{W\, C_i\, V_{DS}} \left(\frac{dI_{DS}}{dV_{GS}}\right)$$

$$\mu_{sat} = \frac{2 \cdot \left(\frac{\partial \sqrt{I_D}}{\partial V_{GS}}\right)^2}{C_i \frac{W}{L}}$$

The field-effect mobility is used to characterize the efficiency of charge transport in the active semiconducting thin layer.

The measured I-V characteristics of OFET device can be plotted by either varying the drain voltage at a constant gate voltage (output characteristics) or changing the gate voltage at a fixed drain voltage (transfer characteristics), both representations are illustrated in **Figure 3.5**.

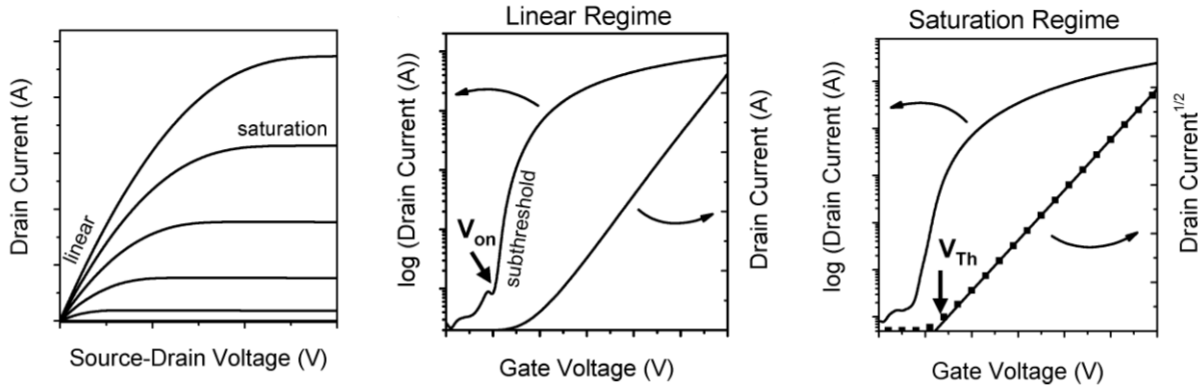

a) **b)** **c)**

Figure 3.5. I-V characteristic curve of an organic n-channel transistor. **a)** The OFET output curve showed the linear and saturation regime, **b)** The OFET transfer curve (I_D vs V_{GS}) in the linear regime and the logarithmic scale of drain current log (I_D) vs V_{GS}. **c)** The transfer curve (I_D vs V_{GS}) in the saturation regime, showing the threshold voltage V_{th} extracted from the square root of the drain current ($(I_D)^{1/2}$ vs V_{GS}) plot.

3.1.2. Important OFET extracted parameters:

The I-V output and transfer curve showed the OFET device electrical behavior, and are used to provide an approximation on the OFET characteristics and extract its basic and important parameters, such as the field-effect mobility (μ, measured in $cm^2V^{-1}s^{-1}$), the threshold voltage (V_{th}, measured in V), subthreshold swing, and the I_{on}/I_{off} ratio.

The mobility describes how fast the electrons and/holes can move through the semiconductor material, it is often considered of merit for comparing electrical performances of different organic materials. The effective mobility extraction from the linear regime (μ_{lin}) is done by fitting the I_{DS}-V_{GS} linear part, whereas the μ_{sat} can be calculated by plotting the square root of the saturation current as a function of the gate voltage, and fitting its linear part, while the extrapolation of the line to the V_{GS} axis corresponds to the threshold voltage (V_{th}).

The threshold voltage is commonly defined by the minimum applied gate voltage value in which electrons and/or holes start to accumulate and form the channel. V_{th} is an important parameter to figure out the OFET performance. In ideal case, the threshold voltage is equal to zero, but in organic FET, values closed to zero are commonly noticed, due to several factors such as the presence of trap carriers, impurities, interface states and large defects in the semiconductor-insulator interface. These

factors affect the V_{th} and can be reduced by the increase in dielectric capacitance (more charge carriers at low biases).

The I_{on}/I_{off} demonstrate the difference between the current in the on state and the current in the off state. The former is noticed when the device is fully operating. However, the latter state is observed when no current is detected in the channel. The on-off ratio is extracted from the transfer curves which correspond to the ratio between the highest and the lowest drain current values.

The subthreshold swing (S, its unit is V/decade) defined by the relationship: $S = (\partial \log I_D / \partial V_{GS})$ is an OFET extracted parameter that determines the gate bias required to switch the device current by a factor of 10. This parameter can be estimated from the slope of $\log I_D$ vs V_{GS} curve in the subthreshold region (the region below the threshold voltage).

Another important aspect that has to consider is the mobility dependence on the electrical outcome from the channel resistance and the contact resistance, the sum is called R_{TOT}, provides a measure of charge injection efficiency in an OFET. (R_{TOT}) is estimated by measuring the current flowing across the device channel is composed of two different components, the contact resistance R_c at the organic semiconductor-metal interface and the channel resistance R_{ch} formed at the organic semiconductor-dielectric interface ($R_{TOT} = R_c + R_{ch}$), both resistance components depend on the choice of metal electrodes.[17] The contact resistance depends on the energetic misalignment between the work function of the source-drain metal and the HOMO (LUMO) of the p-type (n-type) system employed. The resistive contribution given by the channel resistance (R_{ch}) depends on the channel length. The value of the effective mobility in case of large contact resistance is underestimated, large contact resistance can limit the charge transfer in an OFET.[18] The device electrical performances depend not only on the intrinsic carrier mobility of the semiconductor, but also on the charge carrier injection at the source-drain contacts. The contact resistance (R_C) is constituted of two components, R_{int}, the resistance from the mismatch between the Fermi level of the metal contact electrode and the HOMO (LUMO) of the p-type (n-type) semiconductor system. The second resistance component is the R_{bulk}, which is the semiconductor resistance from the metal electrode to the conducting channel. From Mott-Schottky (MS) model,[19] the ohmic contact is preferable to get a good charge injection (in case of good alignment between semiconductor energetic level and the work function of the metal electrode). Contrary, the presence of charge barrier (Φ_B) at the metal-semiconductor interface, that makes charge injection between the metal and the HOMO (LUMO) of the organic material more difficult, results in a non-ohmic contact and a high contact resistance. However, the contact resistance is relatively dependent on the device architecture. In top-contact structure, the contact resistance is lower than that in bottom-contact. Due to the larger metal-semiconductor area, which leads to smaller contact

resistance (see **Figure 3.6**). We can estimate the contact resistance value by the transfer line method (TML).[20-23] This method consists of measuring in the linear regime the total resistance by varying the channel lengths of similar devices. The channel resistance R_{ch} is proportional to the channel lengths, the contact resistance is extracted from the extrapolation to zero length of the resistance Vs channel length plot.

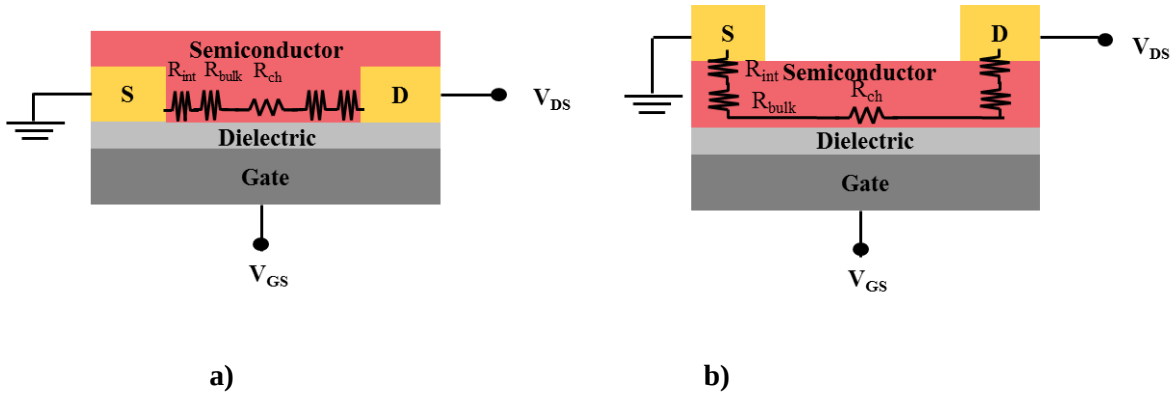

Figure 3.5. Schematic representation of OFET transistors in **a)** top-contact bottom-gate configuration, and **b)** bottom-contact bottom-gate configuration showing the total resistance (channel resistance (R_{ch}) and contact resistance (R_{int}+R_{bulk})) at the meral-semiconducting interface.

3.1.3. OFET device as a tool to unravel the physico-chemical properties of interfaces

Additional OFET charge transport limitation concentrated at the device critical interfaces: namely, the meta-semiconductor and dielectric-semiconductor interfaces. The former is responsible for the limitations coming from contact resistance, while the later comes from defects that leads to charge transport deterioration. For that, it is quietly desirable to characterize OFET devices in various geometries.

As mentioned previously, the choice of metal for source/drain electrodes affects the contact resistance, and so, the charge carriers mobility. In order to have efficient charge injection at the metal-semiconductor interface, the electrodes work function should match with HOMO (LUMO) energy levels for p-type (n-type) semiconductor. Before contact, both energy levels of HOMO (LUMO) of material and the Fermi-level of the metal contact are in their normal state while, in contact of the semiconductor with metal surface, the work function (Φ_M) and ionization energy align leading to charge carriers flow from one to the other.[24-25] One must be considered as important factor is the injection barrier (Φ_B) that forms in the metal-semiconductor interface which is given by the difference between the Fermi-level and the conduction or valance band of the semiconductor. When this energy

is large, the charge injection is poor and leads to high contact resistance. The lower is the injection barrier, the better is the charge injection efficiency (see **Figure 3.6**).

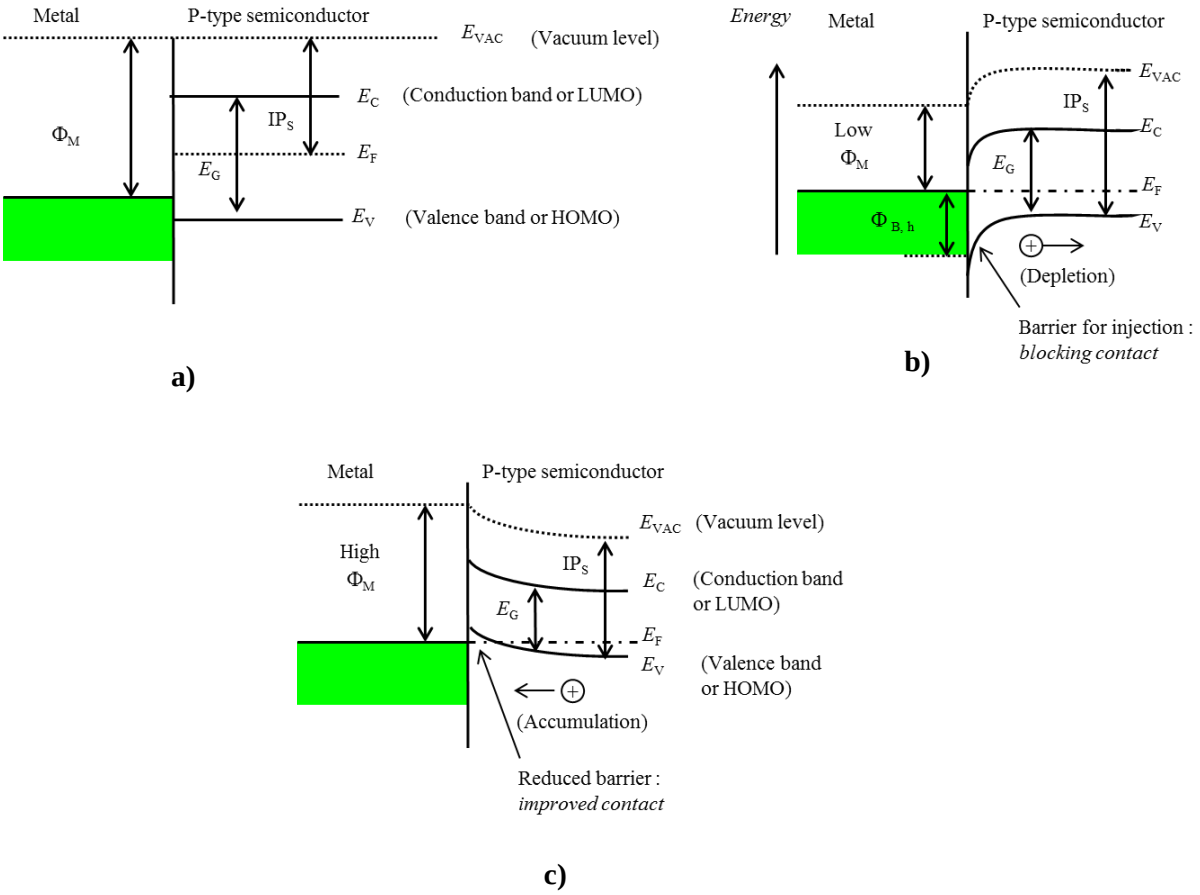

Figure 3.6. Schematic of energy diagram of **a)** a metal and a p-type semiconductor before junction, b) after junction, with a poor contact and high contact resistance due to the high injection barrier (Φ_B), and c) large work function results in a good contact and small injection barrier.

The choice of metal electrodes depends on the nature of the organic semiconductor. For an p-type material, the more suitable is to choose metal electrodes with high work function and a low work function for n-type materials. Typically, the most used metal in OFETs is gold, which has a work function of 5.1 eV close to the ionization potential IP (the distance between the vacuum level E_{vac} and the molecular energetic levels) of most p-type organic semiconductors. However, to inject electrons to the LUMO of n-type organic semiconductors it is more appropriate to use other metals (with low work functions) such as Al, Ca or Mg. The drawback is that these metals tend to oxidize easily. To optimize the metal-semiconductor interface, instead of changing the gold electrodes, another approach can be used is the functionalization of source and drain electrodes with self-assembled monolayers (SAM). The thiol compounds are one of the widely studied solution processed molecules employed in gold

surface functionalization other metals. The SAMs monolayers formation by covalent bonds with the surface metal atoms create a dipole moment, which result to a shift in the metal work function.

The dielectric-semiconductor interface is essential and needs to be optimized to ensure high OFET performances as the charge accumulation occurs within the few nanometers of the organic layer close to the insulator. The traps concentration at this interface can be reduced using self-assembled monolayers. The SAM formation in the dielectric surface influences not only dielectric properties but also the packing and alignment of the deposited semiconductor thin film and results in major cases to the formation of large ordered domains in the semiconducting layer, because the orientation and packing of semiconducting molecules is related to the substrate materials structure. One of the most common family used to chemically modify the silicon dioxide surface is alkylsilane. They react with the surface atoms by covalent bonds forming a monolayer with methyl as terminal group, which increase the surface hydrophobicity and affinity, an example of an alkylsilan used as SAM treatment is illustrated in **Figure 3.7**. More details on metal-semiconductor and semiconductor-dielectric interfaces will be reported in Chapter 5.

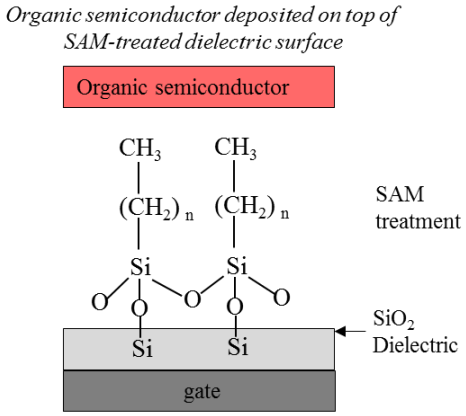

Figure 3.7. Schematic illustration of the formation of an alkylsiloxane SAM at the SiO_2 surface by chemical absorption of an alkyltrichlorosilane.

3.1.4. Ambipolar field-effect transistors

Organic ambipolar materials have attracted a great attention due to their low-cost construction, in several modern applications.[26] Organic ambipolar transistor employing solution processing techniques are of much interest for their ability to transport both holes and electrons in a single semiconductor channel.[27-29] In particular ambipolar transistor are utilized as a single active thin layer in

complementary inverters (CMOS) integrated in logic circuits.[30-31] The fact that ambipolar transistor is able to have both n- and p-type transports, the drain current is not identified by the same manner as unipolar transistors. The organic ambipolar transistor operation mode consists of different regimes, depending on the bias voltage difference between V_{GS}, V_{DS}, and $V_{th,h}$ and $V_{th,n}$ for holes and electrons accumulation respectively (the source electrode is grounded). More details on ambipolar transistors will be provided in Chapter 8.

Unipolar linear regime for electrons (at positive V_{GS} and V_{DS}): When $V_{DS} \leq (V_{GS} - V_{th,e})$ and $V_{GS} > V_{th,e}$, the major charges in the channel are electrons. The drain current is defined by the following equation:

$$I_D = \frac{W}{L} C_i \mu_e \left(V_{GS} - V_{th,e} - \frac{V_{DS}}{2}\right) V_{DS}$$

Unipolar saturation regime for electrons (at positive V_{GS} and V_{DS}): When $V_{DS} \geq (V_{GS} - V_{th,e})$ and V_{DS} $V_{GS} > V_{th,e}$, the electrons drain current saturates and in this case and the drain current is defined as:

$$I_D = \frac{W}{2L} C_i \mu_e (V_{GS} - V_{th,e})^2$$

When $V_{GS} < V_{th,e}$ and $V_{DS} < (V_{GS} - V_{th,h})$, no charge transport occurs into the channel ($I_{DS} = 0$).

When $V_{GS} < V_{th,e}$, and $V_{DS} \geq (V_{GS} - V_{th,h})$, the major charges in the channel are holes. In this case, the drain current can be described by the following equation:

$$I_D = \frac{W}{2L} C_i \mu_h (V_{DS} - (V_{GS} - V_{th,h}))^2$$

Ambipolar regime: When $V_{DS} \geq (V_{GS} - V_{th,h})$ and $V_{GS} \geq V_{th,e}$, In this regime, both source and drain metal electrodes inject one type of charges (holes or electrons) yield to the formation of conduction channel composed of both holes and electrons, that contribute to the drain current as illustrated in **Figure 3.8**. In contrast to unipolar regimes mentioned above, where the channel is formed by just one polarity charges. the drain current is described by the following equation:

$$I_D = \frac{W}{L} C_i \left(\mu_e (V_{GS} - V_{th,e})^2 + \mu_h (V_{DS} - (V_{GS} - V_{th,h}))^2\right)$$

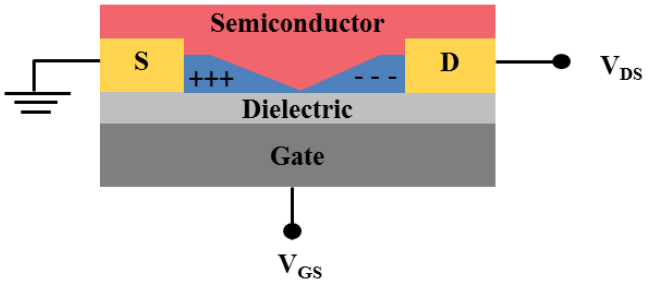

Figure 3.8. Schematic illustration of ambipolar transistor structure in ambipolar regime showing the presence of both electrons and holes in the conduction channel.

3.2. Organic phototransistors (OPTs)

3.2.1. Organic Phototransistor: device structure and operation mode

Organic phototransistors, i.e. OFETs transistor in which an incident light can be employed in addition to a gate field, and considered as the fourth external terminal, in the aim of modulating the charge-carrier density inside the channel. The OPT device can be used not only as signal amplifier, but specially as a light detector. From fundamental science to applications point of views, organic phototransistors have additional advantages over their inorganic counterparts, such as their molecular processability, properties tunability, and their possibility to be assembled on transparent and flexible supports giving rise to new opportunities towards optoelectronic applications.[32-41] Under light-illumination, the semiconductor absorbs light photons and extra charges are generated. These additional charges collected at the drain electrode will increase the measured drain current.[42] The organic phototransistor has similar structure (see **Figure 3.9**) and geometries compared to that of an organic OFET.

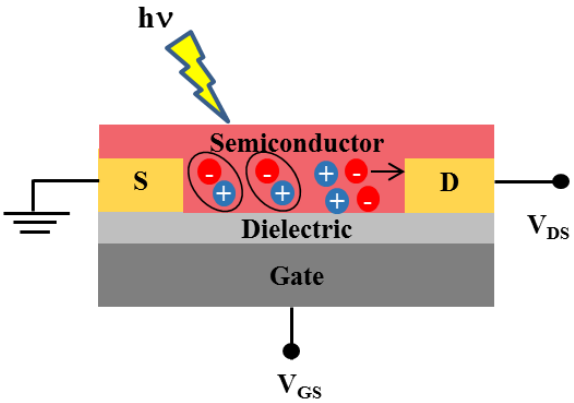

Figure 3.9. Schematic of an organic phototransistor device structures based on an n-type semiconductor under light irradiation, indicating the formed excitons (electron and hole pairs) that dissociate to free charges. The electron charges are moved towards the drain electrode.

3.2.2. Important OPT extracted parameters

The OPT device is characterized by output and transfer curves, from where, the different parameters described above (μ, V_{th}, and I_{on}/I_{off}) are extracted by the same way. Two additional important parameters are usually considered to determine the OPT performances: the photoresponsivity R and the photoswitching ratio, i.e. photosensitivity (P, photocurrent/dark-current). The R (measured in AW^{-1}) is used to provide the device light sensitivity and it's strongly dependent to the channel length. While, the photo-responsivity (P) indicates the drain signal increase upon light irradiation. They are determined by measuring the I-V characteristics in dark and under light irradiation. The R and P values are defined as followed:

$$R = \frac{(I_{light} - I_{dark})}{EWL}$$

$$P = \frac{(I_{light} - I_{dark})}{I_{dark}}$$

Where *W* and *L* are the channel width and length, *E* is the incident illumination power (areal) density on the channel of the device, I_{light} the drain current under illumination, and I_{dark} the drain current measured in dark conditions.

3.3. Organic complementary inverters

3.3.1. Organic inverter complementary device structure

An inverter is a basic unit in electronic logic circuits, it leads to logical inversion (0 - 1 / 1 - 0) of an input that is voltage in our case.[35] The inverter circuit is a key building block for digital electronic circuits and for analog amplifying circuit. Unipolar inverters are based on only p-type or n-type semiconductors. While, Complementary inverters comprised two p-type and n-type transistors (active and load). Organic complementary inverters are organic inverters based on organic n-channel and p-channel transistors. They can be fabricated by using one single organic ambipolar layer or two different organic materials for n- and p-type unipolar semiconductors. The organic complementary devices are characterized by contacting a common gate for both transistors served as the input terminal V_{IN}, a supply voltage (V_{DD}), and an output voltage (V_{OUT}) electrodes and applying positive or negative voltages on V_{DD} and V_{IN}, the resulting curve is called transfer voltage, which measures the output voltage V_{OUT} vs V_{IN}. **Figure 3.10** shows the organic complementary inverter structure and optical image, it presents also an example of an ideal transfer voltage curve.

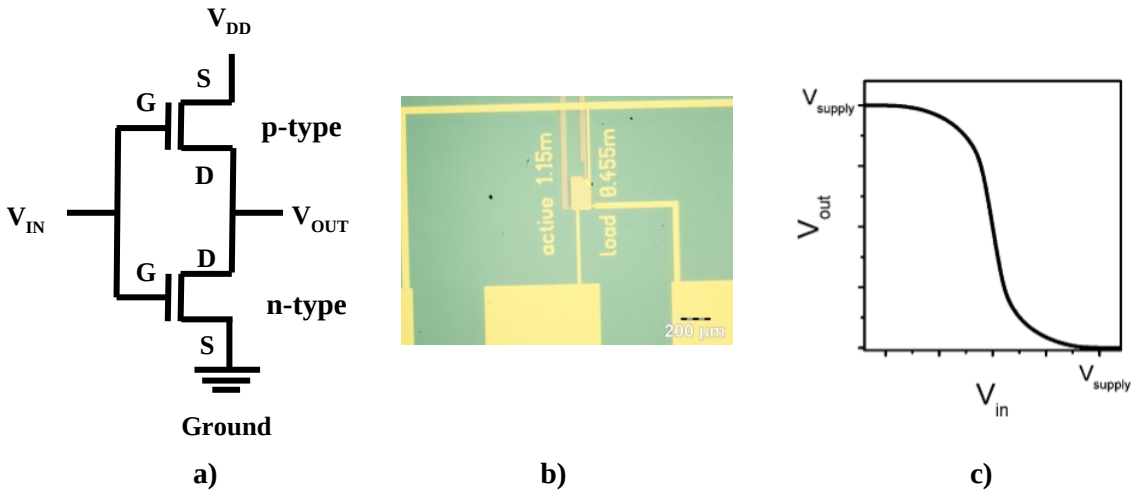

Figure 3.10. a) Schematic illustration of a complementary inverter structure **b)** an optical image of an inverter circuits based on a single ambipolar layer, and **c)** the transfer voltage curve of an ideal complementary inverter.[28]

3.3.2. Important organic inverter extracted parameters

Organic inverters key parameters, such as voltage gain, measured from the transfer voltage curve and defined as dV_{OUT}/dV_{IN}, noise margins, including noise margin low (NML) defined as NML = $V_{OL} - V_{IL}$, where V_{OL} is the Output Voltage Low and V_{IL} is the Input Voltage Low, and noise margin high (NMH), defined as NMH = $V_{OH} - V_{IH}$, where V_{OH} is the Output Voltage High and V_{IH} is the Input Voltage High are extracted from the voltage transfer curve (see **Figure 3.11**). it is known that high OFETs mobilities and I_{on}/I_{off} ratio are considered as the main factors recommended to have high gain voltage and noise margin.

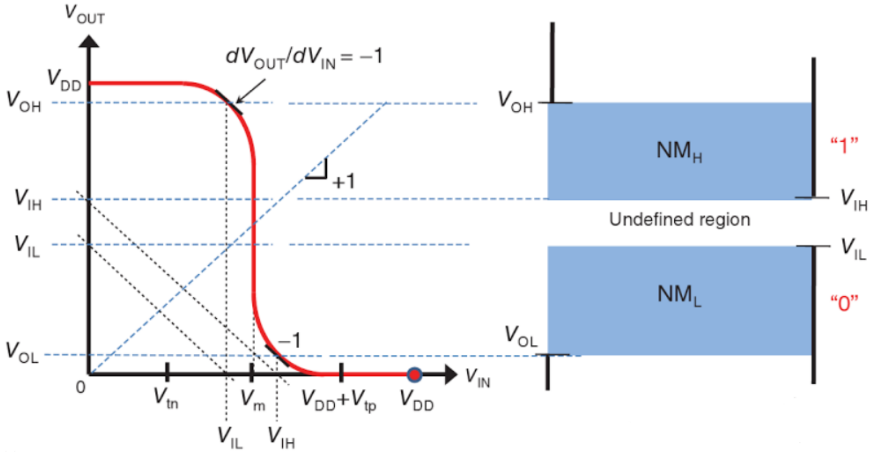

Figure 3.11. The transfer voltage curve indicating the different parameters (V_{OL}, V_{OH}, V_{IL}, V_{IH}) needed to calculate noise margins (high and low) as well as the switching threshold voltage (V_m).

The highest dc gain corresponds to the inverter switching point called also the switching threshold voltage (V_m), which is the point at the intersection in the voltage transfer curve when V_{IN} is equal to V_{OUT}. At this point both n- and p-type operate at the saturation region, the switching threshold voltage of an ideal inverters should be equal to ½ V_{DD}.

In literature, high performance organic complementary inverters have been fabricated using identical ambipolar FET transistors,[31] or by combining n and p semiconductors which gives rise to high gain voltage, and noise margin,[43-44] several examples and more details on organic complementary inverters will be discussed in Chapter 8.

Conclusion

The use of organic semiconductor materials in electronic technology continued to evolve. Strong efforts in the organic based electronics developments are devoted in laboratories environment to be commercialized in near future. In this chapter, we have presented a short description on organic transistors, phototransistors and complementary inverters. We have described their working principle and defined key parameters such as mobility, threshold voltage, I_{on}/I_{off} ratio, photoresponsivity (P), photosensitivity (R), voltage gain and noise margin. Different interfaces and factors that affect their efficiency and electrical performances have been explored.

3.4. References

1. Lilienfeld, J. E., Method and Apparatus for Controlling Electric Currents. *U. S. Patent* **1930**, 1, 745, 175.

2. Kahng, D.; Atalla, M. M., Silicon–Silicon Dioxide Field Induced Surface Devices. *in IRE Solid-State Device Research Conference, Pittsburgh, PA* **1960**.

3. Horowitz, G.; Fichou, D.; Peng, X. Z.; Xu, Z. G.; Garnier, F., A Field-Effect Transistor Based on Conjugated alpha-Sexithienyl. *Solid State Commun.* **1989,** *72* (4), 381-384.

4. Koezuka, H.; Tsumura, A.; Ando, T., Field-Effect Transistor with Polythiophene Thin-Film. *Synth. Met.* **1987,** *18* (1-3), 699-704.

5. Tian, H. K.; Shi, J. W.; Yan, D. H.; Wang, L. X.; Geng, Y. H.; Wang, F. S., Naphthyl end-Capped Quarterthiophene: A Simple Organic Semiconductor with High Mobility and Air Stability. *Adv. Mater.* **2006,** *18* (16), 2149-2152.

6. Facchetti, A., Semiconductors for Organic Transistors. *Mater. Today* **2007,** *10* (3), 28-37.

7. Gao, X. K.; Di, C. A.; Hu, Y. B.; Yang, X. D.; Fan, H. Y.; Zhang, F.; Liu, Y. Q.; Li, H. X.; Zhu, D. B., Core-Expanded Naphthalene Diimides Fused with 2-(1,3-Dithiol-2-Ylidene)Malonitrile Groups for High-

Performance, Ambient-Stable, Solution-Processed n-Channel Organic Thin Film Transistors. *J. Am. Chem. Soc.* **2010,** *132* (11), 3697-3699.

8. Torsi, L.; Farinola, G. M.; Marinelli, F.; Tanese, M. C.; Omar, O. H.; Valli, L.; Babudri, F.; Palmisano, F.; Zambonin, P. G.; Naso, F., A Sensitivity-Enhanced Field-Effect Chiral Sensor. *Nat. Mater.* **2008,** *7* (5), 412-417.

9. Caboni, A.; Orgiu, E.; Scavetta, E.; Barbaro, M.; Bonfiglio, A., Organic-Based Sensor for Chemical Detection in Aqueous Solution. *Appl. Phys. Lett.* **2009,** *95* (12), 123304-123304-3.

10. Arias, A. C.; MacKenzie, J. D.; McCulloch, I.; Rivnay, J.; Salleo, A., Materials and Applications for Large Area Electronics: Solution-Based Approaches. *Chem Rev* **2010,** *110* (1), 3-24.

11. Caboni, A.; Orgiu, E.; Barbaro, M.; Bonfiglio, A., Flexible Organic Thin-Film Transistors for pH Monitoring. *Ieee Sens. J.* **2009,** *9* (12), 1963-1970.

12. Dimitrakopoulos, C. D.; Malenfant, P. R. L., Organic Thin Film Transistors for Large Area Electronics. *Adv. Mater.* **2002,** *14* (2), 99-117.

13. Brabec, C. J.; Cravino, A.; Meissner, D.; Sariciftci, N. S.; Fromherz, T.; Rispens, M. T.; Sanchez, L.; Hummelen, J. C., Origin of the Open Circuit Voltage of Plastic Solar Cells. *Adv. Funct. Mater.* **2001,** *11* (5), 374-380.

14. Burroughes, J. H.; Bradley, D. D. C.; Brown, A. R.; Marks, R. N.; Mackay, K.; Friend, R. H.; Burn, P. L.; Holmes, A. B., Light-Emitting-Diodes Based on Conjugated Polymers. *Nature* **1990,** *347* (6293), 539-541.

15. Greenham, N. C.; Moratti, S. C.; Bradley, D. D. C.; Friend, R. H.; Holmes, A. B., Efficient Light-Emitting-Diodes Based on Polymers with High Electron-Affinities. *Nature* **1993,** *365* (6447), 628-630.

16. Sendler, T.; Luka-Guth, K.; Wieser, M.; Lokamani; Wolf, J.; Helm, M.; Gemming, S.; Kerbusch, J.; Scheer, E.; Huhn, T.; Erbe, A., Light-Induced Switching of Tunable Single-Molecule Junctions. *Adv. Sci.* **2015,** *2* (5).

17. Burgi, L.; Richards, T. J.; Friend, R. H.; Sirringhaus, H., Close Look at Charge Carrier Injection in Polymer Field-Effect Transistors. *J. Appl. Phys.* **2003,** *94* (9), 6129-6137.

18. Hamadani, B. H.; Gundlach, D. J.; McCulloch, I.; Heeney, M., Undoped Polythiophene Field-Effect Transistors with Mobility of 1 cm(2) V(-1) s(-1). *Appl. Phys. Lett.* **2007,** *91* (24), 3.

19. Sze, S. M., *Physics of semiconductor devices, 2nd ed., John Wiley, New York* **1981**.

20. Necliudov, P. V.; Shur, M. S.; Gundlach, D. J.; Jackson, T. N., Contact Resistance Extraction in Pentacene Thin Film Transistors. *Solid-State Electron.* **2003,** *47* (2), 259-262.

21. Zaumseil, J.; Baldwin, K. W.; Rogers, J. A., Contact Resistance in Organic Transistors that Use Source and Drain Electrodes Formed by Soft Contact Lamination. *J. Appl. Phys.* **2003,** *93* (10), 6117-6124.

22. Klauk, H.; Schmid, G.; Radlik, W.; Weber, W.; Zhou, L. S.; Sheraw, C. D.; Nichols, J. A.; Jackson, T. N., Contact Resistance in Organic Thin Film Transistors. *Solid-State Electron.* **2003,** *47* (2), 297-301.

23. Meijer, E. J.; Gelinck, G. H.; van Veenendaal, E.; Huisman, B. H.; de Leeuw, D. M.; Klapwijk, T. M., Scaling Behavior and Parasitic Series Resistance in Disordered Organic Field-Effect Transistors. *Appl. Phys. Lett.* **2003,** *82* (25), 4576-4578.

24. Ishii, H.; Hayashi, N.; Ito, E.; Washizu, Y.; Sugi, K.; Kimura, Y.; Niwano, M.; Ouchi, Y.; Seki, K., Kelvin Probe Study of Band Bending at Organic Semiconductor/Metal Interfaces: Examination of Fermi Level Alignment. *Physica Status Solidi a-Applied Research* **2004,** *201* (6), 1075-1094.

25. Zhang, Z.; Yates, J. T., Band Bending in Semiconductors: Chemical and Physical Consequences at Surfaces and Interfaces. *Chem. Rev.* **2012,** *112* (10), 5520-5551.

26. Baeg, K. J.; Caironi, M.; Noh, Y. Y., Toward Printed Integrated Circuits Based on Unipolar or Ambipolar Polymer Semiconductors. *Adv. Mater.* **2013,** *25* (31), 4210-4244.

27. Zhao, Y.; Guo, Y. L.; Liu, Y. Q., 25th Anniversary Article: Recent Advances in n-Type and Ambipolar Organic Field-Effect Transistors. *Adv. Mater.* **2013,** *25* (38), 5372-5391.

28. Zaumseil, J.; Sirringhaus, H., Electron and Ambipolar Transport in Organic Field-Effect Transistors. *Chem. Rev.* **2007,** *107* (4), 1296-1323.

29. Smits, E. C. P.; Anthopoulos, T. D.; Setayesh, S.; van Veenendaal, E.; Coehoorn, R.; Blom, P. W. M.; de Boer, B.; de Leeuw, D. M., Ambipolar Charge Transport in Organic Field-Effect Transistors. *Phys. Rev. B* **2006,** *73* (20).

30. Singh, T. B.; Senkarabacak, P.; Sariciftci, N. S.; Tanda, A.; Lackner, C.; Hagelauer, R.; Horowitz, G., Organic Inverter Circuits Employing Ambipolar Pentacene Field-Effect Transistors. *Appl. Phys. Lett.* **2006,** *89* (3).

31. Petritz, A.; Fian, A.; Glowacki, E. D.; Sariciftci, N. S.; Stadlober, B.; Irimia-Vladu, M., Ambipolar Inverters with Natural Origin Organic Materials as Gate Dielectric and Semiconducting layer. *Phys. Status Solidi-Rapid Res. Lett.* **2015,** *9* (6), 358-361.

32. Cavallini, M.; Gentili, D.; Greco, P.; Valle, F.; Biscarini, F., Micro- and Nanopatterning by Lithographically Controlled Wetting. *Nat. Protoc.* **2012,** *7* (9), 1668-1676.

33. Cavallini, M.; D'Angelo, P.; Criado, V. V.; Gentili, D.; Shehu, A.; Leonardi, F.; Milita, S.; Liscio, F.; Biscarini, F., Ambipolar Multi-Stripe Organic Field-Effect Transistors. *Adv. Mater.* **2011,** *23* (43), 5091-5097.

34. Qi, Z.; Liao, X. X.; Zheng, J. C.; Di, C. A.; Gao, X. K.; Wang, J. Z., High-Performance n-Type Organic Thin-Film Phototransistors Based on a Core-Expanded Naphthalene Diimide. *Appl. Phys. Lett.* **2013,** *103* (5), 053301.

35. Guo, N.; Hu, W. D.; Liao, L.; Yip, S.; Ho, J. C.; Miao, J. S.; Zhang, Z.; Zou, J.; Jiang, T.; Wu, S. W.; Chen, X. S.; Lu, W., Anomalous and Highly Efficient InAs Nanowire Phototransistors Based on Majority Carrier Transport at Room Temperature. *Adv. Mater.* **2014,** *26* (48), 8203-8209.

36. Kim, J.; Cho, S.; Kim, Y. H.; Park, S. K., Highly-Sensitive Solution-Processed 2,8-difluoro-5,11-bis(triethylsilylethynyl) Anthradithiophene (diF-TESADT) Phototransistors for Optical Sensing Applications. *Org. Electron.* **2014,** *15* (9), 2099-2106.

37. Kim, M.; Ha, H. J.; Yun, H. J.; You, I. K.; Baeg, K. J.; Kim, Y. H.; Ju, B. K., Flexible Organic Phototransistors Based on a Combination of Printing Methods. *Org. Electron.* **2014,** *15* (11), 2677-2684.

38. Loffredo, F.; Bruno, A.; Del Mauro, A. D.; Grimaldi, I. A.; Miscioscia, R.; Nenna, G.; Pandolfi, G.; Petrosino, M.; Villani, F.; Minarini, C.; Facchetti, A., Photoresponse of Pentacene-Based Transistors. *Phys. Status Solidi A* **2014,** *211* (2), 460-466.

39. Yang, D.; Zhang, L.; Wang, H. W.; Wang, Y. S.; Li, Z. X.; Song, T. J.; Fu, C. J.; Yang, S. Y.; Zou, B. S., Pentacene-Based Photodetector in Visible Region With Vertical Field-Effect Transistor Configuration. *IEEE Photonics Technol. Lett.* **2015,** *27* (3), 233-236.

40. Li, M. M.; An, C. B.; Marszalek, T.; Guo, X.; Long, Y. Z.; Yin, H. X.; Gu, C. Z.; Baumgarten, M.; Pisula, W.; Müllen, K., Phenanthrene Condensed Thiadiazoloquinoxaline Donor-Acceptor Polymer for Phototransistor Applications. *Chem. Mat.* **2015,** *27* (6), 2218-2223.

41. Ljubic, D.; Smithson, C. S.; Wu, Y. L.; Zhu, S. P., Highly UV-Sensitive and Responsive Benzothiophene/Dielectric Polymer Blend-Based Organic Thin-Film Phototransistor. *Adv. Electron. Mater.* **2015,** *1* (8).

42. Konstantatos, G.; Sargent, E. H., Nanostructured Materials for Photon Detection (vol 5, pg 391, 2010). *Nat. Nanotechnol.* **2010,** *5* (12), 1.

43. An, M. J.; Seo, H. S.; Zhang, Y.; Oh, J. D.; Choi, J. H., Air Stable, Ambipolar Organic Transistors and Inverters Based Upon a Heterojunction Structure of Pentacene on N,N '-ditridecylperylene-3,4,9,10-tetracarboxylic di-imide. *Appl. Phys. Lett.* **2010,** *97* (2).

44. Vaklev, N. L.; Yang, Y.; Muir, B. V. O.; Steinke, J. H. G.; Campbell, A. J., Bottom-Gate Complementary Inverters on Plastic With Gravure-Printed Dielectric and Semiconductors. *IEEE Trans. Electron Devices* **2015,** *62* (11), 3820-3824.

Chapter 4. Organic semiconductors and molecules encompassed in this study

Introduction

In recent years, the progress in synthetic chemistry of conjugated small molecules/oligomers and polymers have made terrific improvements leading to both tuning of their physical chemistry and materials thereof, and enabling solution processibility. The latter opened the door to the use of low-cost solution processing techniques, as spin-coating, drop-casting, dip-casting or inkjet-printing, to form active materials for organic field effect transistors (OFETs).[1] The performance of OFETs in the last 20 years has enormously improved. The first OFET was reported in 1986 and was based on a film of electrochemically grown polythiophene. Four years later, the first OFET employing a conjugated oligomer (sexithiophene) was fabricated.[2] Typically, transistors based on small molecules exhibit higher mobility and better semiconducting characteristics than polymer semiconductors, due to their higher molecular ordering and their ability to form a well-ordered, polycrystalline films upon vacuum deposition but also from solvent induced precipitation, spin-coating and drop-casting. Polymers possess longer chains and have better solubility when compared to small molecules while the properties of oligomers are intermediate between those of small molecules and polymers. In this chapter, we present and describe the different organic (semiconducting) materials employed throughout the preparation of the doctoral thesis; n-type perylene and fullerene derivatives and an ambipolar semiconductor polymer, with diarylethene molecules integrated into its semiconductor layer, to change its properties upon light irradiation and perform opto-controlled multi-functional organic electronic based devices.

4.1. The studied organic semiconductors

Our work focuses on organic-based electronic devices using different organic materials, processed from solution in different ways and characterized optically, electrically and supported by morphology analysis. These molecules are very promising for applications in real electronics.

4.1.1. N,N'-1H,1H-perfluorobutyldicyanoperylene-carboxydi-imide (PDIF-CN2)

The perylene di-imide (PDI) family holds the distinction of having one of the highest n-type mobilities known in organic electronics particularly those core-functionalized with cyano groups such as PDIR-CN2, are promising materials for electronic and optoelectronic applications due to their ability to yield high performing semiconductors films from solution and to their air-stable device operation.[3-6]. Both the film forming properties and the ambient stability of these molecules arise from the cyano-functionalization of the perylene core which increases the solubility by decreasing the core planarity and stabilizes the charge carriers by lowering the energies of the lowest unoccupied molecular orbital that is associated with electron transport. In core-cyanated perylenes, the LUMO energetic levels are shifted down by 0.4-0.6 eV in comparison with the unsubstituted systems which prevents them from interacting with oxygen and water therefore reducing the degradation issues.[7] The presence of fluroalkyl and cyano substituents leads very high electron mobility values, great reproducibility, which makes PDIF-CN2 a candidate to carry out fundamental studies of electron transport.[8]

The PDIF-CN2 molecule, is stable at room temperature in closed containers under normal storage and handling conditions, this molecule is soluble in organic solvents. The molecular structure is displayed in **Figure 4.1**. This molecule requires sometimes complicated synthetic protocols.[4] In this thesis, typical electrical characteristics of PDIF-CN2 FETs are measured in air and in vacuum inside a glovebox in a nitrogen filled environment.

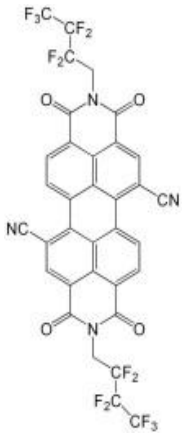

Figure 4.1. Chemical structure of the organic semiconductor PDIF-CN2.

4.1.2. 1',1",4',4"-tetrahydro-di[1,4]methanonaphthaleno[1,2:2',3',56,6':2",3"][5,6] fullerene-C60 (ICBA)

Fullerenes are capable of efficient charge and exciton transport and have therefore gained scientific interest because of their potential use in low-cost electronic device applications.[9] Thus, a variety of potential molecular derivatives has been designed, synthesized, and studied. [6,6]-phenyl-C60 butyric acid methyl ester (PCBM) and phenyl-C71-butyric acid methyl ester (PCBM70) are the most commonly used acceptor materials, respectively. New alternative acceptors are the higher adducts of fullerene derivatives, and have driven the steady enhancement of organic solar cells.[10] One such potential acceptor is indene-C60-bisadduct (ICBA) 1',1",4',4"-tetrahydro-di[1,4]methanonaphthaleno[1,2:2',3',56,6':2",3"][5,6]fullerene-C60 (see **Figure 4.2**), with the LUMO level of 3.74 eV, which is up-shifted by 0.17 eV than PCBM,[11] has demonstrated excellent photovoltaic performance[12-14] once combined with hole-transporting materials in heterojunction solar cells and organic photovoltaics.[15] In our work, we investigate the effect of the annealing temperature of the above-mentioned fullerene molecule that has been purchased from Sigma-Aldrich, and correlate the film morphology with the transport of both electrons and holes in thin-film based transistors.

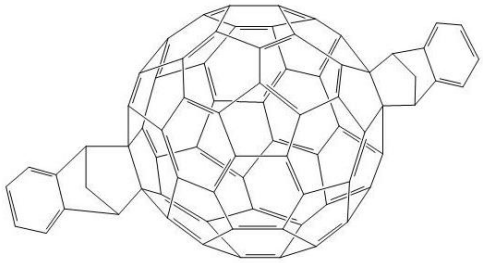

Figure 4.2. Chemical structure of indene-C60-bisadduct (ICBA) organic semiconductor.

4.1.3. Poly(2,5-bis(2-octyldodecyl)-3-(5-(thieno[3,2-b]thiophen-2,5-yl)thiophen-2-yl)-6 (thiophen-2,5-yl)pyrrolo[3,4-c]pyrrole-1,4(2H,5H)-dione) (DPPT-TT)

Organic ambipolar materials have reached much attention to construct the low-cost, flexible displays and large-area electronic products.[16-17] Organic ambipolar semiconductor materials with high electron and hole mobilities processed with simple and cheap solution preparation procedure are of interest for complementary-like logic circuits[18-22] and light-emitting organic field-effect transistors.[23-26] One of the most investigated and promising class of state-of-the-art conjugated polymers, optimized for either p-channel or n-channel OFET operation, achieve high and balanced holes and electrons field-effect mobilities on the order of 1 $cm^2V^{-1}s^{-1}$ is the diketopyrrolopyrrole (DPP)-based donor-

acceptor (D-A) conjugated copolymers.[27-29] The DPP core having a planar skeleton is an acceptor unit with various branched alkyl groups into the two N-positions. Different thiophene-based donor monomers and strong-electron-donating moieties have been employed in DPP-based copolymers in the literature.[29-30] When DPP is used as a strong acceptor unit in D-A alternating copolymers, the DPP building block enables very narrow-band copolymers and enhances the intermolecular interactions with a strong intermolecular overlap through π–π stacking, which offers an attractive n-type and p-type charge transport performance with high balanced ambipolar properties in organic field-effect transistors[24] and organic photovoltaics.[31] DPP-based copolymers solubility can be enhanced and controlled via side-chain engineering. Beside the suitable energy levels, DPP-based conjugated polymers are highly semicrystalline and highly ordered packing with different orientations on the substrate, this also favor the high and balanced OFETs ambipolar performances. Among organic synthetized polymers compressing diketopyrrolopyrrole (DPP), we have used DPPT-TT ambipolar polymer with two thiophene moieties in the repeated unit, called Diketopyrrole-Thieno[3,2-b]thiophene Copolymer (DPPT-TT)[32] (see **Figure 4.3**) in order to investigate its physical properties and device performance in multicomponent-based thin-film transistors and organic complementary inverters. This polymer is highly soluble in common organic solvents such as chloroform, chlorobenzene and toluene after a gentle annealing or a stirring process at room temperature. DPPT-TT polymer has been studied in literature in different OFET architectures and showed high efficient electron and hole field-effect mobilities comparable to the state of the art performing polymer semiconductors. DPPT-TT was thus interpreted as a predominantly hole-transporting polymer, in this thesis, we reinvestigate the DPPT-TT charge transport and ambipolar properties once incorporated in bi-and three-component active layer by optimizing device fabrication and processing materials and surfaces.

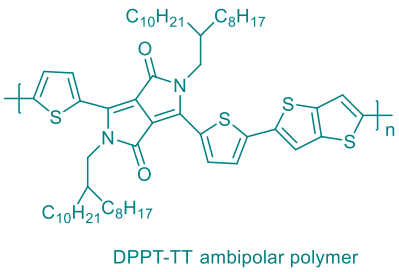

Figure 4.3. Molecular structures of [3,2-b] thiophene Copolymer (DPPT-TT).

4.2. Organic photochromic molecules: Diarylethenes

Photochromic molecules undergo reversible photoinduced isomerization between two (meta)stable isomers that can feature different physical and chemical properties such as absorption,

dipole moments and electronic structure.[33-34-35] Various popular classes of photochromic molecules are of interest of scientists for their potential applications as rewritable optical data storage and electronic devices.[36-38] Molecules exhibiting this behavior attract much interest as they can be used as molecular switches in larger systems. Some of the most promising candidates for photochromic molecules are diarylethene derivatives[33] due to their good thermal stability and fatigue resistance,[39] contrary to that of spiropyrans and azobenzenes. Diarylethenes are a class of photochromic compounds that consist of two aromatic groups connected to a central olefin. However, the use of a cyclic olefin photochemical excitation cannot result in *cis–trans* isomerization. Instead, the photochromic diarylethene will undergo a conrotatory six-electron electrocyclization which results in the formation of a ring-closed isomer. The most used molecular design for diarylethenes is comprised of two substituted thiophene moieties, as diarylethenes are bi-stable systems, they can be synthesized in both open or closed forms. In particular, diarylethene moieties possess different band gap and associated highest occupied molecular orbital (HOMO) and lowest unoccupied molecular orbital (LUMO) levels, depending on their stronger (closed form) or weaker (open form) degree of conjugation, that can be controlled upon irradiation at different wavelengths.[40-41] In this study, we report on the integration of two diarylethene synthesized derivatives, i.e. DAE_tBu (1,2-Bis(5-(3,5-di-tert-butylphenyl)-2-methylthiophen-3-yl)cyclopent-1-ene) (see **Figure 4.4a**) and DAE_F (1,2-Bis(2-(3,5-bis(trifluoromethyl)phenyl)-5-methylthiazol-4-yl)perfluorocyclopent-1-ene) (**Figure 4.4b**), with large fatigue resistance[39] into Diketopyrrolopyrrole derivative, to form multi-component switchable devices.

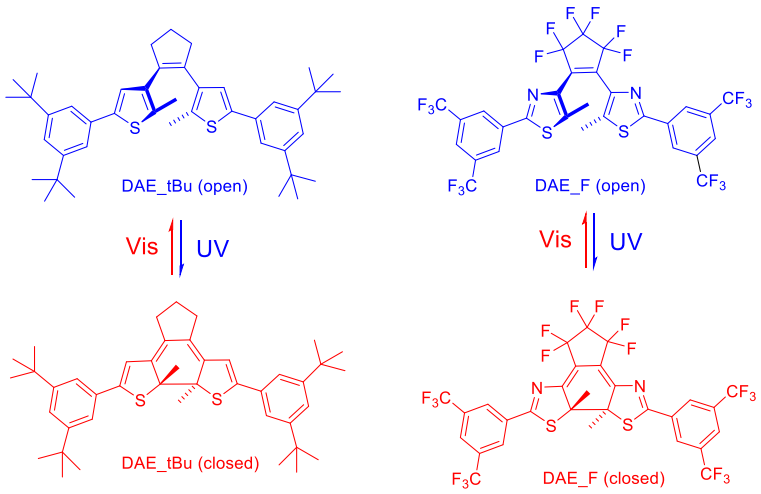

a) **b)**

Figure 4.4. Molecular structure of photochromic molecules: **a)** DAE_tBu and **b)** DAE_F in their open and closed forms.

Conclusions

The big challenge in the world of organic electronic technology is how to design, build and optimize high performance electronic devices with simpler fabrication methods and the ability to be mechanically flexible using cheap and simple processes such as spin-coating, drop casting, which do not require high-end clean room laboratories and giving rise to fast and inexpensive coverage over large areas. Towards this end, different highly performed organic semiconductor materials (n-type, p-type and ambipolar charge transport) that are small molecules, oligomers and polymers have been synthesized and studied, taking in account their optical, morphological and physical properties. In this chapter, we presented the different organic semiconductor molecules used in this thesis work, and described their chemical properties and interest use in electronic area. The Liquid processing and flexible organic materials make them highly favorable for electronic devices used in different applications and could compete in near future silicon-based inorganic electronics, great efforts are devoted to this purpose.

4.3. References

1. Mas-Torrent, M.; Rovira, C., Novel Small Molecules for Organic Field-Effect Transistors: Towards Processability and High Performance. *Chem. Soc. Rev.* **2008,** *37* (4), 827-838.
2. Tsumura, A.; Koezuka, H.; Ando, T., Macromolecular Electronic Device-Field-Effect Transistor with Polythiophene Thin-film *Appl. Phys. Lett.* **1986,** *49* (18), 1210-1212.
3. Schmidt, R.; Oh, J. H.; Sun, Y.-S.; Deppisch, M.; Krause, A.-M.; Radacki, K.; Braunschweig, H.; Koenemann, M.; Erk, P.; Bao, Z.; Würthner, F., High-Performance Air-Stable n-Channel Organic Thin Film Transistors Based on Halogenated Perylene Bisimide Semiconductors. *J. Am. Chem. Soc.* **2009,** *131* (17), 6215-6228.
4. Ling, M. M.; Erk, P.; Gomez, M.; Koenemann, M.; Locklin, J.; Bao, Z. N., Air-Stable n-Channel Organic Semiconductors Based on Perylene Diimide Derivatives Without Strong Electron Withdrawing Groups. *Adv. Mater.* **2007,** *19* (8), 1123-1127.
5. Yoo, B.; Jones, B. A.; Basu, D.; Fine, D.; Jung, T.; Mohapatra, S.; Facchetti, A.; Dimmler, K.; Wasielewski, M. R.; Marks, T. J.; Dodabalapur, A., High-Performance Solution-Deposited n-Channel Organic Transistors and Their Complementary Circuits. *Adv. Mater.* **2007,** *19* (22), 4028-4032.
6. Weitz, R. T.; Amsharov, K.; Zschieschang, U.; Villas, E. B.; Goswami, D. K.; Burghard, M.; Dosch, H.; Jansen, M.; Kern, K.; Klauk, H., Organic n-Channel Transistors Based on Core-Cyanated Perylene Carboxylic Diimide Derivatives. *J. Am. Chem. Soc.* **2008,** *130* (14), 4637-4645.
7. Barra, M.; Di Girolamo, F. V.; Chiarella, F.; Salluzzo, M.; Chen, Z.; Facchetti, A.; Anderson, L.; Cassinese, A., Transport Property and Charge Trap Comparison for N-Channel Perylene Diimide Transistors with Different Air-Stability. *J. Phys. Chem. C* **2010,** *114* (48), 20387-20393.

8. Minder, N. A.; Ono, S.; Chen, Z. H.; Facchetti, A.; Morpurgo, A. F., Band-Like Electron Transport in Organic Transistors and Implication of the Molecular Structure for Performance Optimization. *Adv. Mater.* **2012,** *24* (4), 503-508.

9. Faist, M. A.; Shoaee, S.; Tuladhar, S.; Dibb, G. F. A.; Foster, S.; Gong, W.; Kirchartz, T.; Bradley, D. D. C.; Durrant, J. R.; Nelson, J., Understanding the Reduced Efficiencies of Organic Solar Cells Employing Fullerene Multiadducts as Acceptors. *Adv. Energy Mater.* **2013,** *3* (6), 744-752.

10. Kyaw, A. K. K.; Gehrig, D.; Zhang, J.; Huang, Y.; Bazan, G. C.; Laquai, F.; Nguyen, T. Q., High Open-Circuit Voltage Small-Molecule p-DTS(FBTTh2)(2):ICBA Bulk Heterojunction Solar Cells-Morphology, Excited-State Dynamics, and Photovoltaic Performance. *J. Mater. Chem. A* **2015,** *3* (4), 1530-1539.

11. Sharma, R.; Lee, H.; Gupta, V.; Kim, H.; Kumar, M.; Sharma, C.; Chand, S.; Yoo, S.; Gupta, D., Photo-Physics of PTB7, PCBM and ICBA Based Ternary Solar Cells. *Org. Electron.* **2016,** *34*, 111-117.

12. Voroshazi, E.; Vasseur, K.; Aernouts, T.; Heremans, P.; Baumann, A.; Deibel, C.; Xue, X.; Herring, A. J.; Athans, A. J.; Lada, T. A.; Richter, H.; Rand, B. P., Novel bis-C-60 Derivative Compared to Other Fullerene bis-Adducts in High Efficiency Polymer Photovoltaic Cells. *J. Mater. Chem.* **2011,** *21* (43), 17345-17352.

13. Hoke, E. T.; Vandewal, K.; Bartelt, J. A.; Mateker, W. R.; Douglas, J. D.; Noriega, R.; Graham, K. R.; Fréchet, J. M. J.; Salleo, A.; McGehee, M. D., Recombination in Polymer:Fullerene Solar Cells with Open-Circuit Voltages Approaching and Exceeding 1.0 V. *Adv. Energy Mater.* **2013,** *3* (2), 220-230.

14. Shoaee, S.; Subramaniyan, S.; Xin, H.; Keiderling, C.; Tuladhar, P. S.; Jamieson, F.; Jenekhe, S. A.; Durrant, J. R., Charge Photogeneration for a Series of Thiazolo-Thiazole Donor Polymers Blended with the Fullerene Electron Acceptors PCBM and ICBA. *Adv. Funct. Mater.* **2013,** *23* (26), 3286-3298.

15. Huang, W. C.; Gann, E.; Thomsen, L.; Tadich, A.; Cheng, Y. B.; McNeill, C. R., Metal Evaporation-Induced Degradation of Fullerene Acceptors in Polymer/Fullerene Solar Cells. *ACS Appl. Mater. Interfaces* **2016,** *8* (3), 2247-2254.

16. Baeg, K. J.; Caironi, M.; Noh, Y. Y., Toward Printed Integrated Circuits Based on Unipolar or Ambipolar Polymer Semiconductors. *Adv. Mater.* **2013,** *25* (31), 4210-4244.

17. Ha, T. J.; Sonar, P.; Cobb, B.; Dodabalapur, A., Charge Transport and Density of Trap States in Balanced High Mobility Ambipolar Organic Thin-Film Transistors. *Org. Electron.* **2012,** *13* (1), 136-141.

18. Singh, T. B.; Senkarabacak, P.; Sariciftci, N. S.; Tanda, A.; Lackner, C.; Hagelauer, R.; Horowitz, G., Organic Inverter Circuits Employing Ambipolar Pentacene Field-Effect Transistors. *Appl. Phys. Lett.* **2006,** *89* (3).

19. Petritz, A.; Fian, A.; Glowacki, E. D.; Sariciftci, N. S.; Stadlober, B.; Irimia-Vladu, M., Ambipolar Inverters with Natural Origin Organic Materials as Gate Dielectric and Semiconducting layer. *Phys. Status Solidi-Rapid Res. Lett.* **2015,** *9* (6), 358-361.

20. Gundlach, D. J.; Pernstich, K. P.; Wilckens, G.; Gruter, M.; Haas, S.; Batlogg, B., High Mobility n-Channel Organic Thin-Film Transistors and Complementary Inverters. *J. Appl. Phys.* **2005,** *98* (6).

21. Zhang, X. H.; Potscavage, W. J.; Choi, S.; Kippelen, B., Low-voltage flexible organic Complementary Inverters with High Noise Margin and High dc Gain. *Appl. Phys. Lett.* **2009,** *94* (4).

22. Sonar, P.; Singh, S. P.; Li, Y.; Soh, M. S.; Dodabalapur, A., A Low-Bandgap Diketopyrrolopyrrole-Benzothiadiazole-Based Copolymer for High-Mobility Ambipolar Organic Thin-Film Transistors. *Adv. Mater.* **2010,** *22* (47), 5409-5413.

23. Capelli, R.; Toffanin, S.; Generali, G.; Usta, H.; Facchetti, A.; Muccini, M., Organic Light-Emitting Transistors with an Efficiency that Outperforms the Equivalent Light-Emitting Diodes. *Nat. Mater.* **2010,** *9* (6), 496-503.

24. Tieke, B.; Rabindranath, A. R.; Zhang, K.; Zhu, Y., Conjugated Polymers Containing diketopyrrolopyrrole Units in the Main Chain. *Beilstein J. Org. Chem.* **2010,** *6*, 830-845.

25. Steckler, T. T.; Lee, M. J.; Chen, Z.; Fenwick, O.; Andersson, M. R.; Cacialli, F.; Sirringhaus, H., Multifunctional Materials for OFETs, LEFETs and NIR PLEDs. *J. Mater. Chem. C* **2014,** *2* (26), 5133-5141.

26. Gwinner, M. C.; Khodabakhsh, S.; Giessen, H.; Sirringhaus, H., Simultaneous Optimization of Light Gain and Charge Transport in Ambipolar Light-Emitting Polymer Field-Effect Transistors. *Chem. Mat.* **2009,** *21* (19), 4425-4433.

27. Donaghey, J. E.; Sohn, E. H.; Ashraf, R. S.; Anthopoulos, T. D.; Watkins, S. E.; Song, K.; Williams, C. K.; McCulloch, I., Pyrroloindacenodithiophene Polymers: the Effect of Molecular Structure on OFET Performance. *Polym. Chem.* **2013,** *4* (12), 3537-3544.

28. Lee, D. H.; Shin, J.; Cho, M. J.; Choi, D. H., High-Performance Low-Bandgap Conjugated Polymers Bearing Diethynylanthracene Units for Thin-Film Transistors. *Chem. Commun.* **2013,** *49* (37), 3896-3898.

29. Li, Y. N.; Sonar, P.; Singh, S. P.; Soh, M. S.; van Meurs, M.; Tan, J., Annealing-Free High-Mobility Diketopyrrolopyrrole-Quaterthiophene Copolymer for Solution-Processed Organic Thin Film Transistors. *J. Am. Chem. Soc.* **2011,** *133* (7), 2198-2204.

30. Li, W. W.; Hendriks, K. H.; Wienk, M. M.; Janssen, R. A. J., Diketopyrrolopyrrole Polymers for Organic Solar Cells. *Accounts Chem. Res.* **2016,** *49* (1), 78-85.

31. Jung, J. W.; Liu, F.; Russell, T. P.; Jo, W. H., A high Mobility Conjugated Polymer Based on Dithienothiophene and Diketopyrrolopyrrole for Organic Photovoltaics. *Energy Environ. Sci.* **2012,** *5* (5), 6857-6861.

32. Chen, Z. Y.; Lee, M. J.; Ashraf, R. S.; Gu, Y.; Albert-Seifried, S.; Nielsen, M. M.; Schroeder, B.; Anthopoulos, T. D.; Heeney, M.; McCulloch, I.; Sirringhaus, H., High-Performance Ambipolar Diketopyrrolopyrrole-thieno 3,2-b thiophene Copolymer Field-Effect Transistors with Balanced Hole and Electron Mobilities. *Adv. Mater.* **2012,** *24* (5), 647-652.

33. Irie, M., Photochromism of Diarylethene Single Molecules and Single Crystals. *Photochem. Photobiol. Sci.* **2010,** *9* (12), 1535-1542.

34. Pichko, V. A.; Simkin, B. Y.; Minkin, V. I., Conrotatory and Disrotatory Reaction Paths for Thermal and Photoinduced Ring-Closing Reactions of 1,3,5-hexatriene and its Isoelectronic Analogs. *J. Org. Chem.* **1992,** *57* (26), 7087-7092.

35. Irie, M.; Fulcaminato, T.; Matsuda, K.; Kobatake, S., Photochromism of Diarylethene Molecules and Crystals: Memories, Switches, and Actuators. *Chem. Rev.* **2014,** *114* (24), 12174-12277.

36. Jakobsson, F. L. E.; Marsal, P.; Braun, S.; Fahlman, M.; Berggren, M.; Cornil, J.; Crispin, X., Tuning the Energy Levels of Photochromic Diarylethene Compounds for Opto-electronic Switch Devices. *J. Phys. Chem. C* **2009,** *113* (42), 18396-18405.

37. Frolova, L. A.; Troshin, P. A.; Susarova, D. K.; Kulikov, A. V.; Sanina, N. A.; Aldoshin, S. M., Photoswitchable Organic Field-Effect Transistors and Memory Elements Comprising an Interfacial Photochromic Layer. *Chem. Commun.* **2015,** *51* (28), 6130-6132.

38. Tsujioka, T.; Kondo, H., Organic Bistable Molecular Memory Using Photochromic Diarylethene. *Appl. Phys. Lett.* **2003,** *83* (5), 937-939.

39. Herder, M.; Schmidt, B. M.; Grubert, L.; Patzel, M.; Schwarz, J.; Hecht, S., Improving the Fatigue Resistance of Diarylethene Switches. *J. Am. Chem. Soc.* **2015,** *137* (7), 2738-2747.

40. Perrier, A.; Maurel, F.; Jacquemin, D., Interplay Between Electronic and Steric Effects in Multiphotochromic Diarylethenes. *J. Phys. Chem. C* **2011,** *115* (18), 9193-9203.

41. Nakamura, S.; Yokojima, S.; Uchida, K.; Tsujioka, T., Photochromism of Diarylethene: Effect of Polymer Environment and Effects on Surfaces. *J. Photochem. Photobiol. C-Photochem. Rev.* **2011,** *12* (2), 138-150.

Chapter 5. Experimental techniques and methods

5.1. Device fabrication

In our work, we have characterized organic field-effect transistors (i) based on different molecular semiconductors, (ii) fabricated with different processing techniques and (iii) using different geometries such as bottom-contact top-gate, bottom-contact bottom-gate and top-contact bottom-gate, the two latest configurations were also used to make organic phototransistors. Organic complementary inverters based on ambipolar semiconductor were fabricated in bottom-gate configuration.

5.1.1 General procedure for the device fabrication

Highly doped n-type Silicon wafers purchased from Fraunhofer institute were used as substrates for both organic thin film transistors and phototransistors fabricated on two different configurations: bottom-contact bottom-gate and top-contact bottom-gate and also for OFET bottom-contact top-gate devices. The substrates consist of 230 nm of silicon dioxide (SiO_2) layer thermally grown as gate dielectric onto Si substrates; it is unit area capacitance (Ci) is 15 nF cm^{-2}. For bottom contact bottom-gate geometry, the source drain electrodes are made of gold and are patterned on the insulator by means of microlithographic techniques. The electrode thickness is 40 nm composed of 30 nm Au on top of 10-nm thick adhesion layer of ITO. Each substrate would fit sixteen OFETs of variable channel lengths (L= 2.5, 5, 10 and 20 μm) but same channel width (W = 10 mm) as showed in the optical images of OFET devices in **Figure 5.1**. For top-contact bottom-gate and bottom-contact top-gate devices, we used bare silicon dioxide Fraunhofer wafers with the same characteristics described above while 40-nm thick gold source and drain electrodes were evaporated through shadow masks using Plassys ME300B thermal evaporator (see metal evaporation in 5.1.1.3). In the latter case, such substrates would consist of eight OFET devices, having four different channel lengths (L= 60, 80, 100 and 120 μm) and the same channel width (W = 10 mm).

As to the organic complementary inverter devices in bottom-gate bottom-contact configuration, they would integrate two identical transistors whose active layer was an ambipolar polymer. A different type of OFET substrate from Fraunhofer were used in this case. In particular,

contact electrodes (Au) of these devices were patterned using a conventional lift-off photolithography procedure and consisted of individual FET electrodes having dimensions of L = 5 µm and different channel lengths of both active and load transistors ranging from 0.455 to 1.35 mm.

Before depositing the semiconductor materials onto the substrates surface, both types of Fraunhofer substrates (with electrodes or bare silicon) used for OFET/OPTs fabrication and substrates with patterned electrodes used for performing organic inverters should be thoroughly cleaned to avoid any organic contamination.

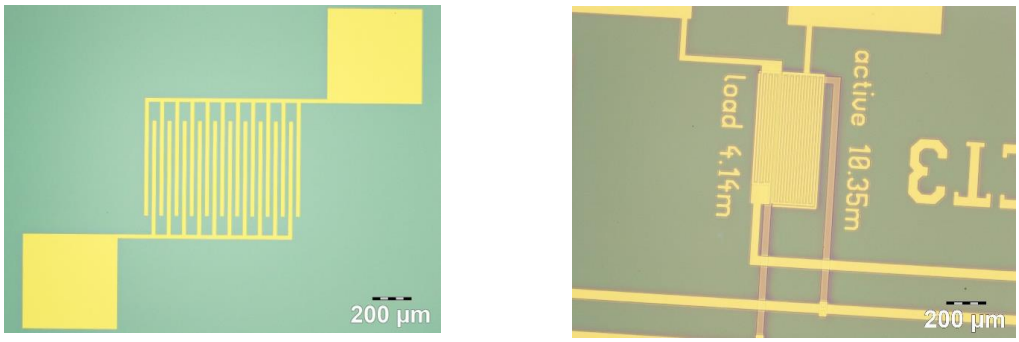

a) **b)**

Figure 5.1. Microscopic images of **a)** an OFETs device (W = 10 mm, L = 20 µm) and **b)** a complementary inverter device consisted of individual FET electrodes having the same channel length of L = 5 µm and different channel width 10.35 mm and 4.14 mm of both active and load transistors respectively.

5.1.1.1. Substrate cleaning

Fraunhofer substrates used in our studies are normally covered by a protective photoresist layer that is washed off prior to use. The substrates were cleaned with acetone (C_3H_6O, 95% GC) and isopropyl alcohol ($CH_3CHOHCH_3$, 99.7 % GC) in an ultrasonic bath (20 minutes in each solvent) followed by a gentle drying under nitrogen gas.

5.1.1.2. UV-Ozone cleaning

After cleaning process with acetone and isopropanol, for some devices, substrates surface was then cleaned with UV-Ozone cleaning. There is an extensive literature describing the use of ultraviolet (UV)/ozone cleaning to remove organic contaminants from the semiconductor surfaces.[1-3] Ultraviolet-ozone cleaning is a well-established, cheap and simple method for cleaning insulator surfaces, it has been previously demonstrated that treating the gate insulator surface, with UV/ozone can improve the

properties of the gate insulator surface and thus enhance the electrical performance of OFET devices.[4] Substrates are placed in the chamber of UV/Ozone cleaner (see **Figure 5.2**) and irradiated with ultraviolet rays. The wavelengths of the ultraviolet rays radiated from a low-pressure mercury vapor lamp are 184.9 nm and 253.7 nm. The O_3 is formed when atmospheric O_2 absorbs the Ultraviolet rays with 184.9 nm by the following reactions:

$$O_2 \longrightarrow O + O$$
$$O + O_2 \longrightarrow O_3$$

After irradiation with wavelength of 253.7 nm of ultraviolet rays, Ozone O_3 absorbs the the rays and decompose O_3. Throughout O_3 formation and decomposition procedure, oxygen atoms (O) with oxidizing capability are generated. Then, the organic contaminant existing on the substrate surface absorbs UV light and lend to photolysis which produced excited molecules, ions, neutral molecules and free radicals, these organic composites react with atomic oxygen forming volatile substances like CO_2, H_2O, N, and O_2, that are removed from the substrates surface.

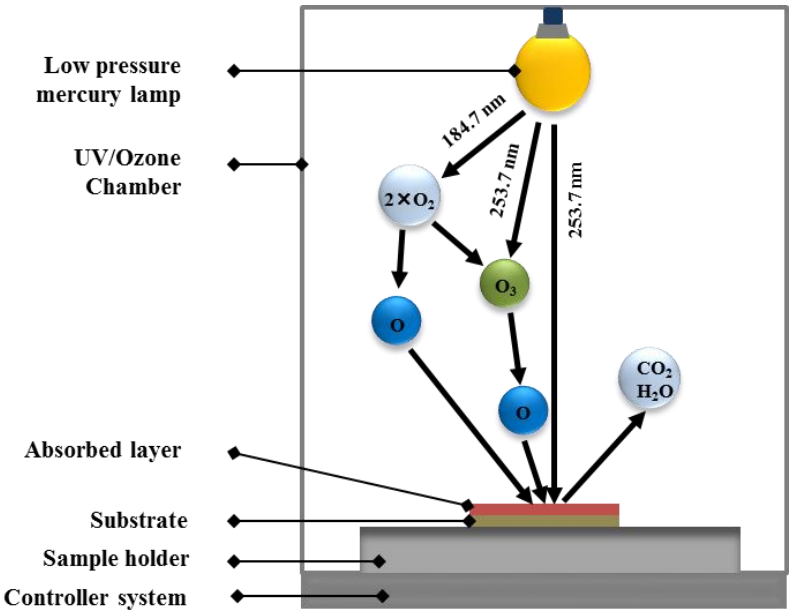

Figure 5.2. Schematic representation of a UV/Ozone cleaner.

5.1.1.3. Metal evaporation

Physical vapor deposition is one of the most used metal deposition techniques. We have used this deposition method to deposit gold metal electrodes. Before depositing gold source and drain

electrodes (50 nm), a thin layer of chromium (Cr, around 3 nm) was deposited on top of bare silicon substrates in order to ensure gold adhesion on silicon substrates for devices based on bottom-contact configuration. In the case of top-contact geometry, 50 nm of Au electrodes were deposited on top of the semiconductor active layer without any intermediate layer (Cr). Aluminum gate electrode (120 nm) was deposited onto the organic insulator polymers (PMMA or CYTOP) for top-gate devices. The metals evaporation is done by using Plassys ME300B and Plassis ME400B thermal evaporators inside and outside the glovebox. Metal vacuum evaporation is based on a thermal principle, in which heating permits the material to reach its melting point and then in a second step its evaporation point. Inside a vacuum chamber (between 10^{-7} and 10^{-6} mbar) where the material, usually is in a boat, heated typically to its melting point, the heating is carried out over a high electrical current (a few hundreds of amperes) through a filament or metal plate on which the material is placed (Joule effect). The choice of this filament material depends on its inertness with the evaporated material. The filament boat used in our work is consisted of tungsten material. The evaporated material is then condensed on the substrate to be deposited on forming a thin film, which is positioned face to the source as shown in the **Figure 5.3** below. The distance between the substrate surface and the source is wide to avoid solid particles attaining the substrate. A crystal detector is placed close to the substrate, which offers an estimation of how fast and how much the metal is being deposited in order to control its thickness. In our case, the evaporation rate was maintained at ~0.02-0.04. The high thermal temperature and goof vacuum play key role for producing a good deposition and contamination free deposits. **Figure 5.3** shows the schematic of the Metal evaporator.

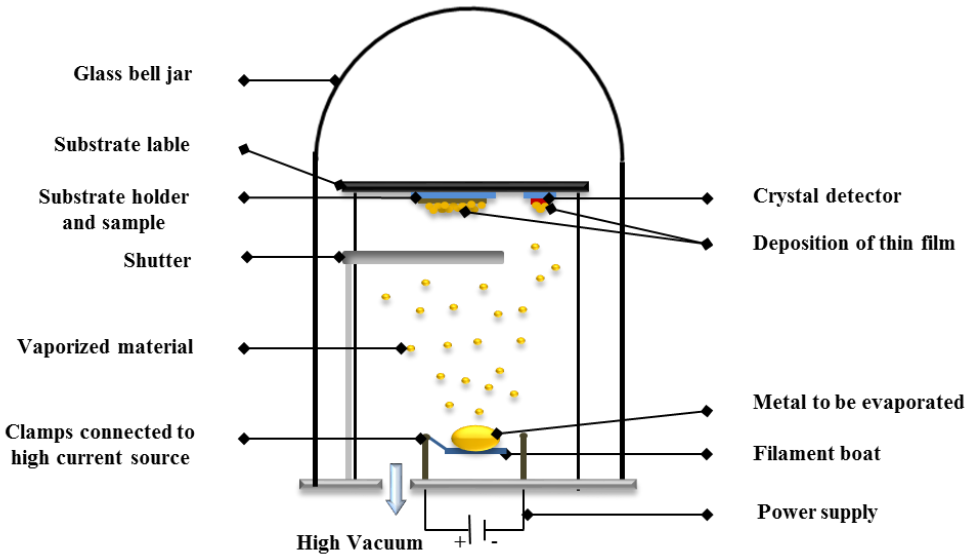

Figure 5.3. Schematic of a physical vapor deposition system.

5.1.2. Substrates functionalization with self-assembled monolayers (SAM)

Self-assembled monolayer (SAM), a well-ordered monomolecular layer formed spontaneously by the reaction of different types of organic molecules with solid substrate materials, has been widely largely explored to modify the supports surface properties in order to enhance or prevent molecules attachment as well as electron trapping. Two distinctive families of SAMs are used, alkanethiol reacting with gold metal and organosilane reacting with oxidized surfaces, in our case SiO_2.

5.1.2.1. Silicon dioxide functionalization

Organosilane SAMs can be formed on various substrates such as glass and oxide silicon. In our studies, hexamethyldisilazane $(CH_3)_3Si\text{-}NH\text{-}Si(CH_3)_3$ (HMDS) and octadecyltrichlorosilane $(CH_3(CH_2)_{17}SiCl_3)$ (OTS) were used as self-assembled monolayers to modify the surface energy of gate insulator and decrease the traps induced by Si–OH groups by the formation of methyl termination $(-CH_3)$[5] of the SAM monolayer adsorbed on the silicon dioxide surface through covalent bonds as showed in **Figure 5.4.** Which make the dielectric surface more hydrophobic and favorable for semiconducting deposition. The use of organosilane SAMs is also inexpensive, and effective insulator surface treatment for improving the performance of an OFET.[4] This passivation treatment is very important to increase the field-effect mobility especially for n-type semiconductors.[6-7]

After UV/Ozone cleaning used to remove organic contaminations, substrates were moved into a nitrogen environment inside a glovebox, where HMDS was self-assembled on the silicon substrates by spin-coating of 100 µl HMDS solutions (0.47 mM) onto the substrate surface for 60 seconds at 1500 RPM, followed by thermal annealing at 100°C for 1 hour. Alternatively, octadecyltrichlorosilane SAMs were grown: in this case the substrates were immersed into a 10 mM solution of OTS in anhydrous toluene and annealed at 60°C for 30 minutes. After that, the substrates were left for 12 hours, washed with anhydrous toluene and dried in the spin-coater (4000 rpm, 60 seconds), and finally annealed at 60°C for 1 hour.

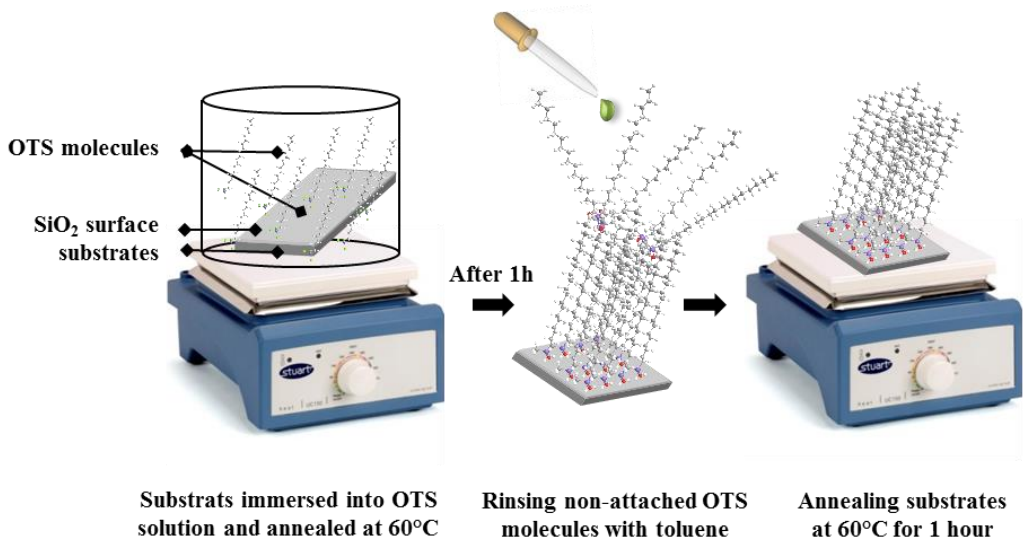

Figure 5.4. schematic illustration showing the different process steps of OTS self-assembled formation on silicon dioxide surface.

5.1.2.2. SAM on gold electrodes

The polarity and amount of injected charge carriers are generally governed by the relative position between the metal work function and the molecular energy levels. The adsorption of undecanethiol ($CH_3(CH_2)_9CH_2SH$) on Au electrode surface decrease the work function of the gold from ϕ = -5.1 eV to ϕ = -4.7 eV to be closer to the LUMO energy level of the n-type semiconductor used materials. OFET substrates were immersed in a 1 mM solution of undecanethiol (C11H23SH) in ethanol for 12 hours in order to form SAMs on the electrodes. After the SAM formation, the substrates were washed with copious amounts of absolute ethanol to get rid of physisorbed undecanethiol molecules from the dielectric and electrode surfaces,[8] then, followed by annealing at 80°C for 1 hour (see **Figure 5.5**).

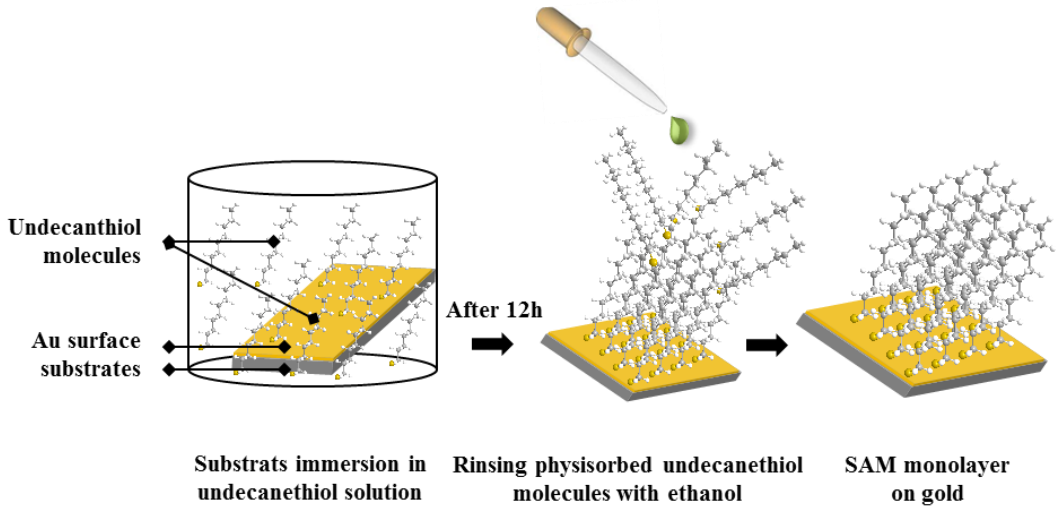

Figure 5.5. Schematic illustration of undecanethiol self-assembled monolayers formation process on Au source-drain electrodes.

5.1.3. Organic materials solution preparation

5.1.3.1. Organic semiconductors solution

Our research focused on solution-processable organic small molecules and polymers that were either synthesized by our collaborators or purchased from Sigma-Aldrich. Organic semiconductor materials were used as received and dissolved in different organic solvents at room temperature for air stable materials and inside the glovebox when more air-sensitive materials were used. Solutions were than stirred and heated to reach complete molecules solvation. More specified details on each semiconductor material preparation are described in the experimental part of each chapter.

5.1.3.2. Diarylethene solution

One of diarylethenes advantages is their compatibility with simple solution-based processing techniques, spin-coating method is the simplest approach for depositing organic materials uniformly through the entire substrate. DAE_tBu and DAE_F derivatives were dissolved in butyl acetate (2 mg/ml) and spin-coated onto polymer layer and thermally annealed at 90°C for 1hour and 30 minutes to induce diarylethenes permeation into the polymer matrix and an ordered crystalline phase in a glove box with a N2 atmosphere. Concerns related to the solvent interaction must be considered, the solvent used for diarylethene layer may interact with previously applied polymer layer. For that reason, the

diarylethene solution must be cautiously prepared and optimized and dissolved in a non-solvent for the polymer to prevent any chemical interactions in polymer-diarylethenes multilayer organic devices.

5.1.3.3. Polymeric dielectric solutions

Because organic FETs are recently used inpotentially inexpensive applications, solution-processable polymer gate dielectrics are interesting alternative method forlow-cost fabrication, which can be deposited by vacuum deposition, spin-coating, printing or spray coating. Polymer dielectrics are ideal due to their multiple properties like optical transparency, flexibility, highly resistant to breakages, and they have excellent insulating perfromences. They have also good film-forming characteristics.[9] In top-gate bottom-contact configuration, we have fabricated devices with two different polymeric dielectric, PMMA and CYTOP.

5.1.3.3.1. PMMA solutions

Typical example of dielectric polymers is poly (methyl methacrylate) (PMMA, ε_i = 3.8), PMMA is a polar plastic, commonly employed as an insulator for organic electronics due to the absence of chemical groups that can act as trap sites for charges, in contrast of dielectric oxides.
For bottom-contact top-gate devices, PMMA (Aldrich, MW = 319 kg.mol^{-1}) was used as a dielectric material. The PMMA film was deposited onto semiconductor layer by spin coating of 350µl of solution (45 mg/ml in anhydrous butyl acetate heated at 80°C and filtered with 0.45µm filter) for 30 seconds at 1000 rpm, followed by annealing at 80°C for 30 minutes (typically the PMMA films were ca. 700 nm thick).

5.1.3.3.2. CYTOP solutions

Another example of polymeric dielectric used in our work, CYTOP (Cyclic Transparent Optical Polymer) poly-(perfluoroalkenylvinyl ether) (CF_2=CF-O-CF_2-CF_2-CF=C_2) purchased from Ashai Glass Japan, is an amorphous (non-crystalline) fluoropolymer. CYTOP is easy to be used and can be deposited in air from solution. It is highly hydrophobic and has a very low permittivity of ε_i = 2.1-2.2. Moreover, this material is a good insulator, its passive surface lends to high performing field-effect transistors with good mobilities.[10]
CYTOP films were deposited by spin-coating 200 µl of solution (190µl of CYTOP and 10µl of solvent) which has been prepared and shacked vigorously one day before to remove the formed bubbles, CYTOP prepared solution must be kept in the fridge before any use. The next day, CYTOP

solution has been moved inside the glovebox and has been deposited at 2300 rpm for 30 second followed by annealing at 80°C for 1 hour and 30 minutes.

5.1.4. Organic materials deposition methods

Thin film materials deposition may be realized over several methods depending on the type of deposited material and the desired application. Different deposition techniques are available for processing organic semiconductor films from liquids, these include spin-coating, drop-casting and solvent induced precipitation (SIP) for crystalline structures formation.

5.1.4.1 Spin-coating method

Spin-coating deposition method is the most used process due to the simple and easy manipulation of its parameters as well as its use to realize a nice and homogeneous films starting from solutions. It leads to highly reproducible formation of thin films with precise control of their coverage and thickness overlarge areas; this method is the principle technique we have used to deposit organic semiconductor layers. The spin-coating process consists in the application of a small amount of solution onto a rotating disc, which will cause ejection and fast solvent evaporation leading to kinetically driven assembly and formation of a liquid or solid thin film.[11] A schematic representation of the spin coating process is presented in **Figure 5.6**. Spin coating is a fast and good method and has several advantages over the other coating techniques. One of the important factors is repeatability of homogenous films. The deposited film parameters can be controlled by varying different spin-coating such as, spin-coating speed, ramping rate. The film thickness depends on drying rate, temperature, and time and the choice of solvent. These parameters are critical to predict and define the formed film properties, and need to be highly considered to achieve a uniform film with the desired thickness.

In general, higher rotation speed during long spin-coating time results to thinner films. The thickness of a spin-coated film is usually proportional to the inverse of the spin speed squared as shown by the equation below. Where *d* is the final thickness, *n* the viscosity coefficient, *w* is the angular velocity, ρ the solution density and *t* is the spinning time.

$$t \propto \frac{1}{\sqrt{\omega}}$$

$$d = \left(\frac{\eta}{4\pi\rho\omega^2}\right)^{1/2} t^{-1/2}$$

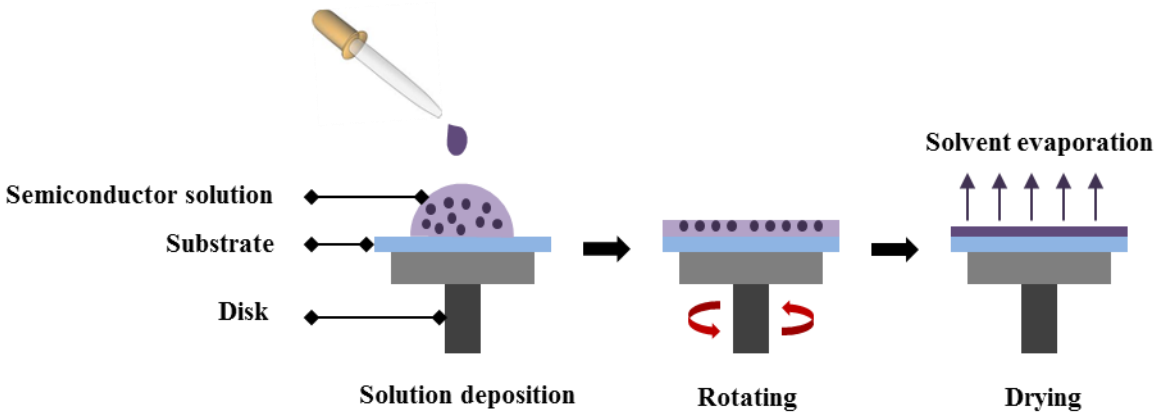

Figure 5.6. Schematic representation of the spin-coating process.[12]

5.1.4.2 Solvent induced precipitation (SIP) method

During Solvent Induced Precipitation (SIP) method, molecules are induced to aggregate and precipitate from solution by modifying the chemical environment by the addition of a non-solvent. This method has been applied to perylene**,** pentacene and HBC-derivatives and has shown to be useful for the formation of self-assembled fiber structuresthat can be used as active layer in organic field-effect transistors.[13] In our work, crystalline fibers were prepared with fast SIP procedure, where a small quantity of solution containing organic semiconductors was rapidly injected into a larger volume of non-solvent (ratio 1: 19). A schematic representation of the fast SIP process is presented in **Figure 5.7**. The fibers were then transferred to the surface by drop-casting.

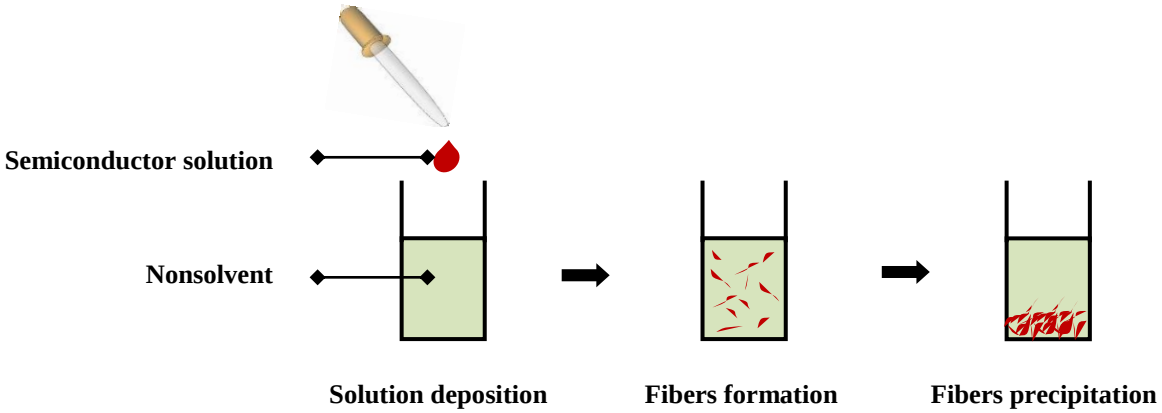

Figure 5.7. Schematic illustration of Solvent Induced Precipitation (SIP) procedure.

5.2. Characterization techniques

5.2.1. Electrical characterization

5.2.1.1. Probe-station

The Current-Voltage (I-V) characteristics of all the OTFT fabricated devices were measured in dark and under illumination, in air at room temperature and inside the glove box in nitrogen atmosphere (oxygen level lower than 10 ppm). Measurements were done by contacting the source, drain and gate electrodes of the substrate device placed on the sample stage, using tungsten-probes under the microscope which are connected to the keithley, and applying different voltages using a Cascade Microtech M150 probe station (**Figure 5.8**) with dual channel Keithley 2636A source-meter and associated softwares Labtracer and Labview. The V_{OUT} - V_{IN} characteristics of the organic inverter devices were performed inside the glove box by contacting a common gate for both transistors served as the input terminal V_{IN}, a supply voltage (V_{DD}), and output voltage (V_{OUT}) electrodes, and applying positive or negative voltages on V_{DD} and V_{IN} using a Cascade Microtech M150 probe station.

Figure 5.8. Schematic representation of the Current-Voltage (I-V) characterization set-up which consists of a Cascade Microtech M150 probe station connected with a dual channel Keithley 2636A source-meter and its associated software.

5.2.1.2. Set-up for experiments requiring light irradiation

Organic field effect transistors and organic inverters devices based on bottom-gate geometry were characterized in dark and under UV/Visible-light irradiation from the top around 1.5 cm distance recording to the sample surface under nitrogen atmosphere using a monochromatic light (Polychrome

V (Till Photonics) which is related to the probe-station described above. Light irradiation was performed at different wavelengths and light intensity depending on the semiconductor absorption properties ranging from 365 nm wavelength at UV region to 546 nm at Visible-region. Both UV and Visible wavelengths were chosen in accordance to DAEs and semiconductor materials absorption spectra. Light intensity was measured using an analogue optical power meter (PM100A, ThorLabs). Time irradiation can be limited to few seconds or more than 10 minutes. OFET based devices in top-gate configuration have been irradiated from the bottom using the same set-up and light intensity.

5.2.2. Morphological characterization

5.2.2.1. Optical and fluorescence microscopy

In our work, we have performed optical and fluorescence images of different semiconductor deposited films, using Olympus BX51 microscope (see **Figure 5.9**).

Figure 5.9. Schematic of Olympus BX51 microscope instrument.

5.2.2.2. Atomic force microscopy

The film surface morphology was studied using AFM with a Veeco Digital Instruments Dimension 3100 scanning probe microscope (SPM). The Atomic Force Microscope (AFM) i.e. Scanning Force Microscope (SFM) or Scanning Probe Microscope (SPM), has been around for almost 15 years. The AFM has undergone a number of developments over the last years, which allows to study not only surfaces topography and morphology but also to measure elasticity, and local resistivity. This instrument is not a 'conventional microscope' that collects and focuses light. The word ‘microscope’ came from its capability to measure and analyze microscopic features. AFM is mostly

useful and widely used as a characterization technique of surface morphology and topography at the nanometric scale for various materials. This method can provide mechanical, thermal, and electromagnetic properties of various surfaces. An atomic force microscope contains a sharp tip mounted at the free end of micro-machined cantilever, which interacts with a sample surface to be investigated. Interatomic forces between the sample surface and the probe tip induce tip and cantilever displacement. The change in the Z axis reflects the surface topography. The AFM operates in different mode; the contact mode, in which the tip stays in close contact with the surface sample during the scanning, which is considered as a major disadvantage in soft material applications. However, in the oscillatory mode, known also as tapping mode, this problem is reduced by having the tip touch the sample surface only for a short time making only brief intermittent contacts. In this thesis, the devices film surface was scanned using AFM tapping mode, where, an electric piezo actuator stack, vertically excited the cantilever oscillating with a constant frequency, allowing the tip to bounce up and down. When the tip gets closer to the surface, Van der Waals forces, electrostatic forces, dipole-dipole interactions, etc. cause the cantilever oscillation amplitude to change. The cantilever motion is magnified with the use of a laser beam, which is deflected from the backside of the cantilever to a photodiode detector that controls the height of the cantilever, generating an electronic signal. The signal is converted to a root mean square (RMS) amplitude value, which is displayed as an AV voltage. The reflected laser beam gives information on the surface height and other sample properties. The AFM resolution is far below the diffraction limit reached by the optical microscopy, which is limited only by the tip radius and the spring constant of the cantilever. The main components of an AFM are (see **Figure 5.10**): the AFM probe, a sharp tip mounted on a soft cantilever, the piezoelectric scanner that moves the tip relatively to the sample, the photodiode detector that measures the cantilever deflections, the feedback loop that monitors the interaction forces between the molecules on the tip with the ones on the surface, and the conversion system acquired by the instrument into an image. The AFM has been used in our studies to determine the crystalline structures (fibers) sizes and morphology and for comparing topographic images of spin-coated films based on the same semiconductor treated with different self-assembled monolayers, annealed at different temperatures or mixed with different chemical molecules.

The AFM was also used in order to characterize the surface roughness of the semiconductor layers under several deposition conditions. The surface roughness (R_{rms}) is the root mean square absolute value of the surface roughness profile, the RMS roughness is a function defined as :[14]

$$R_q = \sqrt{\frac{1}{L}\int_0^L |Z^2(x)|\,dx}$$

Where the function Z(x) describes the surface profile, Z is the height, x is the sample position, and L in the length. The average roughness depends only on the average profile height.

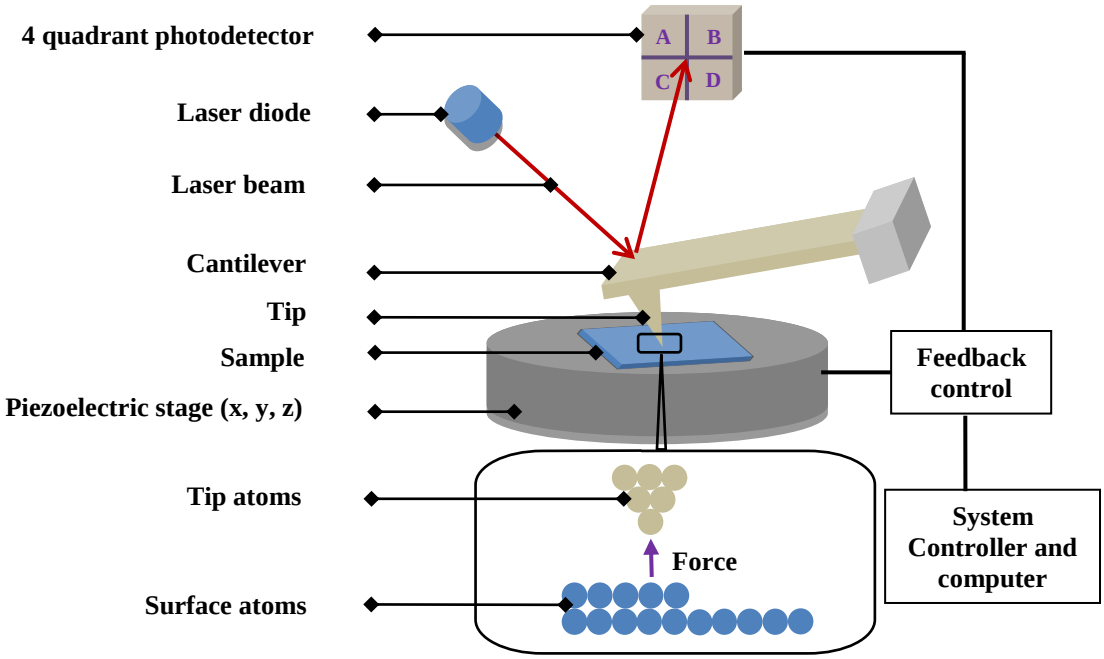

Figure 5.10. Schematic representation of an atomic force microscope set-up.

5.2.2.3. Mechanical contact profilometer

In order to measure the film thickness of deposited materials, we have used a Stylus-based mechanical contact profilometer (KLA-Tencor Alpha-Step IQ) which uses a probe to detect the surface (see **Figure 5.11**). Before measurement, the film surface was scratched to remove the material from a small area. Using the mechanical stylus, it's possible to probe this area and measure the film height recording to the difference between scratched area and the rest of the covered surface. After that, the sample was placed on the sample stage and moved in X, Y axes. A stylus profilometer consists of physical movements in X, Y and Z keeping contact with the surface. The stylus tip moves physically along the surface following the surface morphology, using a feedback system. Tip movements are converted into height using a transducer, constructing the surface profile. The size and shape of stylus tip can impact and limit the measurements resolution. We have measured the film thickness several times in different areas in order to minimize the error and calculate an average value, especially if the film is inhomogeneous. This surface profiler can damage some surfaces.

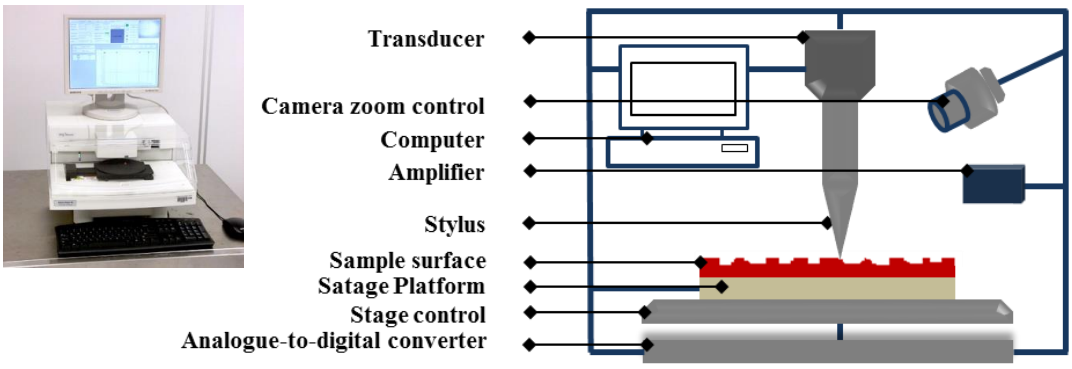

Figure 5.11. Schematic illustration of a mechanical contact profilometer.

5.2.2.4. Scanning electron microscopy

The scanning electron microscope (SEM) is used to produce high-resolution images that reveal different information of small features and object shapes down to 50 nm in size, samples surfaces morphology, and crystalline structures. The main components of a typical SEM are: electron column, scanning system, detector(s), vacuum system, display, and electronics controls (see **Figure 5.12**). The electron column is composed of an electron gun and electromagnetic lenses that operate in vacuum. SEM uses a focused beam of high-energy electrons produced by a thermionic emission gun constructed by a filament (cathode) made of thin tungsten wire (about 0.1 mm) that emits thermoelectrons after being heated at high temperature. These thermoelectrons are then grouped as an electron-beam. The electron-beam following into a metal plate (anode) after applying a positive voltage (1- 30 kV), which accelerates the electrons to energies in the range of 1-40 keV in the SEM. A high-vacuum environment is necessary to allow the electrons to travel without being scattered by the oxygen and water molecules. The electromagnetic lenses (condenser and objective lenses) are used to focus and define the electron beam-diameter in order to form a small focused electron spot on the sample surface, going from ~50 ~50 µm (for a tungsten filament) to a small spot size ranging from 1 to 100 nm. The energetic electrons penetrate into the sample for some distance. Scanning coils are used to deflect the e-beam so that it can scan along x- or y-axis the studied sample surface. The electron beam interacts with the sample to a depth approximately 1 µm and collides with its atom. In doing so, the primary excitation region is generated from primary electron beam, producing signals. The signals produced from electron-sample interactions comprise secondary electrons (SE), backscattered electrons (BSE), X-rays, Auger electrons, and cathodoluminescence. The secondary electrons are provided from the emission of the valance electrons of the constituent atoms of the

sample possessing low energies of less than 50 eV and they are used to generate the topography of the sample surface. The backscattered electrons are those scattered backward and emitted out of the sample after collision with the electrons of the sample atoms, their energy is higher than secondary electrons, ranging from an energy equal to the incident-electron energy down to 50 eV but lower than the incident-electron energy. They are employed to determine crystals structures as the backscattered electrons intensity change is related to the crystal orientation. Another class of signals produced by the interaction of the primary electron beam with the sample is characteristic x-rays. The analysis of characteristic x-rays provides chemical information of the studied surface area and it is the most used in micro-analytical technique in the SEM. All analyzed data are collected from a selected area ranging from approximately 1 cm to 5 microns of the surface sample by several detectors: the SE detector for the secondary electrons collection, solid state BSE detector for BS electrons, energy-dispersive x-ray spectrometer for the characteristic x-rays and photomultipliers for cathodoluminescence. The resulting signals are amplified and displayed on a TV screen or computer monitor, giving rise to a topographic image.

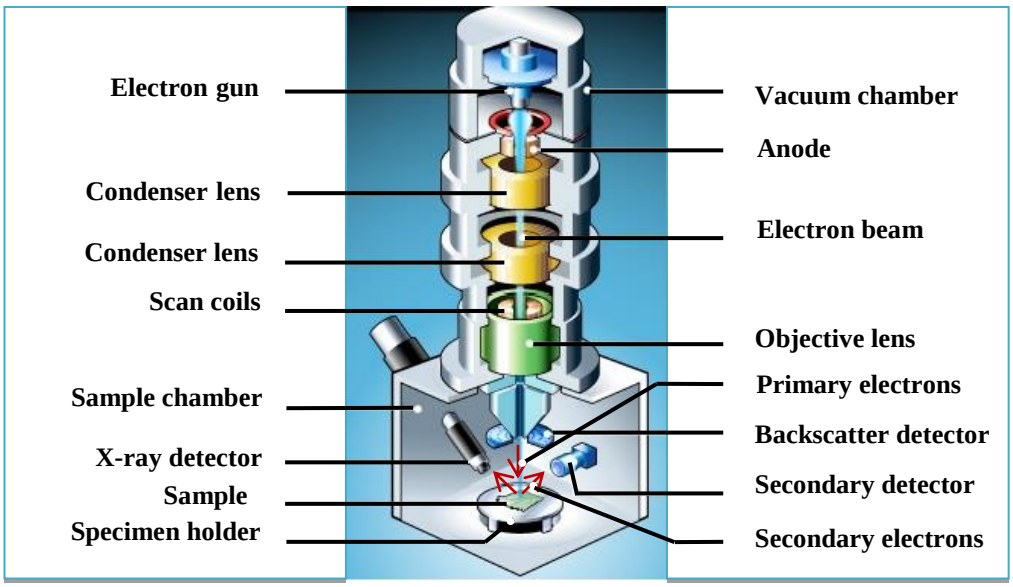

Figure 5.12. Schematic representation of a scanning probe microscope.

5.2.3. Optical characterization: Ultraviolet-Visible absorption spectroscopy

Ultraviolet and visible spectrometers have been widely used over the last 35 years. UV/Visible instrument is one of the important analytical instrument and it is used in many applications. In this thesis, we have used UV/Visible characterization to determine the wavelengths of the maximum

absorption of the employed semiconductors and diarylethene molecules irradiated by light (Chapter 8) and to extract the energy gap (E_G) of used organic semiconductor material (Chapter 7) which corresponds to the electronic transition 0-0 (the larger and intense peak in the spectra). We have recorded UV-Vis absorbance spectra of solution and thin films using Jasco V-670 Spectrophotometer (see **Figure 5.13**) with wavelength range of 190-2700 nm and Xenon lampe for light source. The V-670 double-beam spectrophotometer utilizes a unique, single monochromator and a photomultiplier tube (PMT) as detector for UV/Vis region. When a monochromatic beam radiation of radiant initial intensity I_0 passes through the sample solution or film, absorption takes place and the beam of radiation leaving the sample has radiant intensity I. The amount of radiation absorbed by the sample is experimentally measured in terms of transmittance (T) which is defined as:

$$T = I / I_0$$

The relation between absorbance (A) and transmittance (T) is:

$$A = -\log T = -\log (I / I_o).$$

The Beer-Lambert Law states that the concentration of a substance in solution is directly proportional to the absorbance (A), and the intensity of the emitted radiation depends on the optical path length (l) and the solution concentration (C).

$$A = \varepsilon \, l \, C$$

Where ε is the molar absorptivity with unit of [L mol^{-1} cm^{-1}], l is the path length of the sample which is, the path length of the cuvette in which the sample is contained with unit of [cm] and C is the concentration of the compound in solution, expressed in [mol L^{-1}].

Figure 5.13. Schematic of a V-670 Jasco spectrophotometer.

5.3. References

1. Pearton, S. J.; Ren, F.; Abernathy, C. R.; Hobson, W. S.; Luftman, H. S., Use of Ultraviolet Ozone Cleaning to Remove C and O from Gaas prior to Metalorganic Molecular-Beam Epitaxy and Metalorganic Chemical Vapor-deposition *Appl. Phys. Lett.* **1991,** *58* (13), 1416-1418.
2. Lancaster, C. A.; Shumaker-Parry, J. S., Surface Preparation of Gold Nanostructures on Glass by Ultraviolet Ozone and Oxygen Plasma for Thermal Atomic Layer Deposition of Al2O3. *Thin Solid Films* **2016,** *612*, 141-146.
3. Andersson, E.; Aurino, P. P.; Winkler, D.; Kalabukhov, A., Nondestructive Cleaning of the LaAlO3/SrTiO3 Surface with Ultraviolet Light and Ozone. *J. Vac. Sci. Technol. B* **2016,** *34* (4), 4.
4. Fan, C. L.; Lin, Y. Z.; Huang, C. H., Combined Scheme of UV/Ozone and HMDS Treatment on a Gate Insulator for Performance Improvement of a Low-Temperature-Processed Bottom-Contact OTFT. *Semicond. Sci. Technol.* **2011,** *26* (4), 5.
5. Yamamoto, M.; Umemoto, H.; Ohdaira, K.; Shikama, T.; Nishiyama, T.; Horibe, H., Oxygen Additive Amount Dependence of Rate of Photoresist Removal by H Radicals Generated on a Tungsten Hot-Wire Catalyst. *Jpn. J. Appl. Phys.* **2016,** *55* (7), 5.
6. Xie, Y. T.; Cai, S. C.; Shi, Q.; Ouyang, S. H.; Lee, W. Y.; Bao, Z. A.; Matthews, J. R.; Bellman, R. A.; He, M. Q.; Fong, H. H., High Performance Organic Thin Film Transistors Using Chemically Modified Bottom Contacts and Dielectric Surfaces. *Org. Electron.* **2014,** *15* (9), 2073-2078.
7. Xie, Y. T.; Ouyang, S. H.; Wang, D. P.; Zhu, D. L.; Xu, X.; Tan, T.; Fong, H. H., Performance Improvement in Polymeric Thin Film Transistors Using Chemically Modified Both Silver Bottom Contacts and Dielectric Surfaces. *Chin. Phys. B* **2015,** *24* (9), 5.
8. de Boer, B.; Hadipour, A.; Mandoc, M. M.; van Woudenbergh, T.; Blom, P. W. M., Tuning of Metal Work Functions with Self-Assembled Monolayers. *Adv. Mater.* **2005,** *17* (5), 621-625.
9. Kim, C.; Facchetti, A.; Marks, T. J., Polymer gate Dielectric Surface Viscoelasticity Modulates Pentacene Transistor Performance. *Science* **2007,** *318* (5847), 76-80.
10. Kalb, W. L.; Mathis, T.; Haas, S.; Stassen, A. F.; Batlogg, B., High Performance Organic Field-Effect Transistors with Fluoropolymer Gate Dielectric. In *Organic Field-Effect Transistors Vi*, Bao, Z.; Gundlach, D. J., Eds. Spie-Int Soc Optical Engineering: Bellingham, **2007**.
11. Norrman, K.; Ghanbari-Siahkali, A.; Larsen, N. B., 6 Studies of Spin-Coated Polymer Films *Annu. Rep. Prog. Chem., Sect. C: Phys. Chem.* **2005,** *101*, 174-201.
12. Norrman, K.; Ghanbari-Siahkali, A.; Larsen, N. B., 6 Studies of Spin-Coated Polymer Films *Annu. Rep. Prog. Chem., Sect. C: Phys. Chem.* **2005,** *101*, 174-201.
13. Savage, R. C.; Mativetsky, J. M.; Orgiu, E.; Palma, M.; Gbabode, G.; Geerts, Y. H.; Samori, P., Integration of Self-Assembled Discotic-Based Fibres into Field-effect Transistors: a Comparison of Preparation Approaches. *J. Mater. Chem.* **2011,** *21*, 206-213.
14. Gadelmawla, E. S.; Koura, M. M.; Maksoud, T. M. A.; Elewa, I. M.; Soliman, H. H., Roughness Parameters. *J. Mater. Process. Technol.* **2002,** *123*, 133-145.

Chapter 6: Ambipolar field effect-transistors based on a fullerene derivative

Introduction

Until only a few years ago, low field-effect mobility, environmental instability upon air exposure would hamper the potential of organic field-effect transistors for every day applications. Thanks to the availability of new high performing semiconductor materials and better understanding of the molecular design requirements to avoid such limitations. The application of OFET is coming closer to the market place in large area and low cost applications for electronics [1-15]. Whilst p-type channel organic transistors are the most reported in literature, n-type semiconductors are less studied owing to their tendency to oxidize in air atmosphere.

Fullerene derivatives are easy-to-process semiconductor materials and they feature high electron mobility.[17]One of the most popular fullerene derivative is [6,6]phenyl-C_{61}-butyric acid methyl ester (PCBM), widely used as an n-channel material in heterojunction organic solar cells [10, 18-21] and OFETs.[22-24] More recently, other soluble fullerene derivatives have been synthesized in an attempt to improve the electron mobility.[18, 25-27] Scientific researchers have employed different alkyl chains substituents to induce organic solvents solubility, air stability,[23, 28] good molecular packing, and films order. Among these potential derivatives, indene-C60-bisadduct (ICBA),[29] 1',1",4',4"-tetrahydro-di[1,4]methanonaphthaleno[1,2:2',3',56,6':2",3"][5,6]fullerene-C60 is a promising n-channel material thanks to its high efficiency used in combination with the hole-transporting poly(3-hexylthiophene) polymer in organic solar cells .[18-19, 21, 26, 29]

Within the present work, we have focused our attention onto ICBA and used as the active semiconducting layer in bottom-contact bottom-gate organic field effect transistors (see **Figure 6.1b**). In particular, we have investigated the electrical characteristics enhancements induced by substrate annealing and silicon dioxide passivation treatments. In our study, the OFET electrical characteristics have been correlated with morphological and structural ICBA thin film properties.

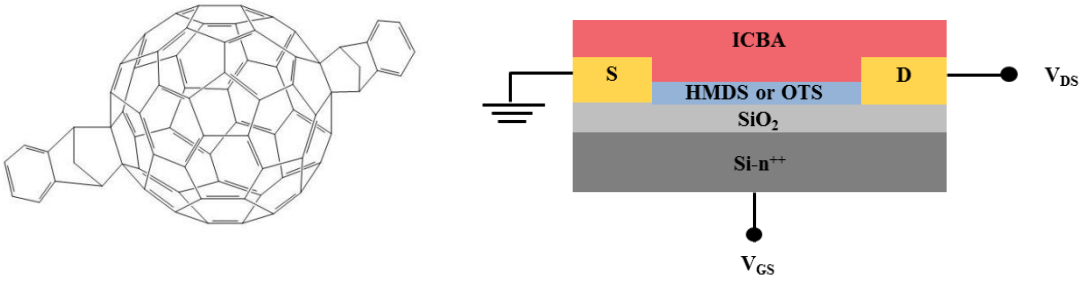

a) **b)**

Figure 6.1. a) Chemical structure of indene-C60-bisadduct (ICBA) organic semiconductor, and **b)** Bottom-contact bottom-gate transistor based on ICBA as the active layer, with Au gold source and drain electrodes.

Further, we have investigated the effect of the surface energy by water contact angle measurements. The silicon dioxide surface energy was tuned and optimized by self-assembled functionalization with octadecyltrichlorosilane (OTS) or hexamethyldisilazane (HMDS). Morphological Atomic force microscopy measurements have been recorded on different type of surface devices (untreated, HMDS or OTS treated) and annealing conditions. The crystallinity of ICBA films was investigated through Grazing Incidence X-Ray Diffraction (GIXRD).

6.1. Experimental

OFET device fabrication and characterization

In this work, we have fabricated bottom-contact bottom-gate field-effect transistors based on ICBA as an active semiconductor layer. This molecule was used as received from Sigma-Aldrich without further purification. Since oxygen has a strong effect on ICBA electronic properties, the solution preparation and OFET devices fabrication were done inside a glovebox in a nitrogen environment (less than 5 ppm for O_2 level and around 3 ppm for H_2O). 230 nm thermally-grown SiO_2 (gate dielectric) with pre-patterned interdigitated gold electrodes substrates have been purchased from IPMS Fraunhofer Institut. In order to get rid of the protecting photoresist layer, substrates were washed with raw acetone, then sonicated in pure acetone (95% GC) and isopropanol (99.7 % GC) in an ultrasonic bath (20 minutes in each solvent), followed by a gentle drying using nitrogen flow. After substrates cleaning, silicon dioxide surfaces were functionalized by either HMDS or OTS self-assembled monolayers (see section 5.1.2 in Chapter 5). Some substrates were left without any further dielectric surface treatments or annealing process and served as references. ICBA organic semiconductor layer was deposited on the insulator surfaces by spin-coating method. Where 170 µl of

ICBA (10mg/ml dissolved in anhydrous chloroform) solution was spin-coated at 3500 RPM for 40 seconds inside the glove box. In case of annealed devices, the thin film deposition is followed by thermal annealing in hot plate at the desired temperature (90 °C, 140 °C, and 200 °C) for 10 minutes, 1 hour, or 4 days. **Figure 6.2** shows an optical microscopic image of an ICBA based OFET transistor performed in bottom-contact bottom-gate configuration.

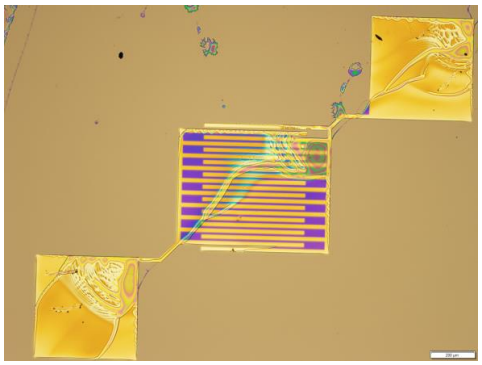

Figure 6.2. OFET device based on ICBA organic semiconductor.

The I–V characteristics of all devices were measured inside the glovebox in nitrogen atmosphere in an inert environment by contacting the source, drain, and gate electrodes and applying positive (to transport electrons) or negative (to transport holes) gate and drain biases, using a Cascade Microtech M150 probe station with dual channel Keithley 2636A source-meter and LabTracer™ associated software. The electrons and holes mobilities were extracted from the saturation regime by the following equation:

$$\mu_{sat} = \frac{2 \cdot \left(\frac{\partial \sqrt{I_D}}{\partial V_{GS}} \right)^2}{C_i \frac{W}{L}}$$

Where I_D is the current measured between source and drain electrodes, V_{GS} is the gate bias applied between the source and gate electrodes, L is the channel distance, W the channel width and C_i = 1.5 $\times 10^{-8}$ Fcm^{-2} is the capacitance per unit area of the gate dielectric layer.

The threshold voltage values were extracted from the extrapolation of the linear part with the x axis (gate voltage) of the sqrt (I_D) vs V_{GS} curve.

Atomic force microscopy

The semiconductor film morphology was explored by Atomic Force Microscopy (AFM) in tapping mode under ambient conditions. We have used a Digital Instruments Dimension 3100 AFM with Nanoscope IV controller. The AFM imaged films were prepared following the same experimental conditions respected for OFET devices, including silicon dioxide surface treatments and annealing process.

The surface roughness, R_{rms} was measured by AFM. R_{rms} represents the variance of the height values acquired in the image (M, N) and defined by the following formula:

$$R_{rms} = \sqrt{\frac{1}{MN}\sum_{(i,j)}^{(M,N)}\left[z_{i,j} - \bar{z}\right]^2}$$

z (i, j) is the matrix element and $\bar{\mathbf{z}}$ is the average value.

Structural Characterization of ICBA films

The crystallinity of different ICBA films was provided by Grazing Incidence X-Ray Diffraction (GIXRD) measurements performed at the ELETTRA-XRD1 beamline at Trieste's synchrotron facility (Italy) using a monochromatic beam with a wavelength (λ) of 1.542 Å and a dimension of 0.2×0.2 (H×V) mm^2. The incident angle of the X-ray beam, αi, was chosen equals and slightly larger than the critical angle for total reflection of the organic film (~0.18° and 0.22°), in order to control the penetration through the full film depth. The diffraction patterns were recorded using a 2D camera (Pilatus detector) placed normal to the incident beam direction at 300mm from the sample. Multiple images were collected translating the sample 0.5 mm in a direction perpendicular to the beam to probe the sample homogeneity.

6.2 Results and discussion

6.2.1. Effect of silicon dioxide passivation with different SAM monolayers and thermal annealing on OFET electrical performances

Bottom-contact bottom-gate organic field-effect transistors based on spin-coated ICBA thin film were fabricated and characterized. The effect of OTS and HMDA self-assembled monolayers

formed on thermally-grown SiO_2 was examined as well as devices thermal annealing at different temperatures (90 °C, 140 °C, and 200 °C) and duration (during 10 minutes, 1 hour, or 4 days). A series of OFET devices that were not thermally annealed were also explored as references. The output and transfer characteristic curves for electron transport within ICBA layer for devices treated with either HMDS or OTS and annealed for 1 hour at 200 °C are showed in **Figure 6.3**. The I-V electrical characteristics revealed typical n-channel output and transfer curves, a high electron drain current and good working OFET devices.

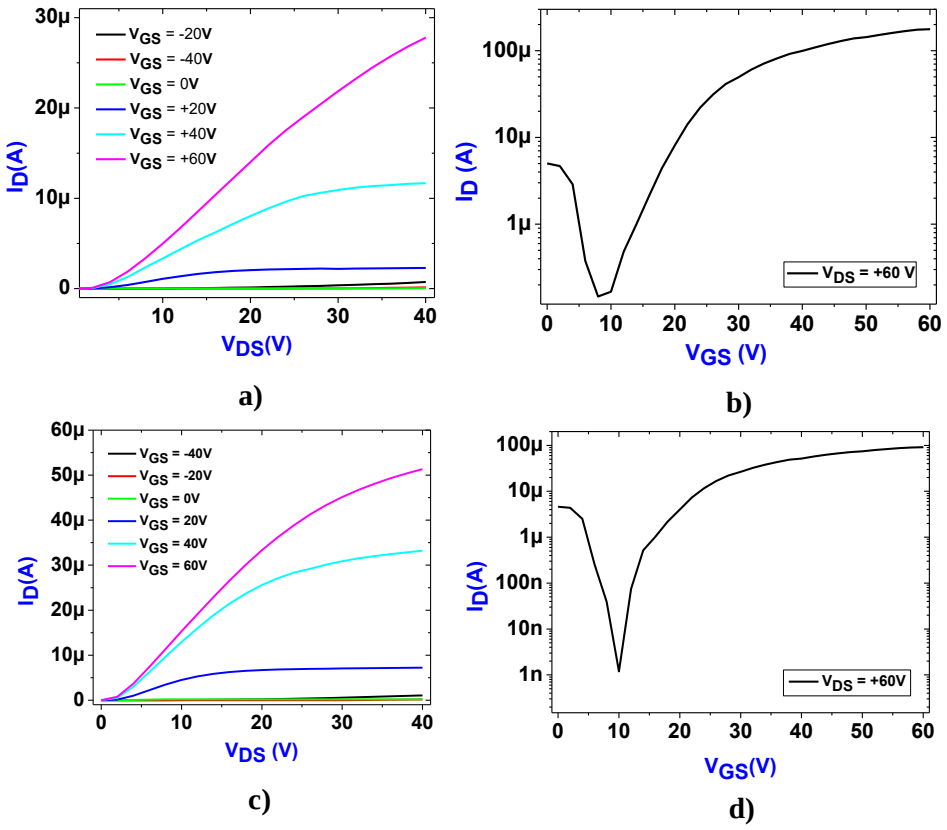

Figure 6.3. Electrons transport transfer **(b, d)** and output **(a, c)** characteristics of ICBA-based transistors upon 1h annealing at 200°C measured in **(a, b)** HMDS-treated, and **(c, d)** OTS-treated devices.

Electron mobility and threshold voltage values for untreated and OTS or HMDS-treated silicone dioxide substrates annealed at different temperatures were reported in **Figures 6.4** and **Figures 6.5** respectively.

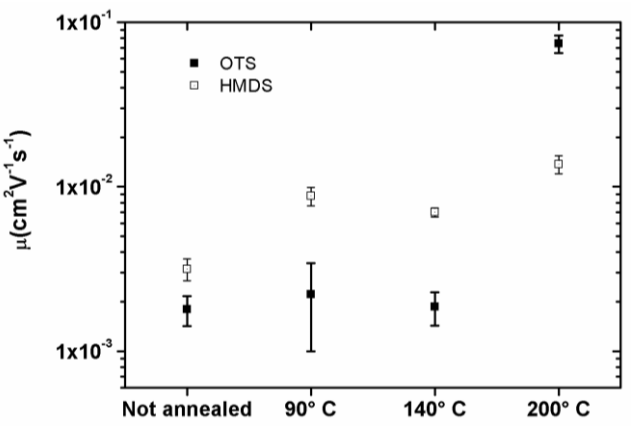

Figure 6.4. A comparative plot displays the electrons field-effect saturation mobility variation in typical ICBA-based OFETs where the active layer underwent annealing at different temperatures (90 °C, 140 °C, and 200°C). A different trend is recorded upon varying the functionalization of the SiO_2 surface with either OTS or HMDS. (W = 10 mm, L = 2.5 μm, the error bars indicate the standard deviation over >4 devices).

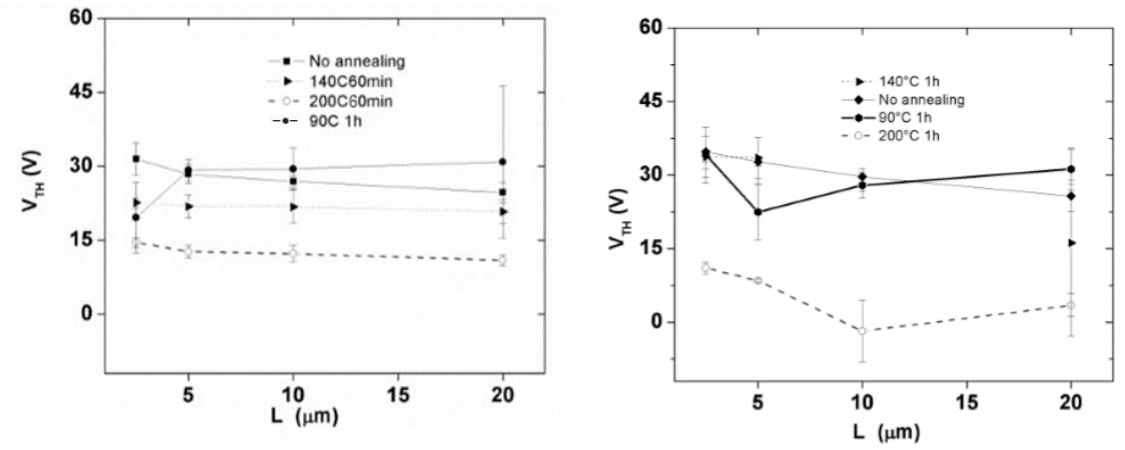

a) **b)**

Figure 6.5. Electrons threshold voltage ($V_{th,e}$) values measured in: **a)** HMDS-treated devices, and **b)** OTS-treated devices at different channel lengths and annealing temperature. (Error bars indicate the standard deviation over >4 devices).

As seen in the previous figures (**Figures 6.4 - 6.5**) showing mobility and threshold voltage values, electrons mobility values obtained from OTS-treated substrates are higher than those obtained from HMDS-treated dielectric layer. This is explained in view of an enhanced surface affinity. OTS treated SiO_2 surface yield to a more hydrophobic surface compared to HMDS. For OTS-treated device annealed at 200 °C, the electron mobility increased by two orders of magnitude with values

approaching 0.1 $cm^2 V^{-1}s^{-1}$ compared to that of non-annealed treated device (in the range of 10^{-3} $cm^2 V^{-1}s^{-1}$), which is the highest ever reported value of electron mobility for ICBA. These improvements in electron mobility are attributed to the thermal annealing which tend to enhance the films morphology and crystallinity. Concerning the threshold voltage, the reported values in the curves presented in **Figure 6.5** ($V_{th,e}$) are all positive values in the range of 0-40 V. In most cases, threshold voltage values are shifted towards the zero with the increase in annealing temperature. The latter behavior was found to be more pronounced in the case of OTS-treated SiO_2 (see **Figure 6.5b**). The threshold voltage shift towards zero is indicative of a film with improved crystallinity accompanied by lower number of defects. In view of that, we put forward the hypothesis that the remarkable mobility increase, especially when OTS is used, stems from a peculiar thermodynamically-favorable assembly of the ICBA molecules. All devices featured a high I_{on}/I_{off} ratio ranging from 10^3 to 10^5.

6.2.2. Correlation between device morphology and electrical properties

The ICBA thin films of untreated and OTS or HMDS treated OFETs annealed at 90 °C, 140 °C and 200 °C were imaged by Atomic Force Microscopy and presented in **Figure 6.6**. Films surface roughness was recorded in **Table 6.1**. AFM images exhibited smoother HMDS films compared to those of OTS (see **Table 6.1**). This can be related to the surface energy. The surface wettability modified by OTS or HMDS was determined by static water contact angle (CA) measurements. The experimental measurements revealed a larger water contact angle (CA) on OTS/SiO_2 (95.5 ± 2.9)° compared to that measured on $HMDS/SiO_2$ surface (62.5 ± 0.5)°. This gives rise to a higher HMDS surface energy, which lend to a better surface affinity of the ICBA molecules on OTS/SiO_2 compared to that of HMDS treated SiO_2 surface.

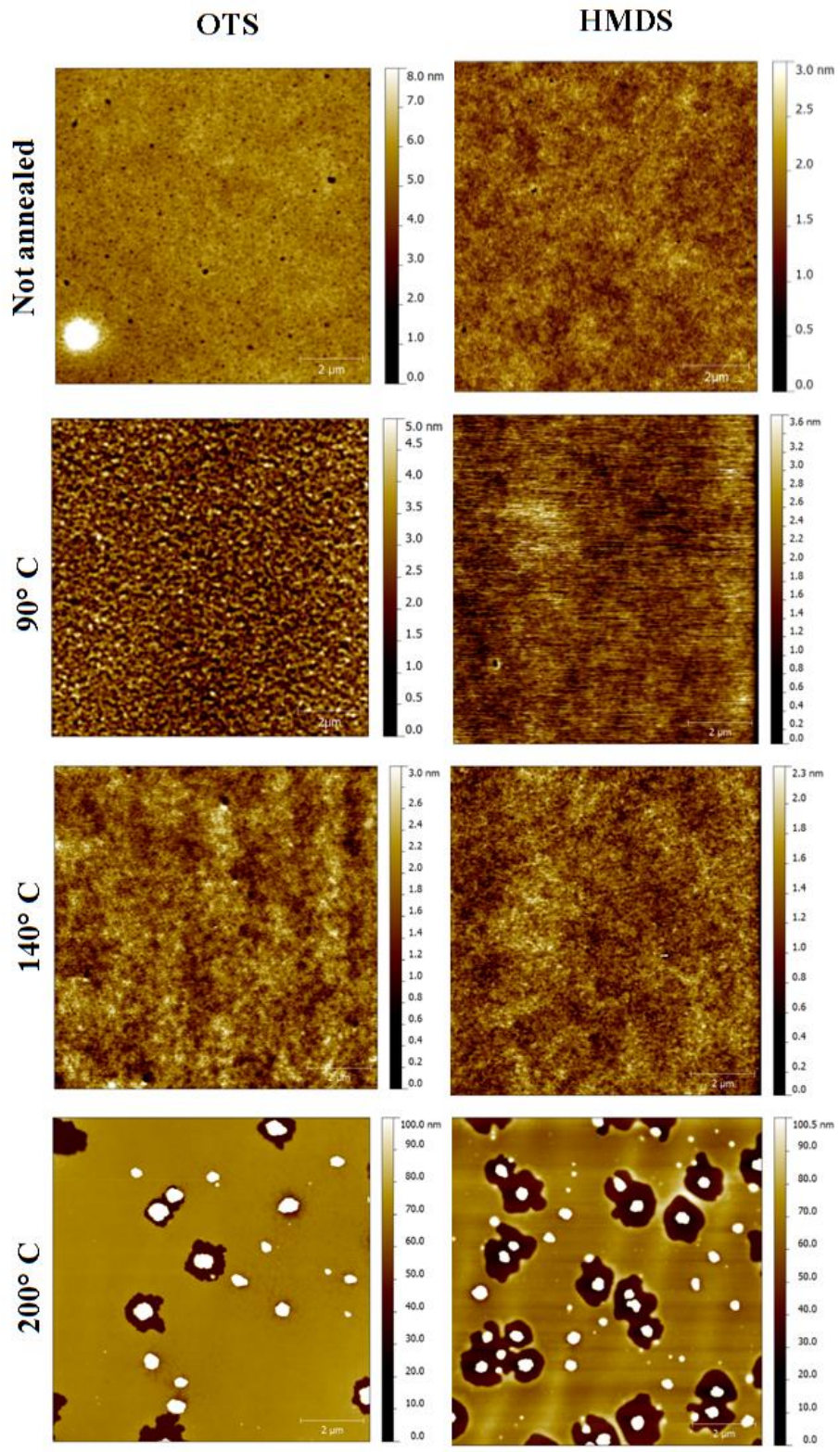

Figure 6.6 Topographical Atomic Force Microscopy images (10 μm x 10 μm) of spin-coated ICBA films (10 mg/mL in chloroform) annealed for 1 hour at different temperature on either OTS or HMDS treated silicon dioxide surface (the scale bar is 2 μm).

	No annealed device	Annealed at 90 °C	Annealed at 140 °C	Annealed at 200 °C
R_{rms} for OTS-treated device	0.504	0.791	0.431	1.200
R_{rms} for HMDS-treated device	0.313	0.428	0.331	2.200

Table 6.1: Film root mean square roughness (R_{rms}) was measured by AFM on the different ICBA films images presented in Figure 6.7.

At 200 °C, both OTS and HMDS treated films are characterized by the presence of tall structure aggregates (see the AFM image showed tall structures in **Figure 6.7**) surrounded by bare silicon oxide and most likely do not take part in the charge transport across the surrounding film whose general thickness decreases due to the local concentration increase of ICBA material in the aggregates. The formation of the latter type of films occurs at > 170°C of temperatures annealing for 1 hour (see **Figure 6.8**). for annealing at 200 °C, aggregates start to form within 10 minutes as recorded in AFM image in **Figure 6.9**.

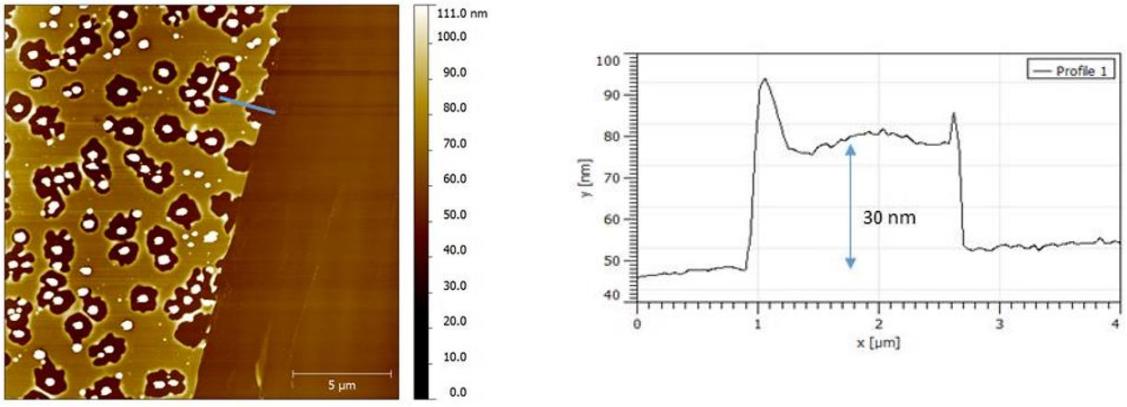

Figure 6.7. Atomic Force Microscopy image showing the step-height (more than 30 nm) of a typical hollow filled by tall structure aggregate within the ICBA film annealed at 200 °C.

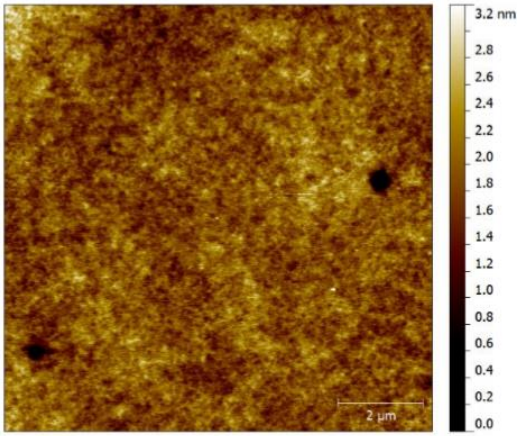

Figure 6.8. Atomic Force Microscopy image of an ICBA film on OTS-treated SiO_2 after annealing at 170°C for 1hour. The surface roughness (Rrms) is equal to 0.37 nm.

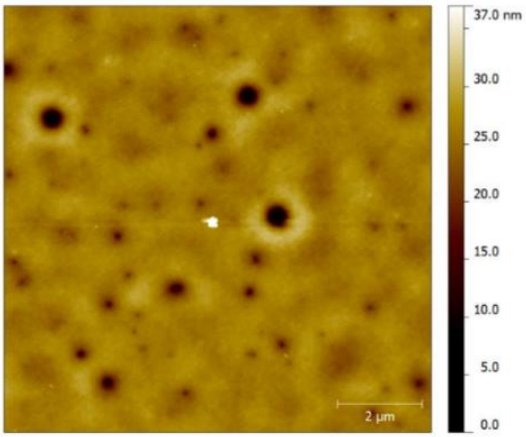

Figure 6.9. Topographic Atomic Force Microscopy image of an ICBA film deposited on OTS-treated SiO_2 after annealing at 200°C for 10 minutes. The surface roughness (R_{rms}) is equal to 2.1 nm.

6.2.3. Correlation between film crystallinity and electrical properties

Grazing Incidence X-Ray Diffraction (2D-GIXRD) measurements using synchrotron light radiation were performed to demonstrate the relationship between the film structural order and crystallinity with the device thermal annealing (see **Figure 6.10**).

Figure 6.10 reports the 2D-GIXRD patterns collected for ICBA films without annealing and with annealing at 200°C (1h), respectively. Isotropic rings are visible at q~0.71 $Å^{-1}$and 1.32 $Å^{-1}$ when the 2D-GIXRD images collected at different incidence angles, are radially integrated (**Figure 6.10c**). Before annealing, the peak width is typical for amorphous films but after annealing at 200°C, the

peaks become slightly narrower which is indicative of an early stage of crystallization. This confirm that the enhanced ICBA electrical performances at 200 °C is related to the structure crystallinity. This comportment is unexpected comparing ICBA to other fullerene systems, like PCBM, which is known to crystallize upon thermal annealing already at 150 °C.[29]

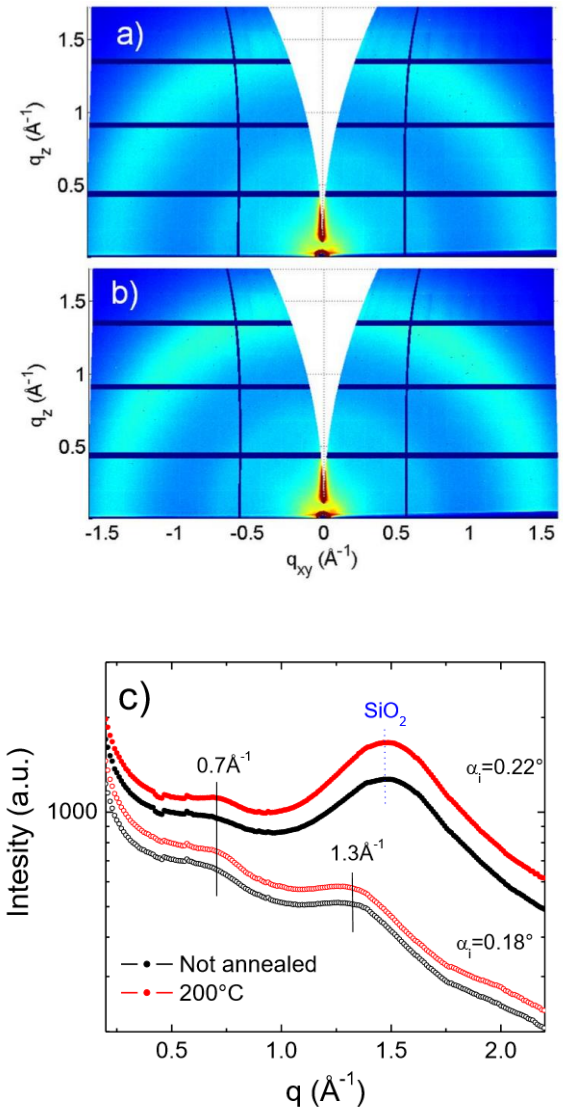

Figure 6.10. 2D-GIXRD patterns of (a) not annealed ICBA film and (b) after thermal treatment at 200°C for 1h collected at α_i=0.22°. c) Radially integrated scattering intensity of 2D-GIXRD images collected at α_i=0.22° (full dots) and at α_i=0.18° (open dots).

6.2.3. Correlation between electrical performances and annealing duration

We have noticed that not only the annealing temperature strongly affected the ICBA film assembly and electrical properties, but also the annealing time of the films was a key parameter.

Figure 6.11 displays electron transfer curves for samples annealed at 200 °C for 10 minutes, 1 hour, and 4 days. The drain current induced by electrons transport in ICBA channel is completely degraded after 4 days annealing time, which is explained by the formation of more tall disconnected aggregates that cover almost all the channel conduction without continuous film around them to bridge source and drain electrodes as showed in the microscopic image in **Figure 6.12**. While, the measured current after 1 hour of annealing is significantly higher than that measured after 10 minutes at the same temperature annealing, this behavior confirms the improved molecular assembly and morphology (see **Figure 6.6** and **Figure 6.12**) resulting to a large mobility difference μ[annealed at 200 °C for 1 h]/μ[annealed at 200 °C for 10 min] ~ 250.

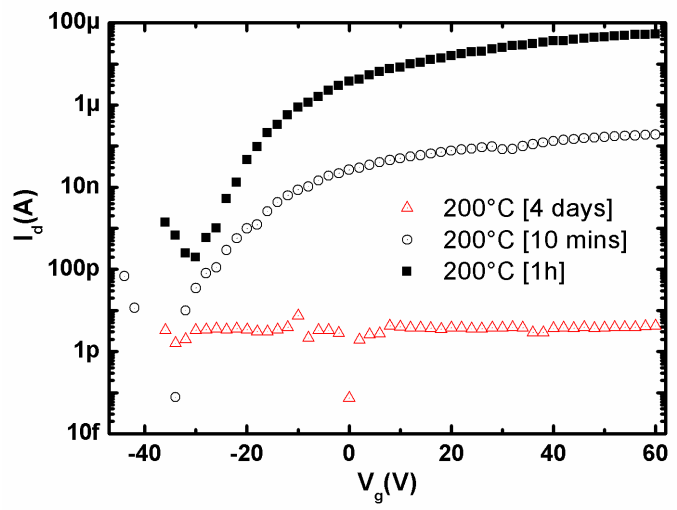

Figure 6.11. Comparative electron transport transfer curves at V_{DS} = 60 V of field-effect transistors based on ICBA with OTS-treated SiO_2, where the active layer underwent annealing at 200 °C for 10 minutes, 1 hour, or 4 days (W = 10 mm, L = 20 μm).

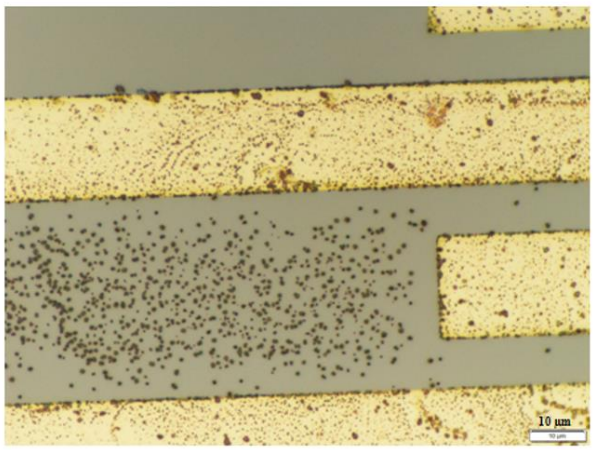

Figure 6.12. Optical Microscope image of an OFET device morphology based on ICBA film deposited on OTS-treated SiO_2 surface, the device was annealed for 4 days at 200°C, the scale bar is 10μm.

6.2.4. Preliminary results on ICBA ambipolar transport

Finally, we investigated the ambipolar character of ICBA through field-effect transistor measurements which revealed ambipolar characteristics with dominant electron transport (μ_e = 0.1 $cm^2V^{-1}s^{-1}$ fore OTS-treated device and annealed at 200 °C) and weaker hole transport (in the range of 10^{-3} $cm^2V^{-1}s^{-1}$). **Figure 6.13** showed the hole transfer characteristics of OTS/HMDS treated devices and annealed at 200 °C for 1 hour.

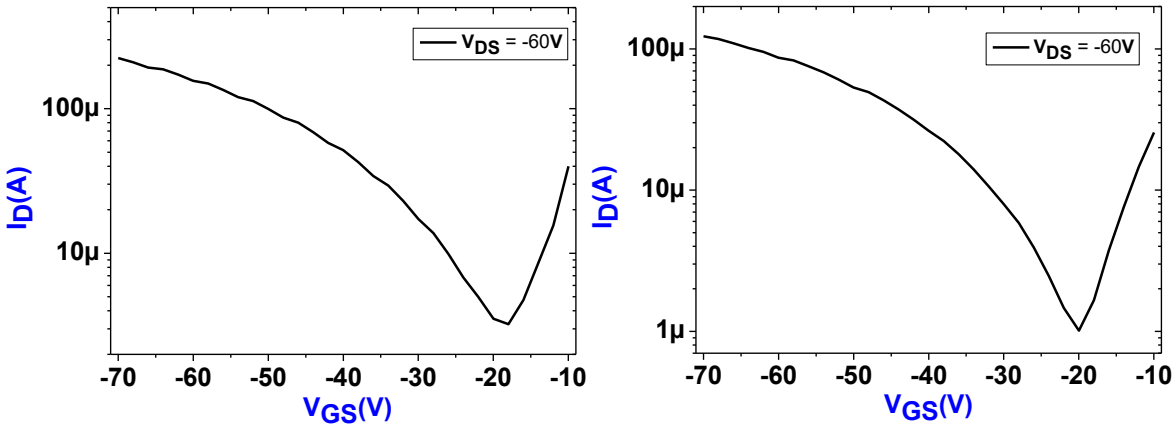

a) **b)**

Figure 6.13. Transfer characteristics for hole charge transport in ICBA-based OFET on which the SiO_2 underwent **a)** OTS and **b)** HMDS surface treatment. Both devices were annealed at 200°C for 1hour (W = 10 mm and L = 2.5 µm).

The I_D-V_{GS} electrical characteristics presented in **Figure 6.3** revealed high holes drain current and good working devices indicating that this system known as an electron transporting material is also able to transport hole charge carriers, which confirm an ambipolar behavior. Such ambipolar behavior has not been yet reported and has been observed in all the fabricated devices in different preparation conditions (OTS or HMDS treatment) before and after thermal annealing at 90 °C, 140 °C, and 200°C.

Fundamental OFET parameters describing ICBA hole transport efficiency, such as hole field-effect mobility (μ_h) and threshold voltage ($V_{th,h}$), were calculated from the saturation regime and plotted in curves presented in **Figure 6.14** and **Figure 6.15** respectively. These parameters were recorded from various samples annealed at 90 °C, 140 °C, and 200 °C, where the SiO_2 is functionalized with OTS or HMDS self-assembled monolayers.

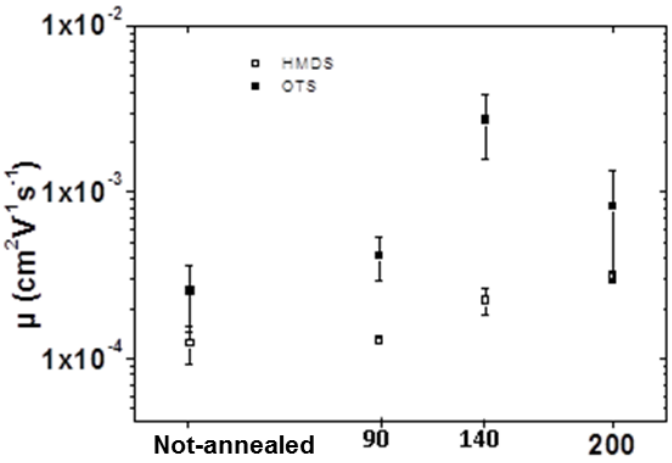

Figure 6.14. A comparative plot displays the hole field-effect saturation mobility variation in typical ICBA-based TFTs where the active layer underwent annealing at different temperatures (90 °C, 140 °C, and 200°C) compared with non-annealed OFETs. A different trend is recorded upon varying the functionalization of the SiO_2 surface with either OTS or HMDS. (W = 10 mm, L = 2.5 μm, Error bars indicate the standard deviation over >4 devices).

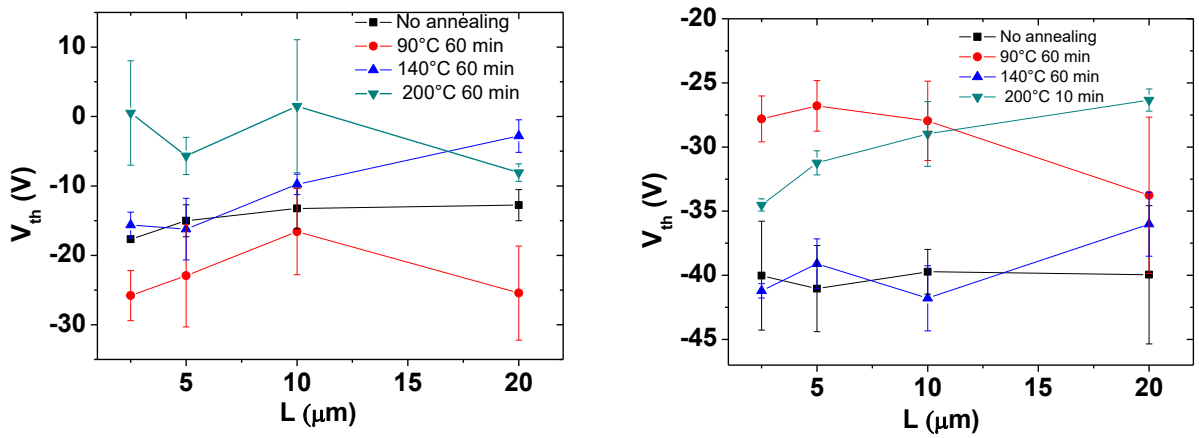

a) **b)**

Figure 6.15. Holes threshold voltage ($V_{th,h}$) values measured on **a)** HMDS-treated devices, and **b)** OTS-treated devices at different channel lengths and annealing temperature. (Error bars indicate the standard deviation over >4 devices).

The enhanced hole transport mobility (from 10^{-4} and 10^{-5} in some untreated devices to 10^{-3} $cm^2V^{-1}s^{-1}$) showed in Figure 6.14 strongly depends on the dielectric surface modification and thermal annealing temperature. The highest hole mobility (2.7×10^{-3} $cm^2V^{-1}s^{-1}$) was extracted from OFET

device treated with OTS and annealed at 140 °C for 1 hour, while at higher temperature annealing, mobility was lower in the range of 10^{-4} regarding all devices with different channel lengths. However, HMDS based devices showed hole mobilities slightly higher than non-annealed OFETs. The hole threshold voltage values are ranging between 0 and -40 V with a tendency to shift towards zero in OTS-treated devices. To be able to explain these electrical results, and the fact that hole mobility seems to reach a high value at 140 °C and tend to be degraded at higher temperatures (the case of 200 °C), it is necessary to provide more analysis and further theoretical studies.

Conclusions

In this work, we have reported on the electrons and holes charge transport properties within Indene-C60 Bis-Adduct (ICBA) thin films, the hole charge transfer in ICBA π-conjugated system is still under investigation by performing theoretical calculation on molecular dynamics. However, the charge transport in ICBA derivative seems to be more complex and will require more in-depth charge transport simulations,[30] to understand from a theoretical point of view the relationship between the hole-transport and the structure of ICBA semiconductor. We investigated the effect of silicon dioxide treatments as well as the thermal annealing and duration on the electrical properties by studying film crystallinity and morphology. We have demonstrated that both electron and holes mobilities can be enhanced by the SiO_2 functionalization with OTS/SiO_2 and HMDS/SiO_2 hydrophobic surfaces. Preliminary measurements showed that, for the first time, ICBA molecules exhibited ambipolar transport. The electron and hole mobility enhanced upon OTS treatments and reached 2.7×10^{-3} $cm^2V^{-1}s^{-1}$ for hole transport at 140 °C and 0.1 $cm^2V^{-1}s^{-1}$ at 200 °C for electrons, the latter electron mobility is the highest reported value in literature. The chemisorption of hydrophobic HMDS and OTS SAMs on SiO_2 reduces the surface energy of SiO_2 and decreases the trapping effect induced by the Si–OH groups, leading to a more favorable environment for the ICBA organic semiconductor molecules deposition. The best electrons and holes mobilities were measured on OFET devices which underwent OTS treatment followed by thermal annealing at a temperature of 200 °C and 140 °C respectively for 1 hour, this confirms that ICBA system is strongly affected by the processing preparation conditions. When ICBA molecules are deposited on OTS treated surface, they can move and undergo self-assembly due to the lower surface energy. Moreover, the thermal annealing operated at > 170 °C for electron transport was found to be a key method for improving the thin film morphology and thus the electrical properties. GIXRD did not provide strong evidence in atomic scale of the structural order. In the future, other structural analysis can be realized using different techniques like Grazing incident small angle scattering to explore the formed aggregates at the nanoscale.

6.3. References

1. Lopez, A. M.; Mateo-Alonso, A.; Prato, M., Materials Chemistry of Fullerene C-60 Derivatives. *J. Mater. Chem.* **2011,** *21* (5), 1305-1318.

2. Arias, A. C.; MacKenzie, J. D.; McCulloch, I.; Rivnay, J.; Salleo, A., Materials and Applications for Large Area Electronics: Solution-Based Approaches. *Chem. Rev.* **2010,** *110* (1), 3-24.

3. Klauk, H.; Zschieschang, U.; Pflaum, J.; Halik, M., Ultralow-Power Organic Complementary Circuits. *Nature* **2007,** *445* (7129), 745-748.

4. Halik, M.; Klauk, H.; Zschieschang, U.; Schmid, G.; Dehm, C.; Schutz, M.; Maisch, S.; Effenberger, F.; Brunnbauer, M.; Stellacci, F., Low-Voltage Organic Transistors with an Amorphous Molecular Gate Dielectric. *Nature* **2004,** *431* (7011), 963-966.

5. Klauk, H., Organic Thin-Film Transistors. *Chem. Soc. Rev.* **2010,** *39* (7), 2643-2666.

6. Sirringhaus, H.; Bird, M.; Richards, T.; Zhao, N., Charge Transport Physics of Conjugated Polymer Field-Effect Transistors. *Adv. Mater.* **2010,** *22* (34), 3893-3898.

7. Sirringhaus, H., Device Physics of Solution-Processed Organic Field-Effect Transistors. *Adv. Mater.* **2005,** *17* (20), 2411-2425.

8. Zaumseil, J.; Donley, C. L.; Kim, J. S.; Friend, R. H.; Sirringhaus, H., Efficient Top-Gate, Ambipolar, Light-Emitting Field-Effect Transistors Based on a Green-Light-Emitting Polyfluorene. *Adv. Mater.* **2006,** *18* (20), 2708-2712.

9. Vandewal, K.; Widmer, J.; Heumueller, T.; Brabec, C. J.; McGehee, M. D.; Leo, K.; Riede, M.; Salleo, A., Increased Open-Circuit Voltage of Organic Solar Cells by Reduced Donor-Acceptor Interface Area. *Adv. Mater.* **2014,** *26* (23), 3839-3843.

10. Dennler, G.; Scharber, M. C.; Brabec, C. J., Polymer-Fullerene Bulk-Heterojunction Solar Cells. *Adv. Mater.* **2009,** *21* (13), 1323-1338.

11. Yan, H.; Chen, Z. H.; Zheng, Y.; Newman, C.; Quinn, J. R.; Dötz, F.; Kastler, M.; Facchetti, A., A High-Mobility Electron-Transporting Polymer for Printed Transistors. *Nature* **2009,** *457* (7230), 679-686.

12. Rao, A.; Chow, P. C. Y.; Gélinas, S.; Schlenker, C. W.; Li, C. Z.; Yip, H. L.; Jen, A. K. Y.; Ginger, D. S.; Friend, R. H., The Role of Spin in the Kinetic Control of Recombination in Organic Photovoltaics. *Nature* **2013,** *500* (7463), 435-439.

13. Vandewal, K.; Albrecht, S.; Hoke, E. T.; Graham, K. R.; Widmer, J.; Douglas, J. D.; Schubert, M.; Mateker, W. R.; Bloking, J. T.; Burkhard, G. F.; Sellinger, A.; Fréchet, J. M. J.; Amassian, A.; Riede, M. K.; McGehee, M. D.; Neher, D.; Salleo, A., Efficient Charge Generation by Relaxed Charge-Transfer States at Organic Interfaces. *Nat. Mater.* **2014,** *13* (1), 63-68.

14. Noriega, R.; Rivnay, J.; Vandewal, K.; Koch, F. P. V.; Stingelin, N.; Smith, P.; Toney, M. F.; Salleo, A., A General Relationship Between Disorder, Aggregation and Charge Transport in Conjugated Polymers. *Nat. Mater.* **2013,** *12* (11), 1037-1043.

15. Rivnay, J.; Jimison, L. H.; Northrup, J. E.; Toney, M. F.; Noriega, R.; Lu, S. F.; Marks, T. J.; Facchetti, A.; Salleo, A., Large Modulation of Carrier Transport by Grain-Boundary Molecular Packing and Microstructure in Organic Thin Films. *Nat. Mater.* **2009,** *8* (12), 952-958.

16. Facchetti, A., *Mater. Today* **2007,** *10*, 3.

17. Konenkamp, R.; Priebe, G.; Pietzak, B., Carrier Mobilities and Influence of Oxygen in C-60 films. *Phys. Rev. B* **1999,** *60* (16), 11804-11808.

18. Voroshazi, E.; Vasseur, K.; Aernouts, T.; Heremans, P.; Baumann, A.; Deibel, C.; Xue, X.; Herring, A. J.; Athans, A. J.; Lada, T. A.; Richter, H.; Rand, B. P., Novel bis-C-60 Derivative Compared to Other Fullerene bis-Adducts in High Efficiency Polymer Photovoltaic Cells. *J. Mater. Chem.* **2011,** *21* (43), 17345-17352.

19. Guo, X.; Zhang, M. J.; Cui, C. H.; Hou, J. H.; Li, Y. F., Efficient Polymer Solar Cells Based on Poly(3-hexylthiophene) and Indene-C-60 Bisadduct Fabricated with Non-halogenated Solvents. *Acs Appl. Mater. Inter.* **2014,** *6* (11), 8190-8198.

20. Shoaee, S.; Subramaniyan, S.; Xin, H.; Keiderling, C.; Tuladhar, P. S.; Jamieson, F.; Jenekhe, S. A.; Durrant, J. R., Charge Photogeneration for a Series of Thiazolo-Thiazole Donor Polymers Blended with the Fullerene Electron Acceptors PCBM and ICBA. *Adv. Funct. Mater.* **2013,** *23* (26), 3286-3298.

21. Hoke, E. T.; Vandewal, K.; Bartelt, J. A.; Mateker, W. R.; Douglas, J. D.; Noriega, R.; Graham, K. R.; Fréchet, J. M. J.; Salleo, A.; McGehee, M. D., Recombination in Polymer:Fullerene Solar Cells with Open-Circuit Voltages Approaching and Exceeding 1.0 V. *Adv. Energy. Mater.* **2013,** *3* (2), 220-230.

22. Anthopoulos, T. D.; de Leeuw, D. M.; Cantatore, E.; van 't Hof, P.; Alma, J.; Hummelen, J. C., Solution Processible Organic Transistors and Circuits Based on a C-70 Methanofullerene. *J. Appl. Phys.* **2005,** *98* (5), 054503.

23. Yu, H.; Cho, H. H.; Cho, C. H.; Kim, K. H.; Kim, D. Y.; Kim, B. J.; Oh, J. H., Polarity and Air-Stability Transitions in Field-Effect Transistors Based on Fullerenes with Different Solubilizing Groups. *Acs Appl. Mater. Inter.* **2013,** *5* (11), 4865-4871.

24. Anthopoulos, T. D.; Tanase, C.; Setayesh, S.; Meijer, E. J.; Hummelen, J. C.; Blom, P. W. M.; de Leeuw, D. M., Ambipolar Organic Field-Effect Transistors Based on a Solution-Processed Methanofullerene. *Adv. Mater.* **2004,** *16* (23-24), 2174-2179.

25. Li, C. Z.; Chueh, C. C.; Yip, H. L.; Zou, J. Y.; Chen, W. C.; Jen, A. K. Y., Evaluation of Structure-Property Relationships of Solution-Processible Fullerene Acceptors and Their n-Channel Field-Effect Transistor Performance. *J. Mater. Chem.* **2012,** *22* (30), 14976-14981.

26. Nardes, A. M.; Ferguson, A. J.; Whitaker, J. B.; Larson, B. W.; Larsen, R. E.; Maturova, K.; Graf, P. A.; Boltalina, O. V.; Strauss, S. H.; Kopidakis, N., Beyond PCBM: Understanding the Photovoltaic Performance of Blends of Indene-C60 Multiadducts with Poly(3-hexylthiophene). *Adv. Funct. Mater.* **2012,** *22* (19), 4115-4127.

27. Bonifazi, D.; Enger, O.; Diederich, F., Supramolecular [60]fullerene Chemistry on Surfaces. *Chem. Soc. Rev.* **2007,** *36* (2), 390-414.

28. Ball, J. M.; Bouwer, R. K. M.; Kooistra, F. B.; Frost, J. M.; Qi, Y. B.; Domingo, E. B.; Smith, J.; de Leeuw, D. M.; Hummelen, J. C.; Nelson, J.; Kahn, A.; Stingelin, N.; Bradley, D. D. C.; Anthopoulos, T. D., Soluble Fullerene Derivatives: The Effect of Electronic Structure on Transistor Performance and Air Stability. *J. Appl. Phys.* **2011,** *110* (1), 014506.

29. He, Y. J.; Chen, H. Y.; Hou, J. H.; Li, Y. F., Indene-C-60 Bisadduct: A New Acceptor for High-Performance Polymer Solar Cells. *J. Am. Chem. Soc.* **2010,** *132* (4), 1377-1382.

30. D'Avino, G.; Olivier, Y.; Muccioli, L.; Beljonne, D., Do Charges Delocalize Over Multiple Molecules in Fullerene Derivatives? *J. Mater. Chem. C* **2016,** *4* (17), 3747-3756.

Chapter 7. High-performance phototransistors based on PDIF-CN2 solution-processed single fiber and multifiber assembly

Introduction

Over last few decades, the organic electronics platform has attracted a great attention, and thanks to their potential applications in optoelectronic devices,[1] organic photovoltaics (OPVs),[2] organic sensors,[3] organic memories, flexible and stretchable organic electronics and development of novel and highly efficient organic light-emitting diodes (OLEDs).[4-5] Among those devices, solution-processed organic field effect transistors (OFETs) are a captivating research field,[6-8] because organic transistors not only are cheap, flexible,[9] low-cost,[10] easy to product at low processing temperatures and provide intrinsic characteristics of organic semiconductor materials[11-13] but also they also represent a basic component in electronic circuits.[1] Specifically, OFETs with photosensitive organic semiconductor materials are widely investigated as promising candidates for high-performance phototransistors (OPTs) and more complex systems used as chemical and biological photo-sensing devices.[14-15]

Organic phototransistors, i.e. OFETs in which an incident light is used in addition to a gate field to modulate the charge-carrier density inside the channel, have many advantages over their inorganic counterparts, such as the tunability of the optoelectronic properties via the molecular design and the possibility to be assembled on non-planar supports opening perspectives towards applications in the flexible and wearable electronis.[16-25] Low-dimensional organic architectures such as crystalline micro/nanowire,[26-34] microribbon[35] and quantum dot[36-37] structures have showed high photosensitivity and good charge transport properties. Among the organic semiconducting molecules used as active components in efficient phototransistors, perylene di-imide (PDI) derivatives are particularly suitable because of their characteristic absorption in the visible region combined with the capacity to transport electrons.[38-49] One of the major limitations of organic transistors, especially those based on n-type

systems, is their air sensitivity. To overcome such a limitation, we have focused our attention on air-stable *n*-type perylene di-imide derivative, i.e. N, N'-1H, 1H-perfluorobutyl-dicyano perylene di-imide (PDIF-CN2) (see **Figure 7.1**), which is known to form highly crystalline fibers by solvent-induced precipitation (SIP), which is a simple solution-processable method to produce high-performing crystalline structures with respect to those that are vapor-grown. In this chapter we report on the integration of various types of PDIF-CN_2 architectures, including single fibers, multiple fibers and spin-coated films, in three-terminal devices while evaluating the influence of the different interfaces, i.e. metal/semiconductor and dielectric/semiconductor, on the electrical performances. In addition, we have carried out an exhaustive study of the light responsive properties of these different PDIF-CN_2 architectures making it possible to elucidate the relationship between molecular order and photoresponsivity.

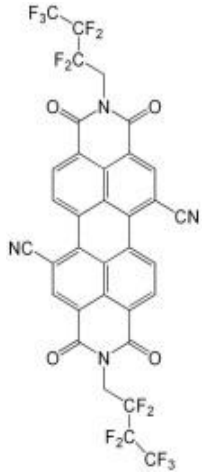

Figure 7.1. Chemical structure of the organic semiconductor PDIF-CN2.

7.1. Experimental

7.1.1. Device fabrication

PDIF-CN2 was dissolved in chloroform (99, 0-99, 4% GC) in a concentration of 2 mg/ml used in SIP process and of 0.5 mg/ml for spin-coating method. The solutions were heated at 50°C until the molecules are completely dissolved. We have fabricated transistors in two configurations, i.e. bottom-contact-bottom-gate and top-contact bottom-gate using highly doped n-type silicon wafers as substrate with thermally-grown SiO_2 layers (230 nm) having a unit area capacitance (C_i) of 15 $nFcm^{-2}$ for all the fabricated organic OFET and OPT devices.

7.1.1.1. OFET devices fabricated on bottom-contact bottom-gate configuration

Micro-lithographed 40 nm thick gold source and drain electrodes were patterned on the dielectric substrate. SiO_2 substrates are protected by a photoresist layer that needs to be washed before use, the substrates were cleaned with acetone (95% GC) and isopropanol (99.7 % GC) in an ultrasonic bath (20 minutes in each solvent) followed by a gentle drying under nitrogen gas. After that, the substrate surface was treated with UV/Ozone cleaning and functionalized with hexamethyldisilazane (HMDS) or octadecyltrichlorosilane (OTS) self-assembled monolayers (see section 5.1.2 in Chapter 5). Afterwards, the gold source-drain electrode surface was modified with (chemisorbed) undecanethiol ($C_{11}H_{23}SH$) SAMs. The presence of such SAM on Au surface lowers the metal work function while rendering it closer to the LUMO energy level of the PDIF-CN2 which amounts to -4.5 eV. The PDIF-CN2 was spin-coated on the dielectric surfaces by applying a 100 µl drop of PDIF-CN2 solution in chloroform onto the substrate and spin it at 1500 RPM for 60 seconds forming thin film layers inside the glove box. The device was then annealed at 60°C for 1 hour concerning FETs based on annealed spin-coated thin films. On the other hand, PDIF-CN2 fibers structures were formed using the solvent induced precipitation (SIP) process, where 150 µl of PDIF-CN2 solution in chloroform (2mg/ml) was injected rapidly in 2.85 ml of methanol (CH_3OH, 99,9% GLC). Within a period of 15 minutes the fibers were formed in solution and precipitated on the bottom of vials. The fibers were then transferred to the surface by dropping multiple times 20 µl until the full surface coverage was reached.

Figure 7.2 presents a schematic illustration of OFET device structure based on multifibers and thin-films performed in bottom-contact bottom-gate geometry including their optical microscopic images.

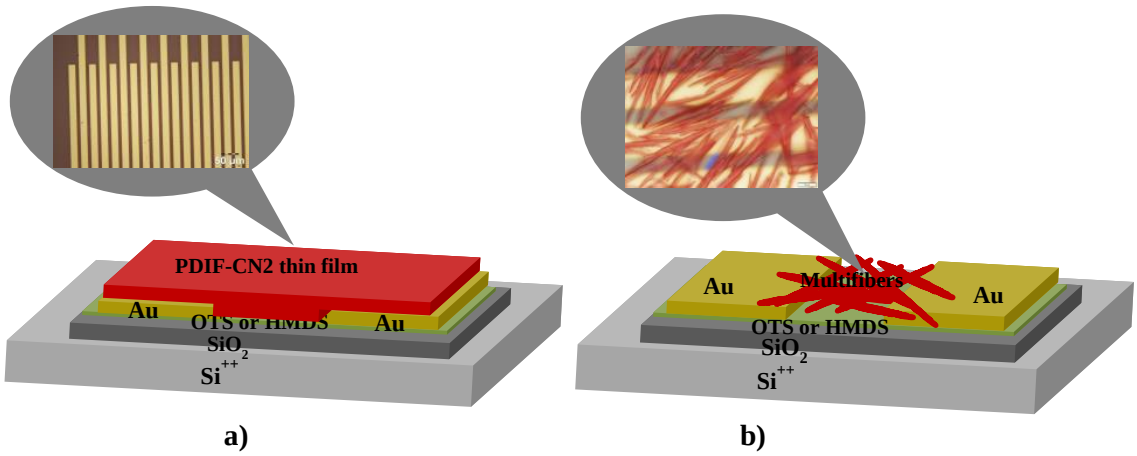

Figure 7.2. Schematic of OFET structures based on PDIF-CN2 a) thin-film and b) multifibers in bottom-contact bottom-gate configuration and their optical microscopic images.

7.1.1.2. Multifibers-based OFETs fabricated in top-contact bottom-gate configuration

To improve the physical contact of multifiber assemblies with source and drain electrodes, we have also fabricated devices in top-contact bottom-gate (see the OFET structure and its optical image in **Figure 7.3**) configuration following the same steps concerning cleaning devices with acetone, isopropanol, UV/Ozone and OTS gate insulator surface treatment (within the same procedure explained above) used for bottom-contact devices. The fibers were deposited by SIP on SiO_2 surfaces, then we evaporated on the top source and drain gold electrodes through a shadow mask inside a vacuum chamber at pressure of 10^{-6} mbar. The evaporation rate was maintained at ~0.02-0.04 nm/s. In this way 50 nm thick films top Au electrodes were grown. The evaporation was done by using Plassys ME300B thermal evaporator.

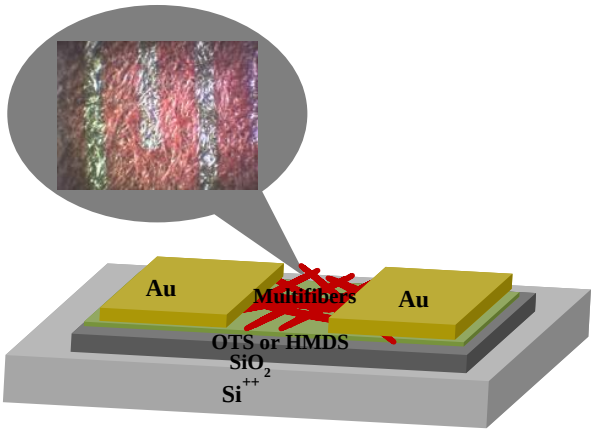

Figure 7.3. Schematic of an OFET structure based on PDIF-CN2 multifibers in top-contact bottom-gate configuration.

Single-fiber devices were fabricated using top-contact bottom-gate geometry (OFET structure and its optical image is presented in **Figure 7.4**). Before depositing the single fiber, the SiO_2 surface was functionalized with OTS to minimize interfacial trapping sites for charges during device operation. SIP fibers were cast onto the functionalized SiO_2 substrates followed by the deposition of 40 nm-thick Au electrodes by thermal evaporation.

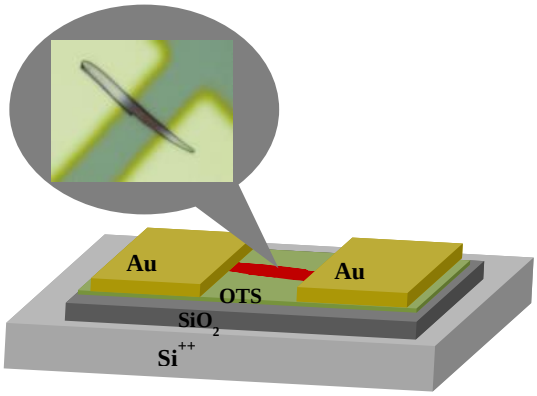

Figure 7.4. Schematic of an OFET structure based on PDIF-CN2 single fiber in top-contact bottom-gate configuration.

7.1.1.3. OPT devices fabrication

Organic thin film phototransistor (OPTs) devices based on spin-coated thin film and multifibers assemblies of PDIF-CN2 in bottom-contact bottom-gate configuration (see **Figure 7.5 a and b**) as well as OPTs based on PDIF-CN2 single fiber in top-contact bottom-gate geometry (see **Figure 7.5 c**) were fabricated and used as analytic system to study the optical and electrical properties of perylene derivative (PDIF-CN2). The active channel of the OTFT devices was illuminated by light radiation of wavelength 525 nm and the irradiation effect on the PDIF-CN2 electrical responses was investigated under different light incident optical powers at room temperature and in nitrogen atmosphere.

Phototransistor devices were characterized in dark and under light irradiation from the top using a Leica LED1000 OLED ring (white light, 5.06 mW cm^{-2}) and an Optometric LLC TLS-25 M tunable light source with a monochromatic beam, light irradiation was performed at 525 nm wavelength at either 4.84 mW cm^{-2} or 7.24 µW cm^{-2} light intensity.

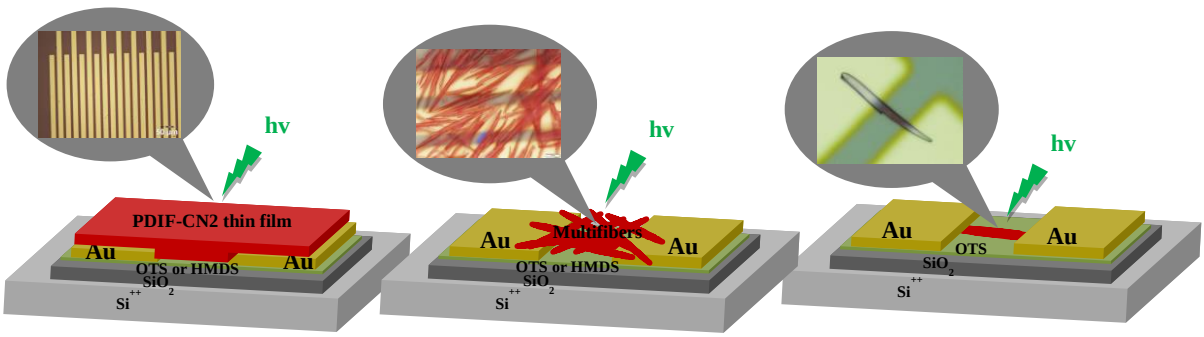

a) **b)** **c)**

Figure 7.5. Schematic of OPT structures based on PDIF-CN2 **a)** thin-film, **b)** multifibers in bottom-contact bottom-gate configuration and **c)** single fiber device in top-contact bottom-gate geometry and their corresponding optical microscopic images.

All the fabricated OFET and OPT devices in different geometries were then characterized. The current−voltage (I−V) characteristics of all devices were measured inside the glovebox in nitrogen atmosphere. The air-stability tests performed under illumination were carried out outside the glovebox at controlled room temperature and humidity (T = 22°C, RH% ~ 25) by contacting the source, drain and gate electrodes and applying different voltages using a Cascade Microtech M150 probe station with dual channel Keithley 2636A source-meter and associated software. The electron mobility was extracted in the saturation regime according to the following equation:

$$\mu_{sat} = \frac{2 \cdot \left(\frac{\partial \sqrt{I_D}}{\partial V_{GS}} \right)^2}{C_i \frac{W}{L}}$$

Where I_D is the current measured between source and drain electrodes, V_{GS} the potential difference measured between the voltage probes, L their distance, W the channel width and C_i the capacitance per unit area of the insulator layer.

7.2. Results and discussion

7.2.1. Organic field-effect transistors based on PDIF-CN2 n-type semiconductor

It is known that OFET device performances are highly dependent on the device geometry. Typicaly, top-contact geometry is characterized by low contact resistance compared to bottom-contact structure, this is attributed to the large charge injection area at the interface metal electrode-semiconductor. On the other hand, the bottom-contact structure is very simple and more robust and preferable for processing because the semiconductor deposition is the only processing step after photolithography technique and devices performances are not affected by other processing steps (like source/drain electrode contacts evaporation). This advantage ensures a minimum process-induced damage of the organic layer. The OFET electrical characteristics improve when the source and drain electrodes are bridged by crystalline structures as semiconductor layer, giving rise to a percolation pathways for charge carriers transport. For this reason, we have fabricated organic devices based on high performance perylene derivative (PDIF-CN2) crystalline structures in different geometries. Such

self-assembled fibers exhibit a much higher degree of crystallinity when compared to spin-coated thin films obtained from the same molecule (see **Figure 7.6**). Selected-area electronic-diffraction (SAED) studies on PDIF-CN2 single fibers deposited on SiO_2 performed previously in our group[50] confirmed that molecules self-assemble in an edge-on orientation on the basal plane of the surface with the fluoroalkyl chains embedded in between the aromatic cores and the SiO_2 dielectric. Different types of architectures based on PDIF-CN2 have shown extremely high field-effect mobilities qualifying this system as a reference n-type semiconductor for organic electronics.[51-56]

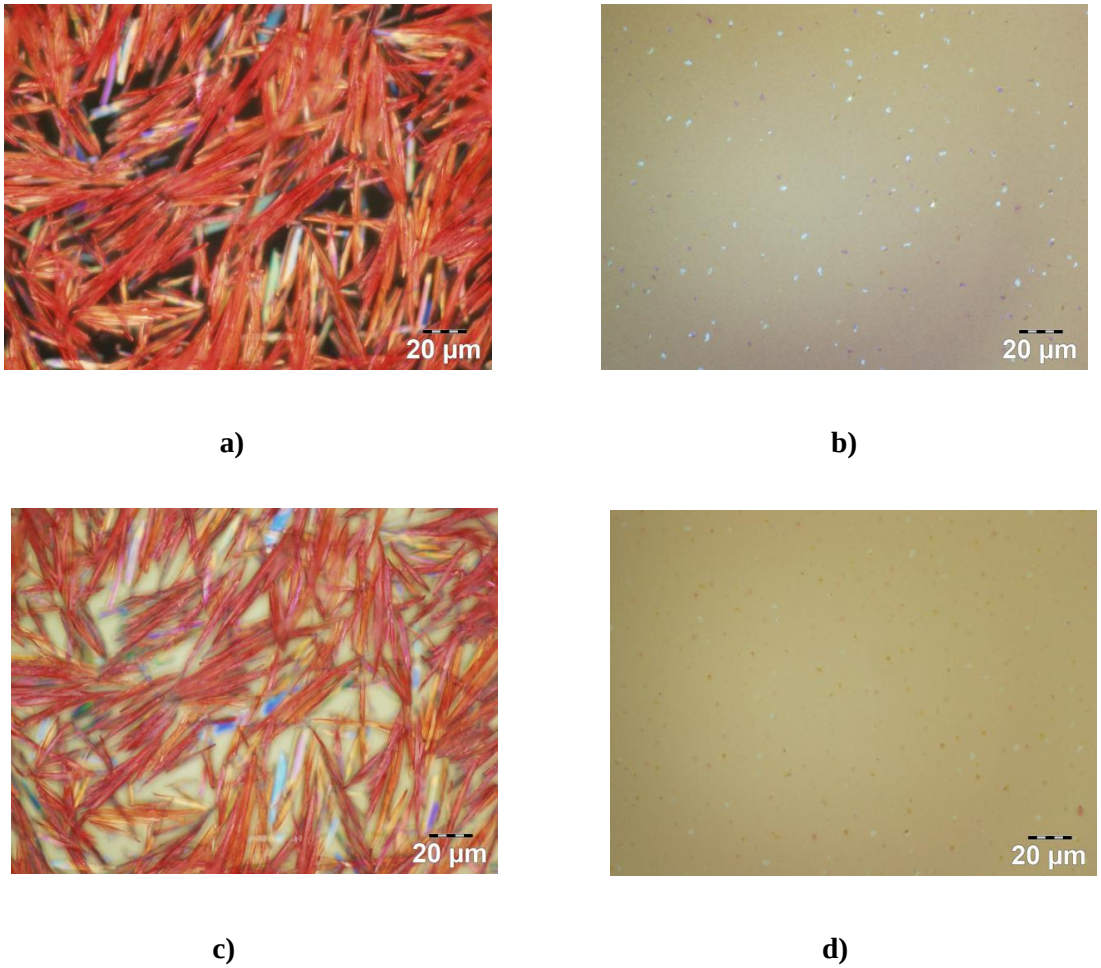

Figure 7.6. Polarized optical microscopic images of **a)**, **c)** multifibers and **b)**, **d)** amorphous spin-coated film-based devises.

7.2.1.1. Effect of SiO_2 surface and gold electrodes functionalization on PDIF-CN2-based OFETs electrical performance

Bottom-contact bottom-gate organic transistors based on PDIF-CN2 spin-coated thin films and multifibers were fabricated and electrically characterized. Organic transistors fabricated on untreated SiO_2 exhibited poor charge transport characteristics for both multifiber assemblies and spin-coated devices (see **Table 7.1** and **Table 7.2**). In order to promote the packing of spin-coated molecules while studying the assembly of the PDIF-CN2 fibers at the surface, the SiO_2 dielectric substrate was modified with UV-Ozone treatment and functionalized with either hexamethyldisilazane (HMDS) or octadecyltrichlorosilane (OTS) self-assembled monolayers. Moreover, the chemisorption of undecanethiols ($C_{11}H_{23}$-SH) on Au electrodes guaranteed simultaneously an improved hydrophobic nature of the metallic surface to promote physisorption of the organic semiconductor, thus ensuring a good physical contact, and an optimization of the injection of charges from the electrodes into the LUMO of the semiconductor by decreasing the Au electrode work function of ca. 250 meV.

Multifiber-based FET		
devices treatment	**V_{th} (V)**	**μ ($cm^2V^{-1}s^{-1}$)**
Non-treated SiO_2	*38 ± 6*	$(4.3 \pm 0.1) \times 10^{-6}$
UV-Ozone cleaning	*30 ± 9*	$(1.1 \pm 0.1) \times 10^{-3}$
UV-Ozone/Thiol	*35 ± 5*	$(1.2 \pm 0.3) \times 10^{-3}$
HMDS SAMs	*-14 ± 4*	$(2.7 \pm 0.9) \times 10^{-3}$
HMDS/Thiol SAMs	*-15 ± 2*	$(3.0 \pm 0.7) \times 10^{-3}$
OTS SAMs	-12 ± 4	$(2.5 \pm 0.4) \times 10^{-3}$
OTS/Thiol SAMs	-18 ± 6	$(3.4 \pm 0.5) \times 10^{-3}$

Table 7.1. Summary of multifiber-based FET parameters measured in saturation regime. [W = 10 mm, L = 2.5 μm].

Table 7.1 summarizes the different field-effect mobility values extracted from saturation regime as well as threshold voltage (V_{th}) for bottom-contact bottom-gate devices based on multifiber structures. It reveals that the best mobilities are measured on OFET devices which underwent OTS or HMDS treatment followed by chemisorption of undecanethiol SAMs on the Au electrodes. Noteworthy, our results show that the charge injection from the functionalized gold electrodes leads to

negligible enhancements in both mobility and V_{th}. The devices with untreated SiO_2 displayed very low mobility values on the order of 10^{-6} $cm^2V^{-1}s^{-1}$ for both multifiber and spin-coated devices. Ideally, the dielectric surface should provide a favorable environment to allow the generation of π-π stacked architectures in order to form highly ordered organic films. The chemisorption of hydrophobic SAMs on SiO_2 reduces the surface energy of SiO_2 while decreasing the trapping induced by the Si–OH groups, giving a more favorable environment for the organic semiconductor molecules deposition, especially for spin-coated films[57]. We recorded a significant improvement in the curve shape, yield of working devices as well as mobility (on the order of 10^{-3} $cm^2V^{-1}s^{-1}$) and threshold voltage when the SiO_2 was treated with OTS or HMDS which favored the fiber affinity for the surface while reducing the inter-fiber aggregation and offering a better interface with the dielectric surface in terms of trapping capacity which decreases when the hydroxyl groups of the silicon dioxide are screened[57] (see **Figure 7.7**).

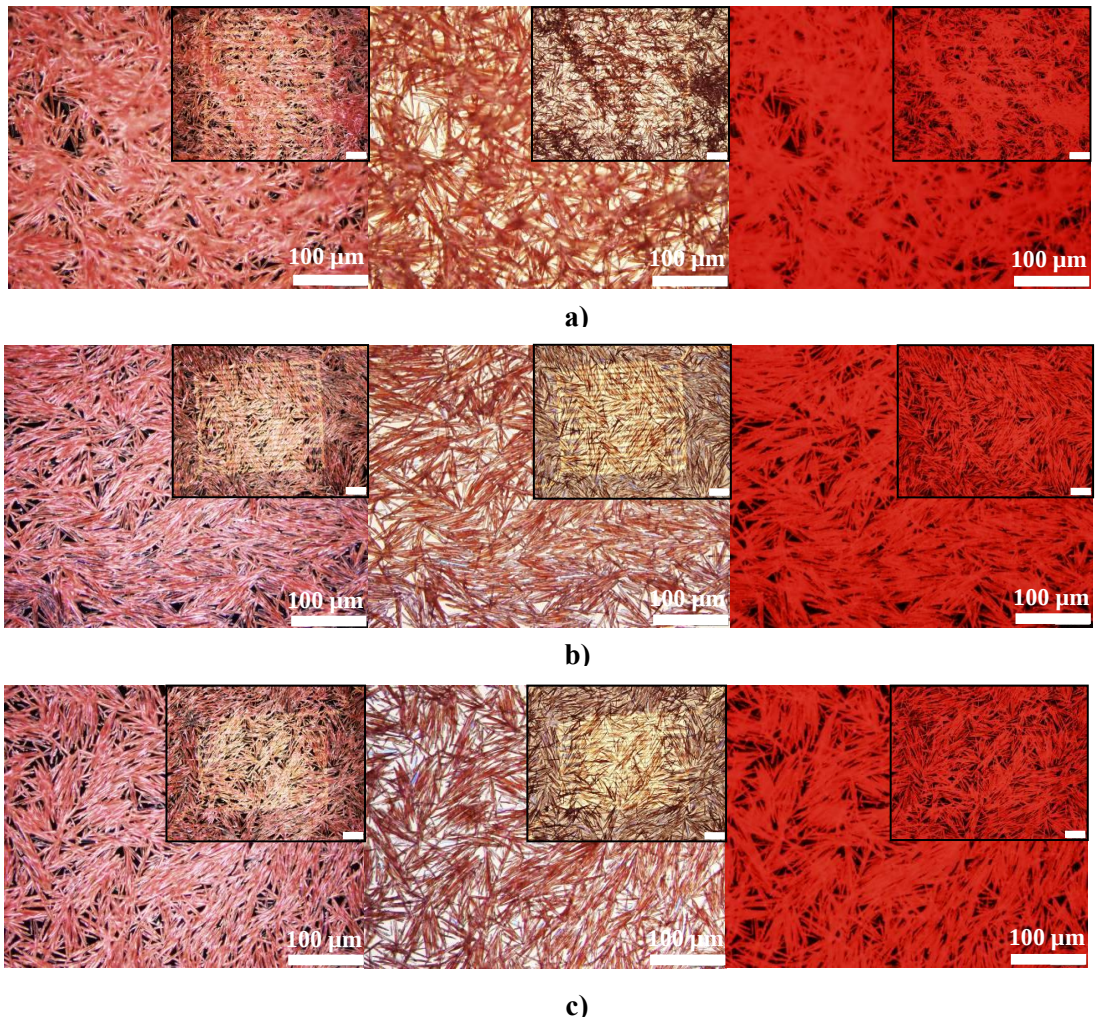

Figure 7.7. Optical microscopic and fluorescence images of multifiber deposited on **a)** untreated SiO_2, **b)** OTS or **c)** HMDS treated SiO_2. Inset scale bar is 100 µm.

Figure 7.7 shows different assembly of fibers on treated and untreated SiO_2 surface. It reveals a propensity to form single layers of fibers on SiO_2 surfaces treated with OTS and HMDS. Morphological and charge transport characterization demonstrated that the hydrophobic nature of the substrate surface has a major impact on the final response of the devices. In order to verify both reliability and reproducibility of the OFET devices based on multifiber assemblies a large number of devices (>100) were prepared on both HMDS-/OTS-treated and untreated silicon dioxide substrates. All fabricated OFETs exhibit the same electrical performances, proving a good reproducibility of the Solvent Induced Precipitation process used to make them.

In addition, the effect of a mild thermal annealing was tested on both thin-film and multifiber FETs in order to improve the degree of crystallinity within the sample. For spin-coated devices, annealing at 60°C for 1 hour led to an increase in their electrical performances as shown in **Table 7.2**.

Spin-coated thin-film based FET		
devices treatment	**V_{th} (V)**	**μ ($cm^2V^{-1}s^{-1}$)**
Non-treated SiO_2	(41 ± 9)	$(6.3 \pm 0.4) \times 10^{-6}$
OTS	(13 ± 8)	$(3.9 \pm 0.1) \times 10^{-4}$
OTS annealed devices at 60°C for 1h	(-23 ± 2)	$(2.8 \pm 0.2) \times 10^{-2}$

Table 7.2. Summary of thin-film based FET parameters (average mobility and threshold voltage values) measured in saturation regime. [W = 10 mm, L = 2.5 μm].

7.2.1.2. Electrical performance of single fiber, multifibers assemblies and thin-film based FETs

In contrast to OFETs based on organic thin film fibers process higher molecular ordering and are more free of grain boundaries. In this context, one-dimensional (1D) organic mesoscopic fibers expected to reveal significantly enhanced charge carrier transport as a result of strong intermolecular coupling between closely packed molecular and of a lower density of structure defects. To this end, organic transistors are fabricated based on single fiber to optimize FETs performances based on packing systems to study the charge transport in the fiber and from one fiber to another one, it is

known that highly ordered self-assembled system yielding high performance, thereby, one has to keep in mind that in organic macromolecular semiconductors the fast charge transport takes place along the backbone, while the limiting factor for the bulk electronic properties is the hopping between the conjugated backbones.

The PDIF-CN2 single fiber based-transistors performed on untreated substrates show no working devices as we can see in **Figure 7.8** and no further current modulation was observed.

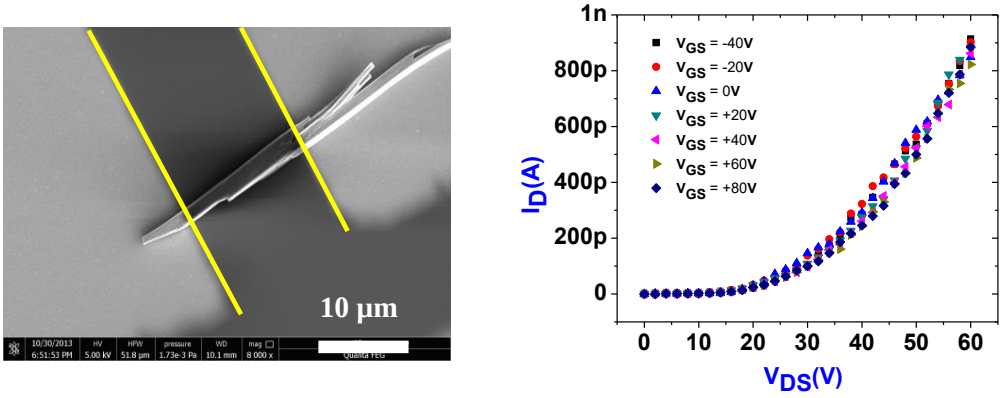

a) **b)**

Figure 7.8. SEM image **a)** and output characteristic **b)** recorded on untreated device based on single fiber. (L = 14.28 µm and W = 1.10 µm measured from SEM image). The yellow lines in the SEM image serve as a guide to the eyes and indicate the source and drain electrode edges.

Figure. 7.9 showed SEM image of FET device based on single fiber PDIF-CN2 and its output curve. The electrical responses measured for the single fiber devices performed on OTS treated substrates demonstrate a clear correlation between the substrate surface energy, well-ordered structures and the related charge transport performance. The output curve reported in **Figure 7.9 b** reveals ideal electrical features.

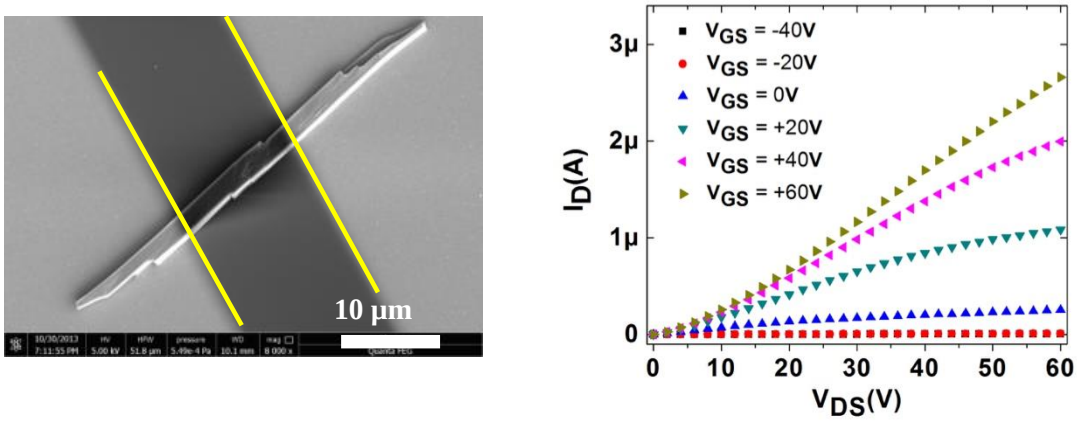

a) **b)**

Figure 7.9. SEM image **a)** and output characteristic **b)** of OTS treated device based on single fiber. The yellow lines in the SEM image serve as a guide to the eyes and indicate the source and drain electrode edges. (L = 14 µm and W = 1.2 µm measured from SEM image).

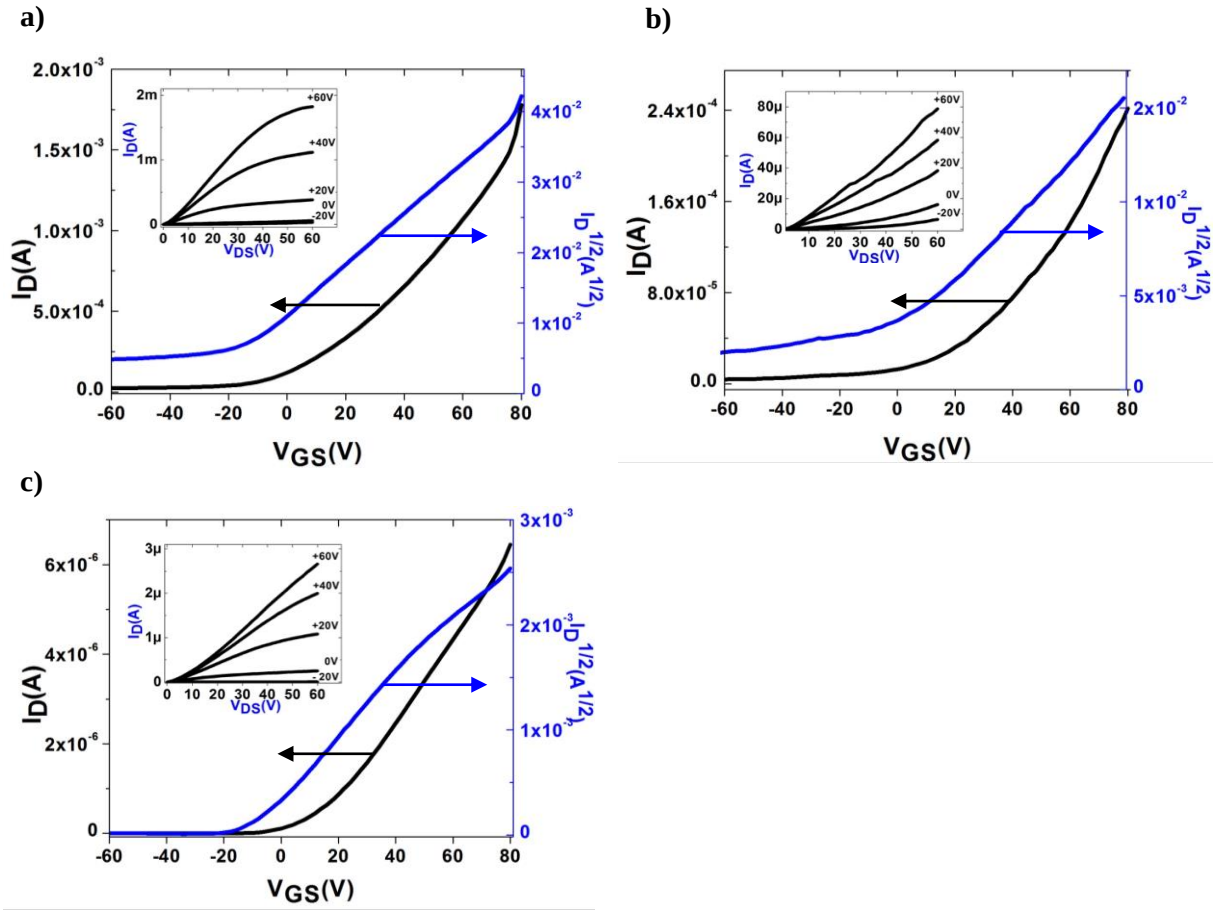

Figure 7.10. Transfer characteristics at V_{DS} = 60 V of PDIF-CN2 treated with OTS based on **a)** spin-coated thin-film (L = 5 µm and W = 10 mm), **b)** multifiber assembly (L = 5 µm and W = 10 mm), and **c)** single fiber (L = 14 µm and W = 1.4 µm). Insets: output characteristics of each device type.

Single-fiber FET		
	V_{th} (V)	**µ ($cm^2V^{-1}s^{-1}$)**
OTS SAMs	-10 ± 3	0.91 ± 0.04

Table 7.3. Summary of single-fiber top-contact bottom-gate FET parameters measured in saturation regime. [Number of samples > 10].

Figure 7.10 portrays the output and transfer curves of PDIF-CN2 spin-coated thin-films, multi- and single-fiber devices. Single-fibers based FET revealed mobility values as high as 2.3 $cm^2V^{-1}s^{-1}$ (average mobility 0.91 ± 0.04 $cm^2V^{-1}s^{-1}$) and low threshold voltage values around -10 V for single-fiber FET as reported in **Table 7.3** and **Figure 7.10 c**. Such performances provide unambiguous evidence for an enhanced charge transport through crystalline fibers when compared to the amorphous spin-coated films (annealed at 60°C for 1 hour) which featured an average mobility of 2.8×10^{-2} $cm^2V^{-1}s^{-1}$, this confirms that the different molecular order at the supramolecular level correlates directly with the transport properties. On the other hand, multifiber FETs displayed field-effect mobilities of ca. 3.8×10^{-3} $cm^2V^{-1}s^{-1}$, thus being nearly three orders of magnitude lower than those measured in single-fiber FETs. Such a discrepancy can be explained by considering the fiber-to-fiber grain boundaries: in multifiber assemblies, charge carriers may hop from one fiber to the neighboring one(s) in order to be collected at the electrode; this process strongly limits the transport. This observation has been confirmed by probing the electron charge transport between two different interconnected fibers as displayed in **Figure 7.11 a**. The field-effect mobility in the saturation region (see the corresponding output-curve in **Figure 7.11 c**), is ~1.7×10^{-3} $cm^2V^{-1}s^{-1}$ which compares well with those extracted from multifiber devices. To further explain such low mobility, we investigated the charge transport through crossing (and therefore overlapping) fibers (see **Figure 7.11 b and 7.11 d**). This exemplary experiment revealed that in some cases the gate effect in the device can be negligible. Such a behavior can be ascribed to a low and ineffective electrostatic coupling with the gate owing to the presence of (two or more) fibers sitting underneath the measured fiber (the one connected to Au gold electrodes) which separate it from the gate electric field.

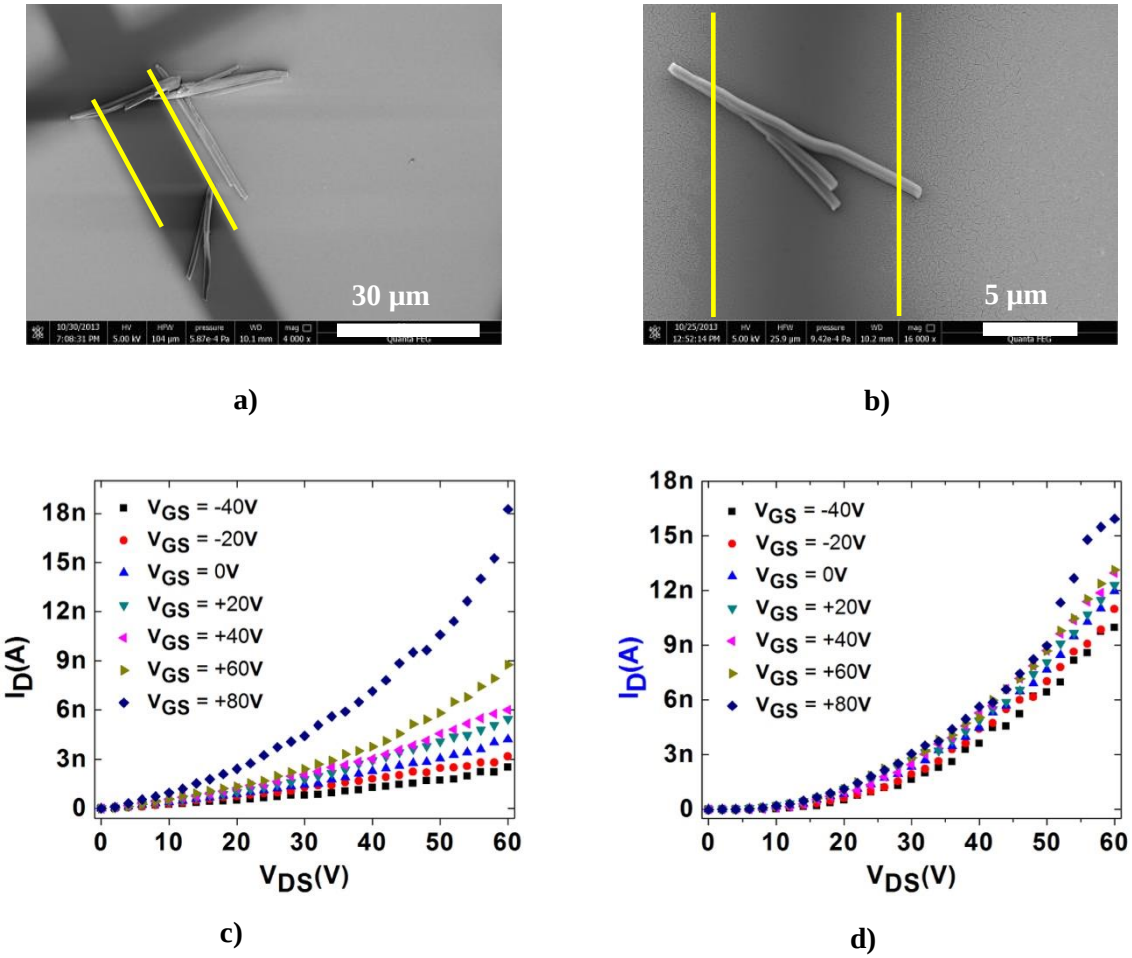

Figure 7.11. (a-b) SEM images and **(c-d)** output characteristics of FET devices treated with OTS based on: **(a, c)** two interconnected fibers, **(b, d)** superposed-fibers. The yellow lines in the SEM images serve as a guide to the eyes and indicate the source and drain electrode edges.

Besides the extraction of the major device parameters, Atomic Force Microscopy characterizations of the fibers were performed in order to gain a deeper insight of this molecular system. The fibers, as measured by AFM, are about 20 µm long, 1-3 µm in wide and hundreds of nanometers high (**see Figure 7.12**).

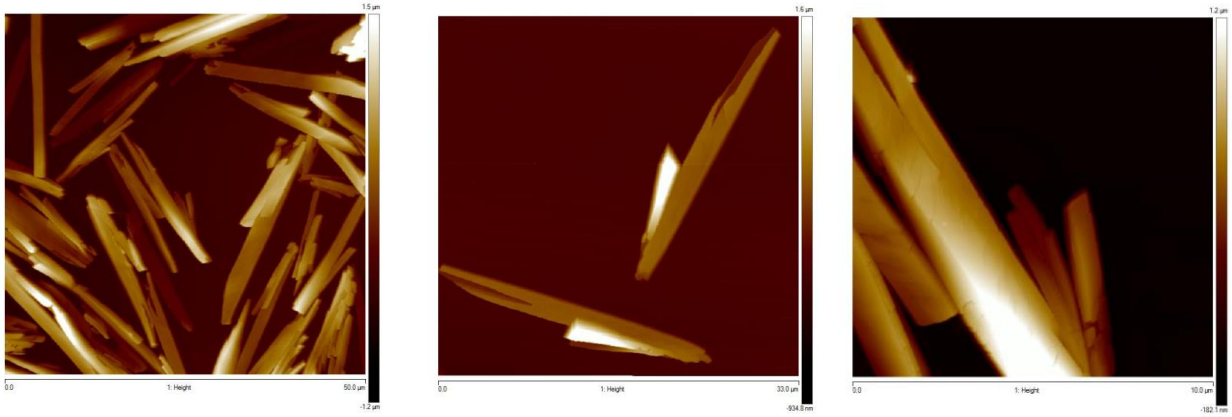

a) **b)** **c)**

Figure 7.12. Topographical tapping mode AFM images at different scan sizes **a)** 50 x 50 μm^2 **b)** 33 x 33 μm^2 and **c)** 10 x10 μm^2 of SIP fibers deposited by drop-casting few µl on silicon dioxide substrates.

With the aim of gaining greater insight into the charge injection at the electrode/semiconductor interface in multifiber-based devices, the top-contact configuration was implemented by thermally evaporating Au source and drain electrodes on pre-assembled fibers physisorbed on a treated SiO_2 surface (top-contact bottom-gate configuration). Unfortunately, the use of top electrodes does not allow the electrode functionalization with thiolated molecules, to guarantee optimal metal/semiconductor interface energetics. The deposition of gold electrodes on the top of the fibers led to non-functioning devices (see **Figure 7.13 a)** owing to an uneven and not continuous top gold layer connecting the fibers (fibers' average thickness being within few hundreds of nm). Unfortunately, the scenario was unchanged even upon evaporation of gold layers with a thickness up to 150 nm (see **Figure 7.13 b**).

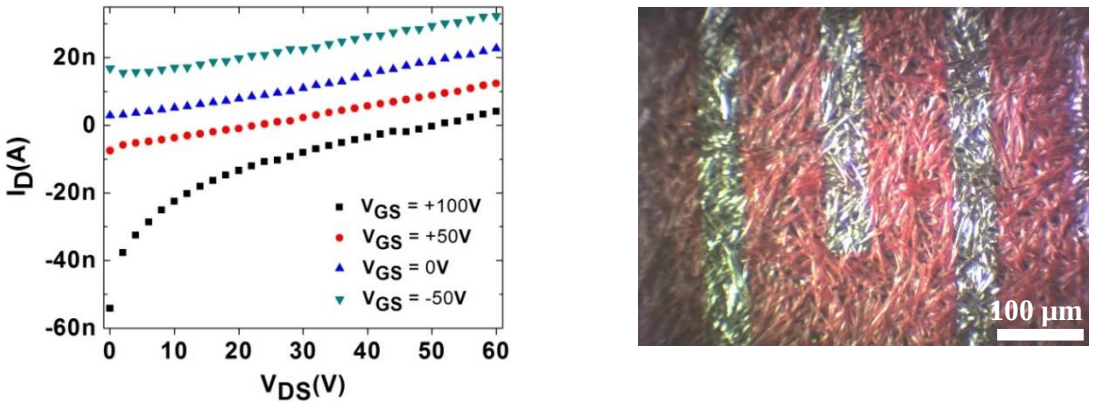

a) **b)**

Figure 7.13. a) Typical output curve recorded on top-contact FETs in case of devices with 150 nm of Au electrodes thickness reveals non-functioning devices. Device dimensions are L = 60 μm and W = 10 mm and **b)** optical microscopic image (bright field) of a top-contact device based on SIP fibers.

7.2.1.3. Effect of the channel length on OFETs electrical performances

Another important aspect one has to consider is also the dependence of the electrical characteristics on the channel length. Upon variation of the channel length the channel resistance decreases and as a result, the effect of the electrodes becomes more important as a voltage drop constantly occurs. If one looks at the relationship $R_{TOT} = R_{ch} + R_{contact}$, it is evident that the total resistive contribution (R_{TOT}) estimated by measuring the current flowing across the device channel is composed of two different components. A voltage drop at the electrode is normally called contact resistance ($R_{contact}$) and is constant with changing the channel length as it only depends on the energetic misalignment between the work function of the source-drain metal and the HOMO (LUMO) of the p-type (n-type) system employed. The resistive contribution given by the channel resistance (R_{ch}) depends on the channel length, instead, as it varies as $R_{ch} = \rho \times (L/A)$, where ρ is the film resistivity, L is the distance between the electrodes and A is the film section.

However, in our system (fiber-based FETs) the variation of the mobility properties with the channel length showed an increase in shorter channels (see **Figure 7.14**) which reflects the fact that the longer the channel the more grain boundaries between fibers are encountered by the charges. Such inter-fiber transport can be correlated to the fibers sizes as measured by AFM revealing lengths of about 20 μm.

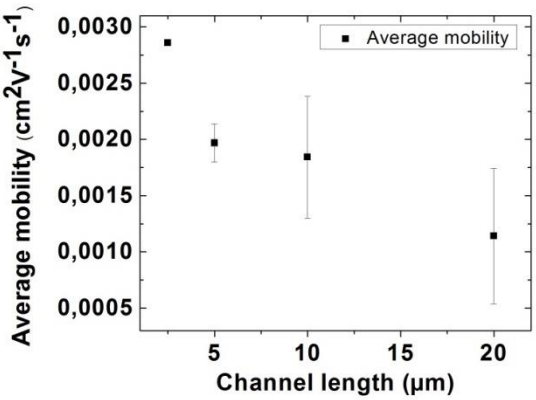

Figure 7.14. Average mobility (μ_{av}) values extracted from curves in the saturation regime measured on fiber-based FETs device treated with OTS. The error bars correspond to the standard deviations.

7.2.3. Organic phototransistors (OPTs) based on PDIF-CN2

An organic phototransistor is an optoelectronic device, having the same source, drain and gate electrodes as the three terminals in OFETs structure. In addition, it has an external light source that play the role of the fourth terminal in OPTs, just as gate electrode for the generation and control of photo-carriers in addition to those induced by the applied gate bias. In organic FET devices, the drain current (I_{DS}) accumulated in between source-drain channel can only be controlled by the magnitude of applied gate voltage (V_{GS}) at a fixed source-drain voltage (V_{DS}). Therefore, in phototransistors, light induced charge carriers are generated in the transistor channel by using light sensitive active organic semiconductors that generally exhibit excellent photocurrent generation efficiency via light absorption. The optoelectronic characteristics (i.e. charge generation, recombination and transport) of PDIF-CN2 organic semiconductor under light illumination can be relatively tunable by controlling their molecular assemblies at the device surface. To this end, we have fabricated and characterized different phototransistors based on PDIF-CN2 active layers having different order of crystallinity and molecular organization related to their morphology and supramolecular packing giving rise to small and large grains of organic semiconductor (spin-coated thin films and fibers based films), which is presumed to enhance OPTs electrical performances.

7.2.3.1. OPTs electrical performances of devices based on spin-coated thin film, multifibers and single fibers.

It was demonstrated that the photo-response properties of organic phototransistor devices cannot be explained and dependent on only device structure and morphology, but it also depends and related to the semiconductor materials intrinsic properties.

The light responsive nature of the electrical characteristics of multifiber-based assemblies compared with those of thin-film and single-fiber devices were quantified by determining the photoresponsivity R and the photoswitching ratio, i.e. photosensitivity, P (photocurrent/dark-current) of the devices. This has been accomplished by measuring the I-V characteristics of the transistors under white and monochromatic light irradiation. The R and P values are defined as:

$$R = \frac{(I_{light} - I_{dark})}{EWL}$$

$$P = \frac{(I_{light} - I_{dark})}{I_{dark}}$$

Where *W* and *L* are the channel width and length, *E* is the incident illumination power (areal) density on the channel of the device, I_{light} the drain current under illumination, and I_{dark} the drain current measured in dark conditions. The *R* and *P* values were plotted as a function of V_G for the thin-film, single fiber and multifiber-based devices.

Figure 7.15 displays the difference in transfer and output characteristics for (**a, b**) multifiber-based OPTs, (**c,d**) thin-film OPTs, and (**e,f**) single-fiber OPTs in dark and under illumination with white light ($\lambda > 400$ nm, 5.06 $mWcm^{-2}$). It reveals a general increase of the drain current in the I_{DS}-V_{DS} and I_{DS}-V_G curves upon irradiation as a result of photogenerated charge carriers. In particular, under light irradiation, the off-current of the single-fiber OPT, multifiber OPT and thin-film OPT were significantly higher indicating that the minimum conductivity measurable in the film (σ_{min}) increased owing to the additional contribution of photogenerated charges. In addition, the threshold voltage (V_{th}) shifted towards more negative voltages (n-doping), implying the easier turn-on of the device. This could be ascribed to the more efficient filling of trap sites by the photogenerated extra charge component.

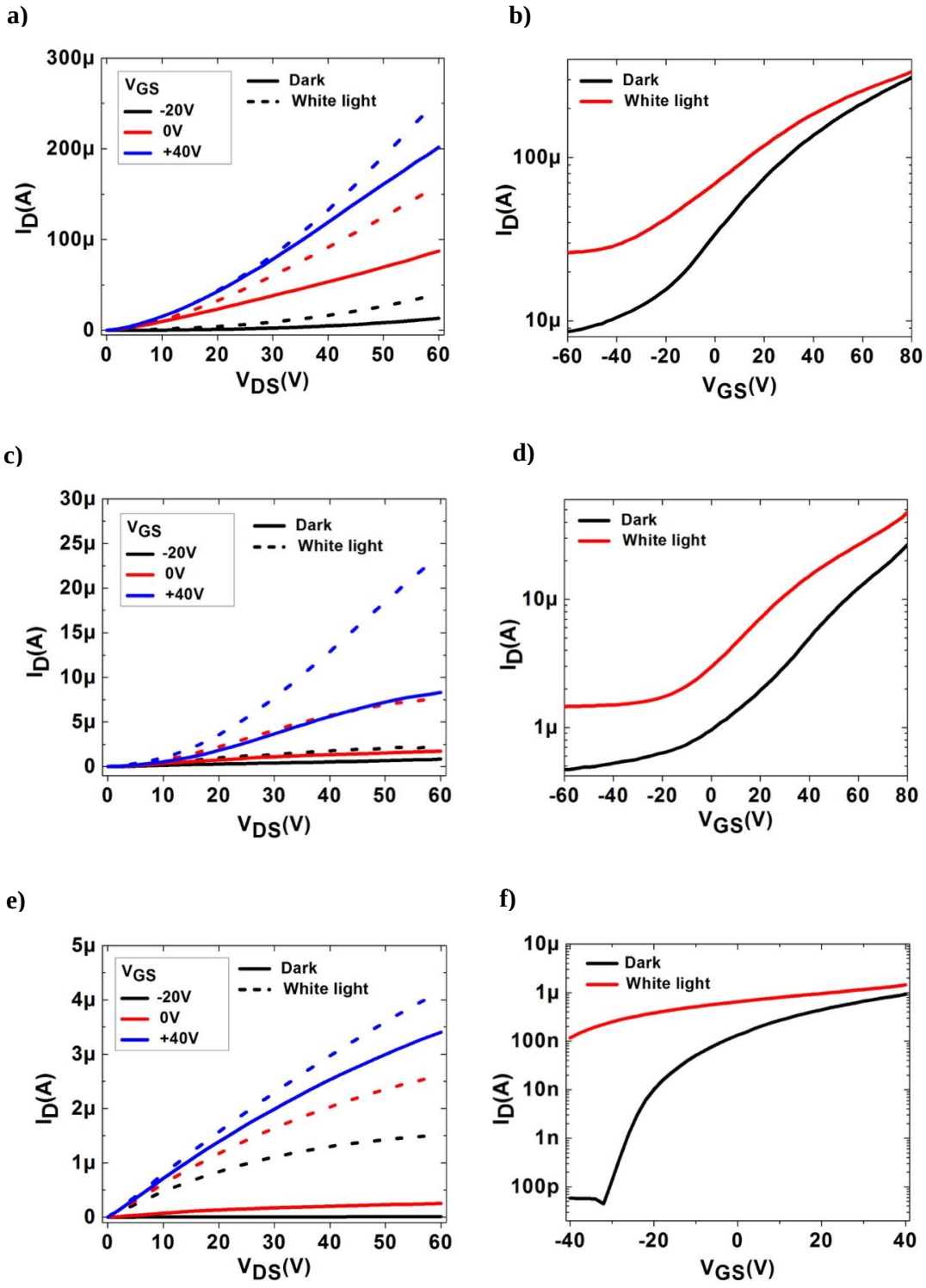

Figure 7.15. Comparison of **(a,c,e)** output and **(b,d,f)** transfer characteristics at V_{DS} = 60 V for **(a,b)** multi-fiber OPT, **(c,d)** thin-film OPT, and **(e,f)** single-fiber OPT measured in dark and under white light irradiation. Channel length (a-d) L= 10 µm, (e-f) L = 14 µm. $E_{\text{white light}}$ = 5.06 mWcm^{-2}.

7.2.3.2. Effect of light intensity on OPTs electrical performances

Different light sources of illumination were used including white light and monochromatic green light at λ = 525 nm. Such a wavelength was chosen in view of the absorption characteristics of PDIF-CN2 (see **Figure 7.16**). We have recorded UV-Vis absorbance spectra of PDIF-CN2 in $CHCl_3$ solution in order to shed light onto the optical properties of the above-mention PDI derivative, the acquired absorbance spectral is presented in **Figure 7.16**. The monomer spectrum displays several well-defined peaks in the 400-550 nm region, whose maxima are placed at λ_{max} = 432, 459, 490, and 525 nm. These peaks correspond to different vibronic bands (3-0, 2-0, 1-0 and 0-0, respectively) associated with the PDI main transition dipole moment, which is aligned along the long axis of the molecule.[58]

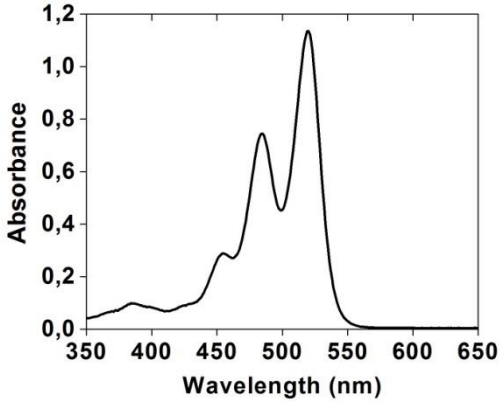

Figure 7.16. Absorption spectra of PDIF-CN2 from solution (2.1×10^{-5} M in $CHCl_3$).

Transfer curves of OPTs based on spin-coated film, multi- and single fiber are illustrated in **Figure 7.17**; green light irradiation at λ = 525 nm with high intensity (4.84 $mWcm^{-2}$ as measured using an analog optical power meter, PM100A, Thorlabs) yielded the largest enhancement in the drain current (I_{DS}) due to the larger absorption of incoming photons. However, it is noteworthy that white light illumination (5.06 $mWcm^{-2}$) exhibited similarly high I_{DS} obtained under green light with high intensity as the photocurrent/dark-current ratio is strongly dependent upon the incident optical power density, while the green light with low intensity (7.24 μWcm^{-2}) exhibited the smaller enhancement in the drain current due to the smaller optical power intensity than the two other light sources.

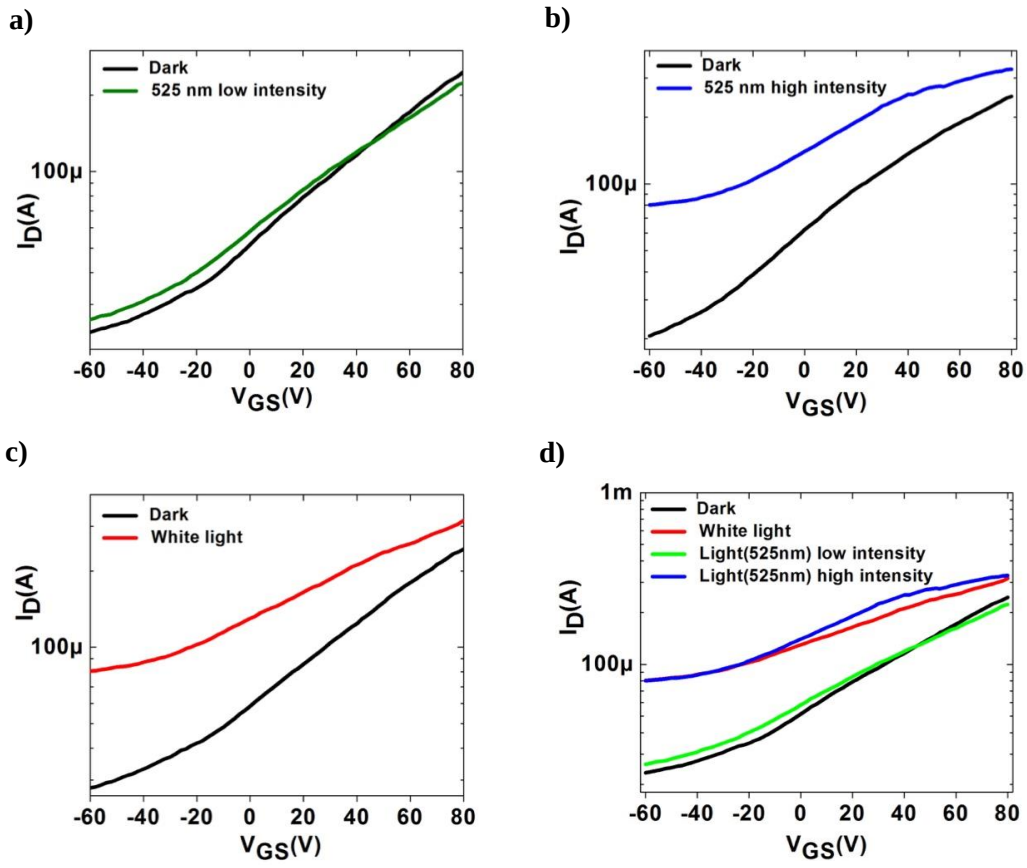

Figure 7.17. Transfer characteristics recorded on multifiber OPT device treated with OTS and undecanethiol self-assembly monolayers, measured in dark and under different irradiation conditions; **a)** under green light at 'low intensity', **b)** green light at 'high intensity', **c)** white light, **d)** comparison between I_D current in dark and under three different illumination conditions. [V_{DS} = +60 V, L = 2.5 µm].

7.2.3.3. The responsivity (R) and photoswitching ratio (P) of phototransistors based on spin-coated thin-film, single-fiber and multifibers assemblies.

Light responsivity (R) and photocurrent/dark-current ratio (P) are important parameters for investigating the capacity of a material to respond to light stimuli. **Figure 7.18** shows that when illuminated with white light the multifiber OPTs exhibit a maximum R value of 200 AW^{-1} with a corresponding P = 3.3, whereas thin-film-OPTs display R_{max} = 24 AW^{-1} and P_{max} = 0.6 (these values were reported from devices with the same channel length for both thin-film and multifiber OPTs). For single-fiber OPTs devices, a maximum R value of 2189 AW^{-1} at a gate voltage of 60 V with a corresponding P value of 5001 were recorded under white light irradiation. In **Figure 7.19**, the same single-fiber OPT device (in **Figure 7.18**) was also irradiated using green light (4.84 $mWcm^{-2}$). The

calculated R and P values were comparable to those obtained under white light irradiation, amounting ca. to 2593 AW^{-1} and 4560, respectively.

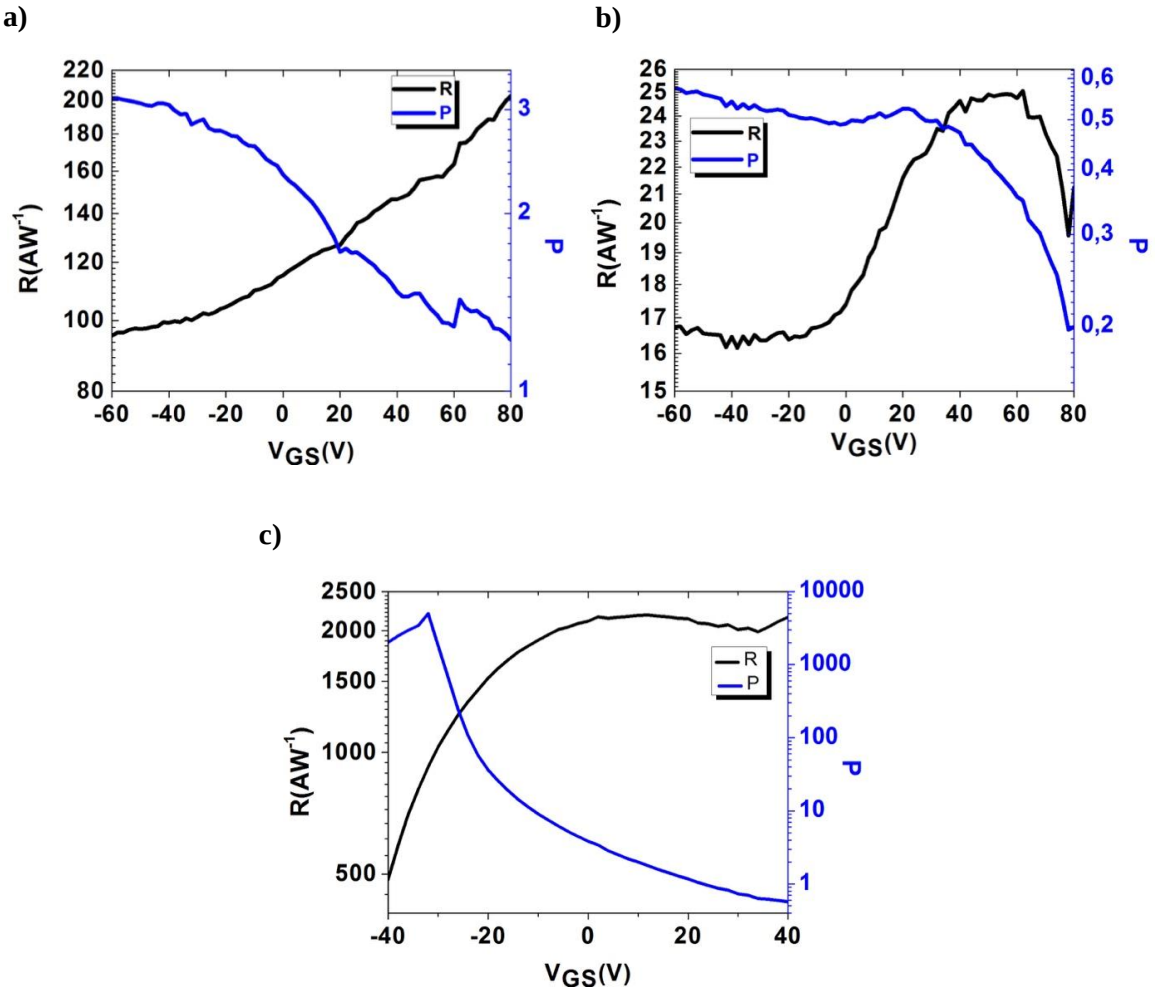

Figure 7.18. Variation of responsivity (R) and photosensitivity (P) with V_G at V_D = 60 V for **a)** multifiber OPT (L = 2.5 µm), **b)** thin-film OPT (L = 2.5 µm), and **c)** single-fiber OPT (L = 14 µm) under white light irradiation, for devices treated with OTS. $E_{\text{white light}}$ = 5.06 $mWcm^{-2}$.

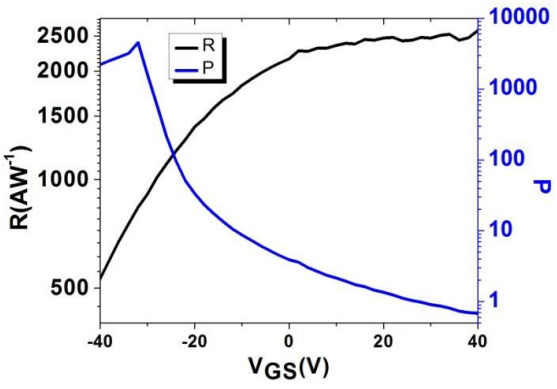

Figure 7.19. Variation of responsivity (R) and photosensivity (P) with V_G at V_D = 60 V for single-fiber OPT (L = 14 µm) under green light irradiation (light intensity is 4.84 $mWcm^{-2}$), for device treated with OTS.

Under white light illumination all investigated PDI-based single-fiber OPTs exhibited responsivity and photoswitching ratio both exceeding 10^3 indicating a pronounced increase of the signal upon irradiation. The multifiber OPTs exhibited responsivity being lower than that of single-fiber OPTs yet one order of magnitude higher compared to those of thin-film based-OPTs. The increase in R in the case of single fibers compared to the thin-film devices can be ascribed to the improved molecular order within the fibers which enables a better transport of the photogenerated carriers to the electrodes. Conversely, the diffusion of the generated Frenkel excitons towards the electrodes is more impeded in the multifiber devices compared to that in single-fiber devices owing to the energetically unfavored fiber-to-fiber energy transfer. The hopping mechanism of excitons in organic semiconductors is generally considered to be a dipole-dipole resonance energy transfer known as the Förster mechanism[59-60]. Such mechanism is based on short-range interactions which vanish as $1/d^6$ where d is the distance between the molecular entities. In our case, the intermolecular π-π distance is of approximately 3.3. Å which is far shorter than two fluorinated alkylchains in a row. Hence, we ascribe the poor photoresponse of multifiber devices to the poor fiber-to-fiber exciton transport.

Significantly, the photoresponsivity R and photocurrent/dark current ratio P values that we obtained in the present study concerning single-fiber OPTs are, to the best of our knowledge, the highest reported in literature for perylene di-imide single crystal-based organic phototransistors.[44-46] For instance, the maximum R reported for BPE-PTCDI NW-OPTs, amounts to ca. 1400 AW^{-1} at a gate voltage of 100 V and photoswitching current of 4960 for top-contact devices irradiated with green light, corresponding to a darkness charge carrier mobility of 1.13 $cm^2V^{-1}s^{-1}$.[46] The photoresponsivity of PTCDI-C_8 (perylene derivative) single nanowires-OPTs was about 7 AW^{-1}.[45] Yu et al. demonstrated that the light response increased by increasing the charge carrier mobility devices,[46] which was observed in previous reports on organic phototransistors[28, 31, 35] and confirmed in our case, where the highest R was obtained from OFET device exhibiting high charge mobility (2.3 $cm^2V^{-1}s^{-1}$). This suggests that PDIF-CN2 single-fiber OPTs are a promising candidate to achieve high light responsivity in electronic devices while keeping high electron mobility.

7.2.3.4. R and P dependence on the channel length (L)

The transfer characteristics of multifiber OPTs devices obtained at V_{DS} = +60 V in dark and under white light illumination are compared in **Figure 7.20 a, b**. In the both cases the devices were

prepared in the same way using the HMDS treatment of SiO_2, the only difference being the channel length, L = 10 µm and 2.5 µm for a) and b), respectively.

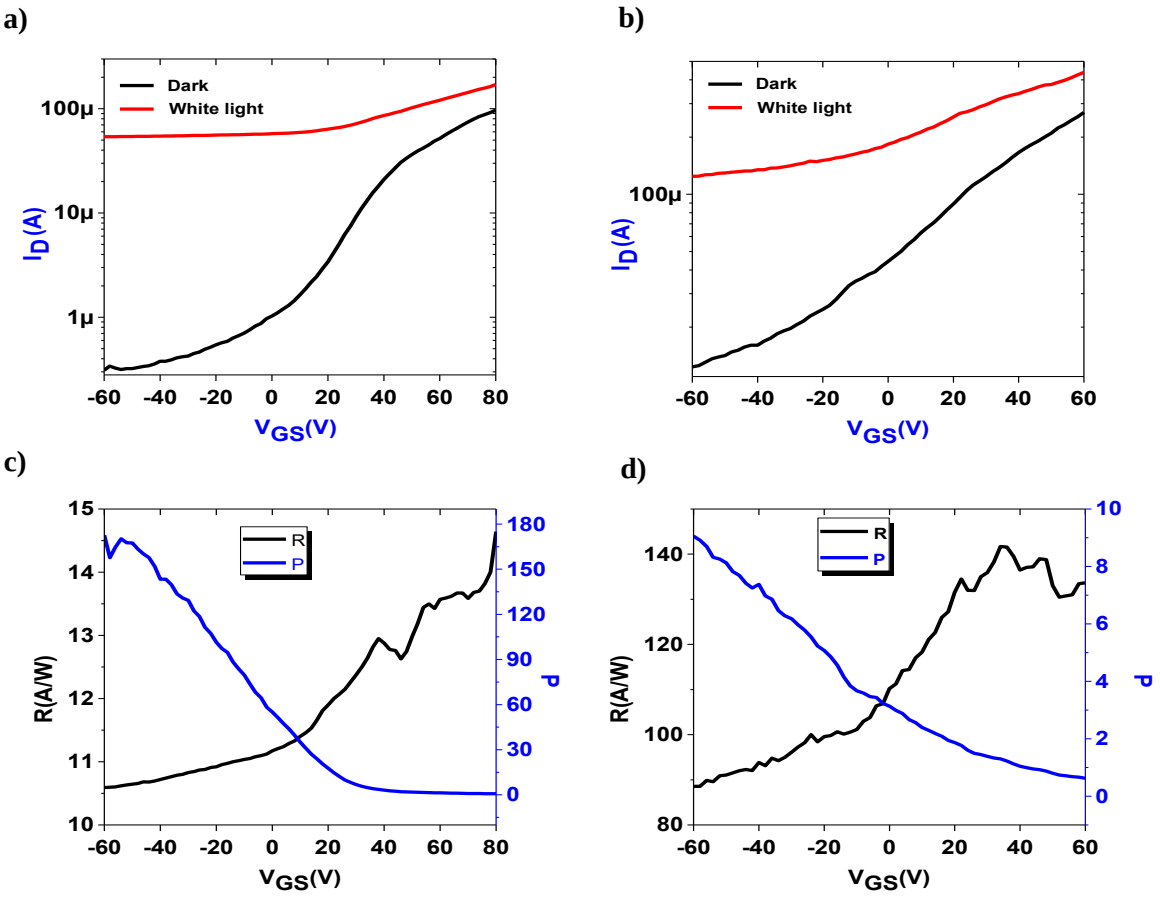

Figure 7.20. Transfer characteristics of multifiber OPT devices in dark and under white light irradiation treated with HMDS with different channel length **a)** L = 10 µm and **b)** L = 2.5 µm, and their responsivity (R) and photosensitivity (P) with V_{GS} at V_{DS} = +60 V for **c)** L = 10 µm and **d)** L = 2.5 µm. $E_{white\ light}$ = 5.06 mWcm^{-2}.

The light responsivity (R) and photocurrent/dark-current ratio (P) were calculated employing the transfer curves presented in **Figure 7.20 a** and **b** and their values are reported in the same figure (panels **7c** and **7.20 d**). The channel length dependence of R and P parameters is of particular interest, because it permits a better understanding of the factors contributing to the PDI device photoresponse. **Figure 7.20 (a)** shows the transfer characteristic curves of OPTs with channel lengths of 10 µm. It reveals the largest enhancement in the drain current (I_{DS}) under light irradiation due to the larger absorption of incoming photons and exhibited a photoswitching ratio P = 180. This value is 20-fold greater than the one detected in device with the shorter channel length of L = 2.5 µm (P = 9) (see **Figure 7.20 c** and **d**). On the other hand, the photoresponsivity R is one order of magnitude greater in

the OPT devices with L = 2.5 µm. Based on these results and others obtained on thin-film devices revealing a similar behavior, we conclude that the photoswitching ratio P is independent from the channel length of PDIF-CN2 based devices, but it is dependent upon the incident optical power density (see Figure S6). However, the photoresponsivity R is strongly dependent on the channel length for both multifiber- and thin-film OPTs.

7.2.3.5. PDIF-CN2 air stability

Figure 7.21 shows the difference in drain current in dark vs. white light irradiation for multifiber and thin-film devices measured in dry nitrogen (inside the glovebox) and in a controlled ambient air (T = 22 °C, RH ~25%).

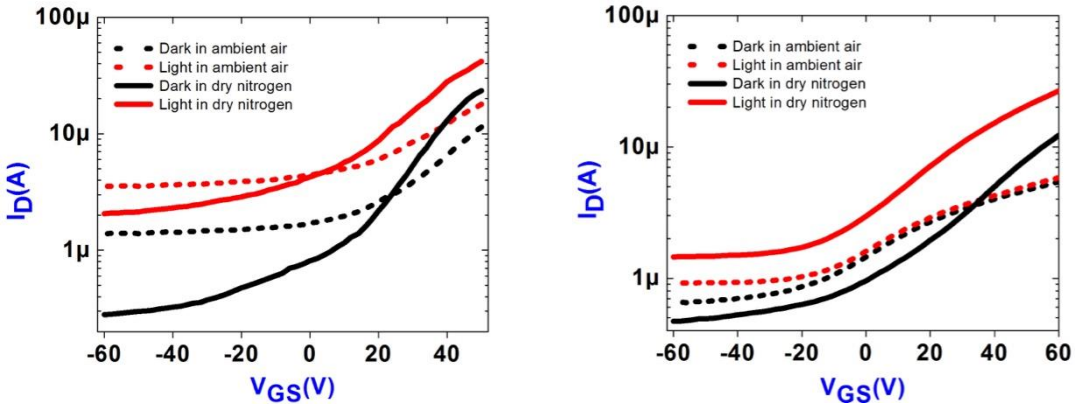

Figure 7.21. Transfer characteristics of **a)** multifiber OPT and **b)** thin-film devices in dark and under white light irradiation measured in dry nitrogen and air atmosphere. [V_{DS} = +60 V, L = 2.5 µm].

It reveals an increase in drain current upon light irradiation for multifiber-based devices by almost 1 order of magnitude, whereas a slight increase in drain current was observed for thin-film-based OFET in a few devices while for the others a decrease in drain current were observed in dark and under white light irradiation, as a result of the semiconductor layer instability in air environment. **Table 7.4** in the Supporting Information shows different mobility and threshold voltage values extracted from the saturation regime of FET devices measured in dry nitrogen and ambient air, $\Delta\mu$ ($\mu_{\text{ambient air}} / \mu_{\text{dry nitrogen}}$) % measures the change between the mobility values in dry nitrogen and ambient air given in percent and $\Delta V_{th} = |V_{th\,(\text{ambient air})} - V_{th\,(\text{dry nitrogen})}|$, which is the threshold voltage difference between dry nitrogen and ambient air.

FET Devices		μ ($cm^2V^{-1}s^{-1}$)	V_{th} (V)	Δμ ($\mu_{Air}/\mu_{Nitrogen}$)	ΔV_{th} $\lvert(V_{th\ air} - V_{th\ Nitrogen})\rvert$
Multifiber	Dry nitrogen	2.0×10^{-3}	+ 10.8	no variation (1)	9.4
	Ambient air	2.0×10^{-3}	+ 20.2		
Spin-coated films	Dry nitrogen	5.3×10^{-4}	+ 3.3	0.09	56.4
	Ambient air	4.9×10^{-5}	-59.7		

Table 7.4. Summary of multifiber-based and spin-coated FET parameters measured in dry nitrogen and ambient air in dark.

The mobility values reported in **Table 7.4** reveal that FETs based on multifiber assemblies are not affected by the exposure to oxygen, as evidenced by the unchanged mobility values measured in dry nitrogen and ambient air. For spin-coated film based devices, the electron mobility measured in ambient air drops down by almost a factor of 4 compared with that of the same device measured in dry nitrogen ($\Delta\mu = 0.09$). On the basis of these results, we can conclude that PDIF-CN2 air stability is strongly influenced by the molecular packing and the morphology of the semiconductor films. For multifiber assemblies, the devices electrical characterizations were almost stable in ambient air; such a result may be explained by the presence of tight packing between PDI cores, providing a kinetic barrier to the diffusion of oxygen into the channel.[61] Piliego et al. have reported on PDIF-CN2-based devices that the decrease in mobility cannot be attributed to semiconductor chemical degradation, but to the physisorption of atmospheric gases[62] at the material grain boundaries that will act as electron traps.[63] Zschieschang et al. showed that PDIF-CN2 vapor deposited thin-films feature a mild mobility reduction from dry nitrogen to ambient air ($\Delta\mu = 0.97\%$), which was ascribed to the electrochemical instability of the semiconductor radical anion via the following equation:

$$O_2 + 2\ H_2O + 4\ e^- \longrightarrow 4\ HO^-$$

The presence of both oxygen (O_2) and water (H_2O) molecules in air environment leads to the formation of HO^- groups that act as charge traps, causing a slow decrease in carrier mobility.[64]A similar observation on electron mobility degradation in ambient air was previously reported by Morpurgo et al. on PDIF-CN2 vapor-deposited single crystals.[65] Concerning the threshold voltage

values (**see Table 7.4**), a shift toward more positive values was observed in the case of multifiber-based devices. According to Kumaki et al., this positive shift is due to the water molecules which induced a deprotonation of Si−OH groups present on the dielectric surface not passivated with OTS self-assembled monolayers, forming charge traps following the reaction: SiOH + H2O → SiO^- + H_3O^+.[66] On the other hand, a negative shift was observed for FETs based on spin-coated thin films measured in ambient air, indicating an electron doping of the semiconductor layer.

Multifiber devices	**μ ($cm^2V^{-1}s^{-1}$)**	**V_{th}(V)**	**$\Delta\mu(\mu_{light}/\mu_{dark})$**	**$\Delta_{Vth}\|(V_{th\text{-}light}-V_{th\text{-}dark})\|$**
Dry nitrogen_Dark	2.0×10^{-3}	+10.8	no variation (1)	13.8
Dry nitrogen_Light	2.0×10^{-3}	-2.9		
Ambient air_Dark	1.9×10^{-3}	+20.2	no variation (1)	32.5
Ambient air_Light	1.9×10^{-3}	-12.3		

Table 7.5. Summary of multifiber-based FET parameters measured in dark and under light irradiation in dry nitrogen and ambient air.

Spin-coated devices	**μ ($cm^2V^{-1}s^{-1}$)**	**V_{th}(V)**	**$\Delta\mu(\mu_{light}/\mu_{dark})$**	**$\Delta_{Vth}\|(V_{th\text{-}light}-V_{th\text{-}dark})\|$**
Dry nitrogen_Dark	5.3×10^{-4}	+3.3	0.96	26.8
Dry nitrogen_Light	5.1×10^{-4}	-23.5		
Ambient air_Dark	7.6×10^{-5}	-65.8	0.76	2.2
Ambient air_Light	5.8×10^{-5}	-68		

Table 7.6. Summary of spin-coated-based FET parameters measured in dark and under light irradiation in dry nitrogen and ambient air.

Our findings, reported in **Tables 7.5 and 7.6**, correlate μ and V_{th} and their relative variation, Δμ and ΔV_{th}, in dark and under white light irradiation for FET devices upon 1 day of exposure to air conditions for both multifiber assemblies and spin-coated films. We can notice a threshold voltage shift toward negative values upon light irradiation for both multifiber and spin-coated devices. A decrease in electron mobility was also observed between light and dark measured both under dry nitrogen (Δμ = 0.96) and ambient air (Δμ = 0.76) environment for spin-coated-based devices, whereas

no difference in electron mobility for multifibers-based device was monitored, thus confirming the air stable nature of packed PDIF-CN2 fibers.

Conclusions

In summary, we have provided evidence for the influence of the order at the supramolecular level in the semiconducting material on the performance of field-effect transistors supported on SiO_2 substrates. In particular, the comparison of single fibers with high crystallinity fabricated from solution processable method (SIP) and multifiber assemblies with spin-coated thin films revealed that the former outperform by exhibiting good reproducibility and field-effect mobilities up to 2 $cm^2s^{-1}V^{-1}$ when the SiO_2 is treated with OTS self-assembled monolayers. Such outstanding field-effect mobility can be ascribed to intermolecular close packing arrangement within the crystalline fibers, the absence of grain boundaries and the presence of an ordered fluorocarbon layer at the periphery of the edge-on molecules ensuring the isolation of the aromatic cores from the dielectric substrate, thereby reducing the dipolar disorder, overall providing an almost ideal situation for charge transport. This mobility value is approaching those reported by Morpurgo et al. in vacuum vapor deposited single crystal devices with lengths of few millimeters.[65] Spin-coated films showed mobilities 4 orders of magnitude lower as a result of the poor order at the supramolecular level within the films. On the other hand, the multifibers showed mobilities of ca. 10^{-3} $cm^2s^{-1}V^{-1}$. Such discrepancy when compared to single-fiber devices can be ascribed to the fact that charges need to hop between adjacent fibers in order to reaching the metallic electrode. This clearly highlight that the properties of PDIF-CN2 fiber assemblies and their related electrical performances are strongly improved when hydrophobic surfaces treated with OTS or HMDS self-assembled monolayers are used for the film growth.

We have also described the fabrication of organic phototransistors based on either single or multifibers integrated in three-terminal devices. The optoelectronic properties of these self-assembled fibers-based devices have been compared to devices incorporating more disordered spin-coated PDIF-CN2 thin-films. The improved crystallinity allows efficient collection of photogenerated Frenkel excitons, which results in the highest reported responsivity R ($>5 \times 10^3$ AW^{-1}) for single-fiber PDI-based phototransistors, and photoswitching ratio P ($>2 \times 10^3$) compared with that of thin-film based OPTs, which are to date the highest reported R and P obtained from PDI single crystal OPTs. This result provides evidence that also the device photoresponse depends on the molecular order and an efficient transport of the photogenerated carriers towards the electrodes is a requirement towards high light response. Overall, our SIP processed PDIF-CN2 single fibers do not require any vapor growth and are highly conducting

with a good operational stability as well as photosensitive architectures for fundamental studies on light-matter interaction and for applications in high performance optoelectronic devices. Our results show also that the air-stability performances are superior in devices where highly crystalline supramolecularly engineered architectures serve as the active layer. These findings provide unambiguous evidence for the key role played by the high degree of order at the supramolecular level to leverage the material's properties toward the fabrication of light-sensitive and air-stable organic field-effect transistors.

7.3. References

1. Arias, A. C.; MacKenzie, J. D.; McCulloch, I.; Rivnay, J.; Salleo, A., Materials and Applications for Large Area Electronics: Solution-Based Approaches. *Chem. Rev.* **2010,** *110* (1), 3-24.

2. Brabec, C. J.; Cravino, A.; Meissner, D.; Sariciftci, N. S.; Fromherz, T.; Rispens, M. T.; Sanchez, L.; Hummelen, J. C., Origin of the Open Circuit Voltage of Plastic Solar Cells. *Adv. Funct. Mater.* **2001,** *11* (5), 374-380.

3. Caboni, A.; Orgiu, E.; Scavetta, E.; Barbaro, M.; Bonfiglio, A., Organic-Based Sensor for Chemical Detection in Aqueous Solution. *Appl. Phys. Lett.* **2009,** *95* (12), 123304-123304-3.

4. Burroughes, J. H.; Bradley, D. D. C.; Brown, A. R.; Marks, R. N.; Mackay, K.; Friend, R. H.; Burn, P. L.; Holmes, A. B., Light-Emitting-Diodes Based on Conjugated Polymers. *Nature* **1990,** *347* (6293), 539-541.

5. Greenham, N. C.; Moratti, S. C.; Bradley, D. D. C.; Friend, R. H.; Holmes, A. B., Efficient Light-Emitting-Diodes Based on Polymers with High Electron-Affinities. *Nature* **1993,** *365* (6447), 628-630.

6. Tian, H. K.; Shi, J. W.; Yan, D. H.; Wang, L. X.; Geng, Y. H.; Wang, F. S., Naphthyl end-Capped Quarterthiophene: A Simple Organic Semiconductor with High Mobility and Air Stability. *Adv. Mater.* **2006,** *18* (16), 2149-2152.

7. Facchetti, A., Semiconductors for Organic Transistors. *Mater. Today* **2007,** *10* (3), 28-37.

8. Gao, X. K.; Di, C. A.; Hu, Y. B.; Yang, X. D.; Fan, H. Y.; Zhang, F.; Liu, Y. Q.; Li, H. X.; Zhu, D. B., Core-Expanded Naphthalene Diimides Fused with 2-(1,3-Dithiol-2-Ylidene)Malonitrile Groups for High-Performance, Ambient-Stable, Solution-Processed n-Channel Organic Thin Film Transistors. *J. Am. Chem. Soc.* **2010,** *132* (11), 3697-3699.

9. Caboni, A.; Orgiu, E.; Barbaro, M.; Bonfiglio, A., Flexible Organic Thin-Film Transistors for pH Monitoring. *Ieee Sens. J.* **2009,** *9* (12), 1963-1970.

10. Dimitrakopoulos, C. D.; Malenfant, P. R. L., Organic Thin Film Transistors for Large Area Electronics. *Adv. Mater.* **2002,** *14* (2), 99-117.

11. Murphy, A. R.; Frechet, J. M. J., Organic Semiconducting Oligomers for Use in Thin Film Transistors. *Chem. Rev.* **2007,** *107* (4), 1066-1096.

12. Mas-Torrent, M.; Rovira, C., Novel Small Molecules for Organic Field-Effect Transistors: Towards Processability and High Performance. *Chem. Soc. Rev.* **2008,** *37* (4), 827-838.

13. Klauk, H.; Halik, M.; Zschieschang, U.; Schmid, G.; Radlik, W.; Weber, W., High-Mobility Polymer Gate Dielectric Pentacene Thin Film Transistors. *J. Appl. Phys.* **2002,** *92* (9), 5259-5263.

14. Torsi, L.; Farinola, G. M.; Marinelli, F.; Tanese, M. C.; Omar, O. H.; Valli, L.; Babudri, F.; Palmisano, F.; Zambonin, P. G.; Naso, F., A Sensitivity-Enhanced Field-Effect Chiral Sensor. *Nat. Mater.* **2008,** *7* (5), 412-417.

15. Jang, M.; Kim, H.; Lee, S.; Kim, H. W.; Khedkar, J. K.; Rhee, Y. M.; Hwang, I.; Kim, K.; Oh, J. H., Highly Sensitive and Selective Biosensors Based on Organic Transistors Functionalized with Cucurbit 6 uril Derivatives. *Adv. Funct. Mater.* **2015,** *25* (30), 4882-4888.

16. Cavallini, M.; Gentili, D.; Greco, P.; Valle, F.; Biscarini, F., Micro- and Nanopatterning by Lithographically Controlled Wetting. *Nat. Protoc.* **2012,** *7* (9), 1668-1676.

17. Cavallini, M.; D'Angelo, P.; Criado, V. V.; Gentili, D.; Shehu, A.; Leonardi, F.; Milita, S.; Liscio, F.; Biscarini, F., Ambipolar Multi-Stripe Organic Field-Effect Transistors. *Adv. Mater.* **2011,** *23* (43), 5091-5097.

18. Qi, Z.; Liao, X. X.; Zheng, J. C.; Di, C. A.; Gao, X. K.; Wang, J. Z., High-Performance n-Type Organic Thin-Film Phototransistors Based on a Core-Expanded Naphthalene Diimide. *Appl. Phys. Lett.* **2013,** *103* (5), 053301.

19. Guo, N.; Hu, W. D.; Liao, L.; Yip, S.; Ho, J. C.; Miao, J. S.; Zhang, Z.; Zou, J.; Jiang, T.; Wu, S. W.; Chen, X. S.; Lu, W., Anomalous and Highly Efficient InAs Nanowire Phototransistors Based on Majority Carrier Transport at Room Temperature. *Adv. Mater.* **2014,** *26* (48), 8203-8209.

20. Kim, J.; Cho, S.; Kim, Y. H.; Park, S. K., Highly-Sensitive Solution-Processed 2,8-difluoro-5,11-bis(triethylsilylethynyl) Anthradithiophene (diF-TESADT) Phototransistors for Optical Sensing Applications. *Org. Electron.* **2014,** *15* (9), 2099-2106.

21. Kim, M.; Ha, H. J.; Yun, H. J.; You, I. K.; Baeg, K. J.; Kim, Y. H.; Ju, B. K., Flexible Organic Phototransistors Based on a Combination of Printing Methods. *Org. Electron.* **2014,** *15* (11), 2677-2684.

22. Loffredo, F.; Bruno, A.; Del Mauro, A. D.; Grimaldi, I. A.; Miscioscia, R.; Nenna, G.; Pandolfi, G.; Petrosino, M.; Villani, F.; Minarini, C.; Facchetti, A., Photoresponse of Pentacene-Based Transistors. *Phys. Status Solidi A* **2014,** *211* (2), 460-466.

23. Yang, D.; Zhang, L.; Wang, H. W.; Wang, Y. S.; Li, Z. X.; Song, T. J.; Fu, C. J.; Yang, S. Y.; Zou, B. S., Pentacene-Based Photodetector in Visible Region With Vertical Field-Effect Transistor Configuration. *IEEE Photonics Technol. Lett.* **2015,** *27* (3), 233-236.

24. Li, M. M.; An, C. B.; Marszalek, T.; Guo, X.; Long, Y. Z.; Yin, H. X.; Gu, C. Z.; Baumgarten, M.; Pisula, W.; Müllen, K., Phenanthrene Condensed Thiadiazoloquinoxaline Donor-Acceptor Polymer for Phototransistor Applications. *Chem. Mat.* **2015,** *27* (6), 2218-2223.

25. Ljubic, D.; Smithson, C. S.; Wu, Y. L.; Zhu, S. P., Highly UV-Sensitive and Responsive Benzothiophene/Dielectric Polymer Blend-Based Organic Thin-Film Phototransistor. *Adv. Electron. Mater.* **2015,** *1* (8).

26. Di Maria, F.; Olivelli, P.; Gazzano, M.; Zanelli, A.; Biasiucci, M.; Gigli, G.; Gentili, D.; D'Angelo, P.; Cavallini, M.; Barbarella, G., A Successful Chemical Strategy To Induce Oligothiophene Self-Assembly into Fibers with Tunable Shape and Function. *J. Am. Chem. Soc.* **2011,** *133* (22), 8654-8661.

27. Gentili, D.; Di Maria, F.; Liscio, F.; Ferlauto, L.; Leonardi, F.; Maini, L.; Gazzano, M.; Milita, S.; Barbarella, G.; Cavallini, M., Targeting Ordered Oligothiophene Fibers with Enhanced Functional Properties by Interplay of Self-Assembly and Wet Lithography. *J. Mater. Chem.* **2012,** *22* (39), 20852-20856.

28. Kim, K. H.; Bae, S. Y.; Kim, Y. S.; Hur, J. A.; Hoang, M. H.; Lee, T. W.; Cho, M. J.; Kim, Y.; Kim, M.; Jin, J. I.; Kim, S. J.; Lee, K.; Lee, S. J.; Choi, D. H., Highly Photosensitive J-Aggregated Single-Crystalline Organic Transistors. *Adv. Mater.* **2011,** *23* (27), 3095-3099.

29. Liu, X. H.; Tavares, L.; Osadnik, A.; Lausen, J. L.; Kongsted, J.; Lutzen, A.; Rubahn, H. G.; Kjelstrup-Hansen, J., Low-Voltage Organic Phototransistors Based on Naphthyl end-Capped Oligothiophene Nanofibers. *Org. Electron.* **2014,** *15* (6), 1273-1281.

30. Um, H. A.; Lee, D. H.; Heo, D. U.; Yang, D. S.; Shin, J.; Baik, H.; Cho, M. J.; Choi, D. H., High Aspect Ratio Conjugated Polymer Nanowires for High Performance Field-Effect Transistors and Phototransistors. *Acs Nano* **2015,** *9* (5), 5264-5274.

31. Zhao, G. Y.; Liu, J.; Meng, Q.; Ji, D. Y.; Zhang, X. T.; Zou, Y.; Zhen, Y. G.; Dong, H. L.; Hu, W. P., High-Performance UV-Sensitive Organic Phototransistors Based on Benzo 1,2-b:4,5-b ' dithiophene Dimers Linked with Unsaturated Bonds. *Adv. Electron. Mater.* **2015,** *1* (8).

32. Wu, G.; Chen, C.; Liu, S.; Fan, C. C.; Li, H. Y.; Chen, H. Z., Solution-Grown Organic Single-Crystal Field-Effect Transistors with Ultrahigh Response to Visible-Blind and Deep UV Signals. *Adv. Electron. Mater.* **2015,** *1* (8).

33. Guan, Y. S.; Qin, Y. K.; Sun, Y. H.; Wang, C.; Xu, W.; Zhu, D. B., Single-Bundle Nanofiber Based OFETs Fabricated from a Cyclic Conjugated Organogelator with High Field-Effect Mobility and High Photoresponsivity. *Chem. Commun.* **2015,** *51* (61), 12182-12184.

34. Wang, J. Y.; Peng, H. D.; Yang, J. M.; Yan, J. H.; Pan, G. B., Solvent-Induced Self-Assembly Synthesis of Ultralong Single Crystalline Organic NiOEP Nanowires with High Photoconductivity. *RSC Adv.* **2015,** *5* (91), 74251-74255.

35. Guo, Y. L.; Du, C. Y.; Yu, G.; Di, C. A.; Jiang, S. D.; Xi, H. X.; Zheng, J.; Yan, S. K.; Yu, C. L.; Hu, W. P.; Liu, Y. Q., High-Performance Phototransistors Based on Organic Microribbons Prepared by a Solution Self-Assembly Process. *Adv. Funct. Mater.* **2010,** *20* (6), 1019-1024.

36. Zhang, Y. T.; Song, X. X.; Wang, R.; Cao, M. X.; Wang, H. Y.; Che, Y. L.; Ding, X.; Yao, J. Q., Comparison of Photoresponse of Transistors Based on Graphene-Quantum Dot Hybrids with Layered and Bulk Heterojunctions. *Nanotechnology* **2015,** *26* (33), 335201-335208.

37. Song, X. X.; Zhang, Y. T.; Wang, R.; Cao, M. X.; Che, Y. L.; Wang, J. L.; Wang, H. Y.; Jin, L. F.; Dai, H. T.; Ding, X.; Zhang, G. Z.; Yao, J. Q., Bulk- and Layer-Heterojunction Phototransistors Based on Poly 2-methoxy-5-(2 '-ethylhexyloxy-p-phenylenevinylene) and PbS Quantum Dot Hybrids. *Appl. Phys. Lett.* **2015**, *106* (25), 253501-253501-5.

38. Nollau, A.; Hoffmann, M.; Fritz, T.; Leo, K., Dissociation of Excitons in Organic Dye Layers of Perylene Derivatives. *Thin Solid Films* **2000,** *368* (1), 130-137.

39. Chesterfield, R. J.; McKeen, J. C.; Newman, C. R.; Ewbank, P. C.; da Silva, D. A.; Bredas, J. L.; Miller, L. L.; Mann, K. R.; Frisbie, C. D., Organic Thin Film Transistors Based on N-Alkyl Perylene Diimides: Charge Transport Kinetics as a Function of Gate Voltage and Temperature. *J. Phys. Chem. B* **2004,** *108* (50), 19281-19292.

40. Sergeyev, S.; Pisula, W.; Geerts, Y. H., Discotic Liquid Crystals: A New Generation of Organic Semiconductors. *Chem. Soc. Rev.* **2007,** *36* (12), 1902-1929.

41. Feng, Y.; Feng, W., Photo-Responsive Perylene Diimid–Azobenzene Dyad: Photochemistry and its Morphology Control by Self-Assembly. *Opt. Mater.* **2008,** *30* (6), 876-880.

42. Schmidt, R.; Oh, J. H.; Sun, Y.-S.; Deppisch, M.; Krause, A.-M.; Radacki, K.; Braunschweig, H.; Koenemann, M.; Erk, P.; Bao, Z.; Würthner, F., High-Performance Air-Stable n-Channel Organic Thin Film Transistors Based on Halogenated Perylene Bisimide Semiconductors. *J. Am. Chem. Soc* **2009,** *131* (17), 6215-6228.

43. Anthony, J. E.; Facchetti, A.; Heeney, M.; Marder, S. R.; Zhan, X. W., n-Type Organic Semiconductors in Organic Electronics. *Adv. Mater.* **2010,** *22* (34), 3876-3892.

44. El Gemayel, M.; Treier, M.; Musumeci, C.; Li, C.; Müllen, K.; Samorì, P., Tuning the Photoresponse in Organic Field-Effect Transistors. *J. Am. Chem. Soc.* **2012,** *134* (4), 2429-2433.

45. Mukherjee, B.; Sim, K.; Shin, T. J.; Lee, J.; Mukherjee, M.; Ree, M.; Pyo, S., Organic Phototransistors Based on Solution Grown, Ordered Single Crystalline Arrays of a pi-Conjugated Molecule. *J. Mater. Chem.* **2012,** *22* (7), 3192-3200.

46. Yu, H.; Bao, Z. A.; Oh, J. H., High-Performance Phototransistors Based on Single-Crystalline n-Channel Organic Nanowires and Photogenerated Charge-Carrier Behaviors. *Adv. Funct. Mater.* **2013,** *23* (5), 629-639.

47. Pfattner, R.; Pavlica, E.; Jaggi, M.; Liu, S. X.; Decurtins, S.; Bratina, G.; Veciana, J.; Mas-Torrent, M.; Rovira, C., Photo-Induced Intramolecular Charge Transfer in an Ambipolar Field-Effect Transistor Based on a pi-Conjugated Donor-Acceptor Dyad. *J. Mater. Chem. C* **2013,** *1* (25), 3985-3988.

48. Tozlu, C.; Kus, M.; Can, M.; Ersöz, M., Solution Processed White Light Photodetector Based N, N '-di(2-ethylhexyl)-3,4,9,10-perylene Diimide Thin Film Phototransistor. *Thin Solid Films* **2014,** *569*, 22-27.

49. Yu, H.; Joo, P.; Lee, D.; Kim, B.-S.; Oh, J. H., Photoinduced Charge-Carrier Dynamics of Phototransistors Based on Perylene Diimide/Reduced Graphene Oxide Core/Shell p-n Junction Nanowires. *Adv. Opt. Mater.* **2015,** *3* (2), 241-247.

50. Mativetsky, J. M.; Orgiu, E.; Lieberwirth, I.; Pisula, W.; Samorì, P., Charge Transport Over Multiple Length Scales in Supramolecular Fiber Transistors: Single Fiber Versus Ensemble Performance. *Adv. Mater.* **2014,** *26* (3), 430-435.

51. Jones, B. A.; Ahrens, M. J.; Yoon, M. H.; Facchetti, A.; Marks, T. J.; Wasielewski, M. R., High-Mobility Air-Stable n-Type Semiconductors with Processing Versatility: Dicyanoperylene-3,4 : 9,10-bis(dicarboximides). *Angew. Chem., Int. Ed.* **2004,** *43* (46), 6363-6366.

52. Schmidt, R.; Ling, M. M.; Oh, J. H.; Winkler, M.; Konemann, M.; Bao, Z. N.; Wurthner, F., Core-Fluorinated Rerylene Bisimide Dyes: Air Stable n-Channel Organic Semiconductors for Thin Film Transistors with Exceptionally High On-to-Off Current Ratios. *Adv. Mater.* **2007,** *19* (21), 3692-3695.

53. Jones, B. A.; Facchetti, A.; Wasielewski, M. R.; Marks, T. J., Effects of Arylene Diimide Thin Film Growth Conditions on n-Channel OFET Performance. *Adv. Funct. Mater.* **2008,** *18* (8), 1329-1339.

54. Fabiano, S.; Wang, H.; Piliego, C.; Jaye, C.; Fischer, D. A.; Chen, Z. H.; Pignataro, B.; Facchetti, A.; Loo, Y. L.; Loi, M. A., Supramolecular Order of Solution-Processed Perylenediimide Thin Films: High-Performance Small-Channel n-Type Organic Transistors. *Adv. Funct. Mater.* **2011,** *21* (23), 4479-4486.

55. Minder, N. A.; Ono, S.; Chen, Z. H.; Facchetti, A.; Morpurgo, A. F., Band-Like Electron Transport in Organic Transistors and Implication of the Molecular Structure for Performance Optimization. *Adv. Mater.* **2012,** *24* (4), 503-508.

56. Willa, K.; Hausermann, R.; Mathis, T.; Facchetti, A.; Chen, Z.; Batlogg, B., From Organic Single Crystals to Solution Processed Thin-Films: Charge Transport and Trapping with Varying Degree of Order. *J. Appl. Phys.* **2013,** *113* (13).

57. Chua, L. L.; Zaumseil, J.; Chang, J. F.; Ou, E. C. W.; Ho, P. K. H.; Sirringhaus, H.; Friend, R. H., General Observation of n-Type Field-Effect Behaviour in Organic Semiconductors. *Nature* **2005,** *434* (7030), 194-199.

58. Delgado, M. C. R.; Kim, E. G.; da Silva, D. A.; Bredas, J. L., Tuning the Charge-Transport Parameters of Perylene Diimide Single Crystals via End and/or Core Functionalization: A Density Functional Theory Investigation. *J. Am. Chem. Soc.* **2010,** *132* (10), 3375-3387.

59. Beljonne, D.; Pourtois, G.; Silva, C.; Hennebicq, E.; Herz, L. M.; Friend, R. H.; Scholes, G. D.; Setayesh, S.; Mullen, K.; Bredas, J. L., Interchain vs. Intrachain Energy Transfer in Acceptor-Capped Conjugated Polymers. *Proc. Natl. Acad. Sci. U.S.A.* **2002,** *99* (17), 10982-10987.

60. Mollay, B.; Lemmer, U.; Kersting, R.; Mahrt, R. F.; Kurz, H.; Kauffman, H. F.; Bassler, H., Dynamics of Singlet Excitations in Conjugated Polymers - Poly (PhenyleneVinylene) and Poly (PhenylPhenyleneVinylene). *Phys. Rev. B* **1994,** *50* (15), 10769-10779.

61. Weitz, R. T.; Amsharov, K.; Zschieschang, U.; Villas, E. B.; Goswami, D. K.; Burghard, M.; Dosch, H.; Jansen, M.; Kern, K.; Klauk, H., Organic n-Channel Transistors Based on Core-Cyanated Perylene Carboxylic Diimide Derivatives. *J. Am. Chem. Soc.* **2008,** *130* (14), 4637-4645.

62. Jones, B. A.; Facchetti, A.; Wasielewski, M. R.; Marks, T. J., Tuning Orbital Energetics in Arylene Diimide Semiconductors. Materials Design for Ambient Stability of n-Type Charge Transport. *J. Am. Chem. Soc.* **2007,** *129* (49), 15259-15278.

63. Piliego, C.; Jarzab, D.; Gigli, G.; Chen, Z. H.; Facchetti, A.; Loi, M. A., High Electron Mobility and Ambient Stability in Solution-Processed Perylene-Based Organic Field-Effect Transistors. *Adv. Mater.* **2009,** *21* (16), 1573-1576

64. Zschieschang, U.; Amsharov, K.; Jansen, M.; Kern, K.; Klauk, H.; Weitz, R. T., Separating the Impact of Oxygen and Water on the Long-Term Stability of n-Channel Perylene Diimide Thin-Film Transistors. *Org. Electron.* **2015,** *26*, 340-344.

65. Molinari, A. S.; Alves, H.; Chen, Z.; Facchetti, A.; Morpurgo, A. F., High Electron Mobility in Vacuum and Ambient for PDIF-CN2 Single-Crystal Transistors. *J. Am. Chem. Soc.* **2009,** *131* (7), 2462-+.

66. Kumaki, D.; Umeda, T.; Tokito, S., Influence of H2O and O2 on Threshold Voltage Shift in Organic Thin-Film Transistors: Deprotonation of SiOH on SiO2 Gate-Insulator Surface. *Appl Phys Lett* **2008,** *92* (9), 093309-093309-3.

Chapter 8. Optically switchable organic-based inverters with photomodulable gain

Introduction

One among the greatest challenges in the field of organic electronics is the development of multicomponent materials that can combine a set of properties. Organic ambipolar materials have gained much attention as active components in low-cost, flexible displays and large-area electronic products.[1] Integrated in organic field-effect transistors (OFETs),[2-4] they have been studied and processed with different fabrication methodologies as a basic fundamental element for organic integrated circuits (ICs) incorporating both p- and n-type transistors used in several applications such as organic complementary inverters (CMOS).[5] Organic ambipolar transistors relying on solution processing have an additional advantage that are able to transport both electrons and holes, in comparison to devices which transport only single types of unipolar charge carriers. In particular, ambipolar transistors have been utilized as a single active layer in organic complementary inverters;[6] these inverters are capable to operate in both first and third quadrants of transfer characteristics with low power dissipation and a good noise margin. In contrast, organic inverters based on unipolar transistors operate only in one quadrant; either in the first or third. Usually, inverters based on heterojunction p-n channels have higher gain compared to those based on one single ambipolar layer.[7] Ideally, for high operating complementary organic circuits, one would like to have both n-type and p-type transistor channels (OFETs) with high electrons and holes carrier mobilities, smaller n- and p-channels dimensions, with simpler device configuration and easy solution fabrication processing. Since ambipolar charge transport has been discovered as an intrinsic property in organic materials, it should, in principle, be possible to realize ambipolar organic semiconductors that combine such high hole and electron mobilities in a conjugated polymer. However, most current, high-mobility polymers for p-channel or n-channel OFETs do not exhibit balanced ambipolar transport because of their chemical structures and molecular energy levels are optimized for one type of charge carrier only. In order to achieve such an efficient electron and hole charge transport, researchers combined p- and n-type semiconductors via blending. [8-10] New multifunctional devices can be fabricated combining

organic semiconductors with other molecules possessing different chemical, optical and electrical properties. Among them, photochromic molecules are small organic molecules capable of undergoing efficient and reversible photochemical isomerization between (at least) two (meta)stable states which exhibit markedly different properties such as absorption, dipole moments and electronic structure.[11-12] Photochromic molecules can be used to tune the semiconductors functional performances, forming light-responsive optoelectronic devices such as switches[13] and OFET memories.[14-15] Many are the reports which can be found in literature on organic electronic devices containing photochromic molecules which are used as photo-sensitive components. In the device, photochromic molecules can be placed either at the semiconductor-insulator interface [16] or inside the semiconductor layer, blended with different organic materials[17], carbon nanotubes[18] and single molecules[19] to enhance devices optical and electrical characteristics.

Photochromic molecules are well known by their reversible color changes uder light irradiation, which is described to the photoinduced electronic structural changes of the molecules going from left- to right-side isomers.[20] One among the most promising candidates for photochromic molecules are diarylethene derivatives [21] which combine a good thermal stability and fatigue resistance.[22] In particular, diarylethene moieties possess different band gap and associated highest occupied molecular orbital (HOMO) and lowest unoccupied molecular orbital (LUMO) levels, depending on their stronger (closed form) or weaker (open form) degree of conjugation, that can be controlled upon irradiation at different wavelengths.[23-24]

Here we have developed for the first time three-component photo-switchable devices by diarylethene integration into an ambipolar polymer featuring good electron and hole mobilities as the active layer. Within the present work, we demonstrated the integration of two diarylethene derivatives, i.e. DAE_tBu (**Figure. 1b**) and DAE_F (**Figure. 1c**), with large fatigue resistance[22] into a matrix of diketopyrrolopyrrole. Diketopyrrolopyrrole-based copolymers are known to have high hole mobility. [27] In this study, we have used an ambipolar polymer called diketopyrrole-Thieno[3,2-b]thiophene copolymer (DPPT-TT)[28] (**Figure.1a**), in order to exploit the optically responsive nature of the photochromic systems cited above to photo-gate the charge transport of both electrons and holes through the three-component material. The basic aim of this work is to fabricate organic inverters based on this polymer (DPPT-TT) and DAE moieties with a photo-controllable voltage gain. The present work describes the fabrication and systematic analysis of an ambipolar-based inverters produced by the successive deposition of organic DPPT-TT polymer and diarylethenes layers using the simple spin-coating method.

In a recent work on DPPT-TT polymer ambipolarity studies upon device optimization via changing the annealing temperature, they obtained high and balanced electron and hole motilities only at high temperature annealing (320 °C). Due to the high temperature at which the chosen polymer films had to be processed (320 ºC for 20 minutes) to exhibit a good ambipolar behaviour, the photochromic diarylethene molecules could be integrated in the material only by thermally activated diffusion into the polymer matrix through a gentle post-processing annealing (90 ºC). This made it possible to fabricate OFETs where the drain current can be photo-tuned thanks to the interactions between the polymer and the DAE species.[25-26] The latter can undergo reversible isomerization between a closed and an open form upon irradiation at different wavelengths. This leads to the facile fabrication of inverters whose gain becomes photo-modulable because it can be tuned by controlling the different population of closed vs. open isomers in the blend by playing with the number and wavelength of the photons shone over the active layer.

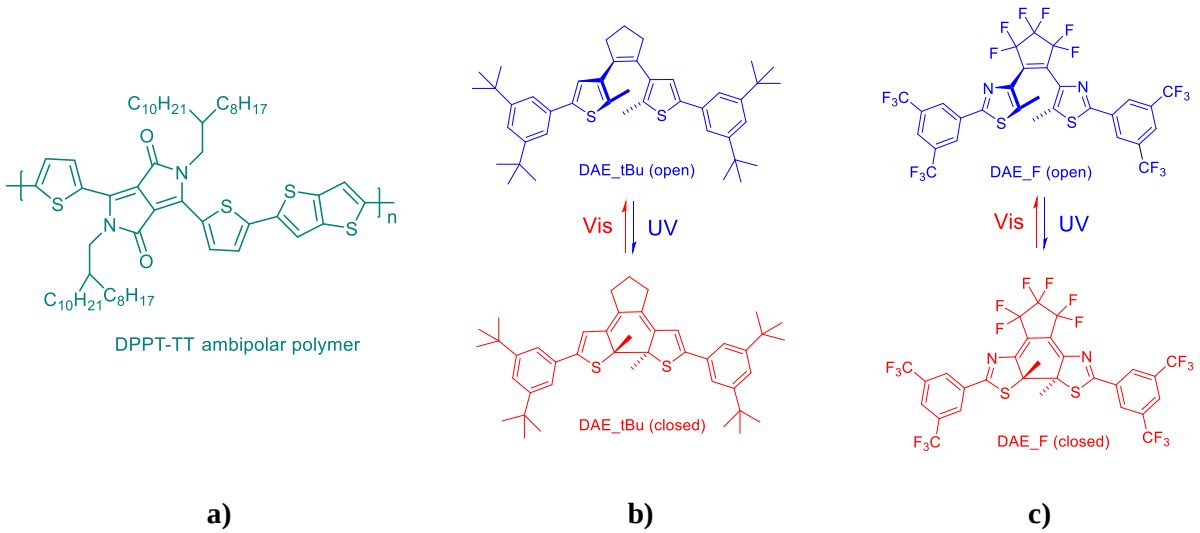

Figure 8.1. Molecular structure of **a)** [3,2-b] thiophene copolymer (DPPT-TT), open and closed form of **b)** diarylethene molecule DAE_tBu and **c)** DAE_F.

8.1. Device fabrication and characterization.

Highly doped n-type silicon wafers were used as substrate for the organic OFETs in bottom-gate geometry. The thermally-grown SiO_2 layer (230 nm) has a unit area capacitance (C_i) of 15 $nFcm^{-2}$. All the substrates were cleaned in an ultrasonic bath with purity acetone (C_3H_6O, 95% GC) and isopropanol ($CH_3CHOHCH_3$, 99, 7 % GC) for 20 minutes each, in order to remove the photoresist layer. The Au (40 nm thick) patterns used for the source/drain electrodes were fabricated using a conventional lift-off photolithography procedure. The semiconducting polymer (DPPT-TT) was

synthesized by our collaborators. The polymer active layer was deposited by spin-coating under N_2; the DPPT-TT solution (10 mg/ml for OFETs and 2 mg/ml for UV/Visible absorption measurements in film) in anhydrous dichlorobenzene was spun onto solid substrate surfaces for 60 seconds at 1500 rpm followed by annealing at 320°C for 20 minutes. After that, DAE_tBu and DAE_F derivatives (10% for each one dissolved in butyl acetate) were deposited and thermally annealed at 90°C for 1 hour and 30 minutes to promote the diarylethenes permeation into the polymer matrix and the formation of an ordered crystalline phase in a glove box with a N_2 atmosphere (see **Figure 8.2**).

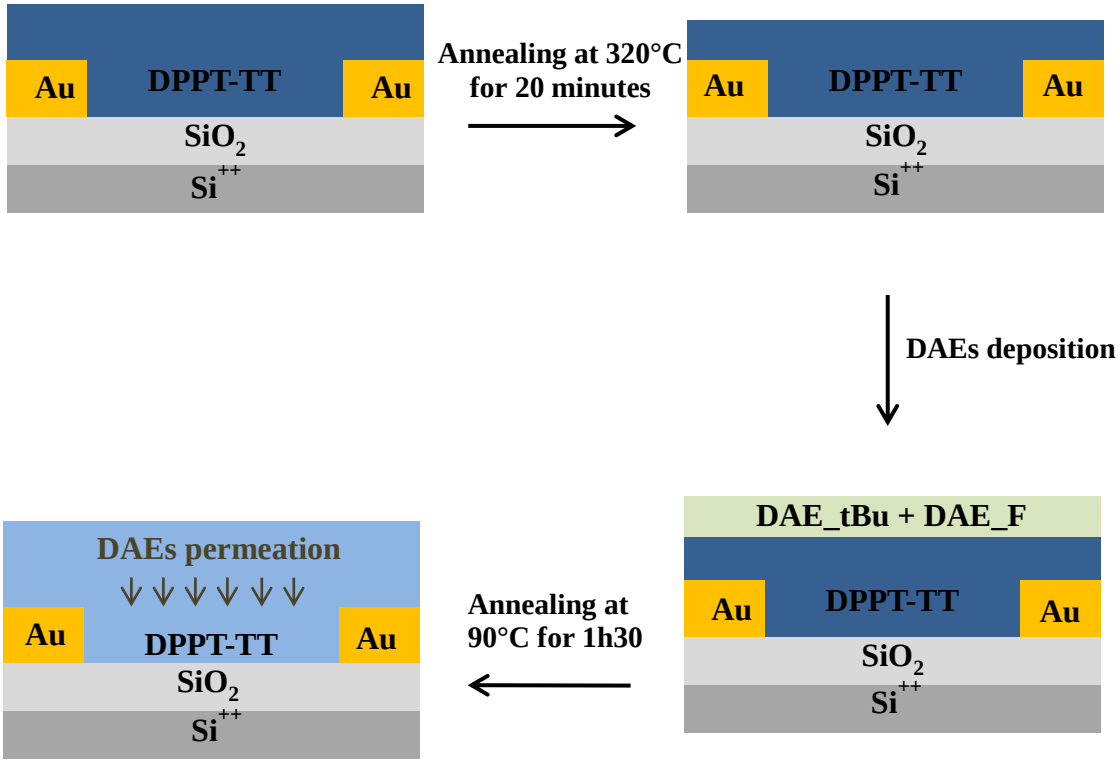

Figure 8.2. Schematic illustration of the preparation steps of FET device in bottom-contact bottom-gate geometry based on DPPT-TT polymer as the active layer with diarylethene molecules permeated into its matrix.

For bottom-contact top-gate devices, glass, barium borosilicate 7059 glass, and Fraunhofer substrates were cleaned by using the same process described above for bottom-gate OFETs. 40 nm layers of gold contact electrodes were thermally evaporated. PMMA (Aldrich, M_w = 319 kg.mol^{-1}) was used as a dielectric material. The PMMA polymeric dielectric film was deposited onto DPPT-TT and DAEs layers by spin coating of 350 µl of solution (45 mg/ml in anhydrous ethyl acetate heated at 80°C and filtered with 0.45 µm filter) for 30 seconds at 1000 rpm, followed by annealing at 80°C for

30 minutes (PMMA film is around 700 nm thick). As a last step, the transistors were completed by aluminum deposition as top gate electrode (~100 nm thick) via thermal evaporation through a metal shadow mask, the OFET structure is illustrated in **Figure 8.3**.

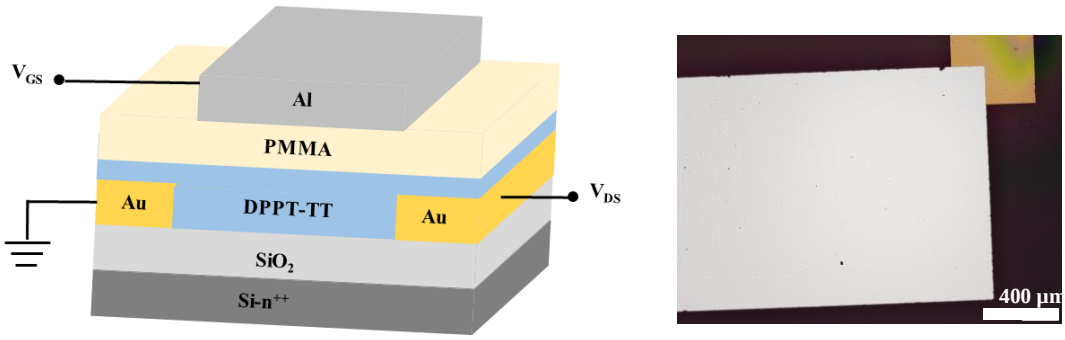

a) **b)**

Figure 8.3. a) OFET device structure in bottom-contact top-gate geometry, b) microscopic image of an OFET device fabricated in top-gate structure.

The current-voltage (I-V) characteristics of all OFET devices were measured inside the glove box in a controlled nitrogen atmosphere through a Cascade Microtech M150 probe station interfaced with a dual channel Keithley 2636A source-meter and its associated software.

Electron and hole mobility was extracted in the saturation regime according to the well-known transistor equation:

$$\mu_{sat} = \frac{2 \cdot \left(\frac{\partial \sqrt{I_D}}{\partial V_{GS}} \right)^2}{C_i \frac{W}{L}}$$

Where I_D is the current measured between source and drain electrodes, W the channel width and L the channel length, V_{GS} the potential difference measured between the voltage probes, C_i the gate-dielectric capacitance.

8.2 Absorbance and quantum yield measurements

UV/Vis absorption spectra were recorded using JASCO V-500 spectrophotometer. The irradiation at 312 nm was performed by means of a UV lamp with a source power of 2.5 mW/ cm^2,

while for that at 530 nm a light emitting diode (80 μW/cm^2, M530F1, Thorlabs) was used. The absorption spectra for solution were performed in a 1 cm x 1 cm quartz cuvette, and UVASOL grade solvent were used. For DAE_tBu, the solution concentration is 20 μM in butyl acetate, for DAE_F the concentration of the solution is 45 μM were measured in butyl acetate, and the irradiation were performed at 312 nm until reaching to the photostationary state (PSS). UV/visible absorption spectra of DPPT_TT polymer in the dichlorobenzene at concentration of 20 μg/ml were also recorded through a JASCO V-670 spectrophotometer.

Absorption spectra were also recorded on thin films on glass substrates prepared by using the same conditions as those employed when fabricating OFETs, in order to determine the quantum yield from the closed to the open form. The isomerization quantum yields for the ring opening of DAEs in thin-films were determined by following the change of absorbance with respect to irradiation time. Aberchrome 670 dissolved in toluene has been used as a chemical actinometer,[29] and the quantum flow was measured at 530 nm using light emitting diode (3.8 mW/cm^2, M530F1, Thorlabs).

In solution, the change in absorbance with respect to time is a function of the photonflux (ω), quantum yield (ϕ), molar absorptivity (ε), length of the optical path (l), Avogadro's number (N_A), fraction of absorbed photons (1-10^{-Abs}), and the volume of the sample (V).

$$\frac{dAbs}{dt} = -\frac{\varphi \cdot \omega \cdot \epsilon \cdot l \cdot \left(1 - 10^{-Abs}\right)}{N_A \cdot V}$$

This equation, which was used to determine the photonflux, can be modified to be applicable on thin films by introducing a unit correction factor (that compensates for the non SI units in the molar absorptivity factor), replacing the volume of the sample with the irradiated area, and by modify the unit of the photonflux from Einstein/s to Einstein/(s*cm^2).

$$\frac{dAbs}{dt} = -\frac{\varphi \cdot \omega \cdot \epsilon \cdot unit\ correction\ factor \cdot (1 - 10^{-Abs})}{N_A \cdot area}$$

The photonflux (at 530 nm) was determined using the chemical standard Aberchrome 670, using exactly the same geometry (including a mask with known area) as used when measuring on the films. The molar absorptivity of DAE in DPPT-TT films was approximated with the solution value (19 000 M^{-1} cm^{-1}). An in-house MATLAB© script was used to fit the absorbance contribution of DAE to theory in which the differential equations where solved in each fitting step. More details for calculating quantum yield of DAEs films can be found in previous works carried out at our labs. [30-31]

8.2.1. UV/Visible spectroscopy studies of pure DPPT-TT polymer in solution and in film

Figure 8.4 recorded the UV/Vis absorption spectra of pristine polymer (DPPT-TT) performed in film and in solution, the maximum absorption peak is shifted from 810 nm in the solution to 715 nm in the film.

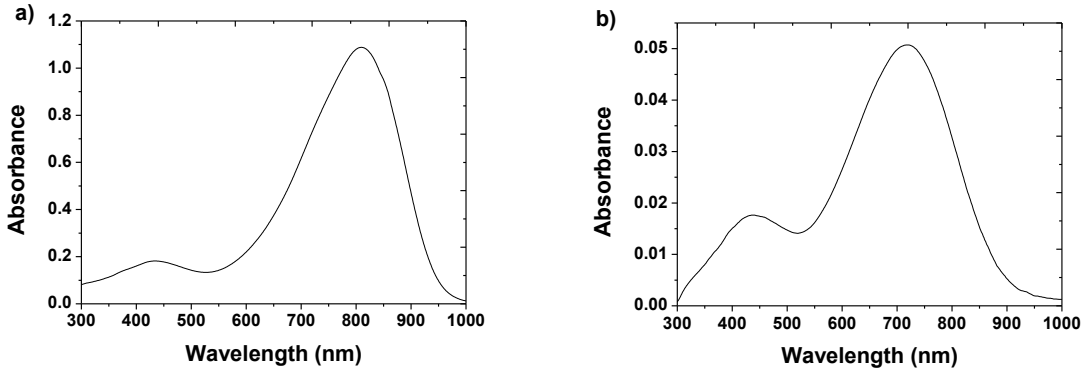

Figure 8.4. UV/Visible absorption spectroscopy of DPPTT-TT in solution and in film. UV/visible absorption spectra of **a)** DPPT-TT solution in dichlorobenzene with the concentration of 20 μg/ml, and **b)** DPPT-TT film on glass substrate spin-coated from a 2 mg/ml solution in dichlorobenzene.

8.2.2. Absorption spectroscopy of pure DAE_F and DAE_tBu in solution

The absorption spectra of pure diarylethene molecules (DAE_F and DAE_tBu) were recorded in solution upon UV light irradiation at λ=312 nm until reaching to the photostationary state (PSS) as displayed in **Figure 8.5**.

In solution, the number of times the isomerization event occurs per absorbed photon by the system, i.e., the isomerization quantum yield has been already calculated and reported in literature for both DAE_tBu and DAE_F, amounting to ca. 0.009 (9 wt%) and 0.039 (3.9 wt%), respectively.[22, 30]

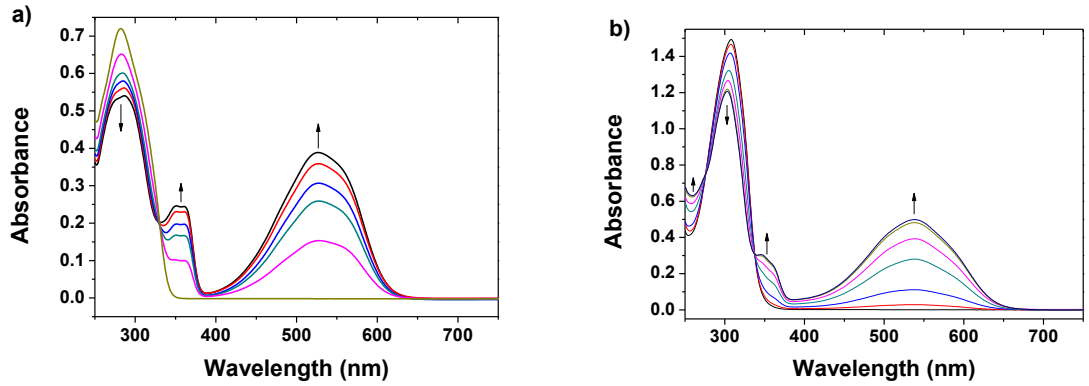

Figure 8.6. UV/Visible absorption spectroscopy of DAE_tBu and DAE_F in solution. UV/vis absorption spectra of **a)** DAE_tBu (20 μM) and **b)** DAE_F (45 μM) in butyl acetate under light irradiation at 312 nm until reaching the photostationary state (PSS).

8.2.3. Isomerization quantum yield measurements in thin films of the closed to open transition

The retainment of photo-switching ability of DAEs diffused into DPPT-TT layer was further envisaged by UV/visible absorption spectroscopy. UV light irradiation at 312 nm leads to an increase in absorption spectra between λ=400 nm and λ=600 nm region for both DAE_tBu (see the absorption spectra presented in **Figure 8.7a** and a zoom-in of this region presented in **Figure 8.9a**), and DAE_F films (see the absorption spectra presented in **Figure 8.8a** and a zoom-in of this region presented in **Figure 8.9b**), corresponding to the formation of ring closed form, which is a common feature of diarylethenes.[34-35] Altering film irradiation with visible light (λ=530 nm), in order to go back to the ring open form, results the spectra recovering to the initial state, presented in **Figure 8.13b** and a zoom-in of this region presented in **Figure 8.9a** for DAE_tBu, and in **Figure 8.8b** and a zoom-in of this region presented in **Figure 8.9b** for DAE_F. Which confirms that the reversible photo-switching of DAEs was retained in the DPPT-TT films.

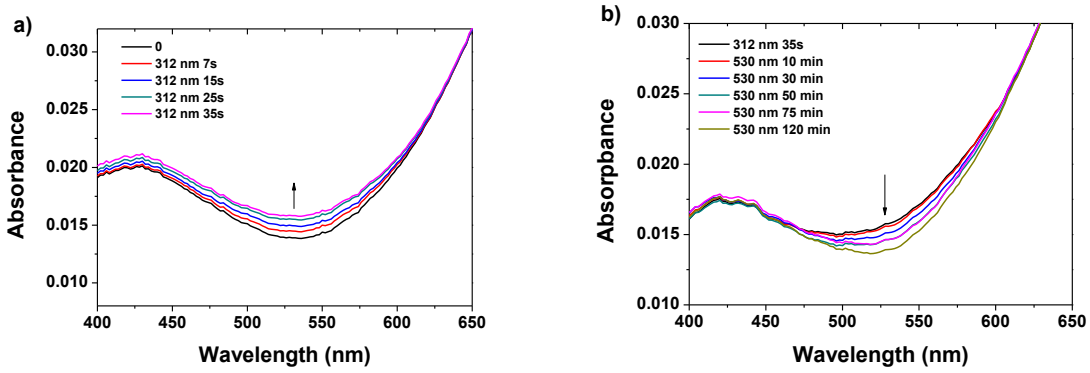

Figure 8.7. UV/Visible absorption spectroscopy of DAE_tBu diffused in DPPT-TT film. UV/vis absorption spectra of DAE_tBu film (spin-coated from 0.2 mg/ml solution dissolved in dichlorobenzene) diffused into DPPT-TT layer (spin-coated from a 2 mg/ml n-butyl acetate solution) on glass substrates upon **a)** UV-light irradiation at 312 nm until reaching the PSS, and **b)** visible-light irradiation (530 nm) until recovering the initial state.

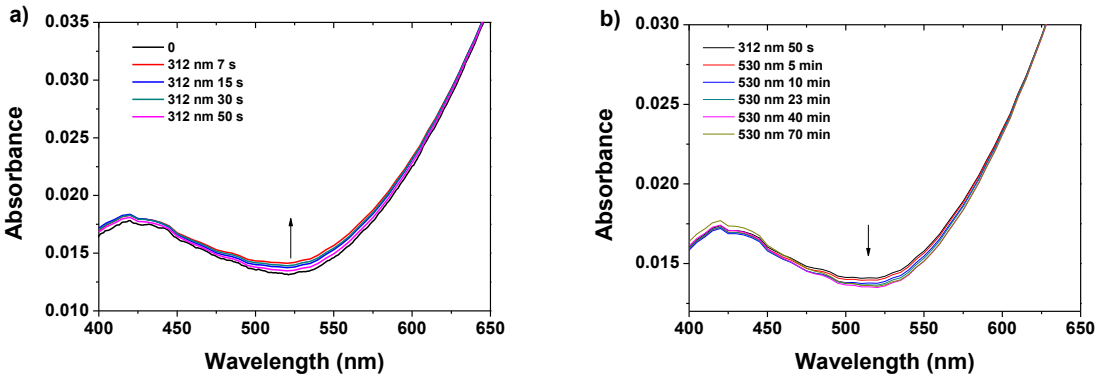

Figure 8.8. UV/Visible absorption spectroscopy of DAE_F diffused in DPPT-TT film. UV/vis absorption spectra of DAE_F film (spin-coated from a 0.4 mg/ml solution dissolved in dichlorobenzene) diffused into DPPT-TT layer (spin-coated from a 2 mg/ml n-butyl acetate solution) on glass substrates upon **a)** UV-light irradiation at 312 nm until reaching the PSS, and **b)** visible-light irradiation (530 nm) until recovering the initial state.

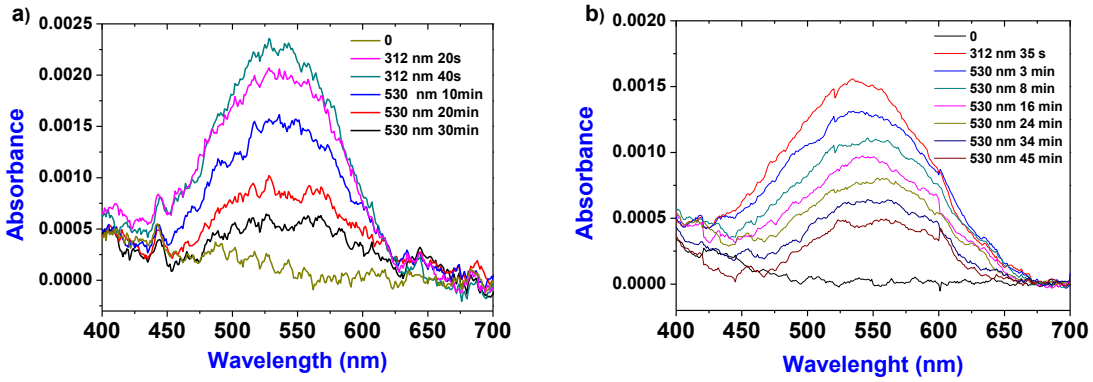

Figure 8.9. UV/Visible absorption spectroscopy of DAE_tBu and DAE_F films. UV/Vis absorption spectra of **a)** DAE_tBu film (0.2 mg/ml dissolved in butyl acetate solution and spin-coated on glass substrates) and **b)** DAE_F-based device (0.4 mg/ml dissolved in butyl acetate solution and spin-coated on glass substrates) under UV-light irradiation at 312 nm to the PSS, and recovered to the initial state under 530 nm visible-light irradiation.

We have determined the photochemical quantum yield (QY) for the photo-isomerization from the ring-closed form to the ring-open form in the film of DAEs molecules diffused into DPPT-TT polymer-matrix. The QY of both DAE_tBu and DAE_F in the film (0.3 wt% and 2.0 wt%, respectively) was lower than the reported values in the solution, [22, 30] which is common as the environment in the films restricts the free change of configuration compared to that in the solution upon light irradiation. Nevertheless, the photoisomerization QY in the film is still high enough to enable the efficient photoswitching in our OFET devices. We notice that DAE_F shows relatively higher QY than that of DAE_tBu, this was also observed in the solutions, and it can explain the faster light-response performance exhibited in DAE_F based devices.

8.3 Device irradiation procedure

Bottom-contact bottom-gate OFET devices were characterized in dark and under UV/Visible-light irradiation from the top of the sample surface under nitrogen atmosphere using a monochromatic light (Polychrome V - Till Photonics). Light irradiation was performed at λ=365 nm at areal power density of either 172 μWcm^{-2} or 212 μWcm^{-2}, and at λ=546 nm with areal power density of 4.01 $mWcm^{-2}$ and 4.57 $mWcm^{-2}$. Both UV and Visible wavelength were chosen in accordance to DAEs absorption spectra (see **Figure 8.4**). Light intensity was measured using an analogic optical power meter (PM100A, ThorLabs). For OFETs in top-gate geometry, the device cannot be irradiated from the top because of the non-transparent nature of the gate electrode; because of this reason, the irradiation was performed from the bottom, beaming light through the quartz substrate, by moving the

light source under the substrate. During the irradiation process, we have performed two cycles alternating Ultraviolet and Visible-light irradiation, each one consists of two steps except the first step which is Step 0 the current value in dark (corresponds to 100 %), step 1 and 2: Ultraviolet irradiation at λ=365 nm (172 μWcm^{-2}) for 10 seconds and 20 seconds respectively. Step 3 and 4 presented the device performances after visible-light irradiation at λ=546 nm (4.01 mWcm^{-2}) for 5 minutes each step. After a few minutes of time relaxation, the second cycle is also divided on two steps of UV and visible irradiation. Step 6 and 7 corresponds to UV illumination at λ=365 nm (212 μWcm^{-2}) for 10 seconds and 20 seconds, respectively. Finally, during steps 8 and 9 the devices were irradiated with visible light at λ=546 nm (4.57 mWcm^{-2}) for 5 minutes each step. For all the steps after irradiation, the light is switched off and the value of the drain current is taken at the same gate bias from the full I_D-V_{GS} curve.

8.4 Results and discussion on ambipolar transistors

Ambipolar transistors based on a DPPT-TT polymer as active layer have been fabricated in bottom-contact bottom-gate and bottom-contact top-gate configurations, using highly n-doped Si wafers. Under N_2 atmosphere in a glove box, the DPPT-TT high concentrated solution (10 mg/ml dissolved in anhydrous dichlorobenzene) was spun onto the solid substrate surfaces followed by annealing at 320°C for 20 minutes. The electrical characteristics of the device were measured by extracting the relevant parameters such as field-effect mobility (μ), threshold voltage (V_{th}), and I_{on}/I_{off} ratio. Ambipolarity of this material was not limited to one particular device or architecture, but it has been observed in different configurations including transistors with different solution-processed gate dielectrics in top-gate structure.

Figure 8.10 depicts the transfer and output characteristics of DPPT-TT-based device in dark (before DAEs deposition) which display typical ambipolar FET characteristics. This figure shows also $\sqrt{I_{DS}}$ vs V_{GS} which represents a sharp turn on of both n- and p-channels with threshold voltages of -4 and 16 V for hole and electron transport respectively. Saturated hole and electron mobilities were extracted from the saturation regime using the standard transistor equation. The OFETs based on the polymer exhibited pronounced hole-transport (μ_h ~ 0.5 cm^{2}v^{-1}s^{-1} and I_{on}/I_{off} ~ 10^7 at V_{DS} = -80 V) but lower electron-transport characteristics (μ_e ~ 0.012 cm^{2}v^{-1}s^{-1}, I_{on}/I_{off} ~ 10^5 at V_{DS} = 60 V) and a bit higher electrons and holes mobilities were obtained in OTS treated devices fabricated in the same configuration (bottom-contact bottom-gate) in the range of 0.6 cm^{2}v^{-1}s^{-1} and 0.017 cm^{2}v^{-1}s^{-1} respectively.

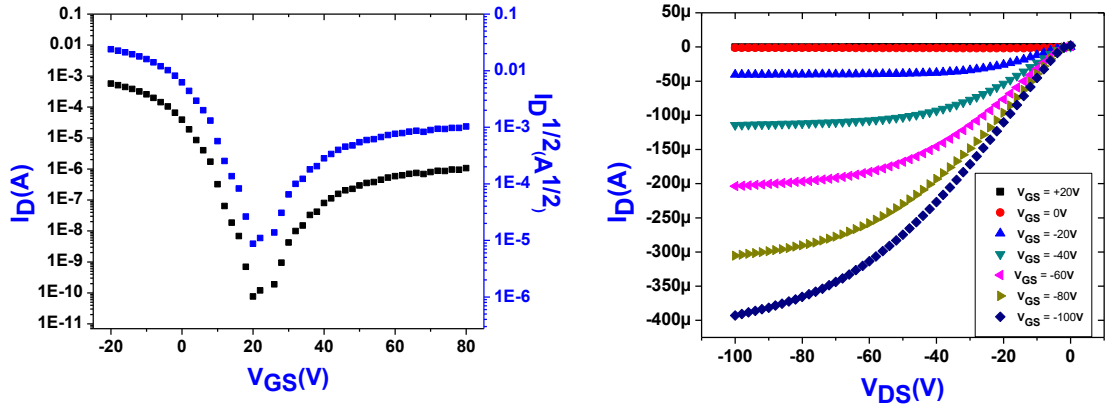

a) **b)**

Figure 8.10. a) OFET transfer and **b)** output characteristic curves in dark for FET devices fabricated in bottom-contact bottom-gate configuration.

The highest extracted hole mobility value is in accordance with the previous report by Zhang et al.[32] on DPPT-TT polymer employed as p-type semiconductor, where they reported 0.4 $cm^2v^{-1}s^{-1}$ as highest value extracted from bottom-gate bottom-contact based OFET devices. A recent work in 2013 on the same polymer reported high balanced electron and hole mobilities (μ_h ~ 1.36 $cm^2v^{-1}s^{-1}$ and μ_e ~ 1.56 $cm^2v^{-1}s^{-1}$) extracted from top-gate bottom-contact devices. We can notice that these mobility values reported in the paper cited above are higher than our extracted values. This difference in mobility can be attributed to the difference in device configuration. In the latter paper, they demonstrated high ambipolar mobilities extracted from top-gate bottom-contact devices using PMMA or CYTOP as polymeric dielectric layer. Whereas in our case, devices were performed in bottom-gate bottom-contact geometry. In order to obtain higher hole and electron mobilities, we have fabricated OFET devices on top-gate bottom-contact configuration. The transfer characteristics for hole and electron transport are presented in **Figure 8.11**, and their extracted electrical parameters are showed in **Table 8.1.** These top-gate devices exhibited much higher mobilities (μ_e ~ 0.11 ± 0.048 $cm^2v^{-1}s^{-1}$, I_{on}/I_{off} ~ 10^5 at V_{DS} = 50 V, and μ_h ~ 4.2 ± 0.016 $cm^2v^{-1}s^{-1}$, I_{on}/I_{off} ~ 10^6 at V_{DS} = -100 V), which are compared to those of bottom-gate devices, they are comparable to the state-of-the-art ambipolar polymers. However, top-gate bottom-contact OFET structure geometry was not compatible with the irradiation setup. For this reason and in order to further explore the diarylethene photochromic effect, we investigated DPPT-TT-DAEs based transistors fabricated on bottom-gate bottom-contact configuration.

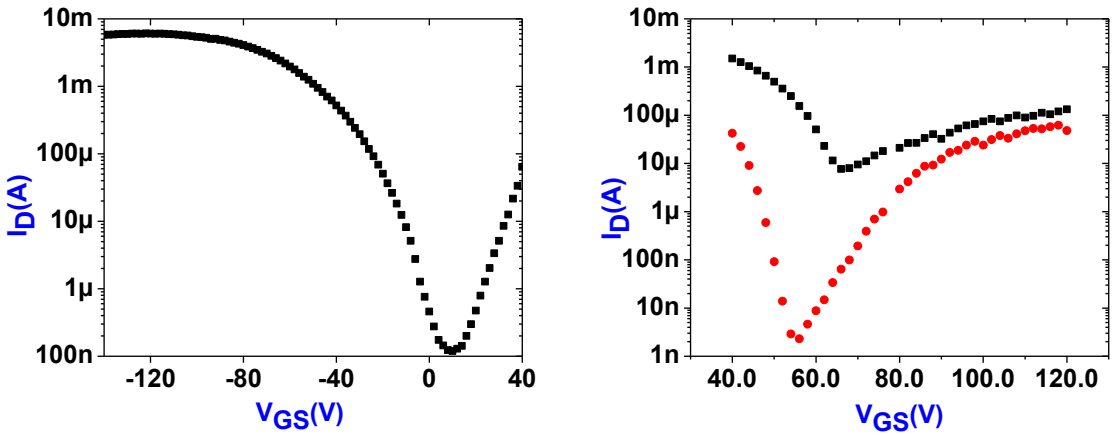

a) **b)**

Figure. 8.11. Transfer characteristics for FET device (L = 100 µm and W = 10 mm) based on DPPT-TT performed in bottom-contact top-gate configuration for **a)** holes transport at V_{DS} = -100 V and **b)** electrons charge transport performed at V_{DS} = + 50 V (red curve) and at V_{DS} = + 80 V (dark curve).

OFET Devices	**μ_p ($cm^{-2}s^{-1}v^{-1}$)**	**μ_n ($cm^{-2}s^{-1}v^{-1}$)**	**V_{th} (V) channel-p**	**V_{th} (V) channel-n**
DPPT-TT	4.2 ± 0.016	0.11 ± 0.048	-14.23 ± 1.211	35 ± 2.431

Table. 8.1. OFETs parameters of DPPT-TT-based devices fabricated in bottom-contact top-gate geometry. Mobility and threshold voltage values for both hole and electron transport reported in the table (L = 100 µm and W = 10 mm) are calculated. Their mean values and standard derivations are extracted from the saturation regime at V_{DS} = -100 V and V_{DS} = 60 V respectively.

After polymer deposition and annealing at 320 °C for 20 minutes, DAE_tBu and DAE_F derivatives in the open forms (the amount added is 10 wt% for each one dissolved in butyl acetate) were deposited on top of DPPT-TT layer and thermally annealed at 90°C for 1 hour and 30 minutes to induce diarylethenes permeation into the polymer matrix and giving rise to an ordered bi- and three-component thin film. Ambipolar OFET devices were characterized in dark before and after DAE addition into the polymer layer in order to investigate the effect of DAEs insertion on the electron and hole mobilities. Transfer characteristics measured at V_{DS} = -50 V are presented in **Figure 8.12**. The transfer characteristics before and after DAE insertion exhibit typical ambipolar behaviour, high hole

and electron mobilities and I_{on}/I_{off} ratio. After DAEs addition, a small decrease in drain current was observed, leading to a negligible decrease in electron and hole mobilities (see **Table 8.2**) due to the permeation process employed which doesn't affect the polymer film morphology and so the charge transport.

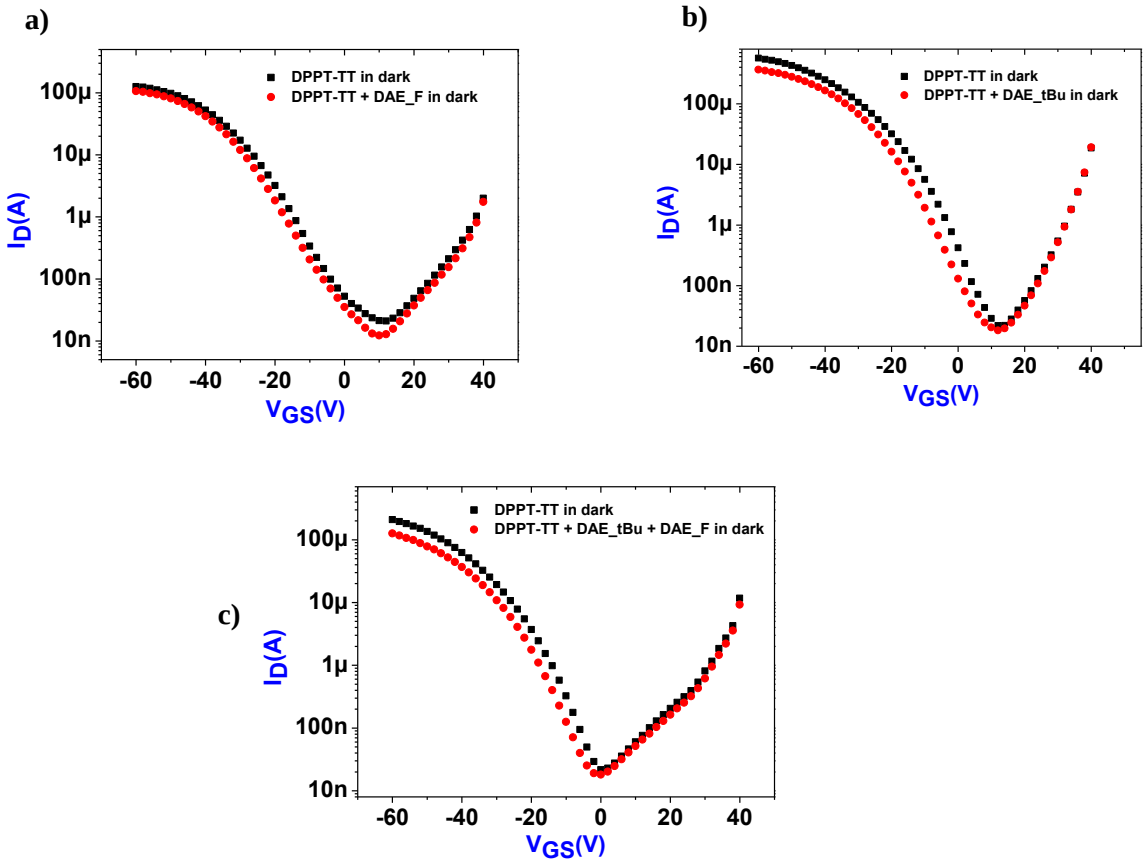

Figure 8.12. OFET Transfer characteristics. Transfer curves in dark for FET devices fabricated in bottom-contact bottom-gate configuration based on **a)** DPPT-TT polymer at V_{DS} = 20 V and at V_{DS} = -60 V for **b)** DPPT-TT-based device before and after DAE_F, **c)** DAE_tBu and **d)** both DAE-F and DAE_tBu permeation.

OFET Devices	μ_p ($cm^{-2}s^{-1}v^{-1}$)	μ_n ($cm^{-2}s^{-1}v^{-1}$)	V_{th} (V) channel-p	V_{th} (V) channel-p
DPPT-TT	0.46 ± 0.038	9.15 ×10^{-3} ± 0.00263	-15.60 ± 1.211	32.67 ± 1.561
DPPT-TT + DAE_F	0.41 ± 0.016	8.46 ×10^{-3} ± 0.00168	-18.60 ± 1.847	24.60 ± 1.221
DPPT-TT + DAE_tBu	0.35 ± 0.023	7.78 ×10^{-3} ± 0.00134	-20.60 ± 2.904	18.07 ± 3.703
DPPT-TT + DAE_F + DAE_tBu	0.38 ± 0.019	7.69 ×10^{-3} ± 0.00185	-16.60 ± 2.531	22.60 ± 2.211

Table. 8.2. Summary of extracted OFETs parameters of DPPT-TT-based devices fabricated in bottom-contact bottom-gate geometry**.**

Averages mobility and threshold voltage values for both hole and electron transport reported in the table from at least ten OFETs (L = 20 μm and W = 10 mm), were extracted from the saturation regime at V_{DS} = -100 V and V_{DS} = 60 V respectively. For devices based on polymer with DAE_F and or DAE_tBu inserted into its polymeric layer, diarylethene molecules were in their open form and all the electrical measurements were performed in dark under nitrogen atmosphere.

Figure 8.13 shows optical microscopic images of the same sample before and after DAEs permeation, with a zoom in of the device channel between source and drain electrodes. From the microscopic images, we can observe a homogenous polymer layer without any kind of aggregation after diarylethenes deposition. To further more explore the films morphology, AFM images have been recorded and presented in **Figure 8.14**.

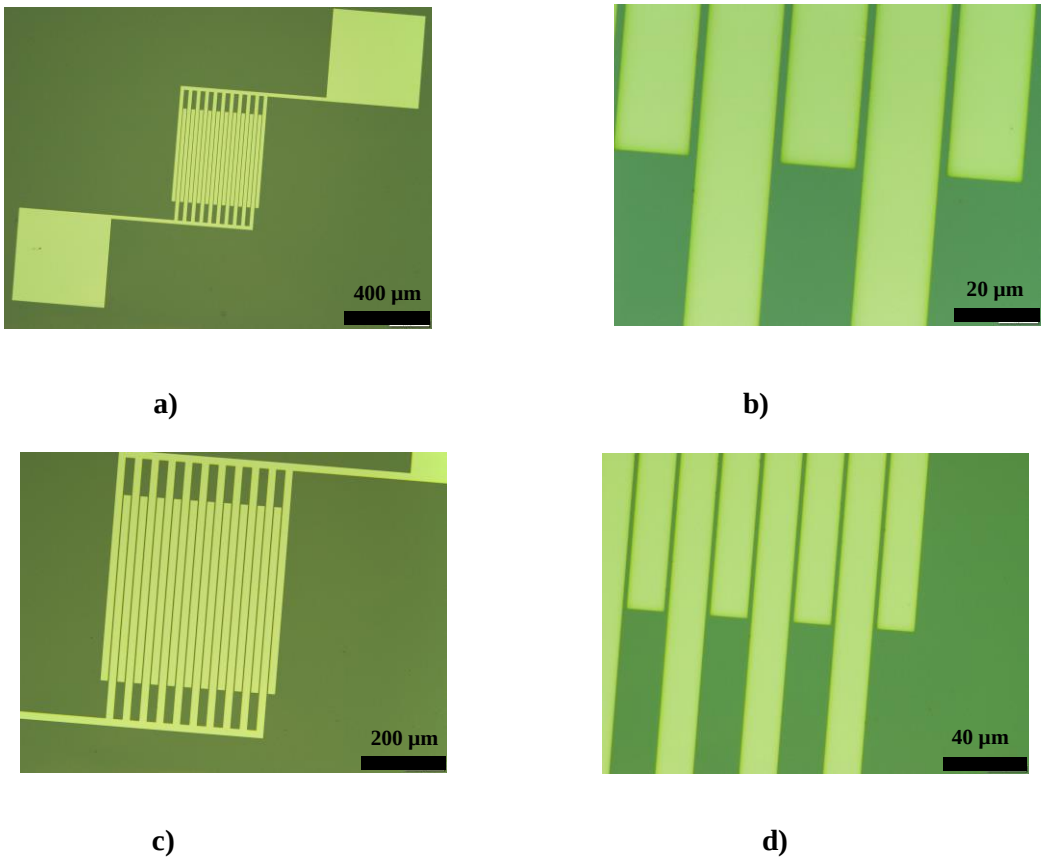

Figure 8.13. optical microscopic images of an OFET (channel length L = 2.5µm) performed in bottom-contact bottom-gate configuration **a)**, **b)** before DAEs addition (DPPT-TT single layer) and **c)**, **d)** after DAEs (DAE_F and DAE_tBu) permeation into the polymer layer (DPPT-TT/DAEs three-component layer). **b)** and **d)** are a zoom in images showing the OFET active channel.

The single, bi-and three-component films morphology of pristine polymer (DPPT-TT) and polymer with DAEs in bi-and three-component was investigated by atomic force microscopy (AFM) (see **Figure 8.14**). AFM investigation on the micrometer scale did not reveal any difference in the film morphology upon addition of DAEs in the active channel. The pristine polymer films showed highly ordered morphology and no significant morphological changes were observed for the same films after DAEs deposition via permeation process on the polymer layer. Which indicates that the photochromic molecules do not effectively change the polymer channel assemblies and morphology. The root mean squared roughness (R_{RMS}) of different polymer films was recorded in **Table 8.3**. It was found that the roughness in bi-and three-component based devices is a bit greater than that of pure DPPT-TT polymer, due to diarylethenes insertion. However, to gain a precise information on the effect of the presence of DAE on the crystalline structure of the polymer, grazing incident x-ray diffraction (GIXD) measurements are needed.

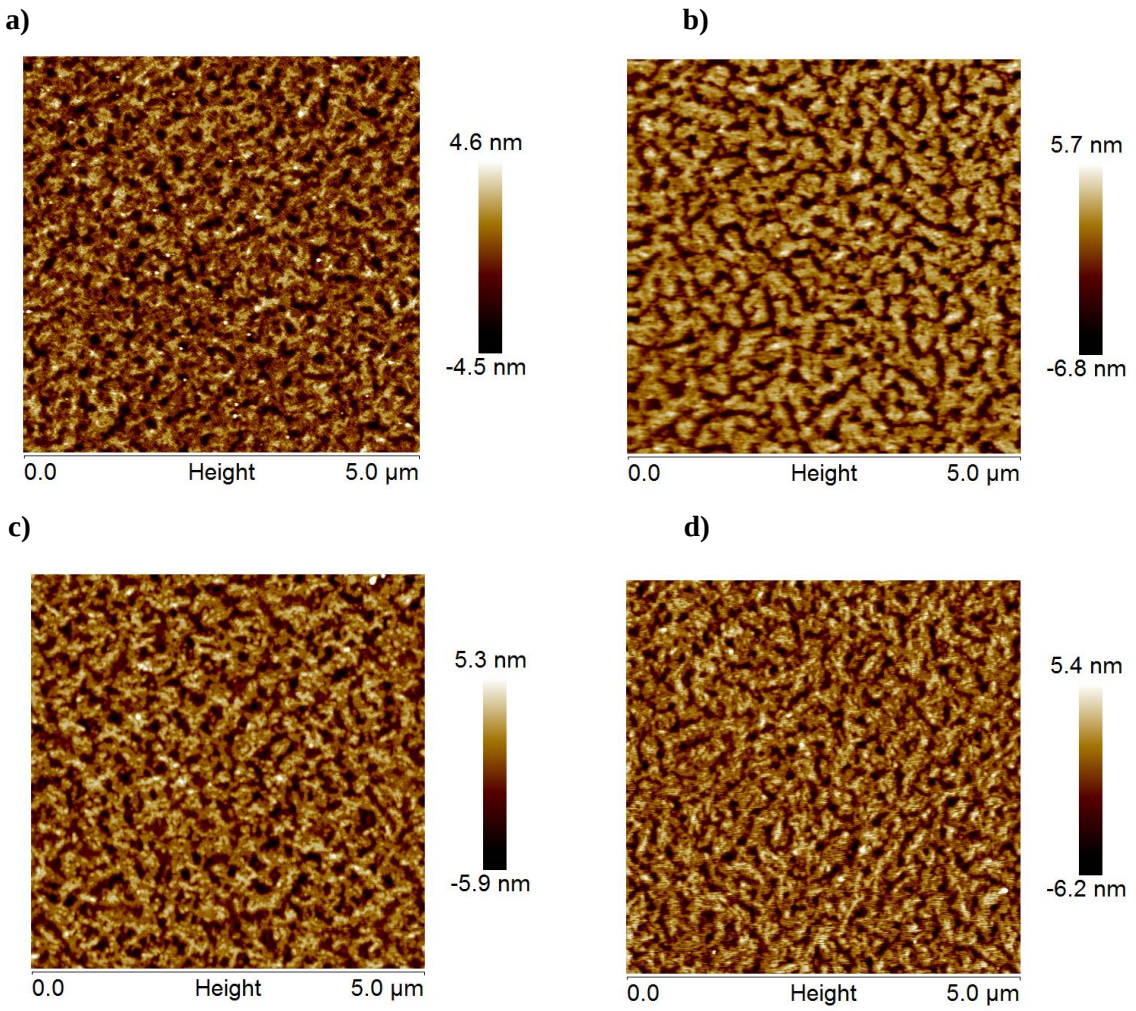

Figure 8.14. AFM images of untreated devices based on DPPT-TT: **a)** before and **b)** after DAE_F (10 wt%), **c)** DAE_tBu (10 wt%) and **d)** both DAE_F (10 wt%) and DAE_tBu (10 wt%) insertion into the polymer matrix by permeation process.

Surface device	Root mean squared roughness (R_{RMS})
DPPT-TT	1.14 nm
DPPT-TT + DAE_F	1.79 nm
DPPT-TT + DAE_tBu	1.47 nm
DPPT-TT + DAE_F + DAE_tBu	1.48 nm

Table 8.3. Summary of calculated Root mean squared roughness (R_{RMS}) from the AFM images presented in Figure. 8.8 for DPPT-TT-based devices fabricated in bottom-contact bottom-gate geometry. This table showed the surface roughness values calculated from different OFET surfaces of pristine polymer (DPPT-TT) and polymer with permeated DAE_F (10 wt%) and or DAE_tBu (10 wt%) molecules.

We have performed photo-switching cycles alternating ultraviolet (λ=365 nm) and green (λ=546 nm) light irradiation onto the OFET devices based on bi- or three-compounds DPPT-TT, 10 wt% of DAE_tBu and or 10 wt% of DAE_F as the active layer. We examined the light-field effect on the drain current modulation. The light-induced electrocyclization of the diarylethene unit changes their molecular structure from open to closed form and vice versa. Such a mechanism is responsible for inducing modulation of the electrical properties of DPPT-TT based OFETs, ensuring a light-control of the drain current.

The DAEs in their open and closed states feature different HOMO and LUMO levels. In particular, when they are in their closed isomeric state the HOMO of DAE_tBu in closed form sits in the bandgap of the copolymer, thus it acts as intragap hole-accepting level. Likewise, is the case for the LUMO of DAE_F in open form, thus for electron-accepting levels. Conversely, the HOMO and LUMO energetic levels of the open form of DAE_tBu and DAE_F respectively sit outside the bandgap, thus no electronic interaction takes place (see the energetic cartoon presented in **Figure 8.15**). This approach has been previously employed in our lab using p-type semiconductors (P3HT, BTBT)[30, 33] and n-type semiconductors (PCBM, ICBA)[31] with different DAE blends.

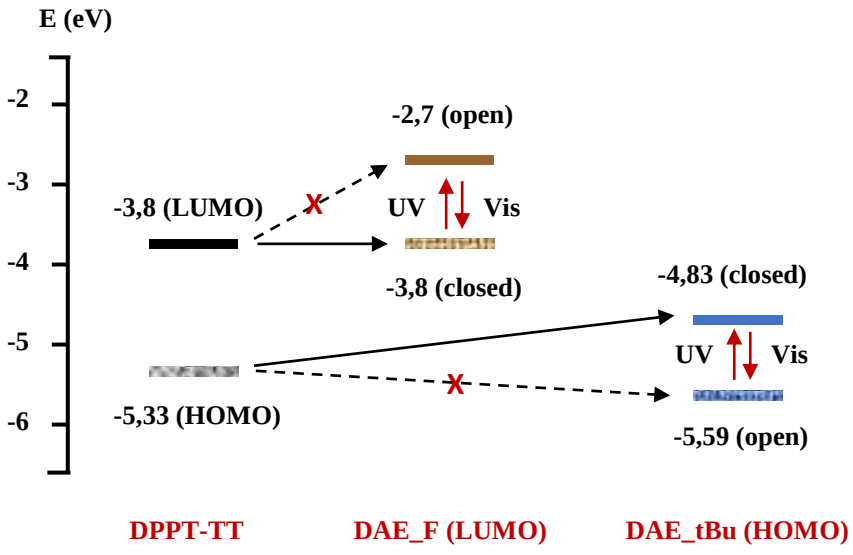

Figure 8.15. HOMO and LUMO Energetic levels. Schematic energy diagram representing the HOMO and LUMO energetic levels of DPPT-TT ambipolar polymer and photochromic diarylethenes (DAE_tBu and DAE_F) in their open and closed states, energetic values are measured from cyclic voltammetry.

Light irradiation was found to induce a marked modulation of the drain current as shown in **Figure 8.16** for either electrons and holes for devices based on the pristine polymer DPPT-TT (**Figure 8.16a**), on DPPT-TT with DAE_tBu (**Figure 8.16b**), or on the polymer with DAE_F (**Figure 8.16c**)

and the three-component based devices; polymer with both DAEs (**Figure 8.16d**). The drain current values were extracted from the transfer characteristics at fixed gate voltage V_{GS} = -100 V and +60 V for holes and electrons transport respectively and drain bias V_{DS} = -80 V and + 60 V respectively, plotted against the irradiation steps. We have observed an important shift in threshold voltage after UV irradiation to more positive values for n-channel and negative values for p-channel. Both electrons and holes current decreased upon 2 steps of UV irradiation lasting 10 seconds and 20 seconds, respectively. The first step is the current value in dark, which corresponds to 100%. Upon UV light irradiation the drain current extracted from three-component devices (see **Figure 8.19d**) exhibited a decrease of 92 % and 85% for holes and electrons, respectively. This evidence confirms that DAE molecules diffuse and reach the semiconductor-dielectric interface. After visible light irradiation divided in two steps of 5 minutes each, electron and hole drain current increased and completely recovered. For the fabricated bi-component devices based on the polymer with inserted DAE_tBu molecules (see **Figure. 16b**), the holes drain current for these devices significantly decreased by more than three orders of magnitude upon 30 seconds of UV illumination, then, it increased upon visible light to 98 % of the initial current value. Whereas, electron current is remained constant upon both UV and Visible irradiation. Concerning OFETs devices based on DPPT-TT and DAE_F, electron currents was switched upon UV and visible illumination, while hole drain currents was stable. These results confirm the completely reversible and selective light-switching process over the insertion of photochromic molecules DAE_tBu (10 wt%) and/or DAE_F (10 wt%).

To gain further insight into the photo-switching of both DAE_tBu and DAE_F.We have determined the DAEs isomerization quantum yield from the closed to the open form. These results confirm the light-switching process, which is completely reversible and selective for holes and electrons charge transport. Furthermore, this high light-induced current modulation was maintained, even after the device storage for several months inside glove box, confirming that diarylethene molecules inserted into polymer matrices has the potential to be used as an optical memory.

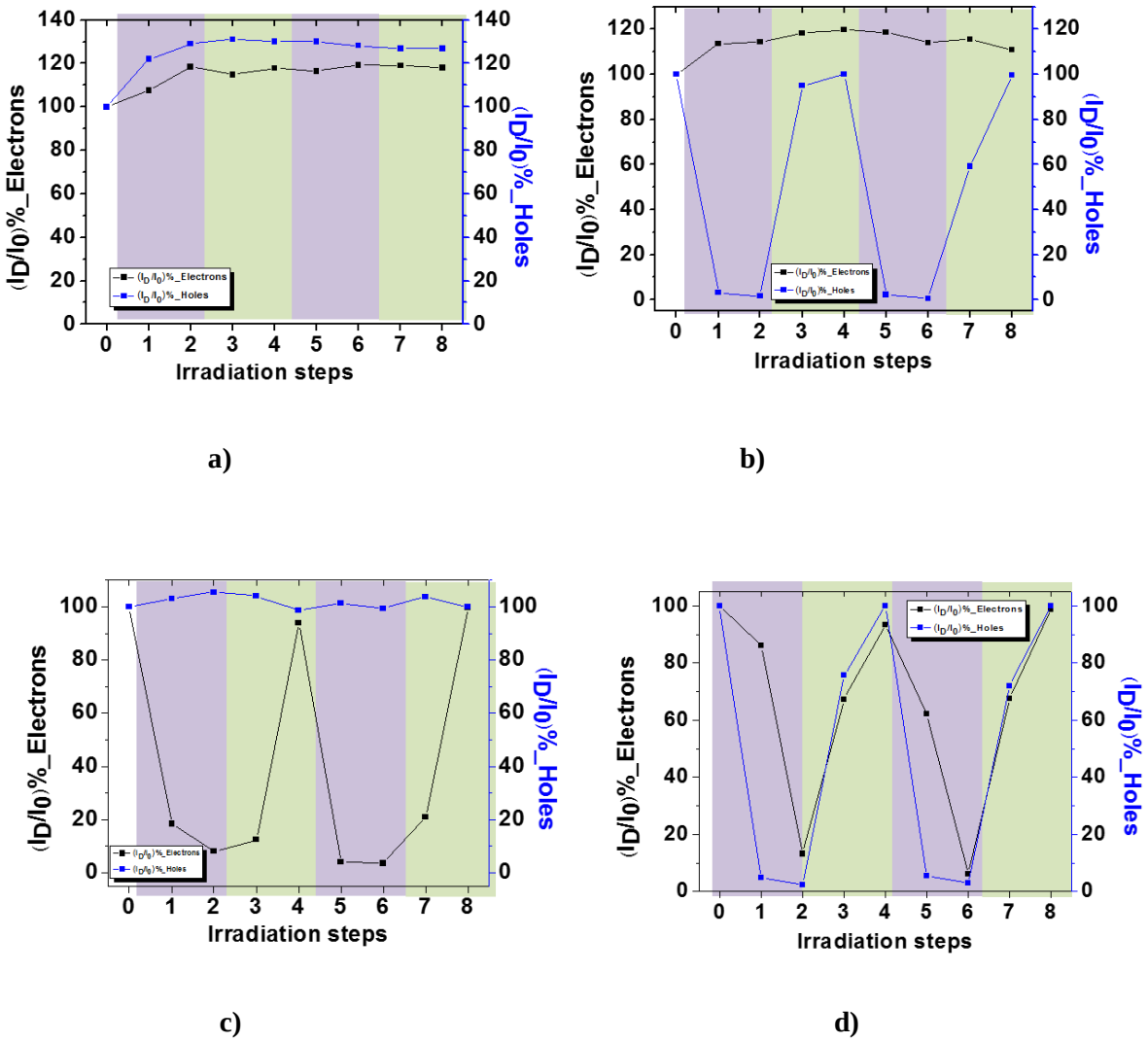

Figure 8.16. OFET Transfer characteristics under Ultraviolet and visible light irradiation. Transfer curves for FET device based on **a)** DPPT-TT polymer with **b)** DAE_tBu (10 wt%), **c)** DAE_F (10 wt%) and **d)** both of them (10 wt% of DAE_tBu and 10 wt% DAE_F) for holes and electrons transport. Light violet and light green shaded areas correspond to the irradiation with light at wavelengths of 365 nm and 546 nm respectively, the irradiation is done from the top.

8.5 High gain complementary inverters based on optically switchable ambipolar transistors

The inverter circuit is a key building block for many digital electronic circuits and for analog amplifying circuits. An inverter is a basic unit in electronic circuits as it leads to logical INVERSION (0 - 1 / 1 - 0) of a given input that is a voltage in our case.[35] It is crucial to simplify the inverters

fabrication processing and circuit designs by incorporating both p- and n-type transistors in a single semiconducting layer using ambipolar transistors. Organic complementary circuits are attractive because the complementary technology has led to the construction of digital circuits with higher operational gain and better noise immunity.[36-37]

We have fabricated organic complementary inverters employing identical ambipolar OFETs based on DPPT-TT polymer with diarylethene molecules (DAE_tBu and DAE_F) inserted via permeation into DPPT-TT matrix in order to tune the voltage gain of complementary-metal-oxide-semiconductor (CMOS) logic by UV/Visible irradiation. Fraunhofer pre-paterned wafers for inverters were purchased from Fraunhofer IPMS institute were used as substrates, contact electrodes (Au) of these devices were patterned using photo-lithography and consisted of individual FET electrodes having dimensions of L = 5 µm and different channel width of both active and load transistors ranging from 0.455 to 1.35 mm. Substrate devices were cleaned by exploiting the same approach described above. Before deposition, the SiO_2 surface was functionalized with octadecyltrichlorosilane (OTS) self-assembled monolayers, to minimize interfacial trapping sites for charges during device operation. Where the substrates were immersed into 10 mM solution of OTS in anhydrous toluene and annealed at 60°C for 30 minutes. After that substrates were left for 12 hours, then washed with anhydrous toluene and dried in the spin-coater (4000 rpm, 60 seconds). Finally, they were annealed at 60°C for 1 hour. An inverter structure and optical image are presented below in **Figure 8.17**.

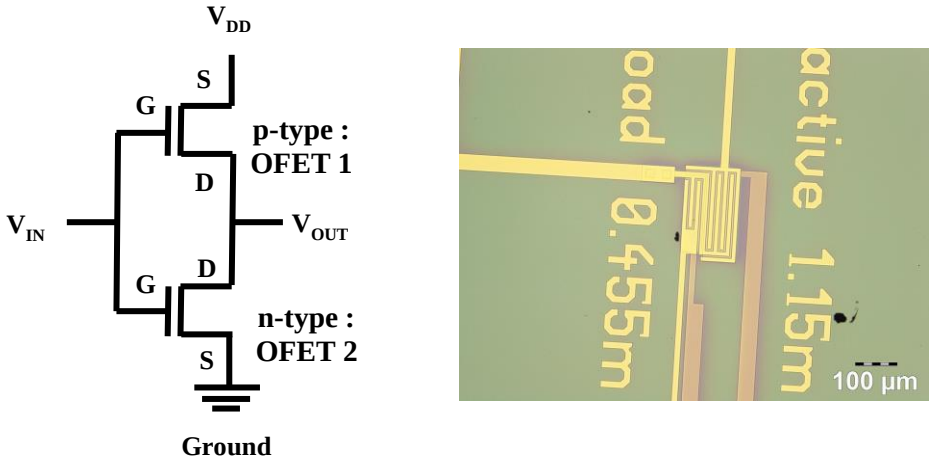

Figure 8.17. a) Schematic illustration of a complementary inverter structure, where S, D, G are source, drain and gate respectively for each separated transistor, V_{IN} is the common gate voltage, V_{DD} is the supply voltage, and V_{OUT} is the output voltage. **b)** shows an optical image of an organic complementary inverter circuit based on a single ambipolar layer, with 1.15 mm and 0.455 mm channel lengths of both active and load transistors respectively.

The transfer voltage (V_{OUT}-V_{IN}) characteristics of all devices were measured inside the glove box in nitrogen atmosphere by contacting a common gate for both transistors served as the input terminal V_{IN}, a supply voltage (V_{DD}), and output voltage (V_{OUT}) electrodes and applying positive or negative voltages on V_{DD} and V_{IN} using a Cascade Microtech M150 probe station with dual channel Keithley 2636A source-meter and associated software.

Complementary organic inverters have been fabricated utilizing DPPT-TT as n and p-type transistors and integrating DAE molecules in order to tune their voltage gain. We have used a bottom-gate configuration, this configuration is preferred by industry, because it allows full use of photolithographic processing. The width channels of p-type transistors were made considerably longer than the channels of n-type transistors to compensate for the difference in mobility of holes and electrons. The channels lengths are identical (5 µm). The voltage transfer characteristics of CMOS inverters based on pure DPPT-TT were measured in dark and their corresponding gain values were calculated (see **Figure 8.18**).

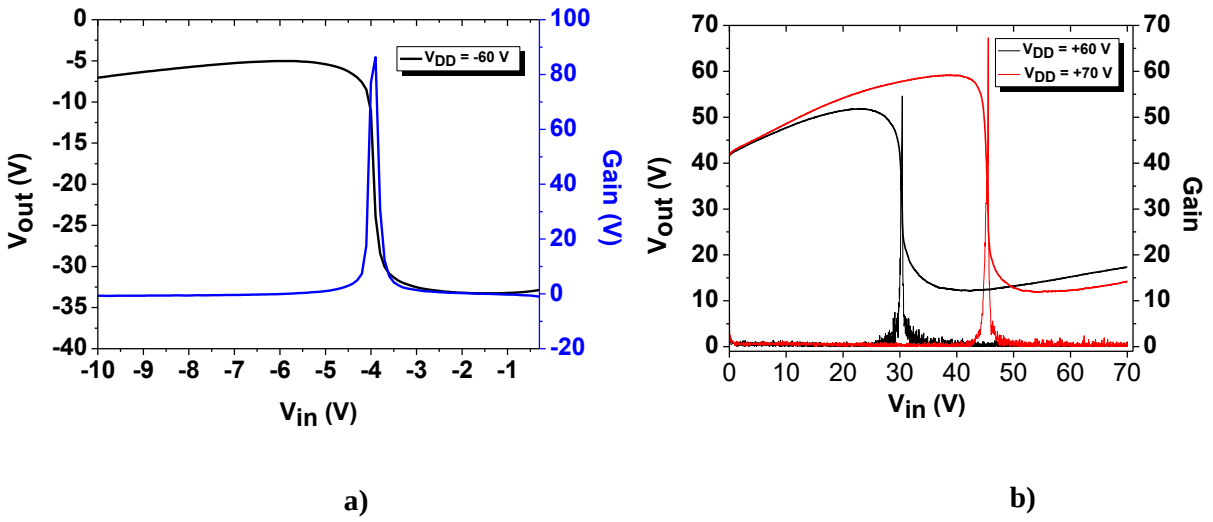

Figure 8.18. Inverter transfer characteristics and their corresponding gain voltage V_{out} vs V_{in} curves. Transfer curve and the corresponding voltage gain of DPPT-TT-based ambipolar inverter with DAE_F and DAE_tBu molecules measured at **a)** negative supply voltage V_{DD} = -60 V and **b)** positive supply voltage of V_{DD} = +60 V and +70 V.

Figure 8.18a and **b** show a typical voltage transfer curve and their corresponding calculated voltage gain for devices based on DPPT-TT and DPPT-TT with DAEs (DAE_F and DAE_tBu), respectively. When the supply voltage (V_{DD}) and V_{IN} are biased positively (see **Figure 8.18b**) the

inverter works in the third quadrant of the output voltage Vs V_{IN} plot with sharp inversions of V_{IN} at near half of V_{DD} = 70 V exhibiting a maximum gain of ~ 67 and a maximum gain of 54 at exactly half V_{DD} for an applied V_{DD} value of 60 V in dark confirming that the voltage gain increased by increasing V_{DD} applied voltage. Under these bias conditions OFET 1 (see **Figure 8.17 a**) acts mainly like p-type transistor of a regular CMOS inverter, while OFET 2 (see **Figure 8.17 a**) operates as the n-type device. If the input and the bias voltage are negative (**Figure 8.18a**), the inverter still operates with n- and p-channel function exchanged between the two devices, in this case, the inverter is operating in the first quadrant exhibiting a maximum gain of ~ 84 at V_{DD} = -60 V. With reference to **Figure 8.18a**, when V_{IN} is close to V_{DD}, the n-channel of both transistors is on with OFET 1 having a smaller overdrive than OFET 2. This explains why the output node cannot be completely pulled down by OFET 2 and why the output voltage slightly decreases with decreasing V_{IN}.
Figures 8.19a and **b** show a typical voltage transfer curves for devices based on DPPT-TT and DPPT-TT with DAEs (DAE_F and DAE_tBu), respectively. **Figures 8.19c** and **d** represent their corresponding calculated gain values upon UV and Visible light irradiation.

Inverters key parameters, such as voltage gain, defined as dV_{OUT}/dV_{IN}, noise margin, including noise margin low (NML) defined as NML = $V_{OL} – V_{IL}$, where V_{OL} is the Output Voltage Low and V_{IL} is the Input Voltage Low, and noise margin high (NMH), defined as NMH = $V_{OH} – V_{IH}$, where V_{OH} is the Output Voltage High and V_{IH} is the Input Voltage High were extracted from the voltage transfer curves in **Figure 8.19a** and **b** corresponding to devices based on pristine DPPT-TT and DPPT-TT with integrated DAE (DAE_F and DAE_tBu) molecules respectively and recorded in **Table 8.4**.

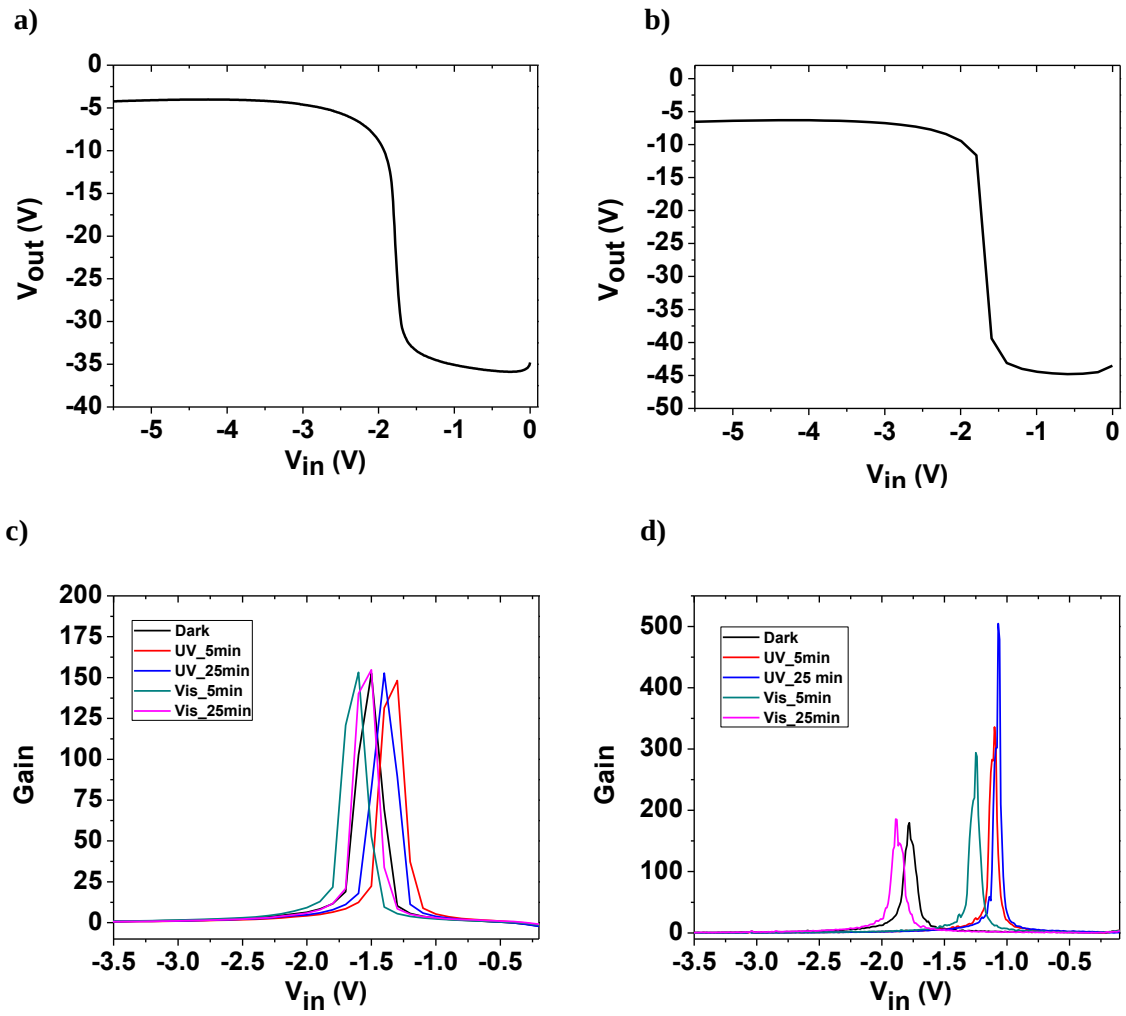

Figure 8.19. Inverters transfer characteristics and dc gain voltage. a) Transfer curve of a CMOS-like inverter comprising two DPPT-TT-based transistors measured at V_{DD} = -70 V, **b)** transfer curve of DPPT-TT-based ambipolar inverter with DAE_F and DAE_tBu molecules, **c)** and **d)** the corresponding measured gain for DPPT-TT and DPPT-TT-DAEs (DAE_F and DAE_tBu) based devices respectively in dark and under UV-Visible irradiation.

The inverter devices fabricated by integrating DAEs in the semiconductor layer operate in the first quadrant at V_{DD} = -70 V, however, did not exhibit sharp inversions of V_{IN} at $V_{DD}/2$, with inversion at a lower magnitude of V_{IN} values in the first quadrant compared to the positive quadrant (in **Figure 8.18**). This asymmetry is highly related to the observed asymmetry in the individual electrons and holes transfer characteristic curves. At V_{DD} = -70 V we have obtained a much higher gain ~ 153 for pristine polymer and ~ 180 for inverter based on two DPPT-TT ambipolar transistors with DAE_F and DAE_tBu in dark, as represented in **Figure 8.19c** and **8.19d** respectively. As showed in **Figure 8.19d**, the gain increased progressively with UV illumination (365 nm) exhibited a high static gain value of 504 after 25 minutes of UV irradiation and noise margin increased by almost 10 %

½ V_{DD} compared to that obtained in dark (see **table 8.4**), under visible light (546 nm), the voltage gain and noise margin values decreased to recover the initial values after 25 minutes of visible irradiation. This behavior confirms the ability to tune the inverters gain using light irradiation.

Device	Irradiation	NML (V)% ½ V_{DD}	NMH (V) % ½ V_{DD}	Gain_max (V)
DPPT-TT	In dark	8 %	85 %	152.5
	After UV irradiation (365 nm)	7 %	84 %	152.7
	After visible irradiation (546 nm)	8.5 %	86 %	153
DPPT-TT + DAE_F + DAE_tBu	In dark	10.9	92 %	184
	After UV irradiation (365 nm)	20 %	86.8 %	504
	After visible irradiation (546 nm)	9.97 %	92.4 %	180

Table 8.4. Gain and noise margin values extracted from devices based on DPPT-TT polymer and DPPT-TT polymer with permeated DAE_F and DAE_tBu molecules into its active layer.

It is known that combining n and p semiconductors to make organic inverters gives rise to high voltage gain. In literature one can find several examples.[38-39] Zhang et al. developed flexible organic complementary inverters using pentacene and C60 as active layer achieving high gain up to 180.[40] Tatemichi et al. fabricated an organic complementary inverter with N,N′-ditridecyl-3,4,9,10-perylenetetracarboxylic di-imide as an n-type semiconductor and pentacene as a p-type semiconductor of organic inverter, which exhibited a gain of 500.[41] All these examples are based on different n- and p- type semiconductors. Concerning inverters based on single ambipolar polymer; the gain values reported in literature to date are very low, the highest value being around 86 as stated by Chen et al.[42] Our gain values before and after UV irradiation are remarkably greater than those of other inverters based on ambipolar organic semiconductors.

Parameter values in **Table 8.5** and **Table 8.6** are extracted from fits of individual transistor curves shown in **Figure 8.20** which shows a good operational ambipolar transistor. It was shown in literature that the values of the subthreshold swing, n- and p-threshold voltage difference and I_{on}/I_{off}

ratio strongly influence the noise margin and voltage gain. A difference in the subthreshold swing of driver and load after UV irradiation was observed, it decreased which is favorable for having a higher gain and noise margins, this explains the gain variation after UV light irradiation. Decreasing the threshold voltage difference between both n- and p- type transistors of the inverter will change the dynamic behavior approaching to the ideal inverter for which $Vth_{n,p}$ = 0 V. After UV irradiation, threshold voltage values became closer to 0 V, the inverter characteristics are shifted along the input voltage axis, and the noise margin and gain values increased. Ideal inverter should also have mobility ratio between n and p OFETs, r = 1. The effect of the difference in mobility between n- and p-type transistors on the static characteristics can be compensated for by design because r also contains the easily accessible design parameters W_n and W_p. An important increase in I_{on}/I_{off} ratio is observed after UV light illumination, it is known that high I_{on}/I_{off} ratio is considered as one of factors described above that are recommended to have high gain and noise margins.

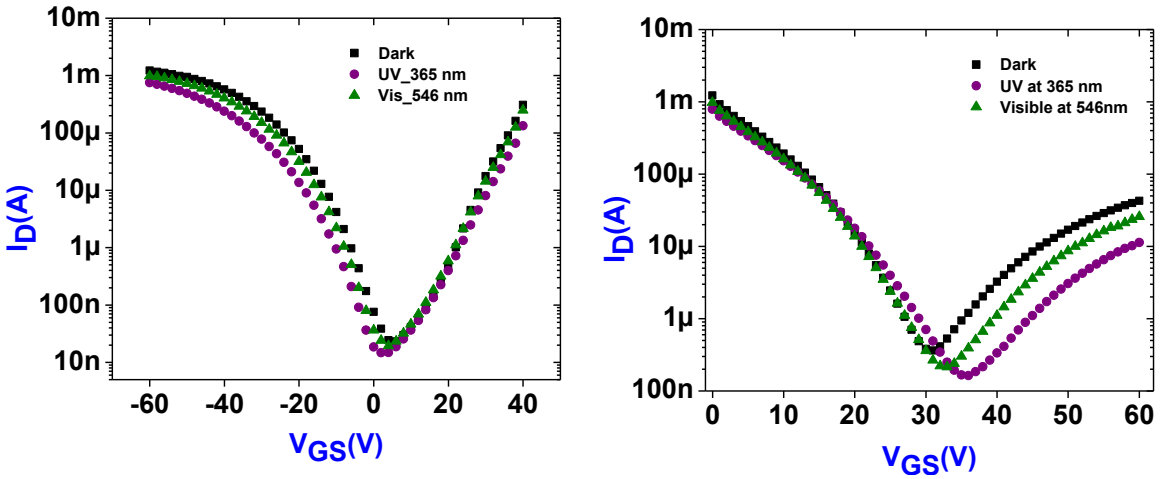

Figure 8.20. Holes and electrons transfer curves. Transfer characteristics of a) individual p- and b) n-channel-OFETs of inverters based on DPPT-TT with DAE_F and DAE_tBu molecules in dark and under UV-Visible light irradiation measured at fixed V_{DS} values at -60 V and +60 V respectively.

	V_{th} (V) for *n*-channel	V_{th} (V) for *p*-channel	I_{on}/I_{off} for *n*-channel	I_{on}/I_{off} for *p*-channel
Dark	29.15 ± 1.38	-9.65 ± 2.90	2.14×10^4	5.30×10^5
UV-irradiation (365 nm)	32.24 ± 1.64	-7.83 ± 2.84	6.45×10^4	7.07×10^5
Visible-irradiation (546 nm)	30.21 ± 1.29	-10.25 ± 3.68	1.93×10^4	5.20×10^5

Table 8.5. OFETs extracted parameters in dark and under UV-Visible light irradiation. Averages Threshold voltage and I_{on}/I_{off} ratio values extracted from saturation regime of n and p-type OFET curves based on DPPT-TT polymer with DAE_F and DAE_tBu molecules.

	Subthreshold swing for *n*	Subthreshold swing for *p*
In dark	22 ± 2.14	6.45 ± 2.74
UV-light irradiation (365 nm)	14 ± 1.94	3.8 ± 1.85
Visible-light irradiation (546 nm)	22 ± 1.65	6.13 ± 1.98

Table 8.6. Extracted parameters from individual OFETs of complementary organic DPPT-TT-based inverters. Subthreshold swing average values extracted from n and p-type OFET curves based on DPPT-TT polymer with permeated DAE_F and DAE_tBu molecules.

Conclusions

We achieved drain-current switching of multicomponent devices based on polymer and diffused diarylethene-channel field-effect transistors with light- and electric-field effects. The drain current was reversibly changed by alternating ultraviolet and visible light irradiation. The light-switching process is completely reversible and selective by using DAE_tBu (10 wt%) and or DAE_F (10 wt%) as photochromic molecules. Bottom-gate inverters based on DPPT-TT ambipolar OFETs integrating diarylethene molecules into the polymer matrix have been fabricated via permeation in order to enhance the gain using light. The CMOS-like inverters showed the highest voltage inversion

gain of 504 up to date for ambipolar semiconductor-based inverter obtained after 25 minutes of UV light irradiation and good noise margins. It is clear that the highest noise margins can only be obtained if $Vth_{p,n}$ is approached to 0 as much as possible, it seems that the threshold voltage shift (to values close to 0) after UV irradiation due to diarylethenes presence in the semiconductor layer improve the voltage gain and noise margins by more than two times compared to values extracted in dark. The resultant inverters average gain of 180 in dark and 504 after UV light at an operating voltage of -70 V qualify them as promising potential candidates for the construction of high-performance, organic thin film-based integrated circuits.

8.6. References

1. Baeg, K. J.; Caironi, M.; Noh, Y. Y., Toward Printed Integrated Circuits Based on Unipolar or Ambipolar Polymer Semiconductors. *Adv. Mater.* **2013,** *25* (31), 4210-4244.
2. Zhao, Y.; Guo, Y. L.; Liu, Y. Q., 25th Anniversary Article: Recent Advances in n-Type and Ambipolar Organic Field-Effect Transistors. *Adv. Mater.* **2013,** *25* (38), 5372-5391.
3. Zaumseil, J.; Sirringhaus, H., Electron and Ambipolar Transport in Organic Field-Effect Transistors. *Chem. Rev.* **2007,** *107* (4), 1296-1323.
4. Smits, E. C. P.; Anthopoulos, T. D.; Setayesh, S.; van Veenendaal, E.; Coehoorn, R.; Blom, P. W. M.; de Boer, B.; de Leeuw, D. M., Ambipolar Charge Transport in Organic Field-Effect Transistors. *Phys. Rev. B* **2006,** *73* (20).
5. Singh, T. B.; Senkarabacak, P.; Sariciftci, N. S.; Tanda, A.; Lackner, C.; Hagelauer, R.; Horowitz, G., Organic Inverter Circuits Employing Ambipolar Pentacene Field-Effect Transistors. *Appl. Phys. Lett.* **2006,** *89* (3).
6. Petritz, A.; Fian, A.; Glowacki, E. D.; Sariciftci, N. S.; Stadlober, B.; Irimia-Vladu, M., Ambipolar Inverters with Natural Origin Organic Materials as Gate Dielectric and Semiconducting Layer. *Phys. Status Solidi-Rapid Res. Lett.* **2015,** *9* (6), 358-361.
7. Gundlach, D. J.; Pernstich, K. P.; Wilckens, G.; Gruter, M.; Haas, S.; Batlogg, B., High Mobility n-Channel Organic Thin-Film Transistors and Complementary Inverters. *J. Appl. Phys.* **2005,** *98* (6).
8. Tian, H. J.; Cheng, X. M.; Zhao, G.; Liang, X. Y.; Du, B. Q.; Wu, F., Performance Improvement of Ambipolar Organic Field Effect Transistors by Inserting a MoO3 Ultrathin Layer. *Chin. Phys. Lett.* **2012,** *29* (9).
9. Babel, A.; Wind, J. D.; Jenekhe, S. A., Ambipolar Charge Transport in Air-Stable Polymer Blend Thin-Film Transistors. *Adv. Funct. Mater.* **2004,** *14* (9), 891-898.
10. Shkunov, M.; Simms, R.; Heeney, M.; Tierney, S.; McCulloch, I., Ambipolar Field-Effect Transistors Based on Solution-Processable Blends of Thieno 2,3-b thiophene Terthiophene Polymer and Methanofullerenes. *Adv. Mater.* **2005,** *17* (21), 2608-2612.
11. Jakobsson, F. L. E.; Marsal, P.; Braun, S.; Fahlman, M.; Berggren, M.; Cornil, J.; Crispin, X., Tuning the Energy Levels of Photochromic Diarylethene Compounds for Opto-electronic Switch Devices. *J. Phys. Chem. C* **2009,** *113* (42), 18396-18405.

12. Frolova, L. A.; Troshin, P. A.; Susarova, D. K.; Kulikov, A. V.; Sanina, N. A.; Aldoshin, S. M., Photoswitchable Organic Field-Effect Transistors and Memory Elements Comprising an Interfacial Photochromic Layer. *Chem. Commun.* **2015,** *51* (28), 6130-6132.

13. Tsujioka, T.; Kondo, H., Organic Bistable Molecular Memory Using Photochromic Diarylethene. *Appl. Phys. Lett.* **2003,** *83* (5), 937-939.

14. Shallcross, R. C.; Korner, P. O.; Maibach, E.; Kohnen, A.; Meerholz, K., Photochromic Diode With a Continuum of Intermediate States: Towards High Density Multilevel Storage. *Adv. Mater.* **2013,** *25* (34), 4807-4813.

15. Hayakawa, R.; Higashiguchi, K.; Matsuda, K.; Chikyow, T.; Wakayama, Y., Optically and Electrically Driven Organic Thin Film Transistors with Diarylethene Photochromic Channel Layers. *ACS Appl. Mater. Interfaces* **2013,** *5* (9), 3625-3630.

16. Sciascia, C.; Castagna, R.; Dekermenjian, M.; Martel, R.; Kandada, A. R. S.; Di Fonzo, F.; Bianco, A.; Bertarelli, C.; Meneghetti, M.; Lanzani, G., Light-Controlled Resistance Modulation in a Photochromic Diarylethene-Carbon Nanotube Blend. *J. Phys. Chem. C* **2012,** *116* (36), 19483-19489.

17. Sendler, T.; Luka-Guth, K.; Wieser, M.; Lokamani; Wolf, J.; Helm, M.; Gemming, S.; Kerbusch, J.; Scheer, E.; Huhn, T.; Erbe, A., Light-Induced Switching of Tunable Single-Molecule Junctions. *Adv. Sci.* **2015,** *2* (5).

18. Irie, M., Photochromism of Diarylethene Single Molecules and Single Crystals. *Photochem. Photobiol. Sci.* **2010,** *9* (12), 1535-1542.

19. Pichko, V. A.; Simkin, B. Y.; Minkin, V. I., Conrotatory and Disrotatory Reaction Paths for Thermal and Photoinduced Ring-Closing Reactions of 1,3,5-hexatriene and its Isoelectronic Analogs. *J. Org. Chem.* **1992,** *57* (26), 7087-7092.

20. Irie, M.; Fulcaminato, T.; Matsuda, K.; Kobatake, S., Photochromism of Diarylethene Molecules and Crystals: Memories, Switches, and Actuators. *Chem. Rev.* **2014,** *114* (24), 12174-12277.

21. Irie, M., Photochromism of Diarylethene Molecules and Crystals. *Proc. Jpn. Acad. Ser. B-Phys. Biol. Sci.* **2010,** *86* (5), 472-483.

22. Herder, M.; Schmidt, B. M.; Grubert, L.; Patzel, M.; Schwarz, J.; Hecht, S., Improving the Fatigue Resistance of Diarylethene Switches. *J. Am. Chem. Soc.* **2015,** *137* (7), 2738-2747.

23. Perrier, A.; Maurel, F.; Jacquemin, D., Interplay Between Electronic and Steric Effects in Multiphotochromic Diarylethenes. *J. Phys. Chem. C* **2011,** *115* (18), 9193-9203.

24. Nakamura, S.; Yokojima, S.; Uchida, K.; Tsujioka, T., Photochromism of diarylethene: Effect of Polymer Environment and Effects on Surfaces. *J. Photochem. Photobiol. C-Photochem. Rev.* **2011,** *12* (2), 138-150.

25. Kwon, D. H.; Shin, H. W.; Kim, E.; Boo, D. W.; Kim, Y. R., Photochromism of Diarylethene Derivatives in Rigid Polymer Matrix: Structural Dependence, Matrix Effect, and Kinetics. *Chem. Phys. Lett.* **2000,** *328* (1-2), 234-243.

26. Fukaminato, T.; Umemoto, T.; Iwata, Y.; Yokojima, S.; Yoneyama, M.; Nakamura, S.; Irie, M., Photochromism of Diarylethene Single Molecules in Polymer Matrices. *J. Am. Chem. Soc.* **2007,** *129* (18), 5932-5938.

27. Cho, M. J.; Shin, J.; Hong, T. R.; Um, H. A.; Lee, T. W.; Kim, G. W.; Kwon, J. H.; Choi, D. H., Diketopyrrolopyrrole-Based Copolymers Bearing Highly pi-Extended Donating Units and Their Thin-Film Transistors and Photovoltaic Cells. *Polym. Chem.* **2015,** *6* (1), 150-159.

28. Chen, Z. Y.; Lee, M. J.; Ashraf, R. S.; Gu, Y.; Albert-Seifried, S.; Nielsen, M. M.; Schroeder, B.; Anthopoulos, T. D.; Heeney, M.; McCulloch, I.; Sirringhaus, H., High-Performance Ambipolar Diketopyrrolopyrrole-thieno 3,2-b thiophene Copolymer Field-Effect Transistors with Balanced Hole and Electron Mobilities. *Adv. Mater.* **2012,** *24* (5), 647-652.

29. Glaze, A. P.; Heller, H. G.; Whittall, J., Photochromic Heterocyclic Fulgides. Part 7. (E)-Adamantylidene-[1-(2,5-dimethyl-3-furyl)ethylidene]succinic Anhydride and Derivatives: Model Photochromic Compounds for Optical Recording Media. *J. Chem. Soc.-Perkin Trans. 2* **1992,** (4), 591-594.

30. El Gemayel, M.; Borjesson, K.; Herder, M.; Duong, D. T.; Hutchison, J. A.; Ruzie, C.; Schweicher, G.; Salleo, A.; Geerts, Y.; Hecht, S.; Orgiu, E.; Samori, P., Optically Switchable Transistors by Simple Incorporation of Photochromic Systems into Small-Molecule Semiconducting Matrices. *Nat. Commun.* **2015,** *6*.

31. Borjesson, K.; Herder, M.; Grubert, L.; Duong, D. T.; Salleo, A.; Hecht, S.; Orgiu, E.; Samori, P., Optically Switchable Transistors Comprising a Hybrid Photochromic Molecule/n-type Organic Active Layer. *J. Mater. Chem. C* **2015,** *3* (16), 4156-4161.

32. Zhang, X. R.; Richter, L. J.; DeLongchamp, D. M.; Kline, R. J.; Hammond, M. R.; McCulloch, I.; Heeney, M.; Ashraf, R. S.; Smith, J. N.; Anthopoulos, T. D.; Schroeder, B.; Geerts, Y. H.; Fischer, D. A.; Toney, M. F., Molecular Packing of High-Mobility Diketo Pyrrolo-Pyrrole Polymer Semiconductors with Branched Alkyl Side Chains. *J. Am. Chem. Soc.* **2011,** *133* (38), 15073-15084.

33. Orgiu, E.; Crivillers, N.; Herder, M.; Grubert, L.; Patzel, M.; Frisch, J.; Pavlica, E.; Duong, D. T.; Bratina, G.; Salleo, A.; Koch, N.; Hecht, S.; Samori, P., Optically Switchable Transistor via Energy-Level Phototuning in a Bicomponent Organic Semiconductor. *Nat. Chem.* **2012,** *4* (8), 675-679.

34. Irie, M., Diarylethenes for Memories and Switches. *Chem. Rev.* **2000,** *100* (5), 1685-1716.

35. Matsuda, K.; Irie, M., Diarylethene as a Photo Switching Unit. *J. Photochem. Photobiol. C-Photochem. Rev.* **2004,** *5* (2), 169-182.

36. Briseno, A. L.; Kim, F. S.; Babel, A.; Xia, Y. N.; Jenekhe, S. A., n-Channel Polymer Thin Film Transistors with Long-Term Air-Stability and Durability and Their Use in Complementary Inverters. *J. Mater. Chem.* **2011,** *21* (41), 16461-16466.

37. Yoo, B.; Jones, B. A.; Basu, D.; Fine, D.; Jung, T.; Mohapatra, S.; Facchetti, A.; Dimmler, K.; Wasielewski, M. R.; Marks, T. J.; Dodabalapur, A., High-Performance Solution-Deposited n-Channel Organic Transistors and Their Complementary Circuits. *Adv. Mater.* **2007,** *19* (22), 4028-4032.

38. An, M. J.; Seo, H. S.; Zhang, Y.; Oh, J. D.; Choi, J. H., Air stable, Ambipolar Organic transistors and inverters based upon a heterojunction structure of pentacene on N,N '-Ditridecylperylene-3,4,9,10-tetracarboxylic di-imide. *Appl. Phys. Lett.* **2010,** *97* (2).

39. Vaklev, N. L.; Yang, Y.; Muir, B. V. O.; Steinke, J. H. G.; Campbell, A. J., Bottom-Gate Complementary Inverters on Plastic With Gravure-Printed Dielectric and Semiconductors. *IEEE Trans. Electron Devices* **2015,** *62* (11), 3820-3824.

40. Zhang, X. H.; Potscavage, W. J.; Choi, S.; Kippelen, B., Low-Voltage Flexible Organic Complementary Inverters with High Noise Margin and High dc Gain. *Appl. Phys. Lett.* **2009,** *94* (4).

41. Tatemichi, S.; Ichikawa, M.; Kato, S.; Koyama, T.; Taniguchi, Y., Low-Voltage, High-Gain, and High-Mobility Organic Complementary Inverters Based on N,N'-ditridecyl-3,4,9,10-perylenetetracarboxylic diimide and Pentacene. *Phys. Status Solidi-Rapid Res. Lett.* **2008,** *2* (2), 47-49.

42. Chen, Z. Y.; Lemke, H.; Albert-Seifried, S.; Caironi, M.; Nielsen, M. M.; Heeney, M.; Zhang, W. M.; McCulloch, I.; Sirringhaus, H., High Mobility Ambipolar Charge Tansport in Polyselenophene Conjugated Polymers. *Adv. Mater.* **2010,** *22* (21), 2371-2375.

Chapter 9. Conclusions and outlooks

9.1. Conclusions

This thesis is centered around the self-assembly of high-performing n-type and ambipolar small molecules (PDIF-CN2, ICBA) and polymer (DPPT-TT) semiconductors at surfaces and interfaces, at their multiscale physical chemistry characterization and at their use to fabricate field-effect transistors which exhibit novel properties especially when combined with other functional molecules, towards the fabrication of multifunctional electronic devices expressing new functionalities, that never been reported before.

It is notorious that n-type charge transport in field-effect transistors based on electron-accepting organic semiconductors severely suffers from charge trapping at the dielectric-semiconductor interface when SiO_2 is used as a substrate. In this regard, the use of silane chemistry to grown a self-assembled monolayer on SiO_2 was demonstrated by Peter Ho to be key in order to cover the dielectric surface with a hydrophobic SAM, unfavouring the absorption of water at the dielectric-semiconductor interface.

In this thesis, we have exploited the controlled dielectric surface modification to improve the electrical properties of organic field-effect transistors based on a fullerene derivative. In particular, we have focused our attention on indene-C60 Bis-Adduct (ICBA), i.e. a liquid processable fullerene derivative. We have treated the surface of SiO_2 with HMDS or OTS. We found that OTS SAM exhibit better device performances, high mobility and low threshold voltage close to zero. After functionalization of the SiO_2 surface rendering it more hydrophobic, the devices were annealed at various temperatures (90 °C, 140 °C, and 200 °C) in a nitrogen filled glovebox. The ICBA exhibited both electrons and holes transport within the film. Field-effect mobilities improvements were detected as a result of thermal annealing with values enhancing from 10^{-3} to 10^{-1} $cm^2V^{-1}s^{-1}$ for electron transport and reaching 2.7×10^{-3} $cm^2V^{-1}s^{-1}$ for hole transport. We can conclude from this work that the thermal annealing, SAM functionalization of the insulating gate dielectric are key parameters to optimize the films structural and morphological properties and thus lead to significant improvements in OFETs characteristics.

Most of the organic semiconducting materials are composed of polycrystalline structures consisting of crystalline domains separated by amorphous regions. Such structural characteristic determines a major limitation of the charge transport within the material/film and leads to lower field-effect mobilities compared to inorganic semiconductors. To overcome such a limitation, highly crystalline structures are particularly desired for field-effect transistors and applications thereof, including light-sensitive devices. In light of this we have focused out attention to the realization of organic transistors and phototransistors based of self-assembled crystalline structures formed by solvent-induced precipitation. In particular, we have fabricated and optimized organic phototransistors based on either single or multi-fibers structures integrated in three-terminal devices. These self-assembled crystalline fibers have been produced by solvent-induced precipitation of an air stable and solution-processable perylene diimide derivative, i.e. PDIF-CN2. This molecule is well-known for its electron transport efficiency and environmental stability. We have demonstrated that the charge mobility of PDIF-CN2-based transistors is highly affected by the films crystallinity by comparing the electrical characteristics of spin-coated, single fiber, and multifibers films. Moreover, we have found that the dielectric functionalization with OTS and HMDS self-assembled monolayers is influencing the resulted electron charge current within PDIF-CN2 channel layer. The silicon dioxide passivation minimizes electron traps and ensures a good charge transport behavior. The opto-electronic properties of crystalline fibers-based devices were compared to those of devices incorporating more disordered spin-coated PDIF-CN2 thin-films. The single-fiber devices revealed significantly higher field-effect mobilities, compared to multifiber and thin-films, exceeding 2 $cm^2V^{-1}s^{-1}$, such a high electron mobility performed by solvent processed deposition method is comparable to that recorded on organic transistors prepared by vapor deposited n-channel semiconductors, the latter being an expensive method, especially for opto-electronic industrial applications. We showed that it is possible to fabricate high organic photo-sensitive devices employing simple processing method. This approach can open new opportunities and provides additional strategies for optoelectronic technology featured excellent performances with low-cost and easy manufacturing fabrication. The phototransistors based on crystalline PDIF-CN2 fibers revealed an efficient electron charge transport, a result of strong intermolecular coupling between closely packed PDIF-CN2 molecules and of a low density of structural defects. The improved crystallinity allows efficient collection of photogenerated Frenkel excitons which gives rise to high responsivity (R) for single-fiber PDI-based phototransistors, and photosensitivity (P) exceeding 2×10^3 AW^{-1}, and 5×10^3, respectively. These excellent R and P values are to best of our knowledge the highest reported in literature. These statements prove an evidence for the key role played by the high degree of order at the supramolecular level to improve the material's properties towards the fabrication of light-sensitive organic field-effect transistors. We can conclude that crystalline supramolecular engineered PDIF-CN2 architectures, that have served as the active

layer of transistors and phototransistors, have a greater tendency to affect devices electrical conduction performances.

Photochromic molecules have the capability to change their properties over a simple absorption of photons, without being continuously irradiated. Upon photo-isomerization, the change in their absorption spectra, energetic levels, and geometrical structure can be exploited as optical switches components in light-sensitive optoelectronic devices such as data storage and memory media. Among photochromic molecules, diarylethenes are promising solution processable photo-sensitive molecules that exhibit a good fatigue resistance under UV and Visible light illumination.

In the last topic that we have discussed in this thesis, two diarylethene derivatives (DAE_tBu and DAE_F) were employed together with an ambipolar polymer semiconductor (DPPT-TT) in the fabrication of multi-component light-controlled devices. Our ultimate goal was to induce electrical modulation upon light irradiation of organic transistors and complementary inverters based on DPPT-TT ambipolar polymer, including diarylethene molecules (DAE_tBu and/or DAE_F) in their active layers deposited by a separated layer on top of the polymer layer, in order to achieve a high and ambipolar mobility values by thermal annealing of the polymer layer at high temperature annealing (320 °C). No effect of the diarylethene integration on the film morphology was observed via AFM images, after DAE deposition, the change in charge mobility was negligible compared with the same device based on DPPT-TT before DAE insertion. These bi-and three-component devices were irradiated with UV and Visible light irradiation. The electrons and holes drain currents were optically controlled and reversibly changed by alternating ultraviolet and visible light irradiation.

In three-component based devices, where DAE_F and DAE_tBu are inserted into DAE matrix. The hole and electron currents decrease by three orders of magnitude upon UV (at 365 nm) irradiation (open to closed transition) and increased upon visible light irradiation at 546 nm (closed to open transition) reaching the initial values. This confirms the possibility to modulate the drain current by light-irradiation. The photo-switching concept was also observed for bi-component devises based on DPPT-TT polymer with either DAE_tBu or DAE_F, in which their energy (HOMO of DAE_tBu and LUMO of DAE_F) in the closed form are trap states for holes and electrons respectively. We demonstrated that the holes drain current for devices based on DPPT-TT and DAE_tBu significantly decreased upon 30 seconds of UV illumination. Then, it increased upon Visible light, whereas, electron current is remained constant upon both UV and Visible irradiation. Concerning OFETs devices based on DPPT-TT and DAE_F, electron currents was switched upon UV and Visible illumination, while hole drain currents was stable. Which confirm a completely reversible and selective light-switching process over the insertion of photochromic molecules DAE_tBu (10 wt%) and/or DAE_F (10 wt%).

Three-component based organic complementary inverters were performed using a single layer of DPPT-TT polymer with DAE inserted molecules as n- and p-channel transistors. The optimized organic inverters exhibited high gain upon positive and negative input voltage values in dark and under light irradiation. We recorded for the first-time excellent gain light-induced complementary inverters up to 504 based on one single ambipolar layer. Therefore, these excellent gain values of 180 in dark and 504 after UV irradiation at an operating V_{DD} voltage of -70 V are higher than those reported in literature for ambipolar based complementary inverters (the highest is around 86)[1].

9.2. Outlooks

The use of organic semiconductors in the development of optoelectronic devices [2] has been proven to rival conventional inorganic semiconductor and, on the same time, to exhibit some substantial advantages. The devices can be prepared by solution processing methods on large-scale, and they can be supported on plastic and flexible foils.[3-6] Their electrical and optical properties can be optimized by the synthesis of ad-hoc molecule and the control over its self-assembly to form highly crystalline films.

The attractiveness of organic semiconductors involved in electronic devices has interested several companies and start-up as well as fundamental research institutions. The developments of organic electronics depend crucially on our efforts to perform new generation of organic electronic devices with new functionalities. We believe that in the next years, more and more organic materials integrated in different electronic application will be commercialized, until the day where these organic compounds will displace or dominate silicon based technologies. In some areas of electronics, inorganic semiconductors cannot be used, due to their limitations such as non-flexibility. Examples already exist in the market, like certain chemical sensors and liquid crystal displays.[7] The latter, was performed with using solution processed semiconductors. LG Philip's LCD division has fabricated high-resolution active-matrix liquid crystal display (AMLCD) base on solution processed OTFT.[8] In 2007, Sony company presented an active-matrix OLED display driven by organic thin film transistors.[9] Several examples on organic based devices produces by inkjet printing on glass or produced on flexible plastic were commercialized in the last years.[10]

The high structural order and film crystallinity of organic materials allows great enhancements in transistor devices performences.[11] Accordingly, our results on high performed transistors and phototransistors based on highly crystalline PDIF-CN2 structures combine such excellent light sensitivity, photoresponsivity ratio, and a good operational stability in air atmosphere. PDIF-CN2 crystalline fibers produced by simple and easy solution processing technique that is not expensive for industrial technology, can be incorporated in different electronic light-sensitive devices in future.

Another crystalline nanowire of a perylene derivative has demonstrated photovoltaic effect with high light sensitivity which exhibit a signal-to-noise ratio approaching 10^7 and an external quantum efficiency of > 55%.[12]

We have also optimized other transistors based on a fullerene derivative (ICBA). The simple preparation methods and great electrical properties of ICBA material were extended to another recent work in our group that displayed promising results in photovoltaic efficiency in combination with P3HT. Which certainly make ICBA semiconductor a good candidate for replacing PCBM in organic solar cells.[13]

Finally, we have provided a fundamental study on an ambipolar semiconductor with inserted diarylethene molecules in its matrix, these bi-and three-component were successfully integrated in photo-switched transistors and complementary inverters with great electrical performances. These findings enable the incorporation of multicomponent systems with new functionalities into optically switchable transistors,[14] flexible optical memory devices,[15] photovoltaic cells,[16-17] and electronic logic circuits with a high potential to achieve high-performing organic optoelectronic devices. The organic complementary inverters can be integrated in flexible ring oscillators with a light controllable gain. Novel and high performing organic materials employed in electronic circuits for smart cards, cellphones, data storage, identification tags, and in most daily live products can make a high impact in industry market during the next 10 years, which will be very exciting for researcher scientists in this field.

9.3. References

1. Chen, Z. Y.; Lemke, H.; Albert-Seifried, S.; Caironi, M.; Nielsen, M. M.; Heeney, M.; Zhang, W. M.; McCulloch, I.; Sirringhaus, H., High Mobility Ambipolar Charge Transport in Polyselenophene Conjugated Polymers. *Adv. Mater.* **2010,** *22* (21), 2371-2375.
2. Facchetti, A., Semiconductors for Organic Transistors. *Mater. Today* **2007,** *10* (3), 28-37.
3. Arias, A. C.; MacKenzie, J. D.; McCulloch, I.; Rivnay, J.; Salleo, A., Materials and Applications for Large Area Electronics: Solution-Based Approaches. *Chem. Rev.* **2010,** *110* (1), 3-24.
4. Bao, Z. N.; Dodabalapur, A.; Katz, H.; Raju, V. R.; Rogers, J., Organic Semiconductors for Plastic Electronics. *Abstr. Pap. Am. Chem. Soc.* **2001,** *221*, U627-U627.
5. Brabec, C. J.; Cravino, A.; Meissner, D.; Sariciftci, N. S.; Fromherz, T.; Rispens, M. T.; Sanchez, L.; Hummelen, J. C., Origin of the Open Circuit Voltage of Plastic Solar Cells. *Adv. Funct. Mater.* **2001,** *11* (5), 374-380.

6. Caboni, A.; Orgiu, E.; Barbaro, M.; Bonfiglio, A., Flexible Organic Thin-Film Transistors for pH Monitoring. *Ieee Sens. J.* **2009,** *9* (12), 1963-1970.

7. Zhou, L. S.; Wanga, A.; Wu, S. C.; Sun, J.; Park, S.; Jackson, T. N., All-Organic Active Matrix Flexible Display. *Appl. Phys. Lett.* **2006,** *88* (8), 3.

8. Kang, H., High Resolution OTFT-AMLCD Using Solution-Process. Poster presented at the printed *Printed Eectronics USA* **2007**, San Francisco.

9. Organic Seiconductor Analyst Direct (OSAD). *a Weekly Newsletter on the Organic Semiconductor Industry* **Monday, 22 October 2007,** *5* (1), 39. Cintelliq Ltd.

10. BBC News. UK in Plastic Electronics Drive. **Jan 3. 2007**.

11. Molinari, A. S.; Alves, H.; Chen, Z.; Facchetti, A.; Morpurgo, A. F., High Electron Mobility in Vacuum and Ambient for PDIF-CN2 Single-Crystal Transistors. *J. Am. Chem. Soc.* **2009,** *131* (7), 2462-2463.

12. Zhang, L.; Zhong, X. L.; Pavlica, E.; Li, S. L.; Klekachev, A.; Bratina, G.; Ebbesen, T. W.; Orgiu, E.; Samori, P., A Nanomesh Scaffold for Supramolecular Nanowire Optoelectronic Devices. *Nat. Nanotechnol.* **2016,** *11* (10), 900-907.

13. He, Y. J.; Chen, H. Y.; Hou, J. H.; Li, Y. F., Indene-C-60 Bisadduct: A New Acceptor for High-Performance Polymer Solar Cells. *J. Am. Chem. Soc.* **2010,** *132* (4), 1377-1382.

14. Borjesson, K.; Herder, M.; Grubert, L.; Duong, D. T.; Salleo, A.; Hecht, S.; Orgiu, E.; Samori, P., Optically Switchable Transistors Comprising a Hybrid Photochromic Molecule/n-Type Organic Active Layer. *J. Mater. Chem. C* **2015,** *3* (16), 4156-4161.

15. Leydecker, T.; Herder, M.; Pavlica, E.; Bratina, G.; Hecht, S.; Orgiu, E.; Samori, P., Flexible non-Volatile Optical Memory Thin-Film Transistor Device with Over 256 Distinct Levels Based on an Organic Bicomponent Blend. *Nat. Nanotechnol.* **2016,** *11* (9), 769-775.

16. Cho, M. J.; Shin, J.; Hong, T. R.; Um, H. A.; Lee, T. W.; Kim, G. W.; Kwon, J. H.; Choi, D. H., Diketopyrrolopyrrole-Based Copolymers Bearing Highly pi-Extended Donating Units and Their Thin-Film Transistors and Photovoltaic Cells. *Polym. Chem.* **2015,** *6* (1), 150-159.

17. Li, W. W.; Hendriks, K. H.; Wienk, M. M.; Janssen, R. A. J., Diketopyrrolopyrrole Polymers for Organic Solar Cells. *Accounts Chem. Res.* **2016,** *49* (1), 78-85.

List of publications

Orgiu, E.; Squillaci, M. A.; **Rekab, W.**; Bojesson, K.; Liscio, F.; Zhang, L.; Samori, P., The Dramatic Effect of the Annealing Temperature and Dielectric Functionalization on the Electron Mobility of Indene-C-60 bis-Adduct Thin Films. Chem. Commun. 2015, 51 (25), 5414-5417.

Rekab, W.; Stoeckel, M. A.; El Gemayel, M.; Gobbi, M.; Orgiu, E.; Samorì, P., High-Performance Phototransistors Based on PDIF-CN2 Solution-Processed Single Fiber and Multi-fiber Assembly. ACS. Appl Mater. Interfaces 2016, 8, 9829−9838

Liscio, A.; Agalou, K. K.; Kovtun, A.; Gebremedhn, E.; El Garah, M.; **Rekab, W.**; Orgiu, E.; Giorgini, L.; Samorì, P.; Beljonne., D. Exfoliation of Few-Layer Graphene in Volatile Solvents Using Perylene Surfactants. ChemPlusChem. In press, DOI: 10.1002/cplu.201600503.

Rekab, W.; Herder, M.; Schroeder, B.; Hou, L.; McCulloch, I.; Hecht, S.; Orgiu, E.; Samorì, P. High-performing organic-based inverters with photo-modulable gain. Manuscript in preparation.

List of communications

Integration of Supramolecularly Assembled PDI Fibers in Organic Field-Effect Phototransistors.
W. Rekab, E. Orgiu, P. Samorì. 10th International Conference on Organic Electronics (ICOE), Modena, Italie (11-13/06/2014).

Field-Effect Phototransistors Based on Supramolecularly Engineered Perylene Di-imide Fibers.
W. Rekab, E. Orgiu, P. Samorì. 7th International Conference on Molecular Electronics (ElécMol), Strasbourg, France (24-29/08/2014).

Optically Switchable Transistor via Permeation of Photochromic Molecules into an Ambipolar Polymer Matrix. **W. Rekab,** M. Herder, B. Schroeder, L. Hou, I. McCulloch, S. Hecht, E. Orgiu, P. Samorì. 13th European Conference on Molecular Electronics (ECME), Strasbourg, France (01-05/09/2015).

Statement of work

All the experiments and data analysis reported in this thesis have been carried out by myself under the guidance of my Ph.D. supervisors except for those listed below:

Chapter 6: AFM images were performed by Marco Squillaci (Nanochemistry lab). The 2D-GIXRD structural characterization was carried out in collaboration with Dr. F. Liscio (Istituto per la Microelettronica e Microsistemi - CNR, Bologna, Italy).

Chapter 7: SEM images were recorded with the help of Dr Mirella El Gemayel (Nanochemistry lab).

Chapter 8: DPPT_TT polymer synthesis was performed by Bob Schroeder, PhD student in Prof. Lain McCulloch's group (Chemistry Department, Imperial College, London, UK). Diarylethene molecules (DAE_tBu and DAE_F) were synthesized by Dr. Martin Herder under the supervision of Prof. Stefan Hecht (Humboldt Universität zu Berlin, Germany). Quantum yield measurements were performed by Dr. Lili Hou (Nanochemistry lab).

Experimental results have been discussed with my supervisors Profs. Paolo Samorì and Emanuele Orgiu and our collaborators.

Acknowledgements

I would like to thank all the people who contributed in some way to the work described in the thesis and the realization of this dissertation.

Firstly, I want to express my deepest acknowledgement to my advisor Prof. Paolo Samorì for providing me the opportunity to be member of his research group as a Master student and then as a PhD student. I am very grateful for his time, continuous support, patience, motivation, and immense knowledge. His scientific knowledge, inspiring ideas, and enthusiasm about my research project were a real support to me over the last few years. I could not have imagined having a better advisor and mentor for my Ph.D study. It has been a great pleasure and honor to be one of his PhD students.

I would like to extend my sincere thanks and appreciation to my co-advisor Prof. Emanuele Orgiu for all the support and encouragement he gave me. Without his critical comments, thoughtful guidance this work would not have been achievable. He is an excellent scientist and friendly Professor. His expert advice and support during of my PhD thesis have been invaluable for me.

Besides my advisors, I would like to thank the other members of my dissertation committee Prof. Laurence Vignau and Prof. Sabine Ludwigs for accepting to be member of my defense committee, and for their time to review my thesis.

I humbly acknowledge the valuable collaboration with Prof. Vincenzo Palermo group (at ISOF-CNR, Bologna, Italy), particularly Dr. Konstantinos Kouroupis-Agalou and Dr. Andrea Liscio. Also, I would like to thank Bob Schroeder, PhD student in Prof. Lain McCulloch's group (Chemistry Department at Imperial College, London, UK) for the synthesis of DPPT-TT ambipolar polymer. I would like to thank Dr. Martin Herder and Prof. Hecht (Humboldt Universität zu Berlin, Germany) for the synthesis of diarylethene molecules and Dr. Fabiola Liscio (Istituto per la Microelettronica e Microsistemi - CNR, Bologna, Italy) for performing 2D-GIXRD structural characterization on ICBA films.

There are also words of gratitude for my present and former colleagues who worked by my side during my Master and PhD. Particularly, Mirella, Lili, Marc-Antoine, Lei, Mohamed, Marco

Squillaci, Olly, Tim, Sara, Karl, Marcus, Maria, Chiara, Songlin, Marco Gobi, Artur, Marco Caroli, Simone, Thomas, Agostino. Many tanks to all of them for introducing me to the use of equipments and associated software, helping me to solve technical and scientific problems, being involved on my projects by providing experimental studies and for the valuable discussions.

The Nanochemistry laboratory team has been a source of friendships as well as good advice and collaboration. They supported me greatly and were always willing to help me. Thank you all for the nice and cooperative atmosphere at work and useful feedback and insightful comments on my work.

I would like to thank also other member of our team: Corrine, Nicolas, and Axel, they were kept us organized and were always ready to help.

I expand my thanks to all my friends in France and in Algeria, specially Styven and Khalissa. I would like to thank my family and my family-in-law for supporting me during my PhD thesis. Special thanks to my uncle Farid, his wife Estelle and her parents, my aunt dehbea, and uncle Cherif for their unconditional support during my studies at the University of Strasbourg.

Words are short to express my deep gratitude to my parents Youcef Rekab and Salima Boukahoul, for loving me and having faith in me, all the support you have provided me over the years is the greatest gift, this manuscript is dedicated to you.

Also, I would like to thank my brothers: Mohamed, Chihab and sisters: Hadil, Salsabil, and Ibtihal for all their love, emotional support, and encouragement, they raised me with the love of science and supported me throughout all my studies.

Lastly, I would like to express my sincere grateful to my husband Samir, for his love, patience, and faithful support in each moment of our life. Thank you for making my life so special and full of joy.

Wassima Rekab

Assemblage multi-composant pour l'électronique organique

Résumé

Mon travail de thèse porte sur l'assemblage supramoléculaire et le transport de charge des multi-composants utilisés dans le domaine de l'électronique à base organique. En particulier, l'étude et l'optimisation des transistors organiques à effet de champ (OFETs), des phototransistors, et des inverseurs organiques. Nous avons démontré que la température de recuit des dispositifs OFETs améliore les performances électriques d'un dérivé de fullerène (ICBA). Ces dispositifs dont les surfaces de SiO_2 sont fonctionnalisées par OTS ou HMDS ont montrés des mobilités d'électrons de $0.1 cm^2V^{-1}s^{-1}$, qui est la plus élevée par rapport à la littérature. Aussi, nous avons fabriqué des phototransistors à base de mono- et multifibres de PDIF-CN2 qui ont été optimisés par traitements de surfaces du diélectrique (HMDS ou OTS). Les propriétés optoélectroniques de ces dispositifs ont été comparées à ceux des dispositifs à base des couches minces déposés par spin-coating (éduction centrifuge). Nos dispositifs mono-fibres ont montré des valeurs de mobilité plus élevées (supérieure à 2 $cm^2V^{-1}s^{-1}$) par rapport à ceux des multifibres et couches minces. Une telle efficacité de transport d'électrons est le résultat d'une cristallinité très élevée des fibres, qui permet une collecte efficace des excitons photo-générés qui se traduit par la plus haute sensibilité à la lumière (R) et photosensibilité (P) rapportées pour les phototransistors à base de mono-fibre supérieure à 2×10^3 AW^{-1}, et 5×10^3 AW^{-1}. Enfin, un polymère ambipolaire (DPPT-TT) a été utilisé lors de la fabrication de nouveaux dispositifs multifonctionnels par l'addition des molécules diaryléthènes (DAE_tBu et ou DAE_F), dont les propriétés électriques sont contrôlées par la lumière. Cette approche a permis un contrôle optique de gain en tension des inverseurs organiques, ces dispositifs multi-composants sont caractérisés par des gain en tensions très élevées (jusqu'au 504) comparés à ceux reportés dans la littérature (86). Ces travaux réalisés durant cette thèse offrent de nouvelles perspectives dans le domaine de l'optoélectronique et la conception des mémoires optiques.

Mots-clés : Polymère et Petites Molécules Semi-conductrice, Transistors à Effet de Champs, Phototransistors, Transport de Charge Ambipolaire, Inverseurs Organiques, Molécules Photochromiques.

Abstract

This thesis is focused on the investigation of supramolecular assemblies and the charge carriers transport across organic single, bi- and three-component materials, used as the active layer in organic field-effect transistors (OFET), phototransistors (OPT) and complementary inverters. We demonstrated that thermal annealing and duration has high impact in OFET performances based on a fullerene derivative called ICBA. The devices electron mobility enhanced upon HMDS and OTS treated SiO_2 surface and reached 0.1 $cm^2V^{-1}s^{-1}$, which is the highest reported value in literature. We have provided evidence for the influence of the order at the supramolecular level in the semiconducting material (PDIF-CN2) on the performance of OPTs. We compared solution processed single crystalline PDIF-CN2 fibers and multifiber assemblies with spin-coated thin films, which revealed that the former exhibited good electron mobility up to 2 $cm^2s^{-1}V^{-1}$. The improved fiber crystallinity allows efficient collection of photogenerated excitons, results in the highest reported responsivity R ($>5 \times 10^3$ AW^{-1}), and photoswitching ratio P ($>2 \times 10^3$), which are to date the highest reported in literature for PDI-single crystal OPTs. Finally, we have performed for the first time new multifunctional devices combining an ambipolar polymer (DPPT-TT) with inserted diarylethene molecules in its matrix. The fabricated OFET and organic complementary inverters were optically controlled. The resultant inverters gain values are tuned by ultraviolet and visible light irradiation, reaching 504, which is higher than those reported in literature (86). These findings qualify them as promising potential candidates for the construction of high-performance integrated logic circuits and memory chips.

KEYWORDS: Semiconducting Polymer and Small Molecules, Organic Field-Effect Transistors, Organic Phototransistors, Ambipolar Transport, Organic Complementary Inverters, Photochromic Molecule.